STUDIES OF HIGH ENERGY COSMIC RAYS AT PeV REGION

A THESIS SUBMITTED TO THE UNIVERSITY OF NORTH BENGAL

FOR THE AWARD OF

DOCTOR OF PHILOSOPHY [*SCIENCE*]

IN

PHYSICS

BY

RAJAT KUMAR DEY

SUPERVISOR

DR. ARUNAVA BHADRA

DEPARTMENT OF PHYSICS

UNIVERSITY OF NORTH BENGAL

DARJEELING - 734013

MAY 2013

DECLARATION

I declare that the thesis entitled "STUDIES OF HIGH ENERGY COSMIC RAYS AT PeV REGION" has been prepared by me under the guidance of Dr. Arunava Bhadra, Senior Research Physicist of High Energy and Cosmic Ray Research Centre, University of North Bengal. No part of this thesis has formed the basis for the award of any degree or fellowship previously.

Rajat Kr. Dey

Date: 31.05.2013

(Rajat Kumar Dey)

Department of Physics,

University of North Bengal,

P.O. – North Bengal University,

District – Darjeeling,

Pin – 734013,

WB; India.

UNIVERSITY OF NORTH BENGAL
HIGH ENERGY & COSMIC RAY RESEARCH CENTRE

Dr. Arunava Bhadra
Sr. Research Physicist

P.O. NORTH BENGAL UNIVERSITY
Siliguri, West Bengal
India, PIN 734013
Phone: (0353) 2776358 (O)
Fax: (0353) 2699001

CERTIFICATE FROM THE SUPERVISOR

I certify that Sri Rajat Kumar Dey has prepared the thesis entitled "STUDIES OF HIGH ENERGY COSMIC RAYS AT PeV REGION", for the award of PhD degree of the University of North Bengal, under my guidance. He has carried out the work at the Department of Physics and High Energy and Cosmic Ray Research Centre, University of North Bengal.

Date: 27.05.2013

(Dr. Arunava Bhadra)

Dr. Arunava Bhadra
Sr. Research Physicist
High Energy & Cosmic Ray Research Centre
University of North Bengal, Siliguri, 734013

IN MEMORY
OF
MY LATE FATHER

ACKNOWLEDGEMENTS

I express my heartfelt gratitude to Dr. Arunava Bhadra, my research supervisor, for his guidance, valuable suggestions and patience to the development of this work. In particular I appreciated his invaluable help when I was getting started with Monte Carlo Code.

With deep respect I remember the inspiration of my teacher Prof. (Late) Nirmalendu Choudhury, who taught me Nuclear Physics and Cosmic Rays at Post Graduate level. I am grateful to him for his knowledge and introducing me to the world of cosmic rays.

For the inspiration to look beyond India, I would like to thank Prof. Jean Noel Capdevielle, APC, France.

I express my sincere thanks to Dr. Biswanath Ghosh, retired from High Energy and Cosmic Ray Research Centre for always found the time to ask me how the work was going on. I am very much grateful to Dr. Subrata Sanyal for his love and encouragement. I express my thankfulness to Dr. Samir Kumar Sarkar and Mr. Arindam Mukherjee for their support and help. I thank Mr. Sadhan Paul for treating me like one of the members of the centre. I especially thank my fellow student Biplab in consulting the technicality of Monte Carlo codes. I am obliged to Dr. Partha Joardar, Bose Institute for meaningful discussion about M C simulations in the early phase of the work.

I am greatly indebted to my teachers Dr. Nikhilesh Kar, Prof. Pradip Kumar Mandal, Prof. Swapan Kumar Ghosal, Prof. Biswanath Bhattacharjee and Prof. Dhruba Dasgupta for their motivation and help. I would also like to thank my esteemed colleagues Prof. A. Mukhopadhyay, Dr. M. K. Das, Dr. B. C. Paul, Dr. S. Chatterjee and Mr. P. Mali for their tremendous support throughout the work. I am especially grateful to my friend Sripada Haldar with whom I shared my joy and happiness during the good times. I thank also to my University colleagues Prof. Mahendranath Ray, Dr. Ashish Kumar Nanda and my former colleagues Sri Nepal Chandra Gope, M.D.G.M. High School and Dr. B. P. Ghosh, Behala College for their inspiration and love. I acknowledge the help of Mr. Tamal Sarkar, USIC during the installation of Linux OS and other packages in computers. I gratefully acknowledge the technical help of Mr. Rajesh Pradhan from the Physics Department.

I owe a lot of thanks to my mother and family members for their love, encouragement and support. Finally thanks to my wife Swapnali for her endless patience and encouragement at every turn.

ABSTRACT

The present thesis reports research works by the author (in collaboration with few others) on various aspects of cosmic rays in the PeV region. The main objectives of the thesis are **[i]** *to study the detail characteristics of few extensive air shower (EAS) parameters/observables from a detailed Monte Carlo (MC) simulation and to examine their primary mass sensitivity for the purpose of exploiting them in understanding the nature of shower initiating particles in the PeV energy regime through multi-parameter approach of studying EAS,* **[ii]** *to study the role of air shower fluctuations in estimating hadron-air interaction cross section through EAS technique, and* **[iii]** *to quantify the neutrino and gamma-ray signatures of PeV cosmic rays if they are accelerated by polar caps of pulsars.*

For a precise estimation of primary mass, modern EAS experiments are more and more relying on the multi-parameter approach of studying EAS. Under the context one of the main objectives of the present thesis work was to examine whether the shower age parameter that essentially describes the slope of the lateral distribution of electrons in EAS can effectively be utilized for extracting information about the nature of shower initiating particles. We proposed a way for the unambiguous estimation of the lateral shower age parameter from electron densities at different radial distances and then its correlation with other EAS observables has been studied from a detailed MC simulation study. Subsequently we explore the possible role that the parameter may play in a multi-parameter approach of studying EAS to understand the nature of shower initiating particles.

Distinguishing gamma-ray and hadron initiated EASs based on lateral distribution of electrons has been studied using MC simulations which in turn may help to understand the sources of primary cosmic rays in the concerned energy range. The possibility of using the local lateral shower age parameter of EAS for the gamma-hadron separation has been explored. The proposed observable might be particularly useful for surface detector experiments those have no reliable muon measurement facilities.

From an analysis of MC simulation data it is revealed that an asymmetry may develop in positive and negative muon numbers about the shower axis depending on the geomagnetic field at the location of the observation. Such an asymmetry is particularly pronounced at certain zenith and azimuth angle range. From the present investigation a new primary mass sensitive parameter, the so called muonic dipole

length is proposed and is estimated from the asymmetry in muon distributions. The implications of such an effect on EAS observations have been discussed.

The p-air cross-section is estimated from EAS studies either by evaluating the absorption of the proton initiated EAS flux penetrating the atmosphere or from the distribution of the depth of shower maximum. The former approach is, however, affected mainly by the intrinsic fluctuations associated with EASs those are generally disentangled using Monte Carlo simulation technique. Here we have critically examined this aspect and pointed out that the air shower fluctuations has limited effect on cross-section measurements.

From several experimental observations and theoretical considerations it is believed that cosmic rays of PeV energies (in fact up to 100 *or even* 3000 *PeV) are of galactic origin. Supernova remnant and pulsars (including pulsar wind nebulae) are the most promising candidates for the galactic cosmic ray sources. Because of the deflection of charged cosmic rays by the interstellar magnetic fields, the cosmic ray flux loses all the information about the direction of their sources. However, high energy gamma-rays and neutrinos are expected to be produced in the interactions of energetic cosmic rays with the ambient matter in the source environment and thereby cosmic ray sources can be identified by observing appropriate fluxes of gamma rays and neutrinos. In a work of this thesis we derived expressions for flux of gamma rays and neutrinos to be observed at Earth if cosmic rays at PeV energies are accelerated by polar caps of pulsars. We also estimated gamma- rays and neutrino fluxes for some nearby gamma ray pulsars and compared with the available observations.*

PREFACE

The origin of cosmic rays remains one of the greatest challenges in modern physics. Cosmic rays span an enormous range of energy from about 10^9 eV to beyond 10^{20} eV. The energy spectrum of primary cosmic rays exhibits power law behaviour with an energy spectrum that is essentially a continuous power law. At about 3×10^{15} eV the primary cosmic ray spectrum steepens slightly. This feature is commonly called the *knee* of the spectrum. Because of the presence of the *knee* feature the PeV energy region is an area of intense study in cosmic ray research. The proper explanation of the *knee* is supposed to be a corner stone in understanding the origin of cosmic rays.

The knowledge about the composition of primary cosmic rays in the PeV domain is of fundamental importance for understanding the *knee*. However, despite several extensive experimental efforts no definite conclusion on change of composition across the *knee* could be drawn. This is mainly because of the inverse problem of deriving the mass composition of cosmic rays from EAS measurements, which is an indirect but only feasible way of studying cosmic rays at this energy range owing to low flux of primary cosmic rays, is quite difficult.

Under this context various aspects related to PeV cosmic rays, which include MC simulation study of detailed characteristics and primary mass sensitivity of few EAS parameters/observables (shower age and muonic dipole length) for the purpose of employing them to extract the nature of primary particle reliably through a multi-parameter approach of studying EAS, a critical examination of the proton-air and Fe-air interaction cross section measurements by the EAS technique in order to gain physical insight for the deviation of EAS absorption length from interaction mean free path of PeV cosmic ray particles in the atmosphere, and quantifying the neutrino and gamma ray signatures of PeV cosmic rays if they are accelerated by polar caps of pulsars, have been investigated and reported in this thesis.

The important findings of works reported in the present studies are listed below:

[i] The lateral distribution of electrons in EAS exhibits some sort of *scaling* behaviour in terms of the local lateral shower age parameter. This feature is

nearly independent of the primary energy, mass, observational level and hadonic interaction model.

[ii] The local age parameter (LAP) offers a good solution towards an unambiguous estimation of the lateral shower age.

[iii] The lateral shower age offers a good estimator of the longitudinal development of an EAS cascade on a statistical basis, as also noted in some earlier works.

[iv] The local/lateral shower age might be useful for extracting information about the mass of primary cosmic rays. The fluctuation of the LAP has also been found to be sensitive to the nature of the primary particle.

[v] It appears that the local age parameter, if measured with good precision can be employed in discriminating γ-ray initiated EAS from hadron induced EAS.

[vi] The "*muonic dipole length*" in inclined EAS is found sensitive to primary mass; it is larger for iron primary in compare to that for proton.

[vii] From a detail MC simulation study it is found that the air shower fluctuations has limited effect on hadron-air cross-section measurements using EAS technique, rather the characteristics of high energy interactions seem to play the major role for the deviation of EAS absorption length from mean free path of the hadron in air.

[viii] Cosmic rays at PeV energies might be accelerated at polar caps of pulsars. The presence of a hadronic component in the flux of pulsar accelerated particles should result in the emission of high-energy neutrinos and gamma-rays simultaneously as both charged and neutral pions are produced in the interactions of energetic hadrons with the ambient photon fields surrounding the acceleration region. We estimated gamma-rays and neutrino fluxes for some nearby gamma-ray pulsars and compared with the available observations. The present study suggests that pulsars are unlikely to be strong sources of TeV neutrinos.

As an additional support to the candidate, the reprints of the following **published papers** are attached at the end of the thesis.

1. A Bhadra and R K Dey, "TeV neutrinos and gamma-rays from pulsars", *Monthly Notices of the Royal Astronomical Society*, **395**, 1371 – 1375 (2009), e-Print: arXiv: **0812.1845v1** [astro-ph].

2. R K Dey, A Bhadra and J N Capdevielle, "Behaviour of the EAS Age Parameter in the Knee Energy Region", Fermilab *eConf* **C1006284**, *XVI ISVHECRI* (2010), e-Print: arXiv:**1009.5396v1** [astro-ph.HE].

3. R K Dey and A Bhadra, "Gamma-hadron discrimination of primary cosmic rays from EAS observations", *Exploring the cosmos*, ISBN – **978-3-8443-9165-7**, Ed. A Bhadra, *LAMBERT Academic Publishing*, Germany (2011), p 93-105.

4. R K Dey, A Bhadra and J N Capdevielle, "Primary mass sensitivity of lateral shower age parameter in EAS", *Proceedings International Cosmic Ray Conference*, Beijing (2011), HE.**1.2.**, vol. **1/11**, p.174 – 177.

5. J N Capdevielle, R K Dey and A bhadra, "Imprint of Geomagnetic field on charged particle distribution in EAS", *Proceedings International Cosmic Ray Conference*, Beijing (2011), HE.**1.1.**, vol. **1/11**, p. 133-136.

6. R K Dey, A Bhadra and J N Capdevielle, "Scaling behaviour of lateral distribution of electrons in EAS", *Journal of Physics G: Nuclear & Particle Physics,* **39** (2012), 085201.

7. R K Dey and A Bhadra, "Selecting gamma-ray showers from hadronic background using lateral shower age of EAS" *Astroparticle Physics* **44** (2013) 68 – 75.

Communicated to Journal - 01

Work from the following publication is not included in the thesis:

1. A Bhadra and R K Dey, "Physical significance of the lateral shower age", *Proceedings International Cosmic Ray Conf*erence, Germany, Copernicus Gesellschaft (2001), **185**.

(Rajat Kumar Dey)

Department of Physics
University of North Bengal
P.O.- North Bengal University
Darjeeling (WB): India.

TABLE OF CONTENTS

LIST OF TABLES

LIST OF FIGURES

LIST OF APPENDICES

Appendices

CHAPTER 1

COSMIC RAYS AND EXTENSIVE AIR SHOWERS

The Earth is continuously bombarded by charged particles from the cosmos, which are known as Cosmic rays. The discovery of cosmic rays (CRs) has just passed its 100 years last year, in 2012. The study of this non-thermal radiation gives impetus in our understanding of both large objects of the Universe at cosmological distances and the basic building blocks of matter. However, the origin of CRs still remains a subject of much speculation. Attaining a broad range of energy, starting from about 1 GeV up to 10^{20} eV and higher—the highest energies ever observed, the CRs have been, and still are, an important means to look at the Universe and to reveal some its mysteries. An explanation of the origin, propagation mechanisms and nature of the most energetic CRs are still a subject of intense research in Astrophysics and Astroparticle Physics. The main interest of CR studies remains to study them as possible messengers of very powerful astrophysical processes.

The present thesis focuses various aspects of CRs in the PeV energy region. The objectives of the present investigation and the organization of the thesis are given at the end of the present chapter.

1.1 HISTORICAL OVERVIEW

V. F. Hess (Hess 1912) discovered this highly relativistic charged particle radiation in 1912 during several free balloon ascents. He observed an increase of the ionization rate of air with increasing elevation, and inferred that there must be a hitherto unknown radiation penetrating into the Earth's atmosphere from the outer space. In subsequent years W. Kolhörster made further ascends with improved electrometers, measuring the altitude variation of the ionization up to heights of 9 km (Kolhörster 1925).

In 1929 W. Bothe and W. Kolhörster measured coincident signals in two Geiger-Muller counters (Bothe et al. 1929) and concluded that CRs consist of charged particles. Similar conclusions were drawn from measurements by J. Clay, who showed that the intensity of CRs depends on the (magnetic) latitude of the observer (Clay 1930).

In 1938, Kolhörster (Kolhörster et al. 1938) and Auger (Auger et al. 1938) independently discovered that CRs are individual charged particles, which interact with a nucleus in the Earth's atmosphere, and consequently induce a shower of secondary particles. These so-called *extensive air showers* (EAS) were detected with a setup of Wilson cloud chambers and Geiger-Müller tubes, separated by some tens of meters, and operated in coincidence. This finding pioneered a new approach to investigate CRs at the highest energies: the measurement of extensive air showers by means of large ground based detector arrays.

In the 1940s, M. Schein showed with measurements through balloon ascents that the positively charged primary particles were mostly protons (Schein et al. 1941). Cloud chambers and photographic plates were carried into the stratosphere and it was found that CRs are made up of fully ionized atomic nuclei moving at speeds closely to that of light (Brandt & Peters 1948). Many nuclei of the periodic table up to $Z \approx 40$ were found and their relative abundances determined. Hydrogen and helium occur most frequently, and the distribution in mass of the heavier nuclei appeared to be similar to that in the solar system.

In the subsequent years, insights about the shape of the energy spectrum of CRs have been attained. The flux of CRs follows a power law over many orders of magnitude in energy. However, there are a few structure observables. In 1958, Kulikov and Khristiansen (Kulikov & Khristiansen 1958) discovered a distinct steepening in the measured electron shower size spectrum for particle numbers larger than 8×10^5, what corresponds roughly to a primary energy of the shower inducing CR particle of $E \approx 8 \times 10^{15}$ eV. This should be the first measurement of the so called *knee* of the CR spectrum. Three years later, Peters (Peters 1961) concluded that the position of this *knee* will depend on the atomic numbers of the CR particles, if their acceleration is correlated to magnetic fields. He interpreted the *knee* "as a magnetic rigidity cut-off in the source which contributes the bulk of primaries below 10^{15} eV," and, more precisely, to be at "a magnetic rigidity corresponding to that of protons with about 10^{15} eV." However, this would mean that also the spectra of heavier CR primaries ought to exhibit such *knee* structures successively.

The M.I.T. group at Volcano Ranch, New Mexico was built the largest cosmic-ray detector in the 1960s. Two years later the first event with energy of

about 10^{20}eV was recorded with the Volcano Ranch array (Linsley 1963). Bigger air shower arrays were subsequently built (SUGAR (Bell et al. 1974), Haverah Park (Edge et al. 1973), Yakutsk (Afanasiev et al. 2003), and AGASA (Chiba et al. 1992)) and, after some initial attempts, the first successful fluorescence light detector, called Fly's Eye, was set up in Utah (Baltrusaitis et al. 1985). With these detectors, another feature of the CR flux was firmly established and is known as the "*ankle*" (Bird et al. 1993, Lawrence et al. 1991 & Nagano et al. 1992).

It is worthwhile to mention that the Particle Physics was practiced primarily through the study of CRs during several decades of the 20th century. New elementary particles like positron, muon and pion were discovered from 1930s to 1950s through series of investigations of the cosmic radiation. In the subsequent years, new unstable hadrons were found in CR interactions in emulsion chambers, were later identified as *D* mesons. Also, a number of exotic phenomena were observed, none of which could be confirmed in accelerator experiments.

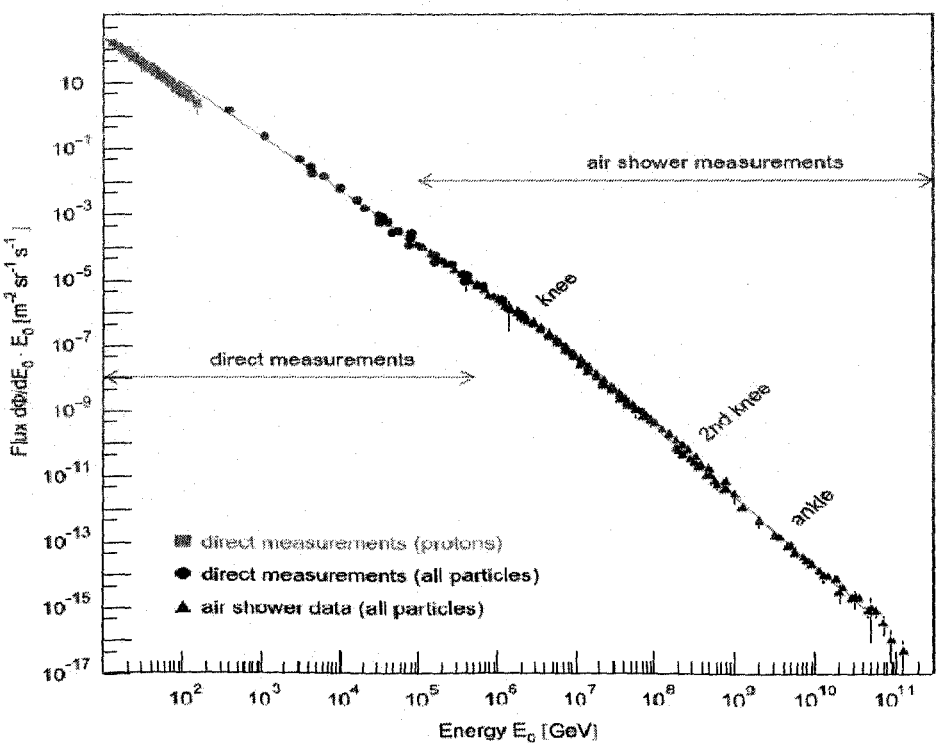

Fig.1.1: All-particle energy spectrum of CRs as measured directly with detectors above the atmosphere and with air shower detectors. At low energies, the flux of primary protons is shown (figure taken from (Blümer et al. 2009)).

1.2 ENERGY SPECTRUM

The solar system is completely bared to a flux of cosmic radiation. The CR energy spectrum extends over 11 orders of magnitude ranging from 1 up to at least 10^{11} GeV. The differential energy spectrum of all CR particles is depicted in **Fig.1.1.** It falls steeply as a function of energy, decreasing by about a factor of 500 per decade in energy. The flux decreases from more than 1000 particles meter^{-2} sec^{-1} at GeV energies to about 1 particle meter^{-2} year^{-1} up to few hundred PeV, and further to less than 1 particle km^{-2} century^{-1} above 100 EeV.

The energy spectrum follows a power law $J(E) = \frac{dN}{dE} \propto E^{\gamma}$ over a wide range of energy, whch is the first indication for non-thermal acceleration processes. The CR spectrum is almost featureless, as can be inferred from **Fig.1.1**. However, small structures become clearly visible when the ordinate is multiplied with some power of the particle energy, as shown in **Fig.1.2**. The spectral index is $\gamma \approx -2.7$ at energies up to several PeV. At an energy $E \approx 3 \times 10^{15}$eV, a steepening of the power law is observed, the so-called *knee* with $\gamma \approx -3.1$ at higher energies. A further steepening, the *second knee*, has been claimed recently around 4×10^{17}eV. The spectrum gets flattened at about 4×10^{18}eV, called the *ankle*.

The tail of the CR spectrum above 10^{20}eV is scarcely populated. A cut-off is predicted by Greisen, Zatsepin and Kuzmin at about 5×10^{19}eV, due to the interaction of the primary particles with the photons of the cosmic microwave background radiation. An updated measurement of the energy spectrum using hybrid events collected by the Auger experiment recently confirmed the CR flux suppression at $log_{10}\left(\frac{E}{eV}\right) = 19.63 \pm 0.02$ (Settimo et al. 2012).

1.3 COMPOSITION

The chemical composition of CRs is rather well known in the low energy regime up to about 10^{14} eV from direct observations. Due to the low flux above this energy a direct measurement of the primary particles is practically not feasible at present. The elemental distributions have been studied by balloon and satellite experiments (Simpson 1983) up to energies of few TeV. About 98% of the primary CR are hadrons, the remaining 2% is composed of electrons and photons. About 87% of the hadronic component are protons, nearly 12% helium nuclei and the rest corresponds to fully ionized nuclei of heavier nuclei.

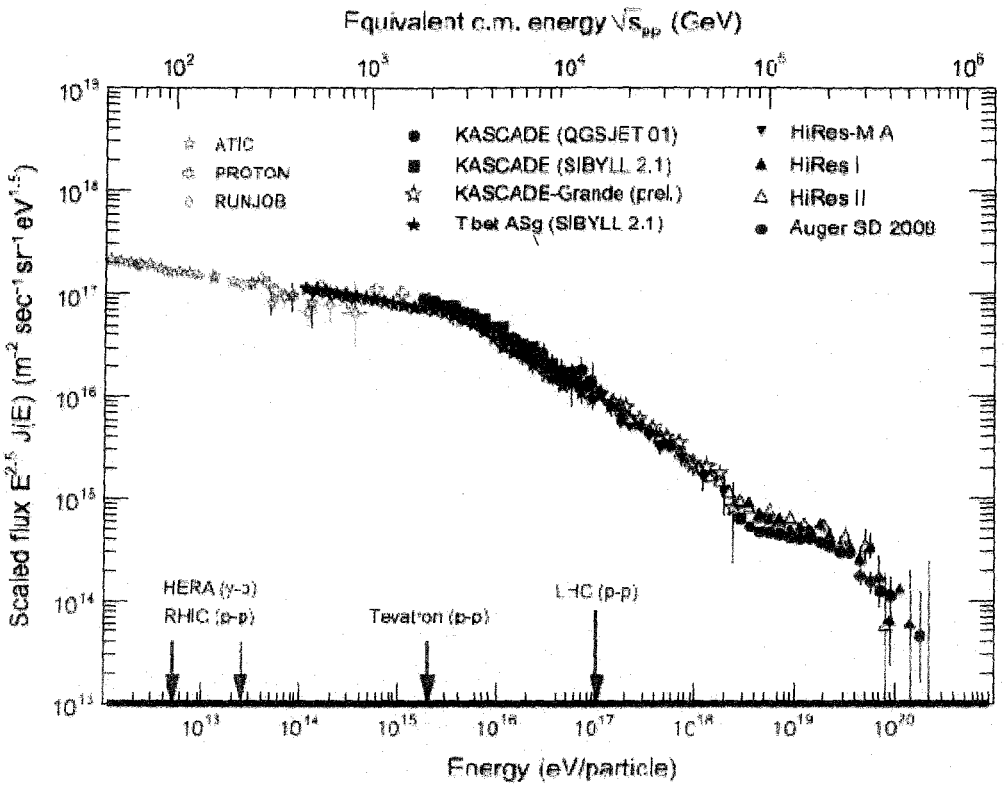

Fig.1.2: All-particle energy spectrum as obtained by direct measurements above the atmosphere by the ATIC, PROTON (Ahn et al. 1971 & Grigorov et al. 1970), and RUNJOB (Derbina et al. 2005) as well as results from air shower experiments. Shown are Tibet ASγ results obtained with SIBYLL 2.1 (Amenomori et al. 2008[b]), KASCADE data (interpreted with two hadronic interaction models) (Antoni et al. 2005), preliminary KASCADE-Grande results (Arteaga-V et al. 2008). The measurements at high energy are represented by HiRes-MIA (Abu-Zayyad et al. 2000 & 2001), HiRes I and II (Abbasi et al. 2008) and Auger (Abraham et al. 2008).

The elementary abundances in the solar system when compared with the one of CRs, important information on the origin as well propagation of the cosmic radiation can be extracted out. The abundance analysis of refractory nuclides has shown similarities between the derived abundances at the sources and the abundances in the Solar System (Wiedenbeck et al. 2003), suggesting that CRs are accelerated out of a sample of well mixed interstellar matter. In CRs, elements like Li, Be and B are overabundant, as well as all the groups with atomic mass lower than Fe. No significant difference is found, instead, in the CNO and Fe groups.

This implies that, on their way through the galaxy, the later nuclei further interact with the interstellar matter, generating lighter nuclei like Li, Be and B through spallation reactions.

The analysis results on the relative abundances of these elements including their isotopes as well and on the basis of diffusion equations for the primary particles, the CRs are found to cross on average a thickness of about 5 g/cm^2, which corresponds to a path length of roughly about 1 Mpc. Given that the thickness of the galactic disk is ≈ 1 kpc, it means that the CRs diffuse into the galaxy before escaping. An average escape time can be estimated from the analysis of the ratio of radioactive secondaries and their decay products, such as ^{10}Be/^{9}B, giving a value of $\approx 10^7$years (Yanasak et al. 2001).

Above 10^{14} eV, information on the chemical composition of CRs comes from studies of the extensive air showers employing various techniques. In the energy region around the *knee*, the composition however is inconclusive. A composition change from iron domination at 10^{17}eV to proton domination at about 10^{18} eV was reported from Fly's Eye (Bird et al. and 1993 & Lawrence et al. 1991) Yakutsk (Knurenko et al. 2008) EAS experiments.

1.4 ACCELERATION AND PROPAGATION

1.4.1 ACCELERATION

The locally observed CR energy density amounts to about $\rho_\sigma \approx 1\, eV/cm^3$. The power required to maintain the CR density can be estimated as $L_\sigma = \rho_\sigma V/\tau_{esc} \approx 10^{41}$erg/s, where τ_{esc} is residence time of CRs in a volume V (the galaxy and galactic halo). In our galaxy about 3 supernovae explosions occur per century, which yields a power of around 10^{41}erg/s. So an efficiency of a few percent ($\approx 10\%$) would be enough for supernovae shock waves to energize the galactic CRs. This had been discovered by Baade and Zwicky (Baade & Zwicky 1934) in 1934. The actual mechanism of acceleration remained mysterious until Fermi (Fermi 1949 & Blandford et al. 1987) proposed a process that involved the interaction of particles with large-scale magnetic fields in the galaxy. Eventually, this lead to the currently accepted model of CR acceleration by the first-order Fermi mechanism, which operates in strong shock fronts powered by supernovae explosions and propagate from a supernova remnant (SNR) into the interstellar medium (Fermi 1949 & Blandford et al. 1987). First hints for acceleration of

hadrons at SNRs were measured by CANGAROO (Enomoto et al. 2002) and H.E.S.S. (Aharonian et al. 2004). These experiments measure TeV gamma-rays created by collision of accelerated protons with atoms and molecules in an interstellar cloud.

Different sites of acceleration could be neighbouring stars of pulsars that are hit by the pulsar wind (Harding & Gaisser 1990), or accreting matter from neighbouring stars or at the shock wave of the galactic wind (Jokipii & Morfill 1987). Further mechanisms of acceleration are direct acceleration in strong electric or magnetic field, e.g. at polar caps, outer gaps or slot gaps of pulsars (Cheng et al. 1986).

For energies above 10^{17} eV the origins of CRs are much speculative. Possible candidates are e.g. jets of Active Galactic Nuclei (Rachen et al. 1993). For energies above 10^{19} eV there exist also various Top-down models in which the CRs are produced as decay products of some super heavy particles X with mass $m_X \geq 10^{12}$ GeV (Guenter 2003).

1.4.2 PROPAGATION

Up to several hundred PeV energy CRs are generally believed to have a galactic origin. The lifetimes of CR particles are longer than the time they need to cross the thickness of the galactic plane (≈ 0.2 kpc) rectilinearly. This and the measured isotropy of the cosmic radiation suggest a diffusive propagation of the charged particles from the sources to the earth. On their way they are deflected by galactic magnetic fields and their original direction is lost when they arrive at the earth. However, the high energy γ-rays may play a vital role for predicting the information about the origin of primary CRs as they point back at their source engines. The particle energy changes during propagation due to spallation, radioactive decay and ionization processes. Furthermore, particles escape with an energy dependent probability from the galaxy. All this affects the energy spectrum of cosmic rays and causes that the spectral index at the source of $\gamma \approx 2$ increases to $\gamma \approx 2.7$ observe at earth. The composition of the cosmic-ray particles changes due to decay and spallation.

1.5 EXTENSIVE AIR SHOWERS

A high-energy CR particle interacts with nuclei in the atmosphere and subsequent collisions initialize cascades of secondary particles. This cascade

develops in the atmosphere and its footprint can be detected at Earth's surface. The cascade of secondary particles is commonly known as extensive air shower (EAS). The first interaction typically occurs at the altitude between 10 to 40 km depending on energy and a type of the primary particle. The total energy of the primary CR particle is distributed to rapidly growing number of secondary particles. The pancake-like shower front with a thickness of ≈ 2 m and a diameter of up to several kilometres depending on primary particle's energy blazes its tail through the atmosphere until the Earth's surface.

The EAS can be subdivided into three components: electromagnetic, muonic and hadronic as shown in **Fig.1.3**. The most of the secondaries come from the electromagnetic part of EAS which is constituted from photons, electrons and positrons. There are also hadronic interactions, which produce short-lived mesons (mainly pions and kaons) of which many decay into muons, electrons and photons. In addition, there are particles not contributing much to the total energy balance, i.e. UV photons (fluorescence and Cherenkov) and radio emission or invisible component (e.g. neutrinos and very energetic muons). The atmosphere itself serves as large calorimeter in which the detected particle interacts and deposits its energy.

Detailed information about EAS is given e.g. in (Blümer et al. 2009, Haungs et al. 2003 & Castellina 2012), and references therein. The main properties of hadron and gamma-ray initiated showers, as far they are important for the understanding of this work, will be discussed briefly in appropriate chapters.

1.5.1 HADRONIC COMPONENT

Hadrons (baryons and mesons) are strongly interacting particles and therefore the largest part of the primary particle's energy goes into the hadronic part. The reactions of the high-energy particles are strongly focussed in forward direction. Consequent upon, they lie in the immediate vicinity of the original arrival direction. This suggests that the shower core is build up by high-energy fragments of nuclei, baryons and mesons. In each hadronic interaction one third of the energy is transferred to the electromagnetic component. The subsequent process works via the decay of neutral pions. The decay of charged pions produces the muonic component of an EAS.

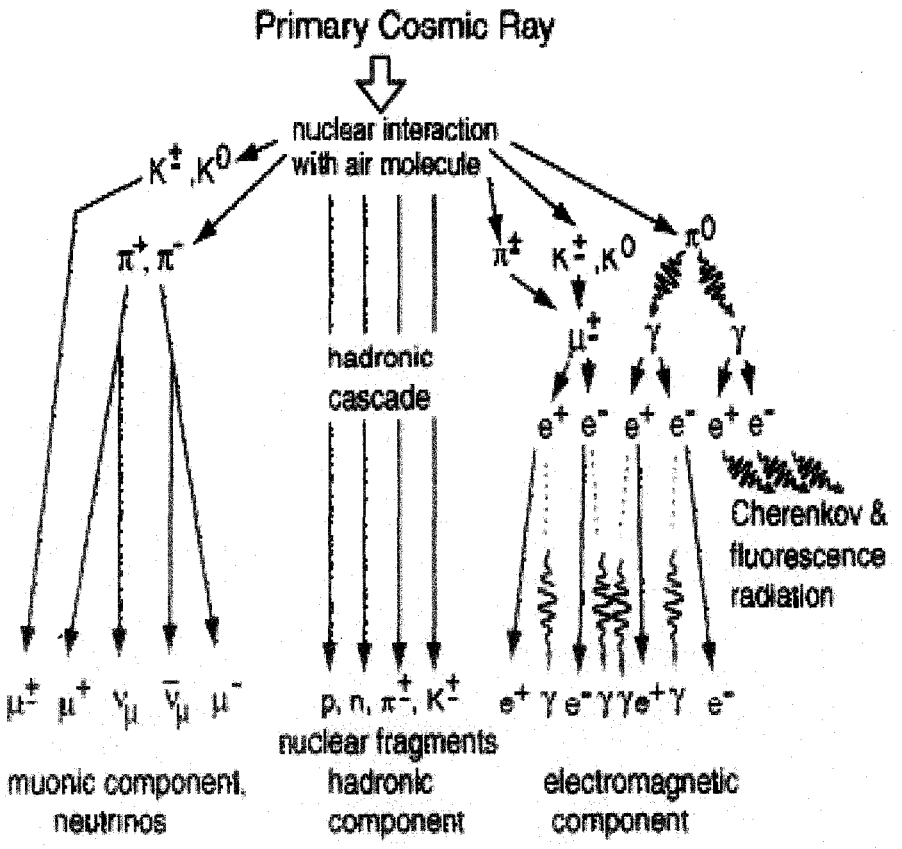

Fig.1.3: Scheme of an EAS with its different components.

1.5.2 ELECTROMAGNETIC COMPONENT

The electromagnetic component consists mainly of electrons, positrons and photons. The decay of π^0 particles into two photons is the feeding source of this EAS component. The produced photons can further produce electron-positron pairs as long as their energy is high enough. The electrons/positrons produce new photons via bremsstrahlung process. Ionization losses start to dominate over the production of new particles below the critical energy ($E_c \approx 84$ MeV in air) and the shower is absorbed by the atmosphere. Thus, the EAS shows a maximum number of particles at some stage of shower development.

The lateral profile of the electromagnetic component in many EAS experiments is very often described by the so-called NKG function (Greisen 1956, Greisen 1960 & Snyder 1989). A comprehensive study of different structure functions for EAS density profile used by various EAS groups will be discussed in *chapter* **3** emphasizing the role of the shower age parameter for studying primary composition.

1.5.3 MUONIC COMPONENT

The muonic component of an EAS originates from the decay of pions and kaons. With a mean lifetime of $\approx 2.2 \times 10^{-6}$s and a Lorentz factor $\gamma \approx 90$ (for $E_\mu = 10$ GeV), muons will penetrate the whole atmosphere practically undisturbed. High energy muons ($E > 100$ GeV) originate in the early stage of the shower development. They lose energy mainly through ionization processes, as the bremsstrahlung emission is strongly suppressed compared to electrons. Low energy muons, descending from a later stage of the development can decay into electrons and neutrinos. The broadening of the spatial distribution of EAS muons due to Earth's geomagnetic field is another interesting area of investigation in context of this thesis (see *chapter* **5**).

1.6 OBSERVABLE PARAMETERS OF EXTENSIVE AIR SHOWERS

The primary reasons to study CRs are to discover their origin, composition and spectral shape. Because the primary CRs are studied indirectly in the PeV region, through their EAS particles, it is indispensable to connect the parameters which can be observed with the nature of the primary particle. The EAS parameters/observables which are most relevant to the present study are namely **[a]** the muon content (N_μ), **[b]** the electron-positron content i.e. electron size/shower size (N_e), **[c]** the lateral shower age ($s_\perp$), **[d]** the local lateral age (s_{local}), **[e]** the muonic dipole length (l_μ), and **[f]** the absorption length/k-parameter (Λ_{abs}/k). The detailed description of these EAS observables can be found in respective chapters of the thesis.

1.7 AIR SHOWER SIMULATIONS

Air shower simulations are a crucial part of the design of air shower experiments and analysis of their data. Numerical simulation of the shower development in the atmosphere is a powerful approach to link the properties of the measured shower to those of the primary particle. To arrive any specific conclusions about CRs from their indirect investigation it is very important to know how they interact with the atmosphere and how the EAS develops. This knowledge is obtained by means of computer MC simulations. In this section a short overview of the MC EAS simulations with CORSIKA (Heck D et al. 1998) code is given. Comparing features obtained from the different adopted techniques applied for data analysis of the simulated showers it is possible to estimate the

mass composition and energy of the primary particle from the measured data. Interaction of the primary CR particle with air and their secondaries are described by high and low energy hadronic interaction models. The information about the primary particle and its interaction history in the cascade is stored in various average EAS observables/parameters.

1.7.1 CORSIKA CODE AND HADRONIC INTERACTIONS

A Monte Carlo technique offers one of the best suited approaches to provide a convolution of all physical processes to form the complex model of an EAS. The main annoying part of the MC technique since its inception lies in the uncertainties arising from the hadronic interactions at high and low energies, is still a major concern in this field in particular. Many code packages for simulating EASs are available. The most frequently used MC programs are CORSIKA (Heck D et al. 1998), AIRES (Sciutto 2001), CONEX (Bergmann et al. 2007), COSMOS (Roh et al. 2013), MOCCA (Hillas 1997) and SENECA (Drescher & Farrar 2003). The predictions obtained with all simulation packages are almost similar. Currently CORSIKA is used by many air shower experiments all over the world. The EAS simulations for the present work are performed with the CORSIKA versions **6.600** and **6.970**. For the hadronic interactions at high energies a number of interaction models have been implemented: QGSJet, DPMJet, EPOS, SIBYLL, VENUS, NEXUS, HDPM while GHEISHA, FLUKA and UrQMD (references there in) are used for hadronic interactions at low energies.

For electromagnetic interactions a modified version of the shower program EGS4 (Nelson et al. 1985) (or the analytic NKG function) can be used. Options for Cherenkov radiation and neutrinos also exist. The code can be used from 10^6 up to 10^{21} eV and beyond and it covers fifty different types of particles and nuclei up to $A = 56$. All these particles can be tracked until they reach the predefined observation level and energy. The code also allows production of shower images and movies of the shower development.

At the heart of a MC program is the generation of pseudo-random numbers which are produced by a random number generator such as RMMARD (between 0 and 1) from the CERN library (James 1988). The atmosphere is composed of 78% nitrogen, 21.5% oxygen and 0.5% argon. All other elements in the air are neglected because they contribute only 1% of the total. The atmospheric model in CORSIKA uses various atmospheres with either planar or curved options that are

parameterised in 5 layers with piece-wise fitted exponential. Special versions for different locations and seasons can be introduced.

Computing time and disk space needed for a shower simulation grow approximately linear with primary energy. A single shower at 10^{20} eV, with about 10^{11} secondary particles, needs about 10^5 hours and ~30 TB disk space. Therefore, statistical sub-sampling (or thinning) (Kobal 2001) is used to discard most of the shower particles and follow only a representative subset of them, which carry a weight to account for the discarded ones. For a good compromise of thinning and weight limitation, typical speed-up factors of 10^4- 10^6 are reached.

Particles information on the observation level from CORSIKA is a starting point for detector simulation in the array. From the particle densities measured in the detector array various EAS observables and their distributions are reconstructed. Development of an EAS is sensitive to a number of parameters and one can try to predict how they should be changed in EAS description to achieve better agreement with observations. As the interaction models are more and more refined now and hence discrepancies between simulations and the measurement are becoming smaller. Using such a model as reference the deficiencies of other models can be understood more clearly. Currently almost all models in the low energy regime describe observed data very well. Differences are viewed in the high energy regime but they are significantly lower at present than earlier.

Over the last $12-15$ years the agreement of simulations with experimental data has greatly improved. Today the simulations describe consistently, within about $15-25\%$, EAS experiments from TeV to PeV (i.e. from γ-ray regime to the region of the *knee*). The method is further extended to EeV (where Haverah Park, AGASA etc. experiments are performed) and up to the 10^{20}eV range of the Pierre Auger experiment.

In the near future the ongoing accelerator/collider experiment at the LHC (14 TeV in cms) is expected to provide new experimental inputs to the cross sections, diffraction and hadronic multi-particle production, additional constraint to the interaction models and thereby improving the predictive power of EAS simulations in the PeV energy range.

1.8 OBJECTIVE OF THE THESIS

The objectives of the present investigation is mainly threefold: First from a detailed MC simulation study of CR EASs initiated by primary CRs we would like to study the characteristics of few air shower parameters/observables (other than the widely used parameters for primary mass extraction such as the muon content and the depth of shower maximum) and examine their primary mass sensitivity. We will particularly focus on the characteristics of the shower age parameter, which essentially describes the slope of the lateral distribution of electrons in EAS, and the possible role that the parameter may play in a multi-parameter approach of studying EAS in order to understand the nature of shower initiating particles in the PeV energy regime. We would also explore whether geomagnetic spectroscopy can be employed cleverly to extract information on primary mass. Secondly we would like to examine the role of air shower fluctuations in estimating CRs-air interaction cross section and finally from theoretical considerations the flux of gamma-rays and neutrinos to be observed at Earth if cosmic-rays at PeV energies are accelerated by polar caps of pulsars will be estimated.

1.9 ORGANIZATION OF THE THESIS

The content of the thesis is organized as follows:

- After a short introduction of CRs (chapter **1**), the characteristics of CRs in the PeV region is reviewed in chapter **2**. The all-particle CR energy spectrum in the PeV region is discussed. Various techniques of estimating composition of CRs from EAS observations is also discussed and the mass composition scenario of primary CRs in the PeV region obtained from experimental observations are summarized. The origin of galactic CRs is also mentioned briefly. Finally a summary on our present understanding has been stated.
- Chapter **3** discusses the lateral distribution of electrons in EAS from a detailed Monte Carlo simulation study. The *universality* property of the lateral density distribution of electrons in terms of *local age parameter* (LAP), as inferred from the simulation data, got support from different experimental observations. The chapter describes the techniques for estimating the LAP, the important characteristics and correlations of the LAP with other EAS observables to understand the nature of shower

initiating particles. The chapter ends with a discussion and conclusions of the present analysis.

- In chapter **4** the identification of the LAP of CR extensive air shower for separating gamma-ray induced showers from hadronic background without doing muon measurement is described. The chapter also discusses about various optimal cuts applied to signal selection parameters employing a selection algorithm for maximizing gamma-ray selection efficiency and minimizing the background contamination. The experimental realization of the adopted technique involving LAP is also discussed here. The chapter concludes with a summary and outlook of the present work.
- Chapter **5** includes a detailed analysis of the asymmetry in muon distributions due to the influence of the Earth's geomagnetic field on the development of EAS from a detailed Monte Carlo simulation study. This muon asymmetry offers a new possibility for the determination of the primary mass composition in the case of EAS events with large zenith angles ($> 50^0$). In this chapter, a novel method is introduced that determines a primary mass sensitive parameter in terms of the *muonic dipole length* (l_μ). The scope of the present proposal for extracting the nature of primary particles by ongoing experiments such as WILLI detector or by future generation large muon detectors is discussed in the last section of this chapter.
- Chapter **6** is devoted to the attenuation phenomena of EAS in air induced by primary CRs. The chapter is mainly focussed on a particular analysis technique to derive the proton air cross section from CR data at the relevant energies. This work is intended to examine critically the role of air shower fluctuations on the cross section measurements from detailed M C simulations.
- Chapter **7** deals with the evaluation of the flux of the TeV gamma-rays and neutrinos to be observed at Earth which are produced in pulsar environments by interaction of polar cap accelerated hadrons with ambient photon fields. In the present work we tried to improve earlier estimation of neutrino flux from pulsar by emphasizing about the constraint imposed by the observed gamma-ray fluxes from several potential pulsars. The importance of consideration of proper polar cap geometry while evaluating the neutrino flux has also been stressed.

Finally the observational situation of neutrino detection from pulsars by the present neutrino telescopes and the possibility of the upcoming neutrino telescopes are discussed.

- Chapter **8** will contain a discussion on the findings.

CHAPTER 2

COSMIC RAYS IN THE PeV REGION

2.1 INTRODUCTION

Cosmic rays in the PeV energy region have several distinguishing features, some of those are the following: **(i)** they are detected (with reasonable statistics) indirectly by means of CR EAS unlike the lower energy CRs those could be detected directly by sending detectors above the atmosphere through balloons and satellites, **(ii)** they are supposed to be originated in the galaxy unlike the highest energy (EeV range) CRs which are believed to be of extra-galactic origin, **(iii)** the energy spectrum of CRs in this energy range exhibits a *knee* feature at about 3 PeV. High energy gamma-rays and neutrinos are expected to be produced in the interactions of energetic CRs with the ambient matter in the source environment and thereby CR sources should be identified, at least in principle, by observing appropriate fluxes of gamma-rays and neutrinos from a CR source. The possibility of observing such high energy (~TeV or above) gamma-rays and neutrinos is high for galactic sources those produce CRs up to PeV energies owing to their smaller distances (relative to extra-galactic sources) and low background noise in compare to CR sources of sub-PeV energies .

In the following we would discuss about the energy spectrum including the *knee* feature and the mass composition of primary CRs. We would also discuss briefly about the origin/sources of primary CRs in the PeV energies.

2.2 ENERGY SPECTRUM AND THE KNEE

Due to steeply falling flux of CRs, the measurements on the energy spectrum were performed so far only by ground based EAS experiments those are being operated in the PeV energy. These experiments improve their energy resolution and the statistics for the all-particle spectrum measurement in the course of time. On the other hand, several experiments extended the energy range and therefore make it possible to connect their own spectrum with the one measured from balloon-borne experiments at low energy and from UHECR experiments at

the highest energy end.

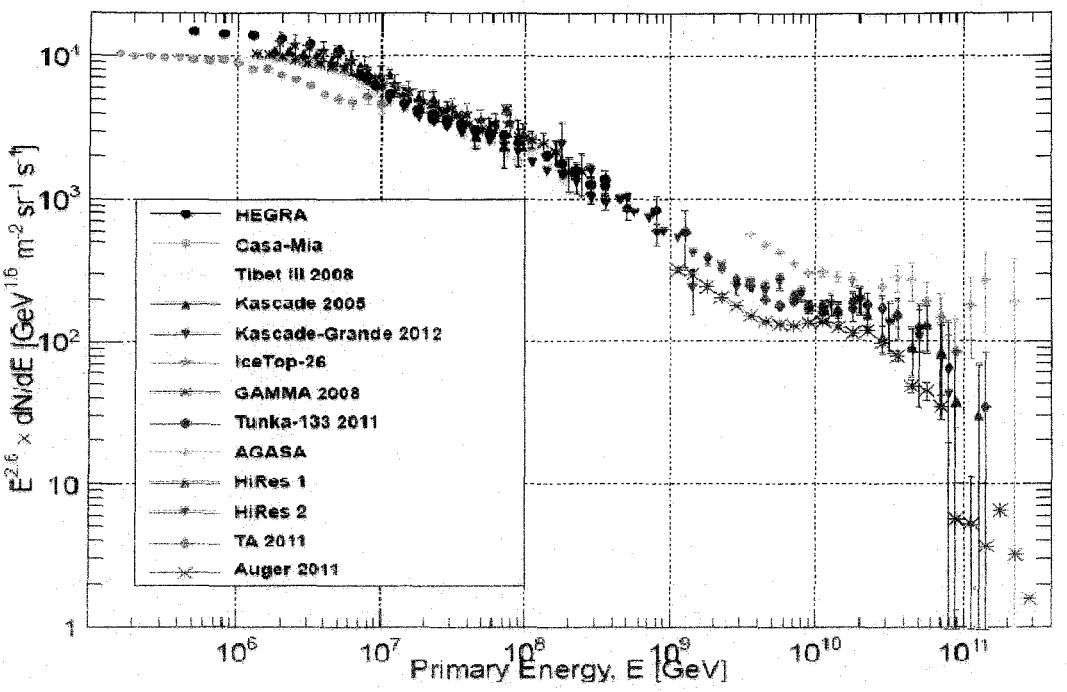

Fig.2.1: All-particle energy spectrum obtained from EAS experiments (Gaisser et al. 2013).

The **Fig.2.1** shows a compilation of currently available spectra for all particles. Interestingly all-particle spectra estimated with various detector techniques agree reasonably well with each other.

A steepening of the spectrum takes place at about 3 PeV as one may notice from the above figure which is known as the *knee* of the spectrum. The differential flux has been multiplied by $E^{2.6}$ and plotted along y-axis to show clearly the change in the slope. The CR spectrum does not have many features. Hence the *knee* is considered as a very important feature that may provide clue regarding the origin of the CRs, the central question of the astroparticle physics.

2.3 PRIMARY MASS COMPOSITION

The EAS measurement aiming at reconstructing the CR mass composition is a very difficult one. The reason lies in the fact that the mass of the primary particle can only be inferred from detailed comparisons of experimental observables with EAS simulations which require hadronic interactions as input. At the air shower energies accelerator data are not yet completely available (though the LHC covers these energies now) for the kinematic region of secondaries

concerning to air showers and also for relevant target–projectile combinations. As a result one has to rely on high energy interaction models leading to an uncertainty of unknown order. The uncertainties of hadronic interactions at high energy in simulations become a dominant source of systematic of estimates of the CR mass composition. Hence, identification of various EAS observables with different sensitivity to the primary mass is of extreme importance as these observables should lead to consistent conclusions about the properties of the primary CRs. Any inconsistent conclusions, on the contrary, would be indicative for incomplete knowledge of the employed hadronic interaction models in simulations.

The EAS experimental data are the convolution of the primary CR distributions with all the effects related to the atmospheric cascading, which is governed by the hadronic and electromagnetic interactions. In order to extract primary information from EAS experimental data, one has to de-convolute them during adopted analysis. The electromagnetic cascading can be well described by the subject quantum electrodynamics, while for different calculations involving hadronic interaction in EAS could be made on the basis of phenomenological models. Currently, quite a good number of hadronic interaction models are available and their agreement with observations keeps improving. For the purpose of CR studies these hadronic interaction models often use interaction cross-sections resulting from the extrapolation of the cross-section versus energy plot. The validation of this extrapolation needs to be tested and further improved.

Low energy hadronic interaction models have been tested recently (Bhadra et al. 2009) with proton and antiproton fluxes measured by BESS and Mt. Norikura experiments. While FLUKA (Fass'o et al., 2001) can describe better the proton spectrum than other two models, UrQMD (Bass et al. 1998 & Bleicher et al. 1999) and GHEISHA (Fesefeldt 1985) on the contrary, show much better agreement with antiproton spectrum. In an interesting study the NBU and the Bose Institute group jointly have reported that even at relatively low energies the BESS antiproton flux could not be accurately simulated by any of the combinations of the above models (Bhadra et al. 2009).

It has also been found that CR experiments might contribute to the betterment of the hadronic interaction models. New measurements of the cross-section between proton and air are presented by the ARGO-YBJ and TienShan experiments. These experiments measured a smaller cross-section than what had

been adopted in the hadronic models. By comparing the model calculation and KASCADE observation, both QGSJET (Kalmykov et al. 1997) and EPOS (Werner et al. 2006 & Pierog et al. 2008[a]) prefer a lower cross-section for the proton-air interaction.

Having very good temporal and spatial resolutions, the ARGO-YBJ carpet containing large number of RPCs has published results on the time structure of the EAS front (Calabrese et al. 2009) distribution and multi-core event search. Their data agree very well with model prediction.

2.3.1 AIR SHOWER OBSERVABLES SENSITIVE TO MASS COMPOSITION

The question of the mass composition of high energy CRs arose very early. The determination of mass composition by EAS measurements requires the identification of quantities at the observation level which can be measured and depend on primary mass. There is a general agreement between different models of high energy hadronic interactions in reference to the observables most sensitive to primary mass. Note that in the context of mass composition at least two orthogonal measurements are needed to estimate both, the mass and energy of the shower initiating primary particle. This is feasible in EAS technique by observing say the longitudinal development or by simultaneous determination of the electromagnetic and muonic component of EAS at observational level. The study of the lateral distribution of EAS charged particles at ground level which is related to the EAS development stage, may also give some insights about the primary composition. We shall elaborate these techniques below:

The determination of the lateral density distribution (LDD) of particles in EAS leads to estimate the total number of charged particles, electrons or muons by fitting the measured densities to proper analytical functions. The mass and energy of the primary particle can then be deduced from the electron and muon numbers. The first method suggested by Linsely *et al* (Linsely et al. 1962) followed from the observation that the number of muons (N_μ) and number of electrons (N_e) in an EAS are related by $N_\mu \sim {N_e}^\alpha$. Taking the simple superposition model one obtains $N_\mu \sim A^{1-\alpha} {N_e}^\alpha$, where '$A$' is the mass number of a nucleus that initiates an EAS and 'α' acts merely as a factor.

The observation of the longitudinal development of the particle cascade in the atmosphere is especially well suited for composition studies. The detection of

produced particles in the shower is done via fluorescence or Cherenkov light through which the signal is transferred to the detector. The mass sensitive estimator that comes out from this measurement is the slant depth (X_m) at which the EAS reaches its maximum in terms of the number of particles. A correlation exists between X_m and the slope parameter of the lateral Cherenkov light distribution which is independent of the type of the primary particle and the angle-of-incidence of the shower. In observations of the Cherenkov light by the imaging technique, the intensity pattern of Cherenkov light coming from the air shower is strongly correlated with the shower size, from which the height of maximum X_m can be determined.

The position of the maximum development of electromagnetic component of EAS in the atmosphere roughly goes as $X_m \propto lnE$ where $E \equiv E_0/A$ is the energy per nucleon. Hence X_m depends on mass as lnA. However, X_m fluctuates event by event basis (interestingly the shower-to-shower fluctuations in X_m also carry important information about the primary particle types). Usually thus average depth of shower maximum is studied as a function of primary energy. The longitudinal development also can be studied with fluorescence technique but it is best suited at a little bit higher energies.

The second oldest method of searching for the mass of the primary CRs is the measurement of fluctuations in EAS development. The widths of the N_μ fluctuations for fixed N_e, measured as $\frac{N_\mu}{<N_e>}$, is the main example. The fluctuations of the shower age parameter and of the height of shower origin are other examples (De Beer et al. 1968).

The average transverse momentum of the secondary particles increases with energy though very slowly. As the longitudinal momentum increases faster than in proportion to the primary energy per nucleon, the emission angle of the secondary particle is smaller in a proton induced shower. As a consequence the lateral distributions of all types of shower particles, electrons, muons and hadrons are expected to be wider in an EAS induced by a heavy nucleus than one initiated by a proton. This feature can be extracted from the EAS initiated by CR particle.

The shape of the LDD of EAS also contains information about the underlying particle physics in the EAS and, thereby also about the mass of the primary particle. Generally, showers initiated by heavy primaries will exhibit a

flatter LDD than those initiated by light primaries. This feature is observed both for electrons and muons. It is worthwhile to mention that the sensitivity of the LDD to the primary mass, however, is weaker as compared to the $N_e - N_\mu$ method or those techniques else.

The reconstruction of the mean heights of production of muons in EAS brings interest to learn about the longitudinal shower development. The technique was revived in the 90ies for tracking electrons and muons with the CR Tracking (CRT) detectors at HEGRA (Bernlohr 1999), the Muon Tracking Detectors at KASCADE (Doll et al. 2002) or at GRAPES (Hayashi et al. 2005) after 60ies of the last century.

There are few other mass sensitive observables, such as muon charge ratio, rise time of Cerenkov signal etc. which are not covered here. Interested readers may see the proceedings of bi-annual conferences of International Cosmic Ray Conferences for the detailed discussion of the mentioned and other techniques.

The KASCADE collaboration proposed a refined procedure few years back in determining mass composition from EAS measurements. The main features of their approach are: (**i**) to measure as many mass-dependent observables as possible in order to average out at least part of the fluctuations and (**ii**) to derive combinations of these measured quantities which give good estimates of energy and mass of the primary for each individual shower.

2.3.2 MEASUREMENTS OF THE PRIMARY MASS COMPOSITION

The reliability of primary composition extracted from EAS experiments can be checked at TeV energies where direct measurements are available. To reach TeV energies, EAS experiments need to locate at high very altitudes such as the ARGO-YBJ (Sciascio & Girolamo 2007) experiment that has a full coverage array ($80m \times 80m$) having resistive plate chambers (RPCs) with excellent resolutions both in time and position. The array is competent enough to allow real time view of a propagating EAS to be obtained including its structure near the core. In the energy range from 10 to 300 TeV, the experiment measured mass composition of light components, such as protons and helium from the knowledge of particle densities in inner and outer regions surrounding the core as shown in **Fig.2.2**. Their spectra agree rather well with direct measurements from CREAM (Zei R et al.

2007). The analysis of ARGO-YBJ data seems to indicate a composition similar to JACEE (Asakimori et al. 1998) than CREAM as can be seen from the **Fig.2.2.**

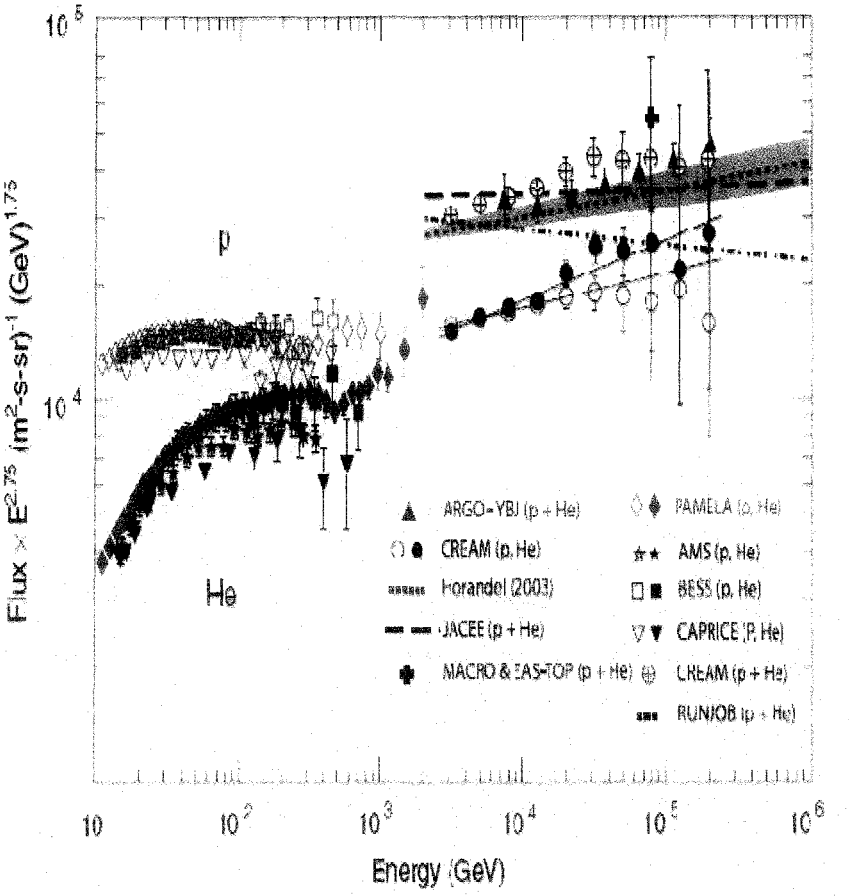

Fig.2.2: Light component $(p + He)$ spectrum of primary CRs measured by ARGO-YBJ compared with other experimental results (Bartoli et al. 2012).

Concerning mass composition at PeV energies muon content (or rather electron content as muon size is used to estimate the primary energy) is widely used to extract primary mass. In this approach, electron-muon discrimination achieved by employing a combination of unshielded and shielded scintillation detectors at ground level. There are number of recent experiments implemented the approach (examples AGASA, CASA-MIA, EAS-TOP, GRAPES, KASCADE and Grande, Maket-ANI, Yakutsk etc.). The muon identification through water Cherenkov detectors were employed in AUGER and Haverah Park detector. IceTop at the South pole uses tanks of frozen ice for the purpose in combination with IceCube at underground. Similar combinations of surface and underground detectors have been used by EAS-TOP and MACRO at the Gran Sasso and Baksan.

One of the major uncertainties occurs in the result due to fluctuations. It is important to realize that electron and muon numbers do not fluctuate independently on event-by-event basis, but are mutually correlated. Such an effect can be properly accounted for by a two-dimensional unfolding technique, first utilized by KASCADE-collaboration (Fuhrmann et al. 2011).

The ICECUBE (Abbasi et al., 2009) collaboration extracts primary composition by using the N_e-$N_\mu$correlation. They had used muon data with $E_\mu^{cut} > 500$ GeV and N_e from ICETOP with $E_e^{cut} > 1$ MeV. However, due to low statistics the composition could be probed only as a combination of protons and iron nuclei. Within error ranges the all particle spectrum was consistent with earlier measurements (Rawlins et al., 2011). Above 100 GeV the muon and muon-neutrino spectra were simulated by using primary CR spectra from KASCADE (Apel et al. 2009) for five nuclei that were extrapolated with a rigidity dependent *knee* for respective nuclei. The Auger spectra were used at UHEs and the difference between Auger and extrapolated KASCADE spectra in the overlap of energy region was attributed to an extragalactic proton component. The spectral shape of muon and muon neutrino appeared to depend on the all-particle spectra rather than the actual composition. This would lead to facilitate accurate calculation of muon and muon-neutrino fluxes at high energies.

Most of the experiments such as the CASA-MIA (Glasmacher et al. 1999), MSU (Fomin et al. 1996), HEGRA-CRT (Bernlohr 1999), KASKADE (Weber et al. 1999), EAS-TOP (Navarra et al. 1998), SPASE-AMANDA (Rawlins et al. 2003), on the basis of muon content relative to electron content in EAS, infer that the composition becomes heavier with increasing energy in the region of *knee*.

Non-imaging observations by operating photo multiplier tube assembly with large Winston Cones looking upwards into the night-sky are perhaps the simplest and most straight forward technique of observations. This method was first successfully applied at energies around the *knee* by the HEGRA array (Karle et al. 1995) and by CASA-BLANCA (Fowler et al. 2001). More recent measurements have extended these measurements at Tunka (Budnev et al. 2009) and Yakutsk (Knurenko et al. 2010) up to ultra-high energies. The slope of the lateral distribution of Cherenkov light measured within nearly 100 m is found to depend on the height of the shower maximum and hence on the mass of the primary CRs. The results of Cerenkov measurements including the DICE (Boothby

et al. 1997), CASA-DICE (Swordy et al. 2001), CASA-BLANKA (Fowler et al. 2001), TUNKA (Cherev et al. 2005), HEGRA (Karle et al. 1995), HEGRA-AIROBICC (Arqueros et al. 2000), SPACE-VULCAN (Dickinson et al., 1999), Yakutsk (Efimov et al., 1991) and few others suggest for a mixed composition below the *knee* with either no significant change in average mass above the *knee* at least up to 10 PeV or a slowly decreasing/increasing average mass beyond the *knee*. A different conclusion is reached by only few experiments such as the CACTI (Paling et al. 1997).

Using muon multiplicity information, GRAPES-III (Gupta et al. 2005) studied the primary composition up to PeV energies with SIBYLL and QGSJET models. Significant differences are seen between the two model assumptions. They found that SIBYLL model better describes data than QGSJET. Similar conclusion was obtained when comparing the composition results of the Tibet ASγ (Amenomori et al. 2006[a]) with the KASCADE experiment (Amenomori et al. 2006[b]).

The Tibet ASγ collaboration in association with a set of new detectors that included Yangbaijing air core detectors (YAC-I and II), water Cherenkov muon detectors and so on, reported several results on mass composition and the uncertainties of hadronic interaction model. They have used an artificial neural network (ANN) for data analysis exploiting extensive MC simulations for EAS events. Preliminary results from data analysis using ANN showed that the data are in good agreement with the QGSJET II and SIBYLL 2.1 models. This agreement persists in the energy range from 30 to 1800 TeV. The Tibet ASγ has also put efforts to separate proton, proton+helium, and iron candidate events that were trained for QGSJET II with a heavy dominated composition. Their technique has been cross checked by the ability to extract known contributions of protons, helium and iron nuclei from the Monte Carlo data. The fraction of proton, helium and iron nuclei were obtained from an analysis using ANN to obtain the all particle spectrum from the Tibet ASγ data.

Fukui et al. (Fukui et al. 1960) and Khristiansen et al. (Khristiansen et al. 1963) were the first to study the muon number fluctuations in the *knee* region and they were also the first concluding an enrichment by heavy nuclei above the *knee* energy (Khristiansen et al., 1994). Similar conclusions were drawn in (Elbert et al. 1976) based on a larger data set.

A noticeable result on the muon production height measurement with KASCADE-Grande is compatible with a clear transition from light to heavy primaries with increasing energy across the *knee*. The time profile of EAS particles was used by Bassi et al. (Bassi et al. 1953) at Haverah Park (Watson et al. 1974) in the context of primary composition in UHE region.

The analysis of Miyake *et al.* (Miyaki et al. 1973) carried out with data from Mt. Norikura (2770 m a.s.l.) for the measurements of primary composition using *shower age* and shower size as observables hinted a change in the composition with heavier domination beyond a size of $\sim 10^7$ (Miyaki et al. 1979). The shower size dependence of the *age parameter* from measurements with the MAKET-ANI array located at Mt. Aragats (3200 m a.s.l.) in Armenia when compared with simulations showing the expected *age* dependence on shower size that would result for a primary beam with heavier domination starts at 10^7 onwards (Chilingarian et al. 2007). The result from Akeno (Hara et al. 1981) taking the variation of *shower age* as a function of muon size for fixed shower sizes maintained the general trend showing a rising *shower age* with an increasing muon number. They had correlated this feature with the primary mass and/or the secondary particle multiplicity.

2.4 ORIGIN OF PeV COSMIC RAYS

It is generally believed that CRs with energy below 10 PeV are accelerated at the shocks in supernova remnants (SNRs). There are also possibilities for their acceleration by other extreme astrophysical environments in the galaxy which include pulsars particularly. In SNR acceleration picture the *knee* could be regarded as an indication of the attainment of maximum energy by the CRs through shock acceleration in SNRs. From an alternative view the *knee* may come from the relatively faster leakage of PeV CRs into the extragalactic space compared to lower energy CRs. It may be due to threshold interactions where e^+-e^-pairs are formed due to interaction of PeV CRs with the ambient infrared photon background near the source (Hong-Bo et al. 2009). Another speculation supports the view that CRs above PeV energies may produce exotic or undetectable particles during their advancement in the atmosphere (Horandel 2006).

Recently, with modern Cherenkov telescopes, γ-ray photons of TeV energies coming from SNRs have been detected, which gives strong indications for an efficient accelerations of charged particles to energies beyond 100 TeV, in

consistency with the models of CR in young SNR shocks (Aharonian et al. 2004). The origin of the γ-ray photons of TeV energies is still uncertain. An experimental validation of the hadonic origin of TeV γ-ray photons over leptonic origin would be eagerly awaited evidence for an acceleration of hadrons in SNRs.

It has recently been suggested that neutron stars inside the shells of young SNRs are the sources of PeV CRs and that the interaction of the particles with the radiation field in the SNR causes electron pair-production, which has relevance to recent observations of high positron fluxes (Erlykin et al. 2011). Even, a pulsar with period 100 ms should be able to reach several PeV if the magnetic field were somewhat bigger than 10^{12}Gauss. In this context, the theoretical estimation of TeV gamma-ray and neutrino fluxes can help to throw light on the question about the origin of PeV CRs.

A test for the models of origin of galactic CRs can be studied through very high energy gamma-ray astronomy. The results mainly from the last decade of the last century made it obvious that new, better gamma-ray telescopes would lead a breakthrough in the field of high-energy gamma-ray astronomy. Also, the stereo-observation technique was generally accepted as the approach that would reach sensitivities around 1% of the Crab nebula flux within 50h observation time for achieving 5σ excess signal. High energy gamma-rays have been detected from several supernova remnants by the Cangaroo III (Enomoto et al. 2006), H.E.S.S. (Aharonian et al. 2007[a] & Wissel et al. 2009), MAGIC (Baixeras et al. 2003 & Magic Coll. 2008), VERITAS (Aliu et al. 2011), HAGAR (Acharya et al. 2009 & Saha et al. 2013), MILAGRO (Sciascio et al. 2011), ARGO-YBJ (Zhang et al. 2009). At relatively higher energies GRAPES III has a very good potential to unearth PeV hadronic sources of CRs. In near future the CTA (Cherenkov Telescope Array) (Actis et al. 2011), which will cover the energy range from 20 GeV to 100 TeV with 10 times higher sensitivity compared to H.E.S.S, is also expected to provide valuable information in this regard.

Four other projects are currently under detailed evaluation or in a first phase of construction. Advanced Gamma-ray Imaging System (AGIS) (Vandenbroucke 2010) and Major Atmospheric Cherenkov Experiment (MACE) (Koul et al. 2005) are Cherenkov telescopes, while the High altitude Water Cherenkov (HAWC) (Salazar 2009) is an extended air-shower array at high

altitude for achieving a low threshold. LHAASO (Cao et al. 2011) is a facility that combines various air shower detectors elements and Cherenkov telescopes.

2.5 SUMMARY

The origin of PeV CRs is still not clearly known. The SN shocks from explosion and SNRs provide sites suitable for CR acceleration up to $E \sim 10^{16} - 10^{17}$ eV. On the other hand, acceleration in compact objects such as Pulsars, X-ray binaries etc., the CR energy may reach even up to $\sim 10^{17}$eV or so.

The proper explanation of the *knee* feature is believed to provide key insight on the origin of the *knee*. In order to understand the full story of the *knee* the mass composition needs to be estimated accurately. As stated above the CR mass composition beyond the *knee* is not definitively established yet, with some observations (Horandel 2004, Kampert & Unger 2012) suggesting that it turns lighter and others instead suggesting that the heavier components become dominant. What will the conclusion on primary mass composition be in the PeV regime: KASCADE, GRAPES or Tibet or else? To improve the situation concerning mass composition multi-parameter study is vital.

A precise estimation of the mass composition of CRs at PeV energies heavily relies on the progress in understanding the hadronic interaction models. The LHCf experiment is studying the very forward region with proton-proton beams at the centre of mass energy of about 10^{17} eV, which is directly relevant to the EAS development in the atmosphere. With the results of this experiment the uncertainties due to our incomplete knowledge of hadronic interactions will be reduced significantly. The information of hadronic interactions extracted from EAS observations also should be important in this regard and may lead to find out new hadronic interaction models.

The ongoing and upcoming high energy gamma-ray and neutrino experiments are expected to provide concrete evidences of the sources of CRs, particularly those are within the galaxy. Meanwhile effort should be made to make the theoretical predictions for the high energy gamma-rays/neutrinos from the potential sources so that they can be effectively compared with observations in searching CR sources.

CHAPTER 3

LATERAL SHOWER AGE PARAMETER

3.1 INTRODUCTION

The primary CR energy spectrum is known to exhibit a power law behaviour with three breaks, a '*knee*' around 3 PeV where the spectral index changes abruptly from -2.7 to about -3, an '*ankle*' at few EeV beyond which the spectrum flattens again to its original slope and a Greisen-Zatsepin-Kuzmin (GZK) suppression around 10^{20} eV (Amsler et al. 2008). Among these interesting spectral features only the *knee* is believed to be associated with solely galactic CRs. Hence measurements of the characteristics of primary CRs including its chemical composition around the *knee* are very important for proper understanding of the origin of this spectral feature as well as to get the idea about the mechanism that pushes CRs to very high energies in the galaxy. However, because of very low and steeply falling (with energy) flux, direct measurements of primary CRs on board satellites or balloons are still limited in the energy region to below a few hundred TeV. Currently the only feasible way to get information about such energetic particles on statistical basis is through the study of CR EASs, which are essentially cascades of secondary particles produced by interactions of CR particles with atmospheric nuclei.

The EAS experiments chiefly measure densities and arrival times of EAS particles in a particle detector array, mostly electrons (positrons and negatrons) and photons, at different lateral distances from which (electron) shower size and the arrival direction of EAS events are obtained. Besides, some of the other EAS components such as muons, hadrons and air shower associated Cherenkov photons are measured in conjunction with electrons. The measurements are usually interpreted in terms of shower initiating particles using detailed MC simulations, which consider interaction mechanisms of energetic particles as input. But due to the limited knowledge of particle interactions at high energies and the large fluctuations, which are intrinsic to any EAS, the conclusions on primary CRs deduced from EAS measurements remain somewhat uncertain; sometimes even there are divergences of conclusions from experiment to experiment. Recent strategies include consideration of several EAS observables simultaneously in

extracting information on primary CRs from EAS observations with lesser uncertainties.

The main parameters associated with the EAS electron component at the given observation level are the shower/electron size (N_e) which is the total number of electrons in an EAS and the lateral (or transverse) shower age ($s_\perp$) which describes the slope of the radial distribution of electrons in EAS. While shower size is often related with the energy of the EAS initiating particle but the lateral shower age has not received sufficient importance so far in deducing information on primaries from EAS observations. In the framework of the cascade theory the parameter is supposed to relate with the stage of development of EAS in the atmosphere (Kamata & Nishimura 1958).

A number of recent studies indicate that the average shape of several distributions of electrons in very high energy EAS, such as the energy distribution or angular distribution, primarily exhibits the so called *universality* (Giller et al. 2005, Nerling et al. 2006, Lipari 2009, Lafebre et al. 2009, Schmidt et al. 2008 & Gora et al. 2006): it depends only on the stage of the longitudinal shower development in the atmosphere or equivalently on the longitudinal shower age parameter ($s_\parallel$ or s_L) that represents the variation of the total number of EAS electrons with the atmospheric depth and hence describes the longitudinal shower development irrespective of the nature of the primary particle and energy. Such a feature was first divulged from the early work by Kamata and Nishimura (Kamata & Nishimura 1958) in the context of the development of CR cascades in the atmosphere and was also described in (Hayakawa 1969). The experimental data also appear to substantiate this *universality* behaviour on an average basis (Yushkov et al. 2008). The universality property is quite advantageous for the analysis of high energy CR data as it helps to parameterize the electron-positron distributions, it seems useful for an accurate estimation of the muon and electromagnetic contents in an EAS (Apel et al. 2008) and also it assists to infer the primary mass composition and the nature of the first few interactions from the observed EAS data (Yushkov et al. 2008).

The observed lateral density distribution (LDD) of EAS electrons is, however, usually described in terms of the lateral shower age ($s_\perp$), which essentially describes its slope or more precisely it gives the slope of the energy spectrum of the electron and photon populations in an EAS. Theoretically, the

relation $s_{\parallel} = s_{\perp}$ holds for both electromagnetic showers and hadron initiated EAS (Lipari 2009 & Hayakawa 1969). In most experiments, however, the estimated $s_{\perp}$ differs from $s_{\parallel}$ for an EAS with hadrons as primary. Here note that $s_{\parallel}$ can be estimated observationally only if the EAS experiment is equipped with Cherenkov or fluorescence detectors, whereas $s_{\perp}$follows immediately from the lateral distributions of electrons, which is a basic measurement of any conventional EAS array consisting of particle detectors. Hence it is imperative to explore the universality of LDD of EAS electrons in terms of the lateral shower age. In KASCADE experiments, the reconstruction procedure to lateral electron density distribution has been employed to obtain the final value of the shape parameter in place of the lateral shower age (Apel et al. 2006).

A major challenge, however, is the reliable and unambiguous estimation of $s_{\perp}$ from experimentally measured electron densities. Usually the LDD of electrons in an EAS is approximated by the well known Nishimura-Kamata-Greisen (NKG) structure function (Greisen 1956, Greisen 1960 & Snyder 1989) and the shower parameters, namely the shower size (N_e) (the total number of electrons in an EAS at an observational level) and $s_{\perp}$ are evaluated by fitting the measured densities with the NKG function. However, experimentally it is observed that the NKG function with a single $s_{\perp}$ is insufficient to describe the LDD of EAS electrons properly at all distances, which implies that the lateral age changes with the radial distance. Subsequently some modifications of the NKG structure function (Lagutin et al. 1979 & Uchaikin 1979) were proposed but the radial dependency on the shower age could not be removed totally. Under the circumstances, the notion of *local shower age parameters* (LAP) was introduced (Capdevielle & Gawin 1982, Bourdeau et al. 1980 & Capdevielle et al. 1990) which is in *essence* the lateral age at a point. Presently, different EAS groups use different structure functions and as a result, in most of the studies lateral shower age parameter is just treated as a mere parameter without assigning any physical meaning to it.

The present research work basically aims to explore for a reliable estimate of shower age parameters (lateral shower age and local age i.e. LAP) and to investigate their important characteristics and correlations with other EAS observables from a detailed MC simulation study and thereby the possible role that the parameters may play in a multi-parameter approach to studying EAS, in order to understand the nature of shower initiating particles. From this study, we have found that the shape of the radial variation of the LAP (and hence the LDD of the

electrons in an EAS) exhibits some sort of *scaling* (energy, mass and altitude independent) behaviour. It is noticed here that the shape of the radial variation of the LAP is, however, found to depend on the choice of the effective Moliére radius in the NKG function. Such a *scaling* feature provides a better description of the radial electron distributions in EAS and should help to estimate the electron content in an EAS accurately.

3.2 SHOWER AGE PARAMETERS

The most simple and earliest description of the electromagnetic cascade was starting with the longitudinal development. The average longitudinal profile of an electromagnetic cascade, which is developed in a medium through a multiplicative process involving the interactions of electrons and photons when passing through it, was provided by Greisen (Greisen 1956, Greisen 1960 & Snyder 1989) on the basis of the calculations of Snyder carried in the so called *Approximation B* (taking into account only three processes of pair-production by the photons, bremsstrahlung by the electrons and the ionization loss suffered by the electrons while neglecting the Compton scattering)

$$N_e = \frac{0.31}{\sqrt{ln(\frac{E_0}{\epsilon_0})}} exp[t(1 - 1.5ln(s_{||})]. \qquad (3.1)$$

Here E_0 is the energy of the primary photon generating the cascade, ϵ_0 is the critical energy (below which ionization losses predominate over that due to pair production) with a value of ~82 MeV. Note that t is expressed here in cascade units (the atmospheric depth has been divided by the electron radiation length in air, taken as 37.1 gm-cm^{-2}). In this useful synthesis a very simple parameterisation of the longitudinal age $s_{||}$ is defined by the relation

$$s_{||} = \frac{3t}{t + 2ln(\frac{E_0}{\epsilon_0})} . \qquad (3.2)$$

As mentioned already the development stage of a pure electromagnetic cascade is characterized by the single age parameter $s_{||}$, known as longitudinal shower age. Mathematically, it was determined earlier as the saddle point in the inverse Mellin transformation of cascade transport equation as indicated by the

previous works in the more simple *Approximation A* (taking into account only the radiation process and the pair creation in their asymptotic forms at high energy). The lateral development was described by Nishimura and Kamata solving by the three dimensional diffusion equations (see *Appendix A*) after the preliminary work of Moliére and Bethe focused on the lateral electron distribution near the cascade maximum. Fitting their numerical results on the electron densities at a distance r from the shower axis, Nishimura and Kamata were able to propose a first semi-analytic lateral distribution in a shower age $s_{\|}$. Under *Approximation B* and taking into account the hegemony of the multiple Coulomb scattering for the lateral deflections electrons, an expression of radial distance dependence of $s_{\|}$ was inferred in the simple form (Kamata & Nishimura 1958),

$$s_{\|}(r) = \frac{3t}{t + 2ln\left(\frac{E_0}{\epsilon_0}\right) + 2ln\left(\frac{r}{r_m}\right)} \qquad (3.3)$$

where r is the radial distance from the shower core and r_m is the Moliére radius (near 80 m at sea level) which is a characteristic constant of a medium defined as the radius of a cylinder containing on average 90% of the electromagnetic showers energy deposition (it is the natural lateral displacement unit in air corresponding to a thickness of 9.4 $gm\text{-}cm^{-2}$: the last value comes from the calculation of the mean scattering angle in the case of multiple Coulomb scattering with a scattering energy $E_S = 21\ MeV$). With the identification $s_{\|} = s(r)$ when $r = r_m$, $s_{\|} = 0$ at the origin of the cascade and $s_{\|} \sim 1$ at the shower maximum.

In the same theoretical context the lateral density distribution of cascade particles given by Nishimura and Kamata can be approximated by the well known *Nishimura-Kamata-Greisen* (NKG) structure function proposed by Greisen (Greisen 1956 & Greisen 1960), given by

$$f(r, s_{\perp}) = C(s_{\perp})(\frac{r}{r_m})^{s_{\perp}-2}(1 + \frac{r}{r_m})^{s_{\perp}-4.5}, \qquad (3.4)$$

where the normalization factor $C(s_{\perp})$ is given by

$$C(s_{\perp}) = \frac{\Gamma(4.5 - s_{\perp})}{2\pi r_m^2 \Gamma(s_{\perp})\Gamma(4.5 - 2s_{\perp})}. \qquad (3.5)$$

The NKG formula has the advantage of normalization as it is integrable in Euler Beta function provided $s_{\perp}$ is independent of r. The normalisation of $f(r)$

implies that $\rho(r) = N_e f(r)$, $\rho(r)$ being the electron density at r (thanks to the properties of the Eulerian function as shown in *Appendix A*).

The relation $s_{\parallel} = s_{\perp}$ was considered to hold for pure electromagnetic showers (Kamata & Nishimura 1958). Such equivalence implies the correlation between steeper lateral distributions ($s_{\parallel} < 1$) or flatter lateral distributions ($s_{\parallel} > 1$) in proportion to the distance to shower maximum; it suggests also the employment of the observable $s_{\perp}$ as a hint of the global shower cascading expected to depend on primary mass and interaction features (cross-section, multiplicity and inelasticity). Hence, the equations (**3.1**), (**3.2**) and (**3.4**) together provide an attractive and a complete procedure of calculating the $3D$ development of the electromagnetic cascade (as first pointed out by Cocconi (Cocconi 1961)).

The superposition of many such pure electromagnetic cascades build the electron component of a hadron initiated EAS. It was also suggested (Kamata & Nishimura 1958, Lipari 2009) that for hadron initiated EAS, both the longitudinal structure and lateral structure of soft components can be described by that of a resulting single cascade, assigning a suitable value to the age parameter. Recent MC simulation studies (Giller et al. 2005, Nerling et al. 2006 & Lafebre et al. 2009) exhibited a possible universality for large EAS with primaries in the EeV energy range in terms of longitudinal age defined through the relation (**3.2**).

However Nishimura, Kamata and Greisen noted some difficulties when comparing the prediction of the cascade theory with the measured lateral electron distributions in EAS and we have listed hereunder some limitation on the validity of the analytical expressions caused by the various approximations in obtaining the solutions as well as due to over-simplification of the adopted $3D$ transport equations. The conditions of validity of relation (**3.4**) are

- $E_0/\epsilon_0 \gg 1$ due to the asymptotic value of the cross-sections.
- $t > 1$ (more than one radiation unit is necessary to consider the continuity in the cascade).
- $|\log(E_0/\epsilon_0)| \gg |\log(r/r_m)|$.

The last condition may be not fulfilled near the shower axis as underlined by Nishimura considering not appropriate to use the data near the shower core.

Nishimura and Kamata have also ascertained that corrections where necessary to their calculations performed for the homogeneous medium. In consequence, taking into account the variation of the air density, they have inferred that in order to compare the theoretical curves with the experimental data, the distribution obtained at about 2 radiation length (in the case of *Approximation B*) above the measurement area has to be employed.

Furthermore, Nishimura ascertained again that near the shower axis the densities were quite lower with NKG than with the original NK formula (Nishimura 1967) for $s \geq 1.2$. Greisen also noticed larger densities in experimental measurements than that given by NKG far from the axis (Greisen 1956, Greisen 1960 & Snyder 1989) which was inferred as a possible contribution of the muon decay. A shorter value of the second momentum of the distribution than in the NKG was observed by Allan for the lateral structure (Allan et al. 1975) and a couple of years later a steeper profile was exhibited by Hillas and Lapikens from MC calculation near 100 GeV (Hillas & Lapikens 1977).

Simultaneously, the $3D$ diffusion equations were solved using adjoint equations, the Bessel Fourier transformation being applied to r and the numerical integration on t and on the energy E being performed by partial polynomial functions (Lagutin et al. 1979 & Uchaikin 1979). This method, which involves several approximate steps and numerical inverse transformations, leads to a limiting (as $E_0 \rightarrow \infty$) radial distribution. An improvement of the NKG function was proposed by adopting a modulated, longitudinal age parameter $s_{\parallel}$ dependent effective Moliére radius so that

$$\rho_{el} = (mr_m)^{-2}\rho_{NKG}(r/m) \qquad (3.6)$$

where $m = 0.78 - 0.21s_{\parallel}$.

We underline here that it is ρ_{el} and not only ρ_{NKG} which has been implemented in the so called subroutine NKG of CORSIKA. The procedure of calculation is the following: N_e is calculated together with $s_{\parallel}$ (via Greisen formula) for each sub-cascade generated by one photon after one pair creation by one secondary of one hadron interaction in the EAS. The electron component is subsequently obtained from the sum of the densities at one given distance of the individual axis of each sub cascade (Capdevielle & Gawin 1982, Bourdeau et al.

1980 & Capdevielle et al. 1990). Of course the procedure doesn't distinguish e^+ and e^- and the annihilation of the positron is not considered.

On the other hand, observing that the experimental LDD of electrons in EAS was steeper than that given by the ρ_{NKG} and was in better agreement with the MC calculations of Hillas (Hillas & Lapikens 1977) at lower energies. Capdevielle *et al* (Capdevielle & Gawin 1982, Bourdeau et al. 1980 & Capdevielle et al. 1990) introduced the notion of *local age*. After testifying the behaviour of the LAP on experimental lateral distributions and reaffirming it with the Akeno observations (Nagano et al. 1984[b]), this approach was validated by the *rapporteurs* of the *International Cosmic Ray Conferences* during the period 1981 to 1985 (Tonwar 1981, Rao 1983 & Clay 1985). The whole procedure was also employed in the calculation of the radio effects of EAS (Suprun et al. 2003).

From two neighbouring points, i and j, we can give the (*local*) *lateral age* parameter (s_{ij}^{local}) for any NKG like distribution $f(x)$ (where $x = r/r_m$) which characterises the best possible description for the electron LDD in $\{x_i, x_j\}$:

$$s_{ij}^{local} = \frac{\ln (F_{ij} X_{ij}^2 Y_{ij}^{4.5})}{\ln (X_{ij} Y_{ij})} \qquad (3.7)$$

where $F_{ij} = f(r_i)/f(r_j)$, $X_{ij} = r_i/r_j$ and $Y_{ij} = (x_i + 1)/(x_j + 1)$. More generally, $r_i \to r_j$, this suggests the definition of the LAP $s_{\perp}^{local}(x)$ at each point:

$$s_{\perp}^{local}(x) = \frac{1}{2x+1}\left((x+1)\frac{\partial lnf}{\partial lnx} + (2+\beta_0)x + 2\right) \qquad (3.8)$$

If $\beta_0 = 4.5$, $f_{NKG}(r)$ with $s_{\perp} \equiv s_{\perp}^{local}(r)$ can be used to fit f in the neighbourhood of r.

Typical behaviour was predicted with a characterized minimum value of $s_{\perp}^{local}(r)$ near about 50 m from the axis, followed by a general increase at a large distance (Capdevielle & Gawin 1982, Bourdeau et al. 1980 & Capdevielle et al. 1990). The relation $s_{\perp}^{local}(r) \equiv s_{ij}^{local}$ for $r = (r_i + r_j)/2$ was found to be valid for the experimental distributions (taking $F_{ij} = \rho(r_i)/\rho(r_j)$ as far as they were approximated by monotonic decreasing functions versus distance).

Such a prediction was substantiated by Akeno (Nagano et al. 1984[b]), North Bengal University (NBU) EAS experiments (Sanyal et al. 1993) and other

experiments (Capdevielle & Gawin 1982, Bourdeau et al. 1980 & Capdevielle et al. 1990). The LAP depends mainly on the logarithmic derivative of the density versus the distance as it appears in the relation (**3.8**); however, this pure mathematical approach may not be attained in practice at any radial distance, due to the experimental uncertainties arising mainly from the use of a finite number of detectors for the density measurements, triggering conditions and errors in the determination of the shower core position. Therefore, $s_{\perp}^{local}(r)$ is estimated via the relation (**3.7**) using physical bands of distance $\{r_i, r_j\}$; for experiments with very dense grids of detectors, such distance bands may be reduced to 5 - 10 m, but they may have to enlarge up to about 20 m for arrays with a lower resolution, as well as in the case of individual showers with large fluctuations. For very large and giant EAS, the interval $\{r_i, r_j\}$ may be required to exceed 100 m or so. We preferred to conserve the characteristic parameters of electro-magnetic cascade in relation (**3.7**) including the value of the Moliére radius to facilitate the comparison with the experimental data, which is most frequently expressed in NKG formalism.

The dependence of $s_{\perp}^{local}(r)$ on r rules out a consistent integration via relation (**3.4**) casting some doubt on the accurate relation between density and size; it was shown that such a dependence on $s_{\perp}^{local}(r)$ on r is mainly a basic feature of pure electromagnetic cascades (Capdevielle & Gawin 1982, Bourdeau et al. 1980, Capdevielle et al. 1990 & Bhadra 1999).

Furthermore, the observed lateral density distribution of air shower electrons is usually described in terms of lateral structure function and hence in terms of lateral shower age and in most experiments the estimated transverse shower age ($s_{\perp}$) differs from the longitudinal age ($s_{\parallel}$) for EAS with hadrons as primary. It was suggested from the experimental results (Dedenko et al. 1975 & Stamenov 1987) that these two age parameters are connected through the (approximate) relation $s_{\parallel} \geq s_{\perp} + \delta$, with $\delta \approx 0.2$. Some early MC simulation results obtained a relation of the nature $s_{\parallel} \sim 1.3 s_{\perp}$ (Capdevielle & Gawin 1982, Bourdeau et al. 1980 & Capdevielle et al. 1990), $s_{\perp}$ being derived from density measurements around 50 m from axis. Here note that the longitudinal age can be estimated observationally only if EAS experiment is equipped with Cherenkov or fluorescence detectors, whereas the lateral shower age parameter follows straightway from the LDD of electrons which is the basic measurement of any conventional EAS array consisting of particle detectors.

3.3 METHOD OF SIMULATION

For generating EAS events, the air shower simulation program CORSIKA (Heck et al. 1998 & Capdevielle 1992) is exploited here. Here our discussions are mainly restricted to CRs in the knee region of the primary spectrum. In the present work, the high energy (above 80 GeV/n) hadronic interaction model QGSJET **01** version **1c** (Kalmykov et al. 1997) was used in combination with the low energy (below 80 GeV/n) hadronic interaction model GHEISHA (version **2002d**) (Fesefeldt 1985) or FLUKA (Fass`o 2001), depending on the primary energy in the framework of the CORSIKA MC program version **6.600/6.970** (Heck et al. 1998 & Capdevielle 1992) to generate EAS events. Note that the low energy interaction model GHEISHA exhibits a few shortcomings (Drescher et al. 2004, Bhadra et al. 2009, Heck 2006 & Ferrari et al. 1996) but the LDD of EAS electrons does not depend much on the low energy hadronic models, except at large distances (Drescher et al. 2004). Hence for very high energy events involving large radial distances we employed FLUKA (Fass`o 2001). A relatively smaller sample was also generated using the high-energy interaction model SIBYLL **v2.1** (Fletcher et al. 1994) to judge the influence of the hadronic interaction models on the results.

The CORSIKA program allows one to choose either of the two options, the EGS4 (electron gamma shower system version **4**) (Nelson et al. 1985) and the NKG for obtaining a lateral distribution of the charge particles. The former option facilitates a detailed MC simulation of the electro-magnetic component of a shower that incorporates all the major interactions of electrons and photons (Rossi & Greisen 1941), whereas the NKG option relies on an analytical approach rather than a full MC simulation. In the NKG option, the electron density of an electro-magnetic sub-shower is calculated straightway using the NKG function with a reduced Moliére radius (Lagutin et al 1979, Capdevielle & Gawin 1982, Bourdeau et al. 1980 & Capdevielle et al. 1990). One gets better accuracy and more detailed information about the electro-magnetic component with the EGS4 option, at the expense of long computing time. We underline here that the NKG option (subroutine NKG inside CORSIKA) is dealing mainly with the relations (**3.6**) and (**3.7**) and not directly with equation (**3.4**). Furthermore the reference (Capdevielle et al. 1977) in CORSIKA original documentation was mismatched with the appropriate references (Capdevielle & Gawin 1982, Bourdeau et al. 1980 & Capdevielle et al. 1990). It was unfortunately reproduced in the user's guide and in

several papers, for instance (Antoni et al. 2001) generating a confuse interpretation of the NKG option.

We have considered the US-standard atmospheric model (NASA report 1976) with a planar approximation. The maximum primary zenith angle was restricted to 50^0 for the present study. The EAS events were generated mainly for proton and iron nuclei as primaries. A few events were also generated for gamma-ray as primary. Irrespective of the nature of the primaries, the slope of primary power law spectra was taken as -2.7 below the knee i.e. 3×10^{15} eV and as -3.0 above. The EAS events were simulated at different geographical positions corresponding to the experimental sites of Akeno (Nagano et al. 1984[b]), KASCADE (Antoni et al. 2001) and NBU (Bhadra et al. 1998). The magnetic fields are provided accordingly. On the observation level, the kinetic energy thresholds were chosen as 3 MeV for electrons (e^+ and e^-) irrespective of the primary species and energies.

3.3.1 GENERATION OF THE EAS MONTE CARLO LIBRARY

The simulated shower library consists of more than 30 000 EAS events with the EGS4 option and more than 180 000 events with the NKG option in the primary energy interval of 10^{14} eV to 3×10^{16}eV. In order to appreciate the asymptotic tendencies at ultra high energies, our library has also been enriched by about 1000 events simulated at $E_0 = 5 \times 10^{17}$ and 10^{18} eV for proton and iron primaries: apart from the thinning factor which is taken as 10^{-6} with optimum weight limitation (Kobal 2001) (i.e., all particles are followed up to an energy E_{th}, where $E_{th}/E_0 = 10^{-6}$, after which only one of those particles is tracked giving appropriate weight to it) the simulation conditions are here identical concerning the hadronic interaction models, the zenith angle range, both the EGS4 and the NKG options. Here we would like to specify that the optimized thinning factor 10^{-6} with the optimum weight limitation for the CORSIKA version used here is considered as the best compromise between the computing time and the accuracy at high energies (Knapp et al. 2003).

In all cases involving the EGS4 option, the longitudinal development is restored numerically and that the longitudinal age parameter is computed (Capdevielle & Cohen 2006[a], 2006[b]), instead of relation (**3.2**) by

$$s_{||} = \exp\left[\frac{2}{3} \times \left\{1 + \frac{\alpha}{t} - \tau\right\}\right] \; with\, \tau = \frac{t_{max}}{t}, \alpha = ln\frac{N_{max}}{N_e} \qquad (3.9)$$

where t_{max} and N_{max} are respectively depth and size read at the cascade maximum. In relation (**3.9**), N_e represents the electron size at the atmospheric depth t which is usually expressed in cascade units.

3.3.2 THE NKG AND THE EGS4 OPTIONS

Taking the opportunity of CORSIKA to calculate the electromagnetic component of EAS via the EGS4 and the NKG procedure, we have used both the options simultaneously for about 30 000 events. In **Fig.3.1** we compare the LDD of EAS electrons obtained with the stated two options for proton, iron and gamma-ray primaries. It is clear from the figure that the NKG option gives a higher density with steeper radial distribution compared to the EGS4 option. A small density excess appears for the pure electro-magnetic cascades near the axis for the NKG options; such an excess presents also in the proton initiated air showers. However, for the proton showers, a tolerable agreement between the output of the two options was noted over a large band of densities between radial distances of $10 - 100$ m from the shower axis; it reconfirms that for proton and photon initiated showers the NKG option is quite useful to calculate a large number of cascades in a short time.

For iron primaries, both the options indicate an older density profile near the axis. The NKG option was found to give an excess density between $2 - 10$ m distances. The average energy of the positrons was quite a bit lower in the case of iron initiated showers and the cross section of positron annihilation becomes more important for the lower part of the cascade. This effect is probably enhanced by the longer path of the electrons in the geomagnetic field and the larger energy loss by ionization. The NKG option is, therefore, not so accurate for the simulation of heavy nuclei initiated showers with large zenith angles after the shower maximum. For vertical showers, the output of the NKG option is nevertheless acceptable. At larger distances a slight deficit in the densities appears with the NKG option; this probably comes from the different treatment of the multiple Coulomb scattering in the NKG option than in the EGS4. Furthermore, Bhaba and Moller scattering are treated in complement with the separated MC procedures. On the other hand, the geomagnetic field of the earth enhances the path of the muons as well. Consequently their losses by ionization and their decay give more electrons, which

were not incorporated in the NKG option. Besides, the NKG option does not accommodate photo-production inside the electro-magnetic sub cascades as the EGS4 code itself contained.

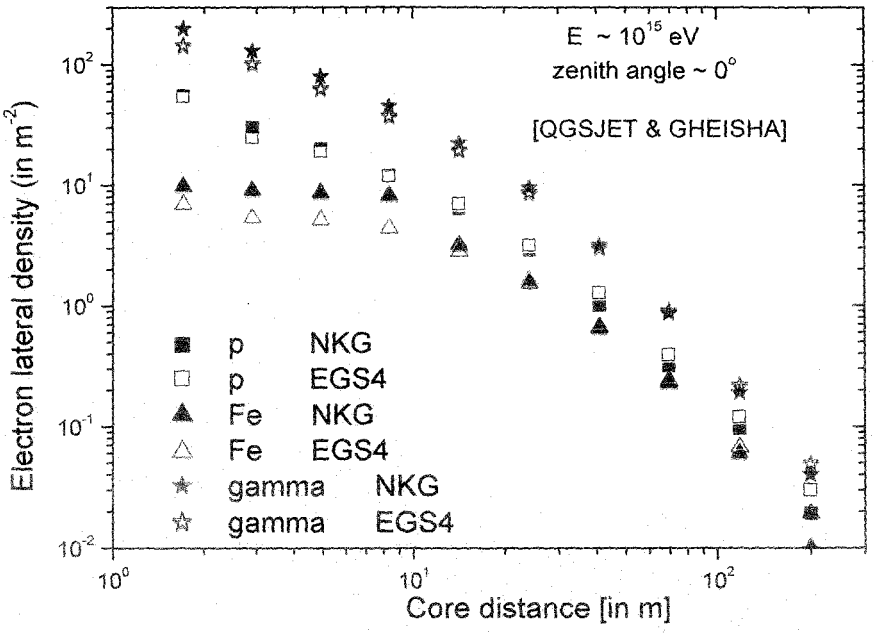

Fig.3.1: Comparison of the EGS4 and the NKG generated lateral distribution of electrons for different primary cosmic ray species. The statistical errors are within the dimensions of the symbols used.

3.4 ESTIMATION OF SHOWER AGE

The simulated data have been analyzed using the reconstruction algorithms developed to obtain shower size and shower age (called basic shower parameters). We adopt two different methods. First following the traditional approach we estimated basic shower parameters by fitting density data with the NKG structure function. Secondly, exploiting equation (**3.7**) we directly estimate local age parameter for each individual event.

3.4.1 LATERAL AGE THROUGH NKG FITTING

In this approach the simulated electron densities at radial distances have been fitted by the method of chi-square minimization through an iterative procedure based on the method of steepest decent to the NKG lateral distribution function of electrons. Here it is to be noted that majority of the EAS groups traditionally estimate basic shower parameters based on the NKG function. In

order to check the goodness of the NKG function in describing the simulated radial density distribution of electrons we first fitted the simulated density data at various radial distances with the NKG function and compare radial density distribution for simulated events with the fitted curve. In **Figs. 3.2a – 3.2c** the simulated particle densities at different radial distances are plotted along with the fitted curves obtained with the NKG function.

As mentioned already the NKG function with a single age cannot describe the EAS particle densities properly over a reasonable radial distances from the shower core. This is reflected in **Fig.3.2a** where the average electron densities over a radial distance range up to about 5800 m from the shower core obtained with the EGS4 option at primary energy 5×10^{17}eV at the geographical site of KASCADE is fitted with the NKG structure function with a single lateral age $s_{\perp}$. The limits in the employment of NKG at very high energy came from both asymptotic representations by simple power laws when $r \rightarrow 0$ and $\rightarrow \infty$. This difficulty in Akeno was reduced by introducing the sum of a pair of NKG functions and in KASCADE by an important reduction of Moliére radius as in earlier experiments at high altitude. A more general function than the Eulerian approach was also proposed in terms of Gaussian hyper-geometric function (Capdevielle & Cohen 2006[a]. 2006[b]) to describe accurately the lateral electron distribution.

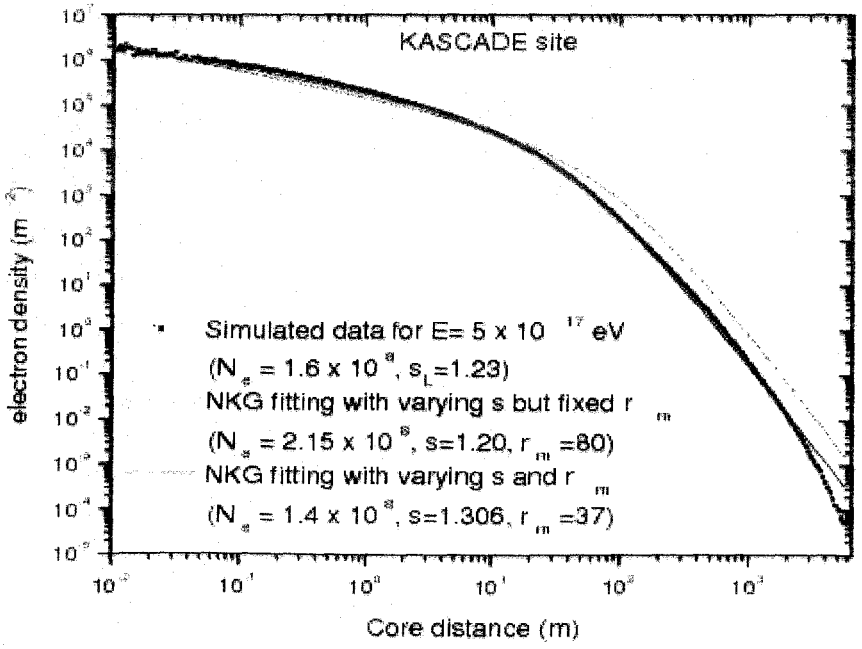

(a)

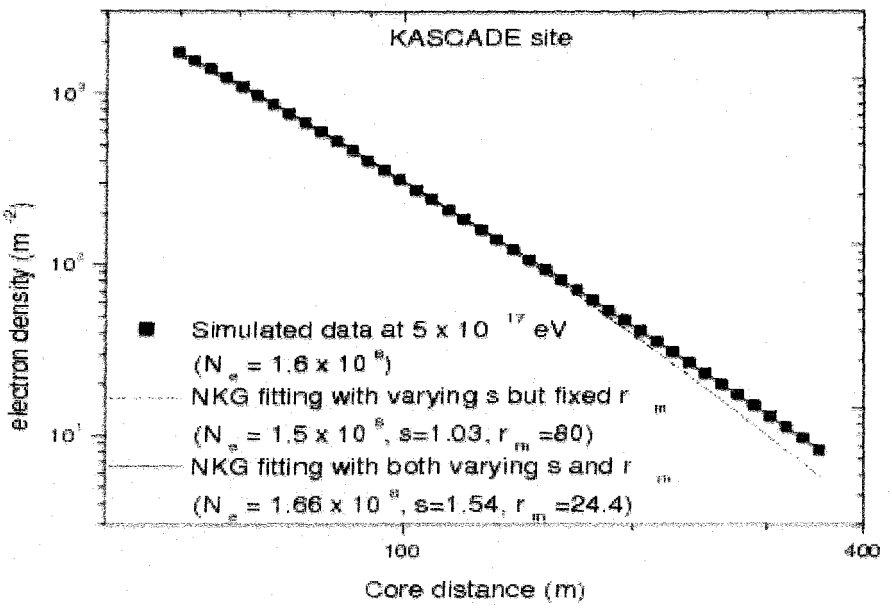

(b)

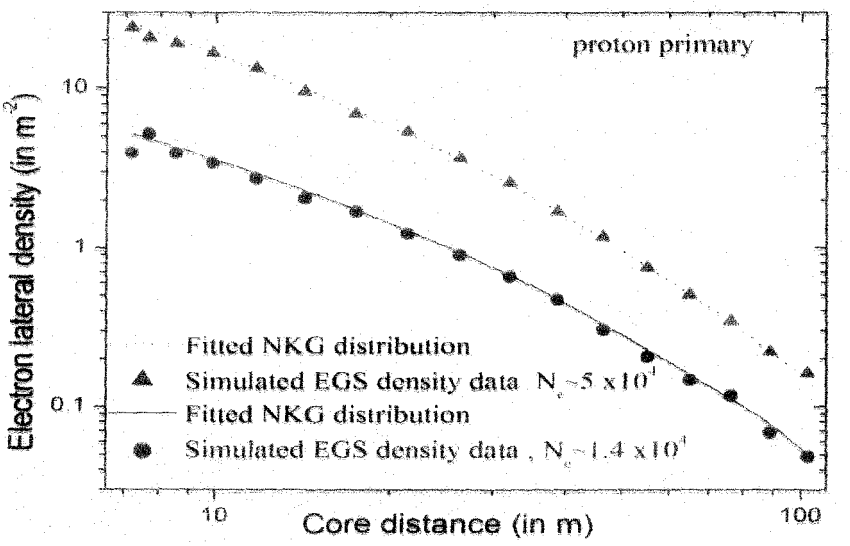

(c)

Fig.3.2: (a) NKG fitting of the EGS4 output of electron density at KASCADE site for p primary covering radial distance more than 5000 m, (b) the same as Fig.3.2a but restricting radial distance between 50 – 350 m and (c) NKG fitting with a constant single age of the EGS4 output of electron density at NBU site restricting radial distance only up to 100 m. The statistical errors are within the dimensions of the symbols used.

We also noted that the description of the data by the NKG function is improved a lot when the Moliére radius is treated as a variable rather than a fixed parameter which is also shown in the same figure. But this better description comes at the expense of very high lateral shower age value which somewhat obscures the physical meaning of the age parameter as assigned in the cascade theory.

In the **Fig.3.2b** we did the same fittings as in **Fig.3.2a** but restricting the radial distance to the range 50 to 350 m. The reason for such a restriction on the radial distance will be clear at the end of this section **3.4**. Here again it is found that the Moliére radius as a free variable improves the description of the simulated data considerably. For small EAS arrays where the radial distance is limited to about 100 m or so, the NKG structure function is found to represent the simulated data reasonably well except at very small distances as is shown in **Fig.3.2c** for two shower size ranges. At very small distances the simulated densities are found higher than those given by the NKG function. The simulated particle densities only in the radial interval 7 - 100 m are thus finally considered for parameter reconstruction and fitted showers with reduced chi square ($\chi^2_{red.}$) less than 5 are only accepted for results on characteristics of shower age parameter.

The error in estimating lateral shower age in the shower size interval 10^3 – 10^5 particles (corresponding to the primary energy range 10^{14} – 3×10^{15} eV) was found to be ±0.03 for the QGSJET model and ±0.05 for the SIBYLL. The larger error for the SIBYLL model seems solely statistical, due to the generation of a relatively fewer number of EAS events using the latter model.

3.4.2 LOCAL AGE PARAMETER

The local age for EAS charged particles was computed for each individual event straightway, applying equation (**3.7**). When estimating the LAP, the main sources of error are the fluctuations in particle density and the uncertainties in radial distance estimation. In simulated data the radial distance of each particle is known with a high accuracy. In this work the error in the LAP, due to uncertainties in radial distance estimation was kept small by taking small radial bins. For minimizing the statistical fluctuations in particle density at different radial bins, a large number of events need to be considered. In this analysis, the error of the LAP for EAS with the primary energy in the PeV range remains within 0.05 for $10\,m < r < 250\,m$, whereas for $r < 10$ m or when $r > 300$ m the error of the LAP is found to be higher, about 0.1. At higher primary energies

(5×10^{17} – 10^{18} eV) the error of the LAP is found at about 0.12 near the core, which decreases to about the 0.07 level when $20\,m < r < 300\,m$ but increases again with the radial distance and reaches to about 0.15 when r approaches $1000\,m$.

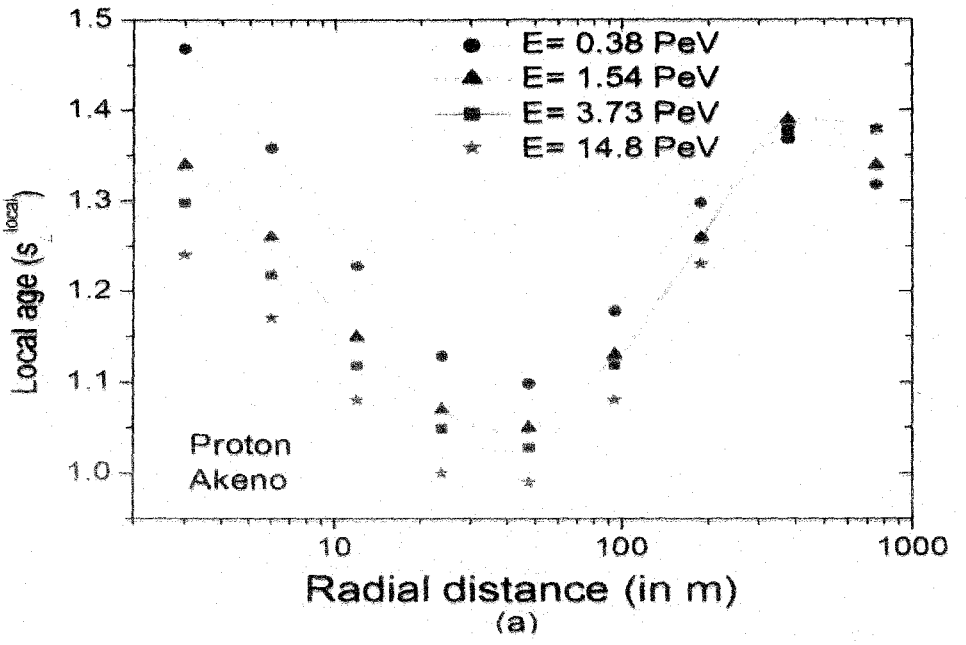

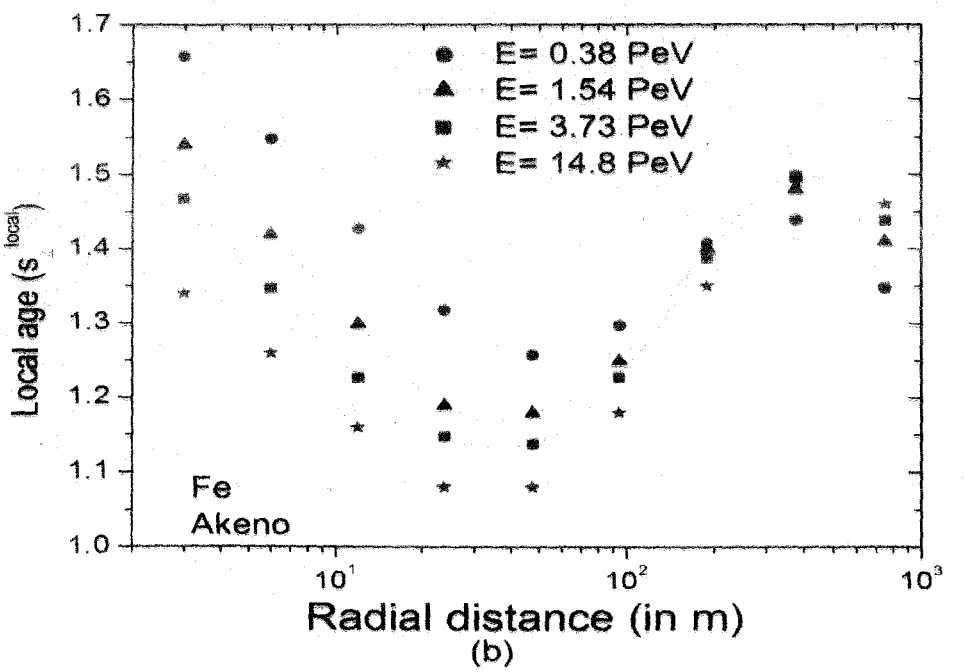

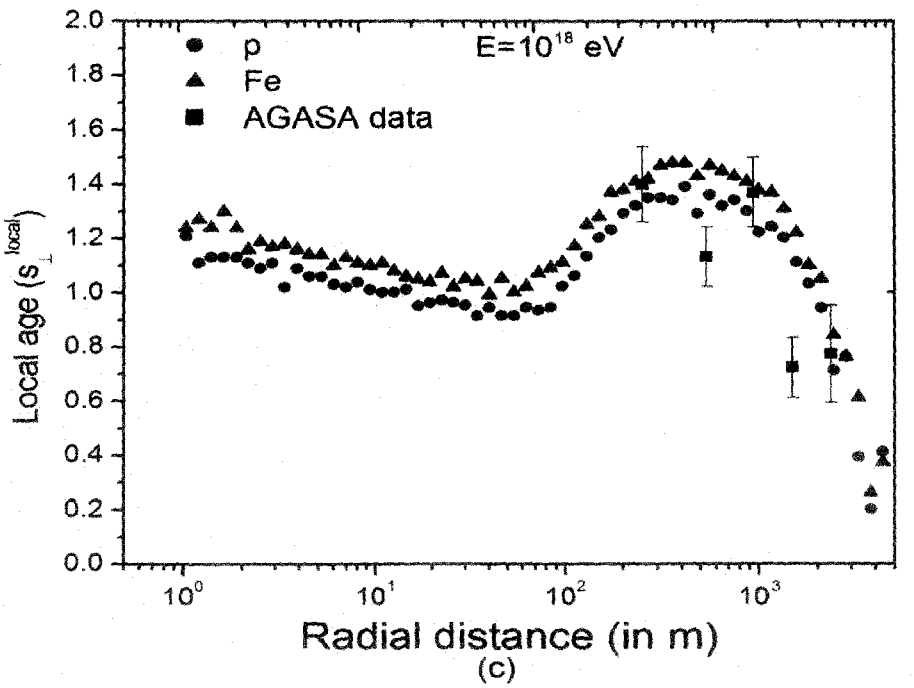
p
Fe
AGASA data
E=10^18 eV
Local age (s^local)
Radial distance (in m)

(c)

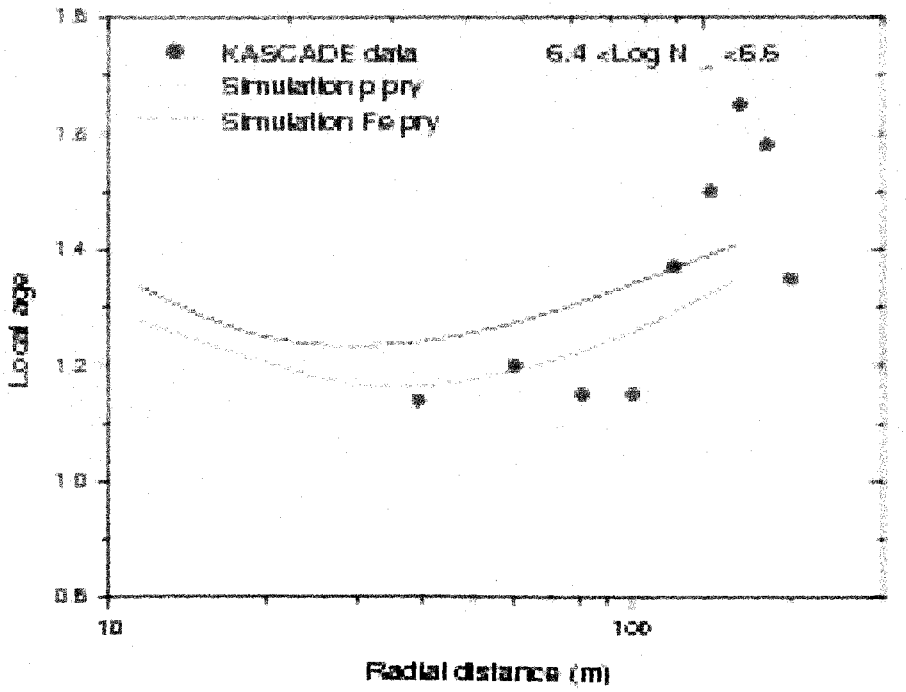
KASCADE data
Simulation p pry
Simulation Fe pry
Local age
Radial distance (m)

(d)

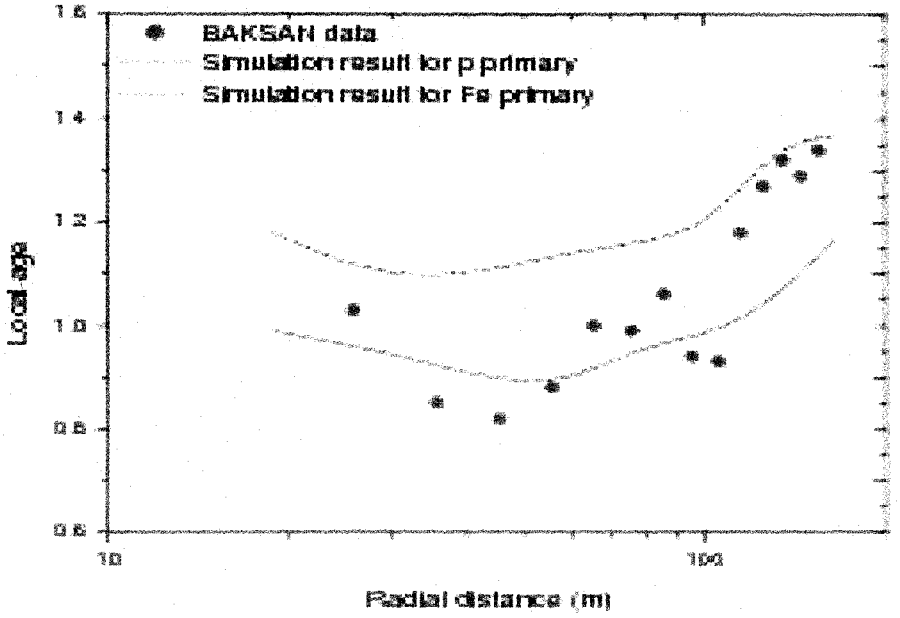

(e)

Fig.3.3: Variation of the LAP (estimated from the simulated data) with radial distance for different primary energies at Akeno site (920 gm-cm^{-2}) for (a) proton (b) iron and (c) for both p and Fe along with the local age obtained from the experimental data. The lines are only a guide for the eye. The same studies are also made for KASCADE and BAKSAN experimental data as shown in Figs. (d) and (e).

The variation of the LAP with the radial distance from the shower core is shown in **Fig.3.3**. It is known from previous studies (Capdevielle & Gawin 1982, Bourdeau et al. 1980 & Capdevielle et al. 1990) that with an increase of the radial distance, the LAP initially decreases, reaching a minimum at around 50 m and then increases, as was also noted from the experimental data (Nagano et al. 1984[b] & Sanyal et al. 1993). Here we noticed two other interesting features (**Figs.3.3a – 3.3e**): the local age again starts to decrease at around 300 – 400 m. To examine whether the experimental data also demonstrates a fall in the local age at large radial distances, we compute the local age from the LDD data of total charged particles, as measured by the AGASA experiment (Yoshida et al. 1994) for primary energy 2×10^{18} eV and compared these values with our simulation results in **Fig.3.3c** using EGS4 output. The experimental data clearly support the trend predicted by the simulation results at larger radial distances. The characteristic high-low-high kind of radial variation in the local age at relatively smaller

distances (within 300 m or so) could not be substantiated by the AGASA data, due to the large separation of the detectors of the array. Here due to limited statistics the position of the minimum of the local age could not be located with good precision but the overall nature of the radial dependence of local age is found the same to that at lower energies. It is worthwhile mentioning that there was an indication for such a decrease of $s_{\perp}^{local}(r)$ at around 300 m in the experimental results obtained by Akeno (Sanyal et al. 1993) and KASCADE-Grande (Ulrich et al. 2008 & 2009[a]). Such behaviour is also depicted in **Fig.3.4** of the KASCADE report (Antoni et al. 2001), where one may notice a maximal deficit at 50–80 m in the ratio of the measured and the fitted electron densities and an excess at larger distances when fitted with the NKG formula. Here we have compared the radial variation of LAP obtained out of the simulated data for proton and iron primaries with those obtained from the experimentally measured density data of KASCADE and BAKSAN (Voevodsky et al. 1993) in **Figs.3.3d – 3.3e** respectively.

These findings are important for an analysis of very large air showers observed/to be observed by the KASCADE-Grande, AGASA, AUGER, Yakutsk and Telescope Array involving large radial distances. The large EAS experiments often treat charged particle densities at large radial distances, such as 500, 600, 1000 m from the shower core as an estimator of the primary particle energy, though such a technique involves several uncertainties (Capdevielle et al. 2009). These findings of a rapid change in the slope of the radial distribution of electrons at large radial distances, suggest that more controls should be adopted in the estimation of the primary energy of large showers, for instance by taking particle densities at more than one radial distance.

Another important observation is that in general the nature of the variation of the local age with the radial distance appears nearly the same for all of the primary energies, *i.e.* the nature of the variation is practically independent of the energy of the shower initiating particles, which implies that the local age (or the lateral distribution of electrons in EAS) exhibits some sort of *scaling* behaviour in respect to the radial dependence from the shower core. This feature of the local age is maintained even for different primary species and observational levels.

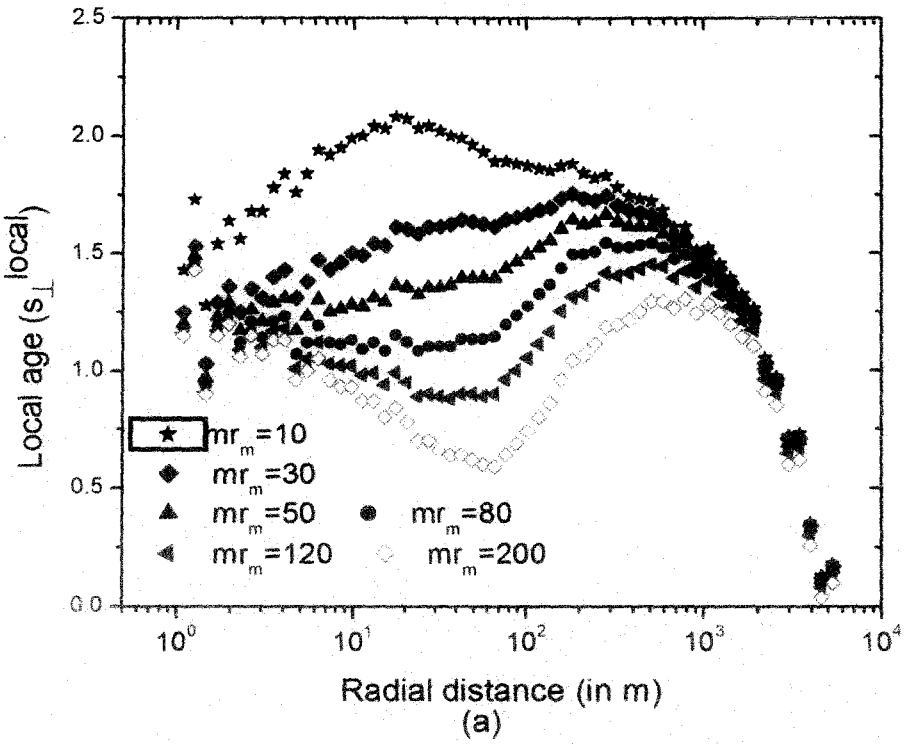
Local age ($s_\perp^{local}$)
Radial distance (in m)
mr_m=10
mr_m=30
mr_m=50
mr_m=80
mr_m=120
mr_m=200

(a)

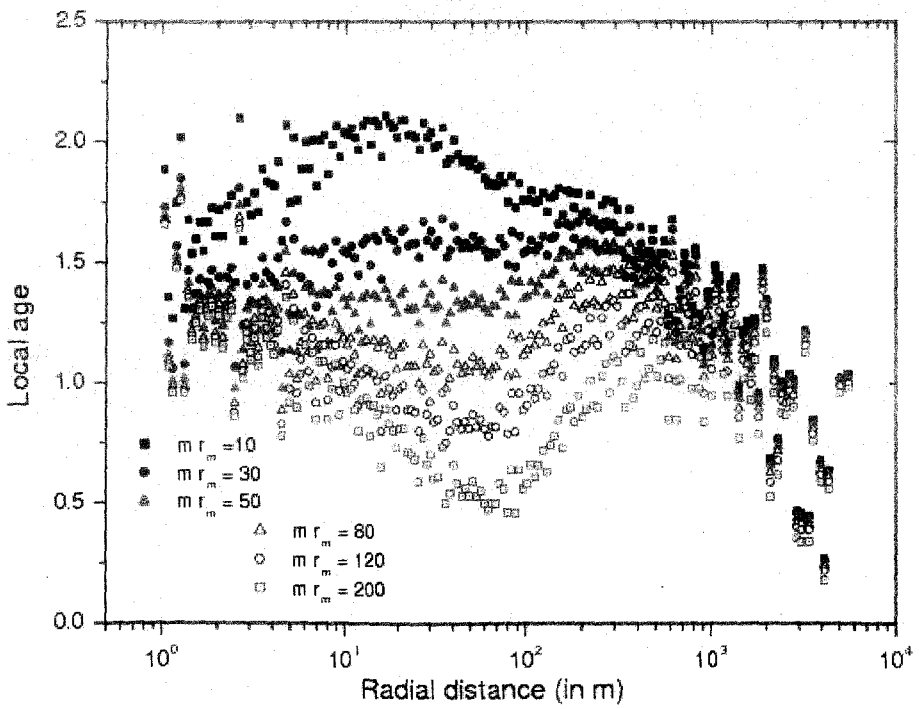
Local age
Radial distance (in m)
m r_m =10
m r_m = 30
m r_m = 50
m r_m = 80
m r_m = 120
m r_m = 200

(b)

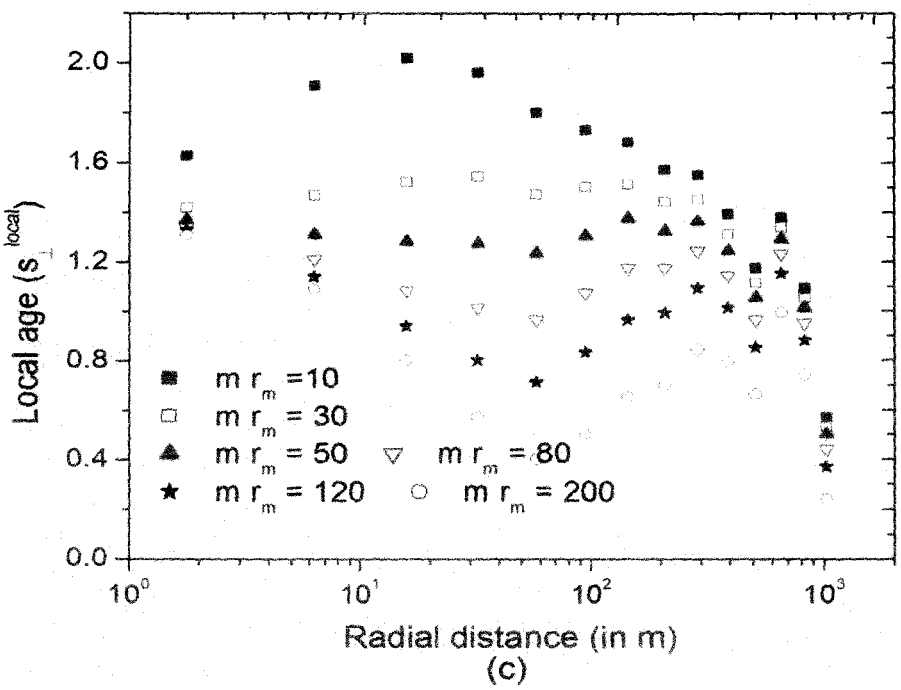

Fig.3.4: Variation of the LAP (estimated from the simulation data) with the radial distance for different choices of the effective Moliére radius at the KASCADE site (a) for proton; (b) for iron with a primary energy 5×10^{17} eV and (c) for γ with a primary energy 10^{15} eV.

To examine systematically the influence of the effective Moliére radius on the shape of the lateral distribution of charged particles in EAS, we study the radial variation of the LAP for different effective Moliére radii, which are shown in **Figs. 3.4a** and **3.4b** for proton and iron primaries with a primary energy of 5×10^{17} eV.

A string-like feature emerged with two nodes, as seen from the figures, one close to the shower core while the other at around $r \sim 400$ m that increases slowly with the effective Moliére radius; the effective Moliére radius behaves somewhat like the tension in a piece of string. Beyond the second node, however, the LAP is found to decrease monotonically with an increase of the radial distance, irrespective of the choice of the effective Moliére radius.

In order to explore the inherent cause of such a feature of the LDD of electrons in hadron initiated EAS, we studied the radial variation of the local age for γ-ray initiated showers, and one such plot at the primary energy 10^{15} eV is shown in **Fig.3.4c**. We found the similar nature of radial variation of the LAP as in the hadron initiated showers. As ascertained in previous simulations (Capdevielle

& Gawin 1982, Bourdeau et al. 1980 & Capdevielle et al. 1990), the behaviour of $s_{\perp}^{local}(r)$ comes mainly from the discrepancies between the EGS4 output and the NKG function, i.e. between the rigorous descriptions of the electromagnetic cascade adopting the basic electromagnetic processes as well as the Moller, Bhaba scattering and positron annihilation, dependence of the cross section on energy on the one hand, *Approximation B* combined with Landau and small angle approximations in a single description of the multiple Coulomb scattering on the other hand. When the experimental data (Antoni et al. 2001, Capdevielle & Cohen 2006[a], 2006[b]) are superimposed on **Fig.3.4**, we understand that a reduced Moliére radius (between 20 - 50 m) is favoured for all primary energies, implying a dramatic reduction in the mean scattering angle connected with the scattering energy of 21 MeV. For primary energies lower than 10^{17} eV, it looks easy to fit the lateral distributions in the range 20 - 100 m and determine the minimum value of $s_{\perp}^{local}(r)$ from the measured densities, as well as its average value over a selected radial distance range. They are representative estimators and a correspondence with $s_{\parallel}$ can be tabulated via adjustments and simulation; at ultra high energy, the detectors are saturated near the core and we suggest a fit of $s_{\perp}^{local}(r)$ around the distances selected for the energy estimator, usually 500, 600, 800 or 1000 m.

3.5 CHARACTERISTICS OF THE SHOWER AGE PARAMETER

To explore the physical nature associated with the lateral shower age parameter, if any, we studied the details of the characteristics of the shower age. For the local age, we considered two different parameters: the minimum value corresponds to the local age at the radial distance, about 50 m, and an average value nearly between 50 to 300 m. Besides, we have taken the NKG lateral age obtained from fitting the density data up to about 100 m.

3.5.1 DISTRIBUTION OF SHOWER AGE PARAMETER

The distributions of the LAP and the lateral shower age were studied for the primary energy range 3×10^{14} to 3×10^{16} eV. Those distributions (for instance **Fig.3.5e**) differ from a Gaussian distribution when the observational level is deeper than the depth of the shower maximum and is found to fit well by an *Extreme Value Distribution* (EVD) defined through

$$\varphi(s) = \frac{1}{\sigma}\exp\left(\pm\frac{\mu - s}{\sigma} - e^{\pm\frac{(\mu-s)}{\sigma}}\right) \qquad (3.10)$$

, where the parameters μ and σ are related to the average size $< s >$ and its variance V_s by $< s > = \mu \pm 0.577\sigma$ and $V_s = 1.645\sigma^2$ (in the case of the histogram of **Fig.3.5f**, $< s > = 1.495$ and $\sigma = 0.07$).

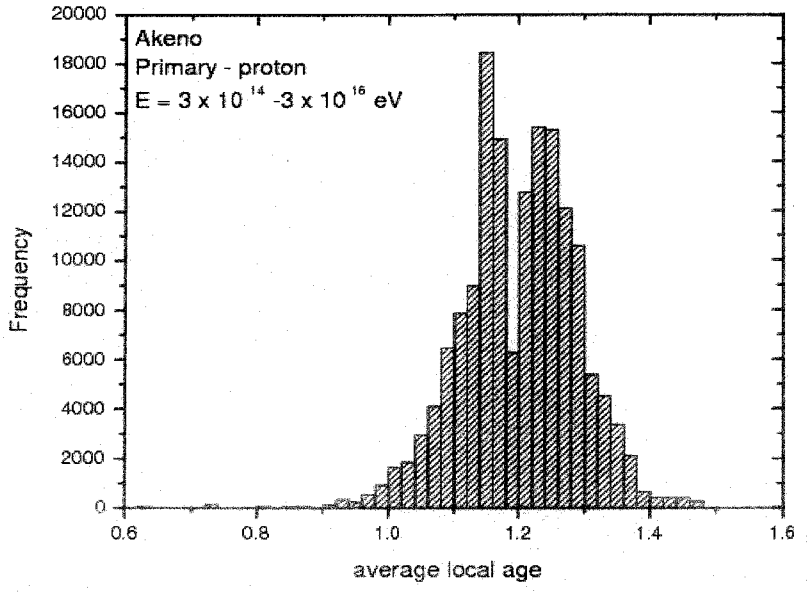

(a)

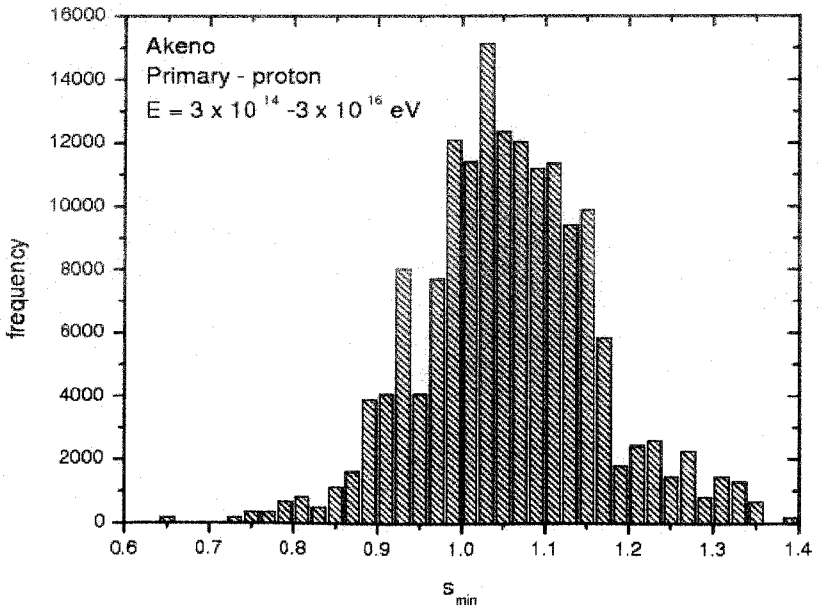

(b)

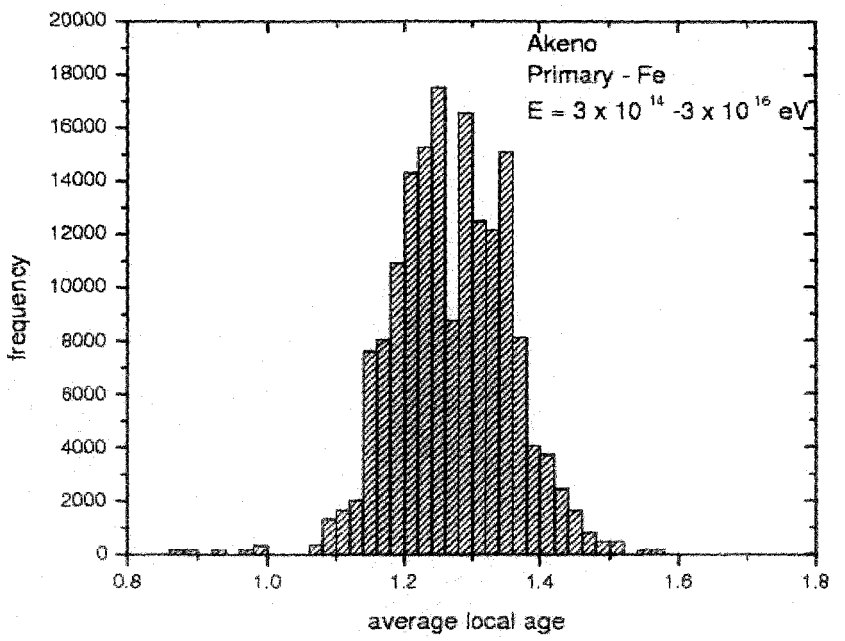
Akeno
Primary - Fe
E = 3 x 10 14 -3 x 10 16 eV
frequency
average local age
0
2000
4000
6000
8000
10000
12000
14000
16000
18000
20000
0.8
1.0
1.2
1.4
1.6
1.8

(c)

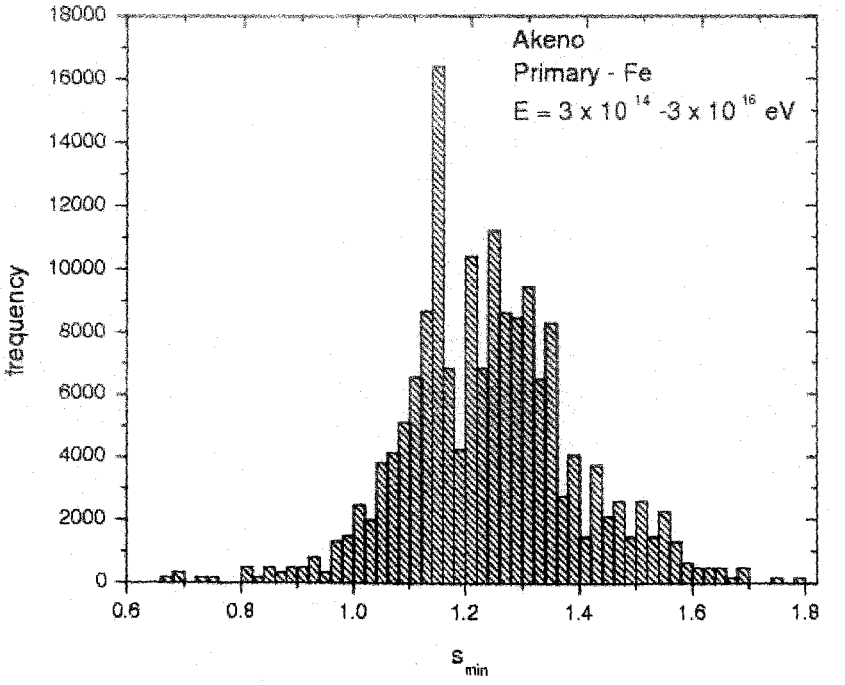
Akeno
Primary - Fe
E = 3 x 10 14 -3 x 10 16 eV
frequency
s min
0
2000
4000
6000
8000
10000
12000
14000
16000
18000
0.6
0.8
1.0
1.2
1.4
1.6
1.8

(d)

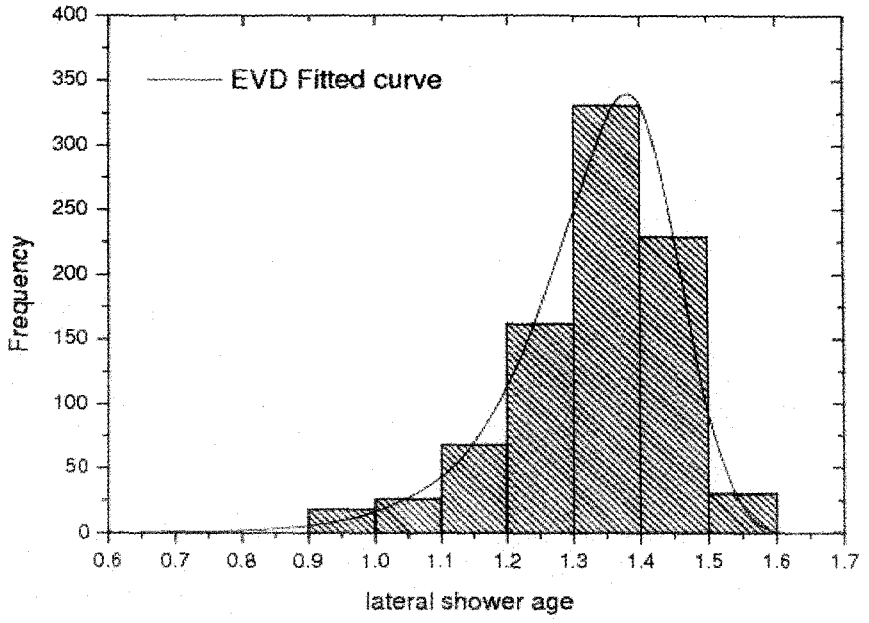
EVD Fitted curve
Frequency
lateral shower age
400
350
300
250
200
150
100
50
0
0.6
0.7
0.8
0.9
1.0
1.1
1.2
1.3
1.4
1.5
1.6
1.7

(e)

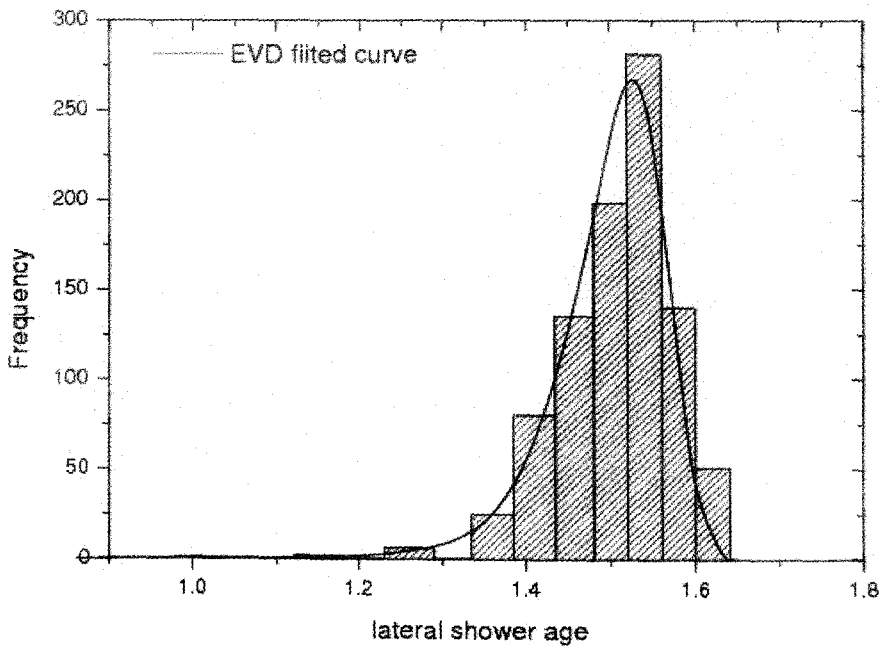
EVD fiited curve
Frequency
lateral shower age
300
250
200
150
100
50
0
1.0
1.2
1.4
1.6
1.8

(f)

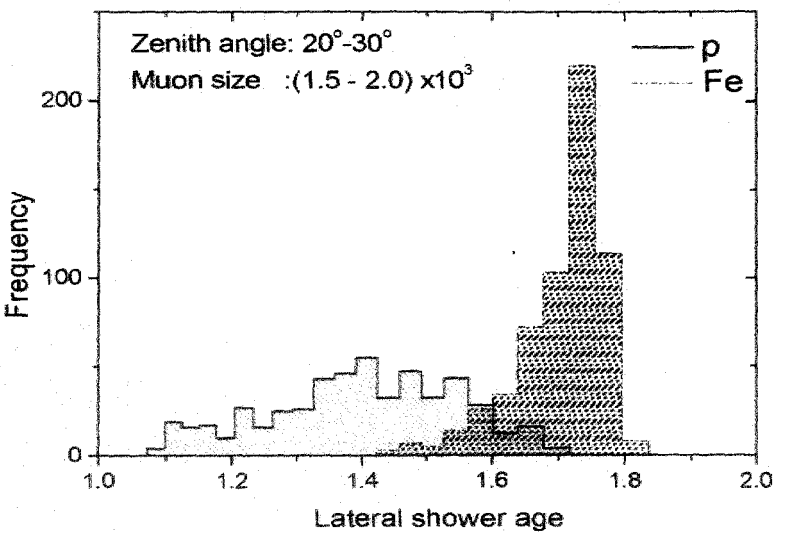

(g)

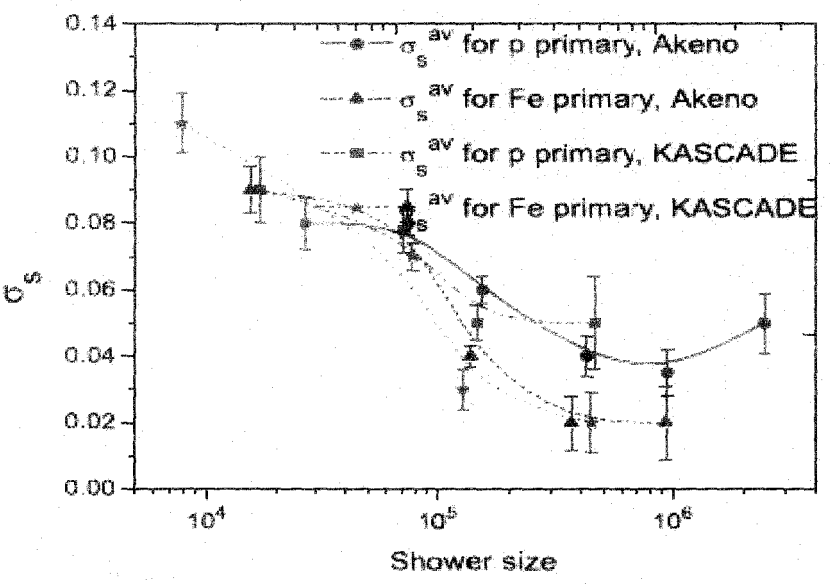

(h)

Fig.3.5: Distribution of age parameter from simulated data: (a) average local age (s_{av}) at Akeno for p primary, (b) minimum local age (s_{min}) at Akeno for p primary, (c) average local age (s_{av}) at Akeno for Fe primary, (d) minimum local age (s_{min}) at Akeno for Fe primary; (e) NKG-fitted lateral age at sea level for p primary, (f) NKG-fitted lateral age at sea level for Fe primary, (g) NKG-fitted lateral age at sea level for p and Fe primaries within a small muon window. (h) The variance (σ) of the LAP as a function of shower size. The lines are only a guide for the eye.

The fluctuations in lateral shower age are much larger for proton initiated showers in compared to those initiated by heavier primary as revealed from the **Fig.3.5**. This is clear on **Fig.3.5e** and **Fig.3.5f** where the frequencies reflect the intensities of primaries around the knee. The long tail in the left wing of **Fig.3.5f** corresponds to very penetrating proton showers of low primary energy and conversely the steep right wing contains showers interacting at very high altitude whereas the central part is populated by showers with an individual maximum close from average maximum at each energy.

Similar features concern the case of the pure iron component (see **Fig.3.5f**) with a general reduction of r.m.s. of the fluctuation. If we consider a small primary energy bin instead of a wide one, for instance by selecting the showers inside a small muon size band, we observed that both the distributions of p and Fe could be separated, which in fact becomes very contrasted as shown in **Fig.3.5g**; this approach, if adopted with the experimental data, may yield important information on the primary composition around the knee region.

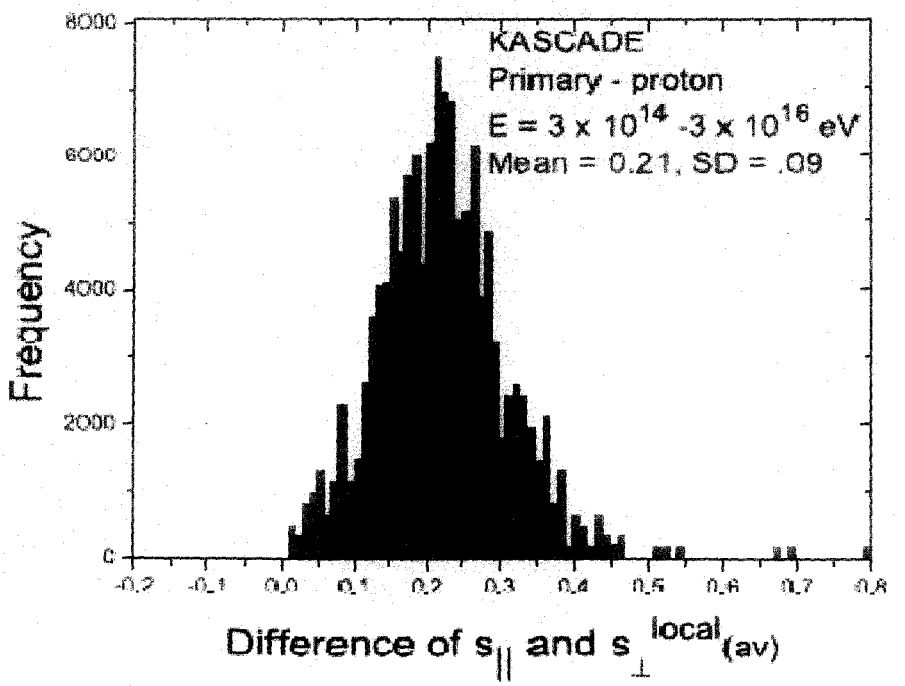

(a)

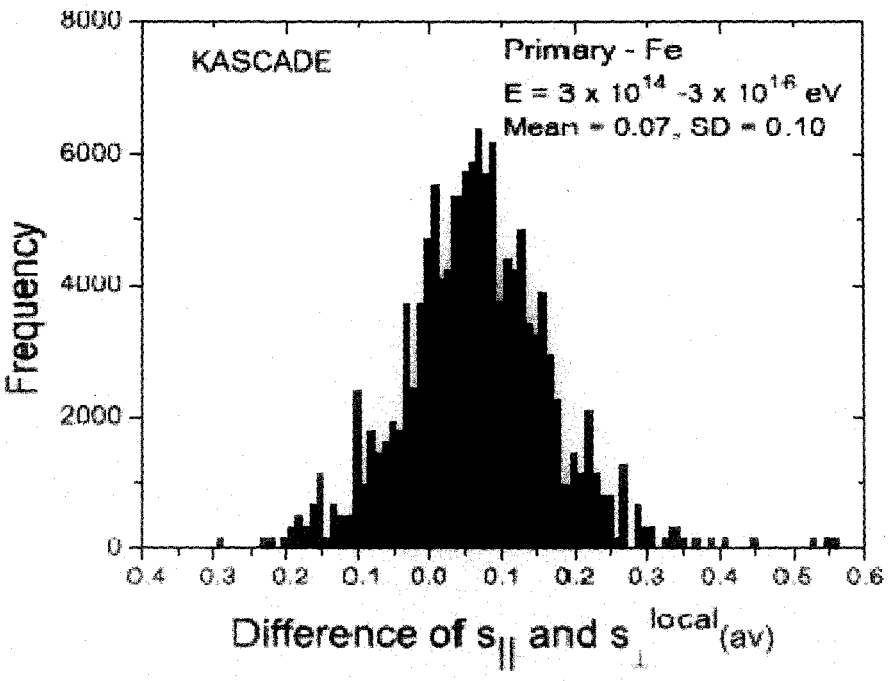
KASCADE
Primary - Fe
E = 3 x 10^14 -3 x 10^16 eV
Mean = 0.07, SD = 0.10
Frequency
8000
6000
4000
2000
0
0.4 0.3 0.2 0.1 0.0 0.1 0.2 0.3 0.4 0.5 0.6
Difference of s|| and s⊥ local(av)

(b)

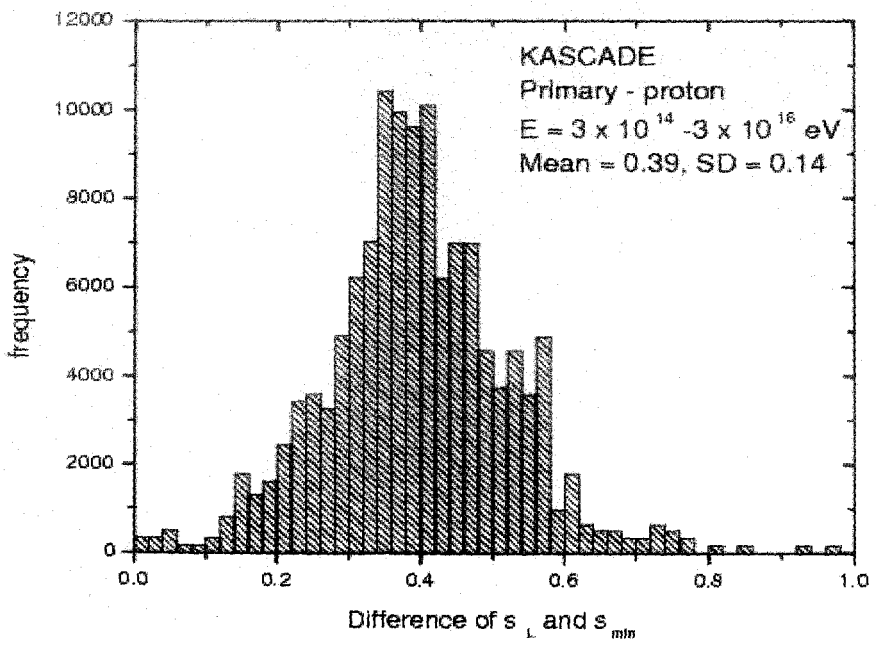
KASCADE
Primary - proton
E = 3 x 10^14 -3 x 10^16 eV
Mean = 0.39, SD = 0.14
frequency
12000
10000
8000
6000
4000
2000
0
0.0 0.2 0.4 0.6 0.8 1.0
Difference of s⊥ and smin

(c)

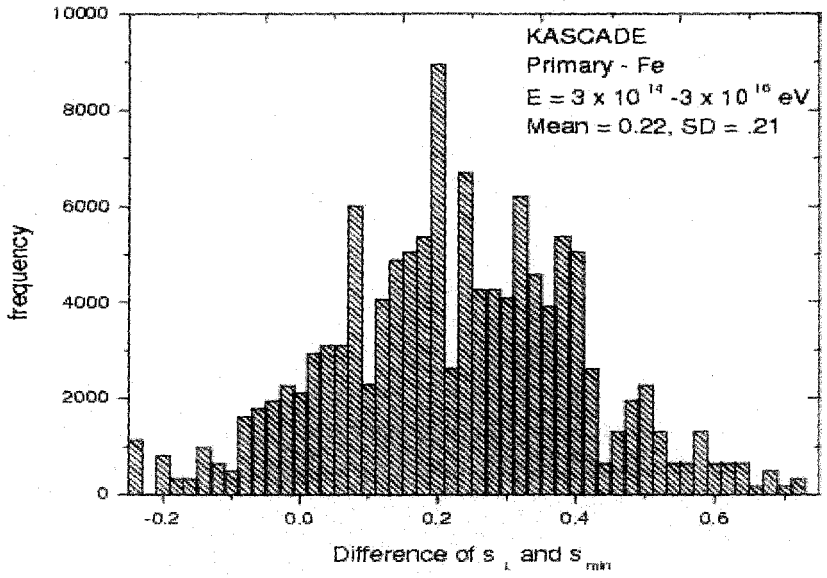

(d)

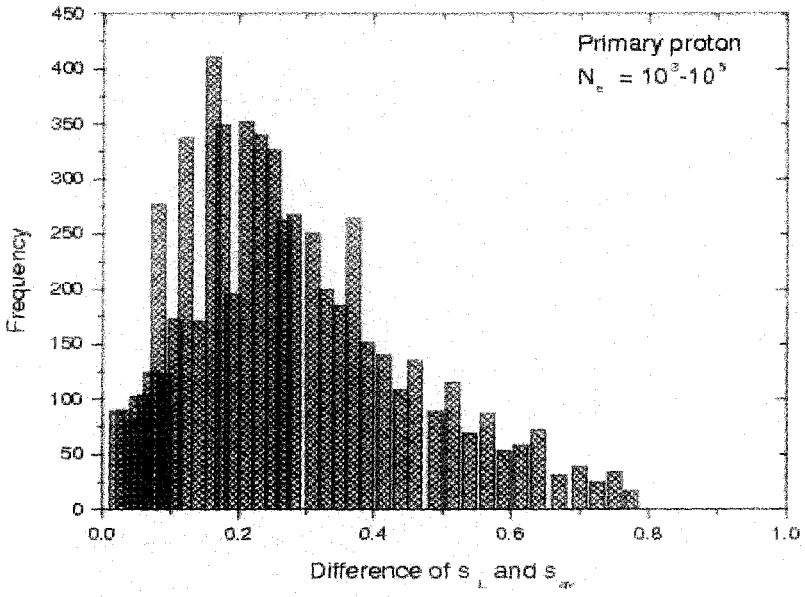

(e)

Fig.3.6: Distribution of the difference between the longitudinal shower age and average local age/minimum local age or NKG-fitted shower age from simulated data. KASCADE: $(s_{\parallel} - s_{\perp}^{local}(av))$ **(a)** p and **(b)** Fe; KASCADE: $(s_{\parallel} - s_{min})$ **(c)** p and **(d)** Fe: KASCADE: $(s_{\parallel}\text{-}\ s_{\perp}(av))$ **(e)** p.

3.5.2 THE FLUCTUATION OF SHOWER AGE PARAMETER

The fluctuations (σ) i.e. variances in the LAP in different shower age bins are estimated and as a function of the shower size are drawn in **Fig.3.5h** for proton and iron primaries for the interaction model QGSJET. In accordance with experiments (Catz et al. 1973), the fluctuations in the LAP were found to be larger for the proton initiated showers in comparison to those initiated by the primary iron, except at lower energies. Similar trends have been found from simulated data when the lateral age parameter and its fluctuation were in use (Dey et al. 2011).

3.5.3 LONGITUDINAL AGE VERSUS LATERAL AGE

For each simulated event the longitudinal shower age has also been estimated exploiting the relation (**3.9**) (or directly obtained longitudinal age delivered by the output of the NKG option of CORSIKA) and the difference between the two age parameters, longitudinal age ($s_{\parallel}$) and average local age $s_{\perp}^{local}(av)$ or NKG fitted lateral age ($s_{\perp}$) is obtained. A frequency distribution of a number of differences between two age parameters at KASCADE site is given in **Fig.3.6**.

The frequency distributions of the differences between two age parameters ($s_{\parallel}$) and $s_{\perp}^{local}(av)$) for proton and Fe primaries are given in **Figs.3.6a – 3.6b**. The frequency distributions of the differences between two age parameters ($s_{\parallel}$ and s_{min}) for proton and Fe primaries are given in **Figs.3.6c – 3.6d**. From **Figs. 3.6a** and **3.6b**, it is clear that the frequency distribution for proton primary exhibits peak, at around 0.2, is consistent with the early observations (Capdevielle & Gawin 1982, Bourdeau et al. 1980, Capdevielle et al. 1990, Dedenko et al. 1975 & Stamenov 1987), whereas for Fe initiated showers the peak difference is much lower, at about 0.07. However, for a non-negligible fraction of events, the differences between the two shower age parameters were found to be substantial. The same study has been made using simulated data at Akeno site for proton and iron primaries in the concerned energy range and the distributions are shown in **Figs.3.7a – 3.7d**.

For the EGS4 data at 10^{18} eV at Akeno site we estimated the average local age between 50 m to the radius of shower disk as may be revealed to an EAS array equipped with particle detectors of area ~ 1 m^2 and found that such an average age is very close to the longitudinal age.

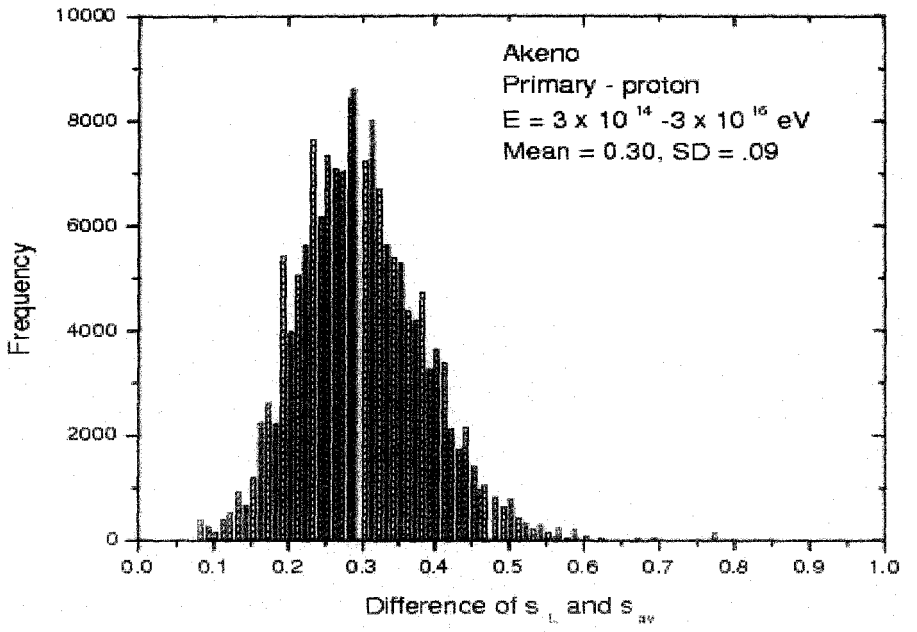
Akeno
Primary - proton
E = 3 x 10 14 -3 x 10 16 eV
Mean = 0.30, SD = .09
Frequency
Difference of s L and s av
10000
8000
6000
4000
2000
0
0.0
0.1
0.2
0.3
0.4
0.5
0.6
0.7
0.8
0.9
1.0

(a)

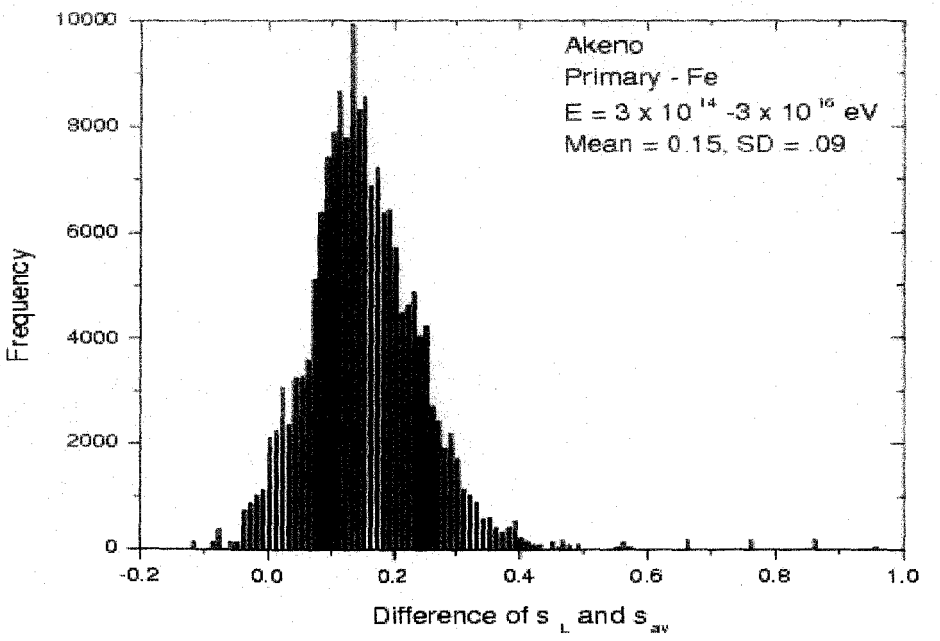
Akeno
Primary - Fe
E = 3 x 10 14 -3 x 10 16 eV
Mean = 0.15, SD = .09
Frequency
Difference of s L and s av
10000
8000
6000
4000
2000
0
-0.2
0.0
0.2
0.4
0.6
0.8
1.0

(b)

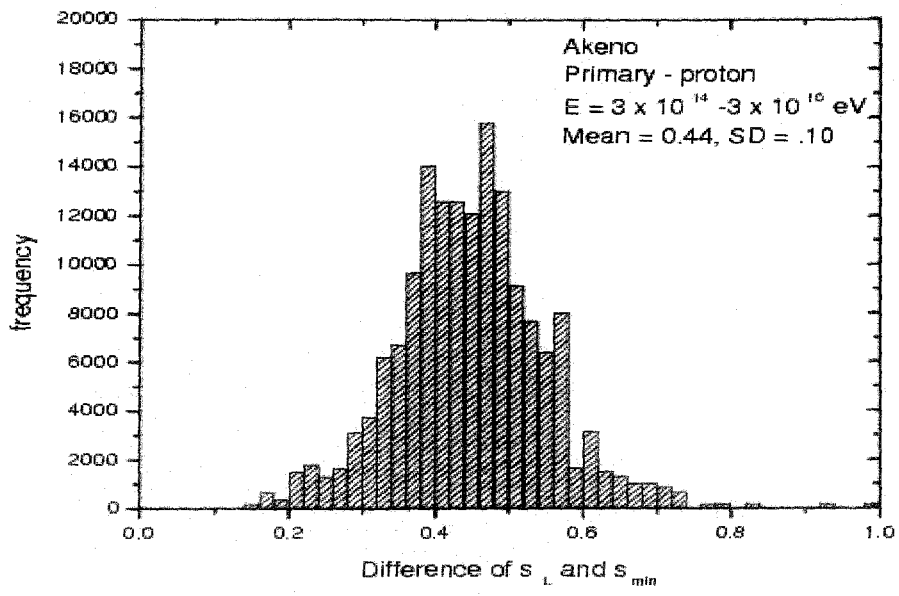

(c)

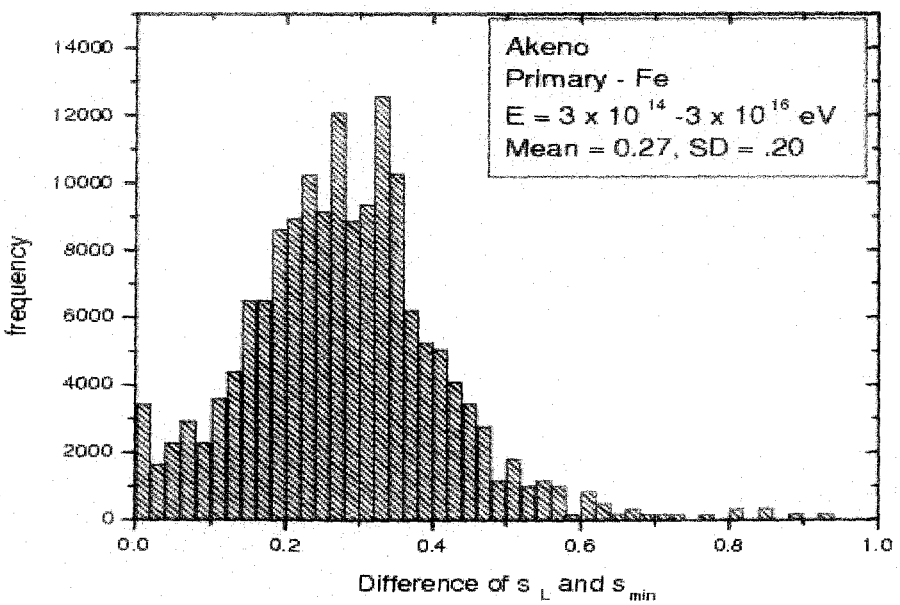

(d)

Fig.3.7: Distribution of the difference between the longitudinal shower age and average local age/minimum local age from simulated data. Akeno: $(s_{\parallel} - s_{\perp}^{local}(av))$ **(a)** p and **(b)** Fe; Akeno: $(s_{\parallel} - s_{min})$ **(c)** p and **(d)** Fe.

3.6 THE CORRELATION OF SHOWER AGE PARAMETER WITH OTHER EAS OBSERVABLES

3.6.1 VARIATION OF LATERAL SHOWER AGE WITH ATMOSPHERIC DEPTH

With the increase of zenith angle a shower traverses an increased thickness of atmosphere which immediately suggests that the EAS with higher zenith angle should be older in shower age than the EAS of smaller zenith angle but of same primary energy. Based on this idea we have studied variation of lateral shower age with atmospheric depth from the simulated data.

The **Fig.3.8a** shows the lateral shower age as a function of $\sec(z)$ for two primary energy intervals at NBU site. Separate samples of proton and Fe initiated showers are considered to investigate the said aspect. The variation of local shower age with atmospheric depth has also been studied for fixed primary energy range which is shown in **Fig.3.8b**. In **Fig.3.8c**, we plot the same variation but for muon size intervals at KASCADE site.

It is seen from the **Fig.3.8** that for both proton and Fe initiated showers the local/lateral shower age monotonically increases with atmospheric depth reflecting a strong correlation of the parameter with longitudinal development.

In order to check the influence of the hadronic interaction models on the results we compare NKG lateral shower age versus atmospheric depth variations for two different models, the QGSJET and the SIBYLL, which is shown in **Fig.3.8a**. The SIBYLL gives comparatively higher value of lateral shower age but the nature of dependence of lateral shower age on atmospheric depth is found similar in both the two hadronic interaction models. This discrepancy may come from the cross section for p-air collisions rising more rapidly versus energy in SYBILL than in QGSJET.

The present simulation study suggests that the lateral shower age/local age can be expressed as a function of zenith angle by the empirical relation

$$s_{\perp} = s_0 + A \sec(z) \qquad (3.11)$$

The value of s_0 and A for different shower size ranges can be obtained by fitting the simulated data generated with either QGSJET or SIBYLL.

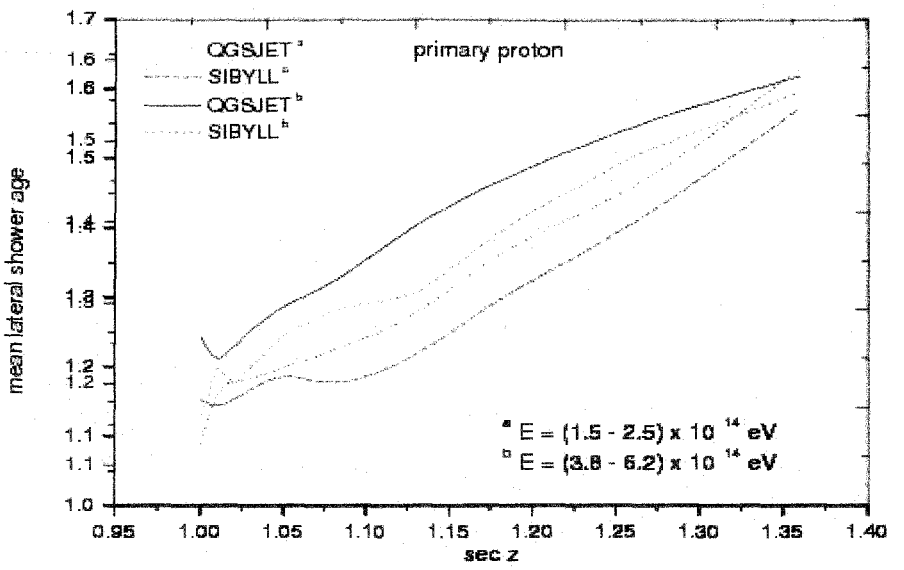

(a)

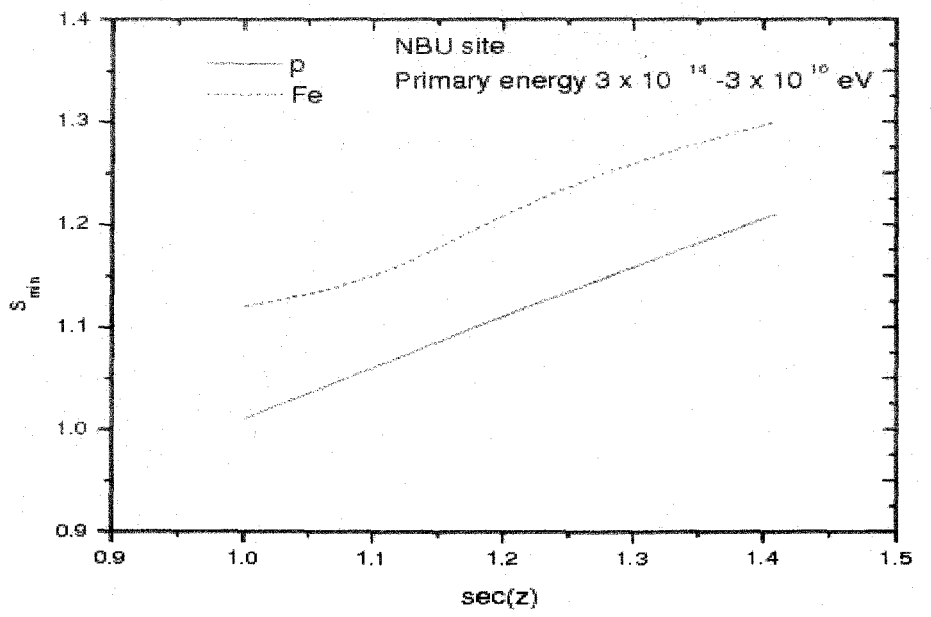

(b)

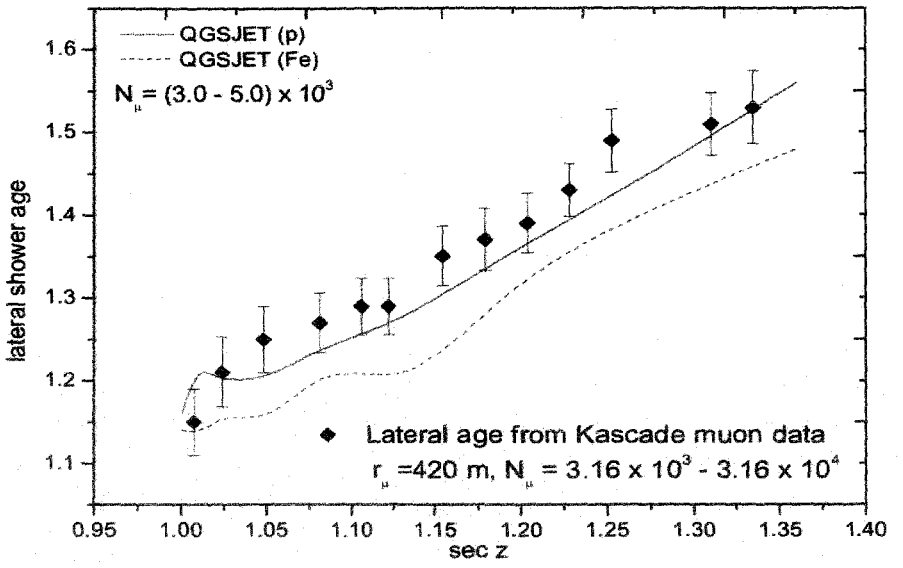

(c)

Fig.3.8: Variation of shower age with atmospheric depth (a) lateral shower age at NBU site for two fixed primary energy intervals and hadronic models, (b) minimum local age at NBU site for a fixed primary energy range and (c) lateral shower age at KASCADE site for a fixed muon size interval along with lateral shower age from KASCADE observed muon lateral distribution data.

Equation (**3.11**) can be written as $s_{\perp} = s_0 + A\frac{x}{x_v}$, where x and x_v are the atmospheric thickness travelled by the EAS and vertical atmosphere depth respectively. It thus immediately follows $\frac{ds_{\perp}}{dx} = \frac{A}{x_v}$. The change of lateral shower age over an atmospheric depth of 100 gm-cm^2 for the simulated data generated with QGSJET lies within $(2 - 4)\times 10^{-2}$ corresponding to the shower size range $10^3 - 10^4$.

3.6.2 VARIATION OF LATERAL SHOWER AGE WITH ELECTRON SIZE

The variation of the local shower age at a radial distance of about 50 m (minimum value) or mean lateral shower age (NKG-fitted) with average shower size, obtained from the simulated results for both proton and iron primaries at the Akeno, KASCADE and NBU locations are presented in **Figs. 3.9a - 3.9c**. The corresponding observational results extracted from the Akeno and KASCADE experimental data are also shown in **Fig.3.9a** and **Fig.3.9b**. For Akeno

experimental data, we extracted a minimum local age for the different shower sizes from reference (Nagano et al. 1984[b]), whereas for KASCADE we estimated it from their measured lateral distribution (Antoni et al. 2001, Apel et al. 2006, Ulrich et al. 2008 & 2009[a]). We note here that being a small EAS array, the radial density measured by the NBU EAS array was restricted to much smaller core distances in compared to the KASCADE or Akeno experiments. As a result shower size estimated by the array, particularly at higher energies corresponding to large electron sizes, may have considerable uncertainties and hence resolving power of the array in respect to primary mass composition is expected to be limited. On the other hand, in the KASCADE or Akeno measurements shower size is basically estimated through NKG fitting considering particle densities up to a larger core distance for EAS with higher primary energies. In view of the radial variation of lateral age such a procedure of estimating shower size may involve some bias on the estimated shower size though the magnitude of such systematic error is not large.

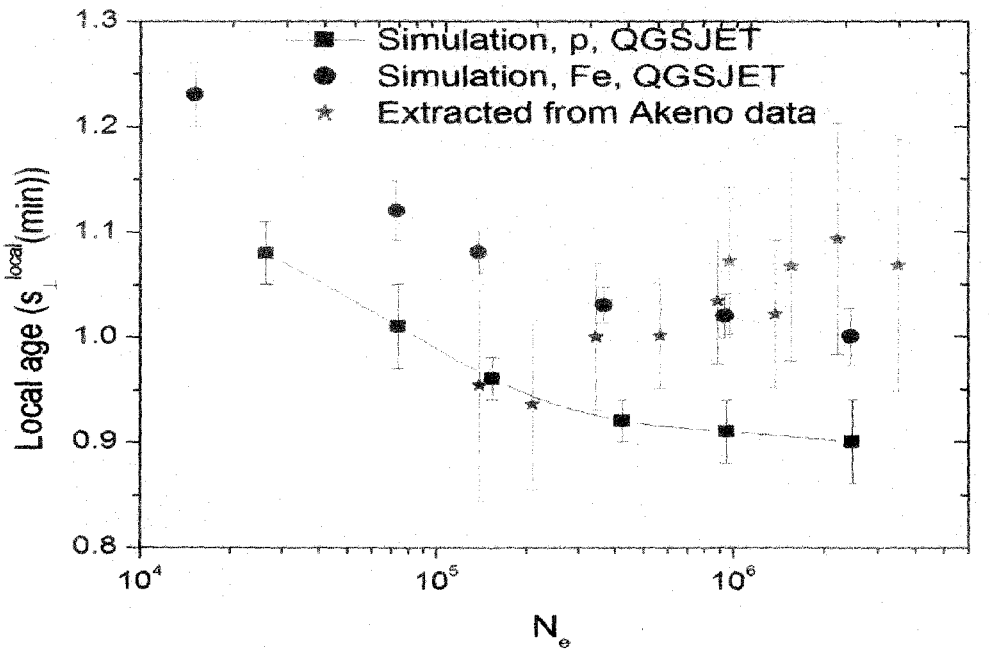

(a)

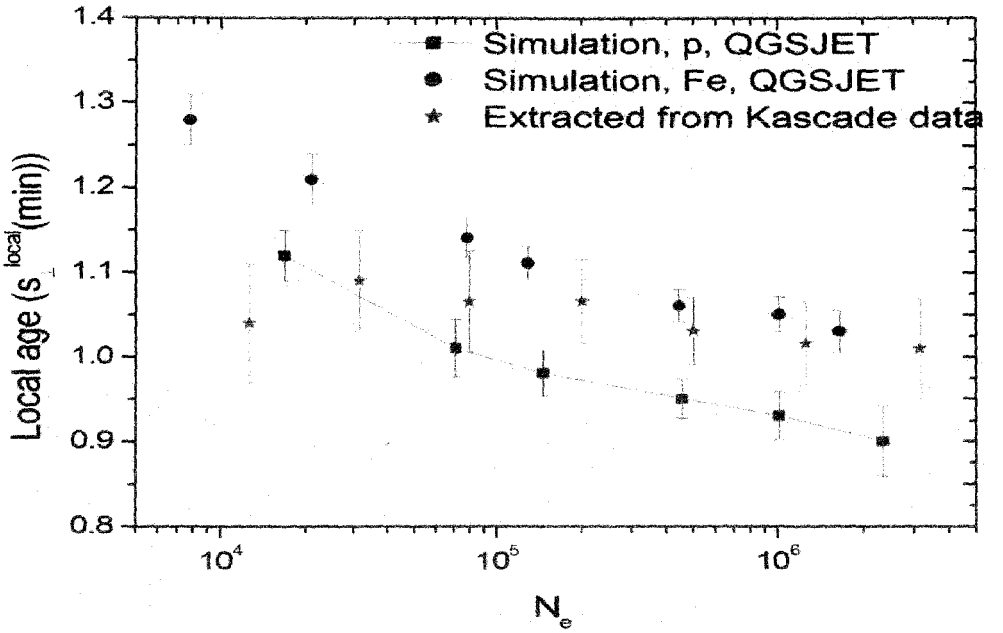

(b)

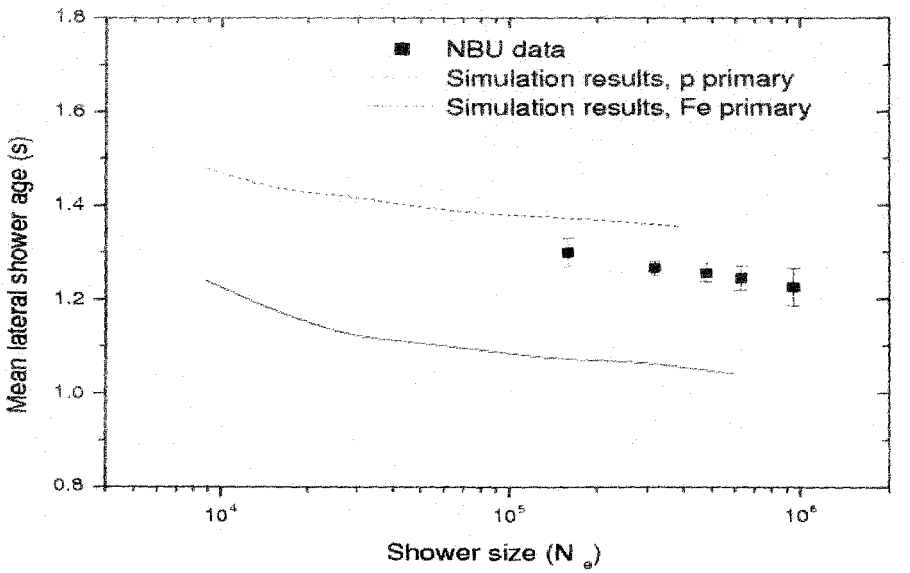

(c)

Fig.3.9: Variation of the lateral shower age with electron size for proton and Fe primaries at (a) Akeno, (b) KASCADE and (c) NBU locations. For KASCADE and Akeno data the estimated minimum value of the local age is used while for NBU data the lateral age is estimated through the traditional shower reconstruction method.

It is noticed from the figures that the local or lateral shower age decreases with shower size but the rate of decrease slows down at higher shower size. With increasing primary energy i.e. with increasing shower size showers penetrate deeper into the atmosphere resulting in steeper lateral distribution indicated by the smaller lateral shower age parameter (Apel et al. 2006). The simulation results show that showers induced by heavier primaries are older compared to those generated by light primaries. The similarity found in the variation of shower age with shower size for two hadronic interaction models QGSJET and SIBYLL indicates that the longitudinal development of the electromagnetic component is alike in both the models.

The comparison of the simulated results with the experimental observations from both the Akeno and KASCADE EAS experiments (**Figs. 3.9a** and **3.9b**) indicate a need for a change in the primary composition towards a heavier primary, as the energy increases across the *knee* of the primary energy spectrum. The KASCADE group also reached a similar conclusion using the shape parameter instead of the shower age (Apel et al. 2006), as well as from the study of the muon content in EAS (Antoni et al. 2002). The present data of the LHC, especially the pseudo-rapidity density distributions, suggest larger multiplicities and inelasticities than in the models used in the CORSIKA simulations (Capdevielle 2010). However, up to energy of 2.6×10^7 GeV, this could result in a very small reduction of the reported enhancement of the primary mass with energy.

3.6.3 VARIATION OF THE LATERAL SHOWER AGE WITH MUON SIZE

The variation of local/lateral shower age with muon size has also been studied for the zenith angle range 0^0 - 45^0 for both proton and iron primaries and are plotted in **Fig.3.10a** and **3.10b** at Akeno, and KASCADE levels. The variation exhibits the same nature as obtained in the KASCADE experiment using NKG fitting for muons with slightly higher threshold energy (Antoni et al. 2001). With increasing primary energy i.e. with increasing muon size showers penetrate deeper into the atmosphere resulting in steeper lateral distribution indicated by the smaller lateral shower age parameter (Apel et al. 2006). The simulation results show that showers induced by heavier primaries are older compared to those generated by light primaries. The similarity found in the variation of shower age with muon size for two models QGSJET and SIBYLL revealing once again that the longitudinal development of the electro-magnetic component is independent of the hadronic interaction models.

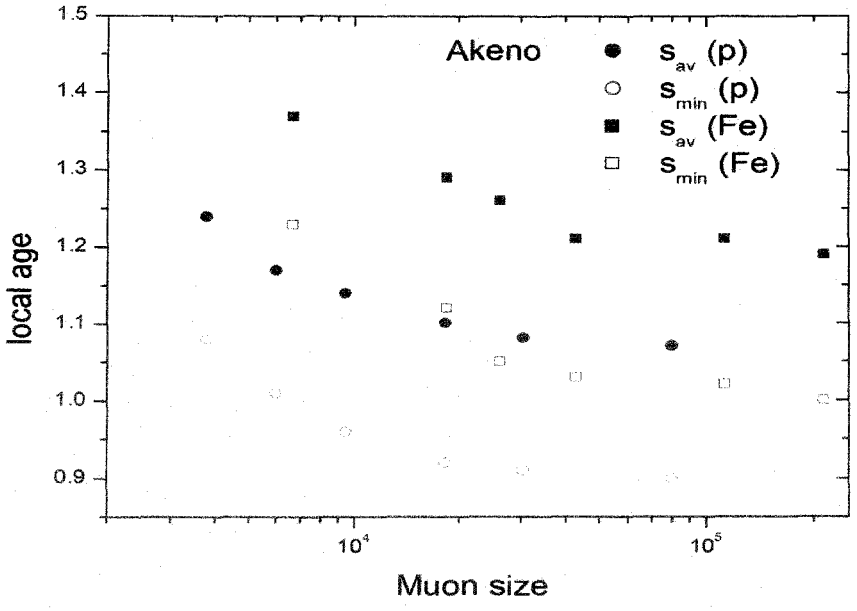

(a)

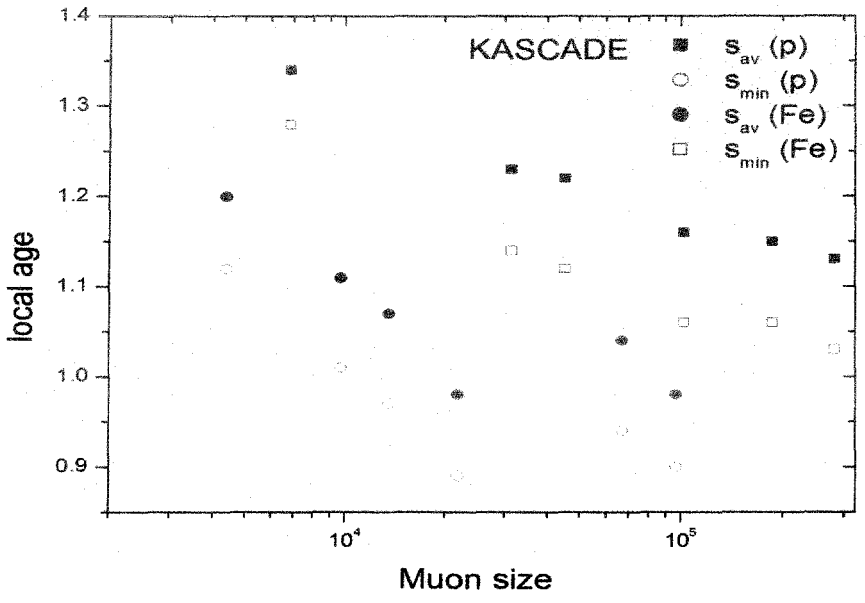

(b)

Fig.3.10: Variation of average/minimum value of the local age with muon size for p and Fe (a) at Akeno and (b) at KASCADE locations.

3.6.4 THREE DIMENSIONAL VARIATION OF N_e, N_μ and s

Muon content of EAS generally used to extract information on the composition of cosmic ray primaries. However, as mentioned earlier due to uncertainties in the interaction model and the difficulties associated with the solutions to the EAS inverse problem, separating the primary energy spectra of elemental groups remains ambiguous. Iron and proton initiated showers may be better separated employing shower age and muon content simultaneously through 3-dimensional plot of shower size and shower age than in either of its 1-dimensional projections. It is also found that accuracy of determining the nature of primary species increases with the simultaneous use of shower age and muon content.

In **Fig.3.11** we plot the 3-dimensional curve between average local shower age at a radial distance about 50 m (minimum value), average shower size and muon size obtained from simulation results for both proton and iron primaries at Akeno and KASCADE levels. The corresponding observational results of the Akeno and KASCADE experiments are also given in the figures. For the Akeno experimental data we extract the minimum local age for different shower sizes from (Nagano et al. 1984[b]) whereas the mean muon content corresponding to those shower sizes are obtained from reference (Dixon & Turver 1974). In the case of KASCADE data, we estimated local age from their measured lateral distribution (Antoni et al. 2001, Ulrich et al. 2008 & 2009[a]) and corresponding muon size are extracted from the $N_e - N_\mu$ curve (Werner et al 2006, Pierog & Werner 2008[a]).

The comparison of simulated results with experimental observation from both the Akeno and KASCADE EAS experiments indicate for a change in primary composition towards heavier primary as energy increases across the *knee* of the primary energy spectrum. The KASCADE group also reached the same conclusion using slope parameter instead of shower age.

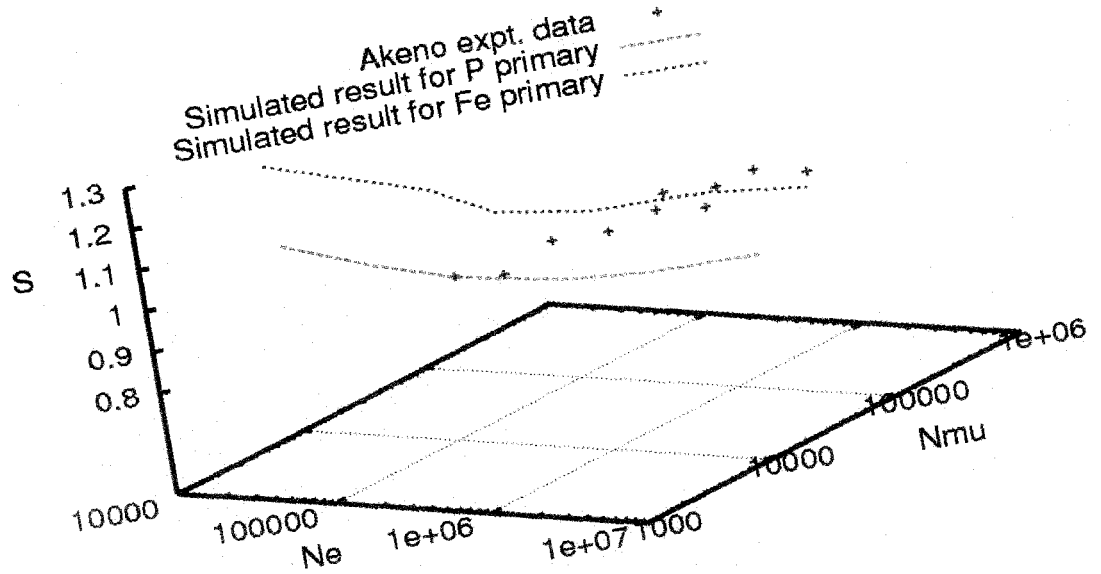

(a)

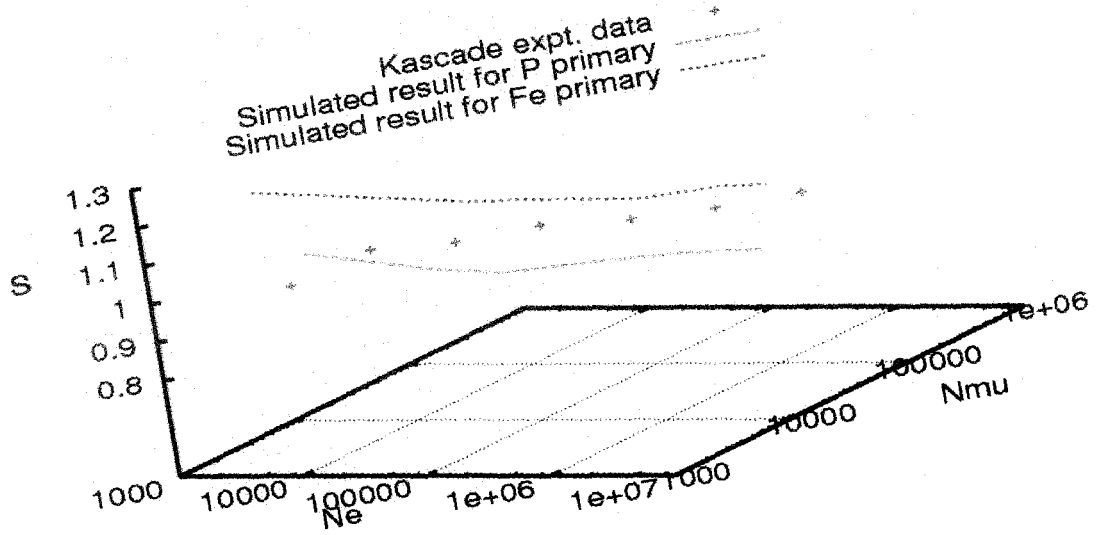

(b)

Fig.3.11: 3-Dimensional plot between shower size, muon size and mean local shower age for proton and Fe primaries at (a) Akeno and (b) KASCADE locations.

3.7 CONCLUSIONS

From the present analysis we conclude the following:

1. The lateral distribution of electrons in EAS exhibits some sort of *scaling* (energy independent) behaviour in terms of the local age. The characteristic feature of the local age versus the radial distance curve is that with an increase of the radial distance, the local age decreases initially and reaches a minimum at around 50 m then it starts increasing, attaining local maxima at around $300-400$ m, and then starts decreasing again. Such a feature appears to be independent of the energy of the EAS initiating particle, at least there is no strong dependence on the primary energy. Such a characteristic radial variation in the local age is found as a generic feature of electromagnetic cascades.
2. The local age offers a good solution towards an unambiguous estimation of the shower age. Since the shower age varies with the radial distance, even for the modified NKG functions, a comparison of the lateral shower age of different EAS experiments is not meaningful, as the radii of the shower discs naturally differ from experiment to experiment, depending on the experimental set up. Even in a single EAS experiment different events have different radial extensions and thus a lateral age obtained through fitting with the NKG function seems ambiguous. The local age at a particular distance (say at about 50 m where it takes the minimum value) is, however, not always practical owing to the large fluctuation in the electron density data in a real measurement. A rational idea could be to take some sort of average local age between the first minimum, at around a core distance of 50 m, and the subsequent local maximum, at around 300 meter. Experimentally the radial variation of the LAP can be checked properly with a full coverage detector array, like ARGO-YBJ (Pierog & Werner 2008[b]). Note that at smaller distances before the first minimum the detectors of EAS experiments often exhibit saturation effect leading ambiguous electron densities at that region.
3. Use of a modified NKG function or more specially employing a reduced Moliére radius in NKG function leads to a constant shower age over a radial distance up to about 350 m but the magnitude of shower age estimated in such a manner is found to be quite higher in comparison with that of

longitudinal age. But even with such reduced Moliére radius, local age is found to decrease sharply after say about 400 m.

From the study of local age in gamma ray initiated showers, it is found that the parameter varies with radial distance and the radial variation of the parameter is alike to what we observe in the case of hadron initiated showers. Which implies that the radial variation of local age in hadron initiated showers is not due to superposition of several gamma ray induced showers but it further reveals the generic feature of pure electromagnetic cascades.

4. The lateral age offers a good estimator of the longitudinal development of an EAS cascade, as already noted in some earlier works (Capdevielle & Gawin 1982, Bourdeau et al. 1980, Capdevielle et al. 1990, Stamenov 1987, Dixon & Turver 1974). However, the parameter correlates with the stage of the shower development on a statistical basis; the average of this parameter increases as air showers traverse an increased thickness of atmosphere. The experimental observations (Bhadra 1999) also substantiate such behaviour. The slope of lateral shower age versus atmospheric depth curve is, however, more or less the same for proton and iron initiated showers. The distribution of the differences between the local age and the longitudinal age also indicate the strong correlation between the two ages. Such a feature has been noted for two different hadronic interaction models, the QGSJET and the SIBYLL, and hence appears robust. It is imperative to examine such correlations using EPOS (Werner et al. 2006, Pierog & Werner 2008[a]), the only model that seems to be providing quite a consistent description of the longitudinal and lateral EAS profiles (Pierog & Werner 2008[b]), which would need to be performed in future work.

   The distribution of differences between local or lateral shower age and longitudinal age also indicate the strong correlation between these two ages.

5. The fluctuation of the LAP was found to be sensitive to the nature of the primary particle. However, the level of uncertainty in determining the lateral shower age from the experimental data is comparable with the magnitude of fluctuation and hence deriving any firm conclusion on the nature of the primary only from the shower age fluctuation is difficult. If showers within a small bin of the primary energy could be selected, for instance by considering shower events in a small muon size interval, the distribution of shower age was found to be quite sensitive on primary composition.

6. The local/lateral shower age takes higher value for iron initiated showers in compared to that of proton initiated which means that lateral distribution of electrons for iron initiated EAS is flatter relative to that of proton initiated EAS. This feature is reflected in the variations of shower age with both electron size and muon content independently. The comparison of the simulated results with the Akeno and the KASCADE observations in respect to a variation of the shower age with shower size around the *knee* indicates a change in the primary composition towards heavier primaries across the *knee*. This finding supports the results obtained from the study of the muon content in EAS.
7. For the study of primary composition the 3-*dimensional* plot of shower size versus muon size and shower age seems to offer better accuracy in compare to the more conventional approach of implementing it through the shower size versus muon size curve. It would be an interesting task to apply such 3-*dimensional* plot to obtain the composition of primary cosmic rays using observed EAS data from a closely packed air shower array with the facility of concurrent muon measurements such as the GRAPES experiment at Ooty (Gupta et al. 2005).

APPENDIX A

ELEMENTS ON THE THEORY OF THE ELECTROMAGNETIC CASCADE

The one dimensional (1D) and the three dimensional theories (3D) are distinguished based on whether the theory addresses just longitudinal or both lateral and longitudinal shower development. In the analytic approach the time distribution can be derived from the solution of the 3D model providing the densities of the particles and their energy distributions. The 4D simulation is more generally reserved to the MC approach where electrons and photons are followed simultaneously in space-time coordinates (Heck et al. 1998 & Capdevielle 1992).

A.1 *Approximations in the theoretical model of the cascade diffusions equations*

The *Approximation A* neglects the ionization losses taking into account the radiation process and the pair creation process. It allows establishing from the elementary gains and losses in particles and energy. In the case of the 1D theory the simplest system of transport equations which are perfectly symmetric (Nishimura J 1967) is given by

$$\frac{\delta\pi}{\delta t} = -A'\pi + B'\gamma \qquad (A1)$$

$$\frac{\delta\gamma}{\delta t} = -\sigma_0\gamma + C'\pi \qquad (A2)$$

We use here the notations of Nishimura in (Nishimura 1967), $\pi(E,t)dE$ and $\gamma(E,t)dE$ representing respectively the average numbers of electrons and photons with energy between E and $E+dE$ at a depth t in radiation lengths. The operators A' and B' correspond respectively to the losses in electron number by bremsstrahlung and gains by pair productions, whereas the operators σ_0 and C' describe the gain in number of photons by C'. C' is calculated in the assumption of complete screening.

The *Approximation A* is better adapted to the growing phase of the cascade and to high energy photons and electrons. The *Approximation B* is more realistic one. In addition to the approximations stated under *Approximation A* it also incorporates the effect of the ionization loss $\epsilon\frac{\delta\pi}{\delta t}$, thus the equation (A1) becomes,

$$\frac{\delta\pi}{\delta t} = -A'\pi + B'\gamma + \epsilon\frac{\delta\pi}{\delta E}. \qquad (A3)$$

In parallel, the 3D diffusion equations can be inferred after introducing the functions $\pi(E,r,\theta)$ and $\gamma(E,r,\theta)$. For instance, in the case of the *Approximation B* they take the simple form in the so called Landau approximation:

$$\frac{\delta\pi}{\delta t} + \theta\frac{\delta\pi}{\delta r} = -A'\pi + B'\gamma + \epsilon\frac{\delta\pi}{\delta E} + \frac{E_s^2}{4E^2}\left(\frac{\delta^2\pi}{\delta\theta_1^2} + \frac{\delta^2\pi}{\delta\theta_2^2}\right) \qquad (A4)$$

$$\frac{\delta\gamma}{\delta t} + \theta\frac{\delta\gamma}{\delta r} = -\sigma_0\gamma + C'\pi \qquad (A5)$$

The more general differential description in *Approximation B* without Landau simplification is obtained by replacing in this last system equation (A5) by the expression

$$\frac{\delta\pi}{\delta t} + \theta\frac{\delta\pi}{\delta r} = -A'\pi + B'\gamma + \epsilon\frac{\delta\pi}{\delta E} + \int[\pi(\theta-\theta') - \pi(\theta')]\sigma(\theta')d\theta' \qquad (A6)$$

The multiple Coulomb scattering governs the lateral deflections submitted by the electrons passing through the atmosphere. The small angle approximation owing a simple expression of the mean scattering angle when the electron passes through an elementary thickness dt is an important step to express the equilibrium described by the equations (A4-5) and (A6), especially (A4-5) with the Landau approximation.

A.2 *Approximations in the Numerical treatment*

The differential equations (A4) and (A5) were solved after application of the Hankel transform to r, Mellin transform to E and Laplace transform to t (Nishimura 1967, Kamata & Nishimura 1958). Retransformations from the solutions expressed in terms of complex functions required further approximated steps, the most important being the saddle point method. The final result expressed

in numerical densities was again fitted with a tolerable agreement with the so called NKG formula following an earliest Nishimura formula.

Another approach to solve the system of equations (A4-5) was performed by the method of adjoint equations (Lagutin et al. 1979 & Uchaikin et al. 1979) and the resulting structure functions were found steeper. Here also several numerical approximations had to make to get the solution.

Surprisingly, $\rho_{el}(r)$ which has not been checked above 10^{17} eV was used *in extensor* to calculate the radio synchrotron emission in giant extensive air showers (Suprun et al. 2003): recalculating those densities with *CORSIKA-EGS4*, we observed that the discrepancies remains small for axis distances lower than $3r_m$ containting fortunately the largest part of the source of radio emission or fluorescence in EAS.

A.3 *Analytic and Monte Carlo solutions*

The calculation of the electrons and photons spectra in shower of the same age obtained by Rossi and Greisen has the limitations that are intrinsic to the realistic but simplified theoretical framework (*Approximation B*) that has been used. This framework introduces several simplifications: the cross-sections for bremsstrahlung and pair-production have always the asymptotic form that is strictly speaking only valid at very high energy, the electron collision losses are treated as a simple energy independent constant, and Compton scattering is entirely neglected. Also in *Approximation B* the electron mass is neglected and the electron spectrum extends down to zero energy. A MC calculation of the spectral shapes can of course avoid all these limitations and is in principle more accurate, even if it has its own limitations and difficulties.

A comparison of the Rossi-Greisen shapes with the numerical results, show remarkable agreement but also some small differences, which could be interesting to explore in more detail. As an illustration, normalizing the high energy spectra to $\pi(E,s)) \rightarrow E^{-(s+1)}$, the quantity

$$s\int_0^\infty dE\pi_e(E,s) \qquad (A7)$$

is given by the function $K_1(s,-s)$ for the Rossi-Greisen calculation. The numerical integration of the Nerling *et al* parameterization (Giller et al. 2005 & Nerling et al.

2006) gives results that differ by 5 - 10 %. The parameterization for the electron spectrum has the form:

$$\pi_e(E,s) = \frac{1}{[E + a_1(s)][E + a_2(s)]^s} \qquad (A8)$$

that has manifestly the same asymptotic behaviour as the Rossi-Greisen shape at both low and high energy: $\pi_e(E) \rightarrow$ constant for $E \rightarrow 0$, and $\pi_e(E) \propto E^{-(s+1)}$ for $E \gg \varepsilon$ (ε being the critical energy).

For the Nerling parameterization the first coefficient is $c_1(s) = -[a_1(s) + sa_2(s)]$, which differs slightly from the coefficient as predicted from Rossi-Greisen solution beyond $s > 1$. The origin of the (small) difference between the analytic and MC solutions (i.e. numerical one) merits further studies. A possible explanation is a more precise description of the physics of the electromagnetic interactions in the MC calculation.

A.4 *Age parameter in longitudinal and lateral developments*

The shower age parameter (s) was first derived from the solution of equations (A1-2) using Mellin transformation, s being the variable in the complex plane. The total number of electrons (obtained by the inverse Mellin transformation) is obtained for $s = \bar{s}$ following the relation,

$$\lambda_1'(\bar{s})t + log\frac{E_0}{E} - \frac{1}{\bar{s}} = 0 \qquad (A9)$$

Taking into account the elementary solutions (where $\lambda_1'(\bar{s})$ is a function varying slowly), the relation between s and t was derived from the approximation at cascade maximum

$$\frac{\delta\bar{s}}{\delta t}\left(\lambda_1'(\bar{s})t + log\frac{E_0}{E} - \frac{1}{s}\right) + \lambda_1(\bar{s}) = 0 \qquad (A10)$$

and the general properties of s were established by the fact that the maximum of the cascade is at $s = 1$, the cascade is developing (growth) when $s \leq 1$, whereas it is decaying (absorption) if $s \geq 1$.

Those considerations in *Approximation B* are brought through the relation (**3.2**) for $s_{||}$, the so called Greisen formula for longitudinal development, along with

the relations (**3.1**) and (**3.4**). One of the clearest presentations of the qualitative relation between longitudinal shower age parameter and the lateral profile of the cascade under *Approximation B* was demonstrated by Cocconi (Cocconi 1961) showing that a lateral distribution is becoming flatter when $s \geq 1$ of course for $s_{||} = s_{\perp}$. The case of relation (**3.3**) for $s_{||}$ was also considered by Cocconi and Nishimura to take into account some effects of density resulting of the atmospheric inhomogeneity. Relation (**3.4**) has several advantages passing from an asymptotic tendency near axis when $r \to 0$ following r^{s-2} to a steeper power law when $r \to \infty$.

The problem of calculating the electron lateral distribution has attracted considerable in the past. Nishimura and Kamata solved numerically the 3-dimensional equations in *Approximation B* to obtain the (energy integrated) lateral distribution of electrons propagating in medium of constant density. Their results were fitted by Greisen (Greisen 1956 & 1960) with the approximate form:

$$\rho_{NKG}(r, s_{\perp}) = N_e f(r)_{NKG} = N_e C(s_{\perp})(\frac{r}{r_m})^{s_{\perp}-2}(1+\frac{r}{r_m})^{s_{\perp}-4.5} \quad (A11)$$

After these works several other authors have given different parameterization of the lateral distribution as a function of an age parameter.

The NKG function is based on the Eulerian Beta function, $B(u,v)$, taken here in the case of cylindrical symmetry, from:

$$N_e = \int_0^{\infty} 2\pi r \rho_{NKG}(r) dr \quad (A12)$$

$$= 2\pi C(s_{\perp}) \int_0^{\infty} (\frac{r}{r_m})^{s_{\perp}-1}(\frac{r}{r_m}+1)^{s_{\perp}-4.5} d\left(\frac{r}{r_m}\right) \quad (A13)$$

where appears the classical form:

$$B(u,v) = \int_0^{\infty} \frac{x^{u+1}}{(1+x)^{u+v}} dx \quad (A14)$$

for $x = \frac{r}{r_0}, u = s - 2 \; and \; v = 6.5 - 2s.$

This normalization via (A12) gives the opportunity to link one single density of electrons to $N_e$as

$$\rho_{NKG} = \frac{N_e}{r_m^2} f_{NKG}(r) \qquad (A15)$$

where $s_\perp$ must be a constant with respect to r corresponding to a fixed value of t in relation (**3.4**), otherwise expressing the integration in terms of Euler Beta function is not valid in general.

In reason of the difficulties observed with the experimental profile, the topological test of the local age parameter (equation **3.7**) was proposed to get an experimental hint of the validity of the lateral structure function. $s_\perp(r)$ is given automatically in the written output of ***CORSIKA*** option *NKG* for several axis distance (**User's Guide of *CORSIKA-6600/6970)***.

When the calculation of the electron component is carried out with relation (**3.6**), the situation with the *NKG* inspired procedure implemented in *CORSIKA* is more close to the experimental data and also of the calculation with *EGS4*.

CHAPTER 4

GAMMA - HADRON DISCRIMINATION

4.1 INTRODUCTION

High-energy γ-ray astronomy provides a very valuable source of information regarding non-thermal processes in the Universe. In recent years this field has progressed significantly. The γ-ray sky at energies over 10 TeV is also of the astrophysical importance since it can give essential clues regarding the origin of galactic CRs of very high energy. The *ultra-high energy* (UHE) CRs arriving at the Earth are mainly charged particles and a small fraction of γ-rays. In their travel through the interstellar medium, charged particles have their paths affected by electromagnetic fields and interstellar gas clouds, although γ-rays arrive directly from their sources, giving information about the physical processes which take place at/near their source engines. Also the heliosphere and interplanetary medium interact with charged particles, while γ-rays retain their original information about sources. When CRs arrive at the top of the atmosphere they generate EASs that develop through the atmosphere until they reach ground level. The EAS thus formed can be detected by observing (**a**) the secondary particles arriving on the ground; (**b**) Cherenkov light emitted by charged secondary particles and (**c**) fluorescence light emitted by charged secondary particles. These particle signals are observed by means of different experimental techniques.

The EGRET telescope aboard the Compton Gamma-ray Observatory (Collmar 2000) has detected over two hundred point sources. A significant number of these sources emit γ-rays with energy up to a few GeV. This upper limit is due to the restricted collection area of satellite-based observatories. Since for many of these sources no spectral cuts have been observed, they are expected to emit γ-rays at higher energies. These promising results have promoted the design of advanced ground based telescopes which detect the secondary particles of the shower. The most successful ground based devices are the so-called *imaging air-Cherenkov telescopes* (IACTs) (Aharonian 2006[a]). The IACTs such as MAGIC (Baixeras et al. 2003 & MAGIC Coll. 2008), H.E.S.S. (Hinton 2004), VERITAS (Weeks 2010 & Beillicke 2008) and the onboard Fermi Large area telescopes (FermiLAT) (Atwood 2009 & Dermer 2012) produce results which agree remarkably well with

the astrophysical model predictions. Observations by FermiLAT revealed more than 1,873 high-energy gamma-ray sources, including several classes of active galaxies, pulsars, pulsar wind nebulae, supernova remnants, binary sources, high-energy gamma-ray bursts, a nova and the Sun (Michelson 2011). The imaging technique provides a method of effectively discriminating between γ-rays initiated showers and the background CR showers, based on the morphology of their Cherenkov images. Careful analysis of anomalies in the structure of EASs is the only possible way to obtain experimental information about UHE γ-rays in primary cosmic radiation and provides the means to study CRs beyond the flux limits of direct observations (energies larger than 10^{14} eV). From the literature study it is known that the EAS observables like shower size (N_e), muon size (N_μ), hadron size (N_h), air shower associated Cherenkov content (N_{Ch}), and morphology of the Cherenkov images and the depth of shower maximum (X_{max}) were generally used for the purpose of gamma-hadron discrimination from time to time. To extract information about primary CRs more accurately from the experimental measurements, detailed MC simulations of the shower development is being used as basis of the data analysis and interpretation. The MC simulations consider the evolution of EAS in the atmosphere initiated by different energetic particles which propagates down to observation level.

In the field of CR air shower physics, the separation of γ-rays from the dominant nuclear component in the cosmic radiation is an important topic for astroparticle physics that still needs more attention (Nestnhoff et al. 1995 & Badran et al. 1997). The UHE γ-rays are considered to be an hadronic origin of primary CRs: a fraction of accelerated hadronic CRs are likely to produce γ-rays through Δ-resonances, bremsstrahlung, inverse Compton etc. non-thermal processes at or very close to the source site by interacting with the ambient matter (Bhadra & Dey 2009). The γ-ray detection suffers from the huge background constituted by ordinary (nucleonic) CRs in the GeV-TeV energy region. The flux of primary γ-rays amongst the CRs has been estimated to be $\sim 10^{-5}$ of the proton flux at 100 TeV (Wolfendale 1990). However, some early works predicted a galactic plane excess higher than this: $\frac{\gamma}{p} \sim 10^{-2}$, 3×10^{-2} and 10^{-2} at 10^2, 10^3 and 10^4 TeV (Wdowczyk et al. 1983). Even at energy of 10^7 TeV, this ratio has been predicted to rise up to 10^{-1}(Wdowczyk et al. 1983). To observe astrophysical sources (emitting undeflected γ-rays and assumed as point-like objects) and to

study the anisotropy properties of primary CRs, one has to eliminate isotropically distributed CRs.

Hadronic showers produce muons in the charged pions and kaons decays that occur in the hadronic interactions, while showers initiated by γ-rays/$e^{\pm}$ are purely electromagnetic except for hadrons photo-production, that is, a hadronic interaction of a photon with an air nucleus. The photo-production cross section increases with primary energy and consequent upon, γ-ray initiated air showers would have a significantly less muon content than those of hadronic cascades at low energy (Gaisser 1990 & Gandhi et al. 1990). Usually poor muon content is considered as the signature of γ-ray initiated EAS. In order to select a γ-ray shower based on such a criterion, an EAS array needs to be equipped with muon detectors covering very large area which is economically very challenging and such a facility is rarely available. So one has to look for some other primary mass sensitive observables based on which γ-ray initiated EASs can be separated out without the need of large area muon detector. In some early works, efforts were made to distinguish γ-ray showers on the basis of developmental stage of EAS in the atmosphere with the idea that γ-ray induced EAS will be younger than the hadron initiated EAS (Samorski et al. 1983 & Protheroe et al. 1984). The lateral shower age ($s_{\perp}$) is essentially the slope of the lateral density distributions of electrons in EAS that reflects the developmental stage of EAS and hence $s_{\perp}$was used as distinguishing parameter (Greisen 1956, Greisen 1960 & Snyder 1989). However, earlier MC simulation results regarding youthfulness of γ-ray showers in terms of shower age were inconclusive (Fenyves 1985 & Hillas 1987). In those simulation works, authors used their own simulation codes and findings could not be cross checked. Since, nowadays standard simulation code like CORSIKA (Cosmic Ray Simulation for KAscade) (Heck et al. 1998 & Capdevielle 1992) is available and our knowledge about the high energy particle interactions is much improved now, it would be imperative to revisit the issue.

4.2 METHODS FOR SELECTING GAMMA-RAY INDUCED SHOWERS

In this chapter, we have presented a detailed study on discrimination of γ-ray induced EAS from the background contributed by hadrons in the multi-TeV range. The lateral shower profiles generated by various primaries within a particular primary energy range are being used here, and they provide some discriminatory power for separating γ-ray showers from the background. The

selection of γ-ray showers is attempted by employing two different approaches – the **Method I** and the **Method II**. In the former approach (Method I), we have taken single (r-independent) lateral age parameter i.e. $s_{\perp}$ as the γ-ray separation parameter. Besides, it has been argued in the literature that the different masses of primary CRs might also be separated out by the simultaneous use of N_e, N_{μ} and f parameters (Sciascio et al. 2007 & Aloisio et al. 2001). The parameter f is giving out the ratio of reconstructed average electron densities at two arbitrary distance bands from the shower core, measuring roughly the rate of absorption of electrons in their lateral developments from the shower core. Experimentally it is observed that the NKG function with a single lateral age is insufficient to describe the lateral density distribution of EAS electrons properly at all distances, which implies that the lateral age changes with the radial distance. Subsequently, the notion of local lateral shower age parameter (LAP) was introduced (Capdevielle & Gawin 1982, Bourdeau et al. 1980 & Capdevielle et al. 1990) which is in essence the lateral age at a point. A detailed description of the LAP has already been outlined in the **chapter 3**. Since experimental electron density data in EAS may fluctuate considerably at a particular radial distance, instead of taking LAP at any particular point we take an average LAP nearly between 50 m and 300 m. In Method II we employed this average LAP (s_{local}) to select γ-ray showers. It is found that when single constant age ($s_{\perp}$) is used, the separation power becomes subdued. In contrast, the average LAP appears as a suitable mass sensitive parameter for classifying γ-ray induced showers.

4.3 OBSERVATIONAL LEVELS OF INTEREST

The present study has been performed mainly at the geographical location of ARGO-YBJ (latitude 30.11^0 N, longitude 90.53^0 E, 4300 m a.s.l.) (Sciascio 2007 & Aloisio 2001). This is because the experiment offers a full coverage array and hence can measure radial density distribution of electrons in EAS with great accuracy, which in turn provides an opportunity to estimate LAP accurately. Moreover, since ARGO-YBJ does not have any muon detector, discrimination of γ-ray showers based on an alternative EAS observable, related to only electromagnetic component should be very useful. The proposed observable may be of interest for surface detectors (SD) experiments, that have no any (or reliable) measurements of the muonic shower size. Since ARGO-YBJ experiment is located at very high altitude, its energy threshold is sub TeV and hence for this location we

simulated EAS events in the energy range from 1 TeV to 3 PeV. However, ARGO-YBJ has not yet studied the radial variation of the lateral shower age while a few other experiments, such as Akeno (Nagano et al. 1984[a] & Nagano et al. 1984[b]) and NBU (Sanyal et al. 1993), successfully tested the predicted radial variation of LAP. We simulated a few events at the geographical location of Akeno and compared with the observations to demonstrate again the importance of considering LAP instead of single shower age. The correlations of $s_{\perp}$ with N_e and/or N_{μ} have been considered as a basis for extracting information on the nature of primary CRs. The KASCADE (Antoni et al. 2001) and the NBU (Bhadra et al. 1998) experiments provide a few results on these aspects. Accordingly we performed simulations at the geographical locations of these experiments and compared with experimental findings in order to examine primary mass sensitivity of lateral shower age parameter.

4.4 SIMULATION CHARACTERISTICS

The MC simulation for generating EAS events considers interaction mechanisms of energetic particles as input. But due to limited knowledge of particle interactions at high energies (and the large fluctuations) the results of simulation may become model dependent. To ensure that the conclusion of the present work is robust, we consider two high energy hadronic interaction models, QGSJet **01** v.**1c** (Kalmykov et al. 1997) and EPOS **1.99** (Werner et al. 2006 & Pierog & Werner 2008[a]) and found that the present findings do not have any strong dependence on the choice of interaction model.

The EAS events are simulated by coupling the high energy hadronic interaction models mentioned in the previous sentence, and the low energy hadronic interaction model GHEISHA (version **2002d**) (Fesefeldt 1985) in the framework of the CORSIKA MC program version **6.970** (Heck et al. 1998 & Capdevielle 1992). For the electromagnetic part the EGS4 (Nelson et al. 1985) program library has been used. The maximum zenith angle of primaries has been restricted to 45 degree here.

The MC simulation data library consists of over 0.1 million EAS events each for p, Fe and γ-ray at the ARGO-YBJ location in the primary energy range 1 TeV to 3 PeV using both QGSJet **01** and EPOS **1.99** models. In addition, we have generated 25,000 EAS events for each primary component p, Fe and γ-ray and

about 10,000 He events with the model QGSJet in the primary energy range from 100 TeV to 30 PeV following a power law with a spectral index of -2.7 below the *knee* and -3.0 above the *knee* at the geographical locations of KASCADE (latitude 49.1^0 N, longitude 8.4^0 E, 110 m a.s.l.) and NBU (latitude 26.8^0 N, longitude 88.4^0 E, ~130 m a.s.l.). Besides, a small size of EAS events for p and Fe primaries are generated at the location of Akeno (latitude 35.78^0 N, longitude 138.5^0 E, 900 m a.s.l.). The magnetic fields are set for all four observational levels accordingly.

Two mixed compositions have been prepared from the generated showers taking 50% p, 25% He, 25% Fe events forming **mixture-I** and 37% p, 37% Fe, 26% γ-ray events constituting **mixture-II** respectively for better understanding of EAS observational results.

4.5 THEORETICAL BACKGROUND AND SIGNAL SELECTION TECHNIQUE

4.5.1 THE LATERAL AND LOCAL AGE PARAMETERS

Extensive air showers propagating in the same density profile of the atmosphere essentially have equal lateral distributions around the shower axis. In the cascade theory, the problem of deriving the electron lateral distribution through an analytical method received an important recognition in the past. Nishimura and Kamata (Lipari 2009) solved numerically the 3-dimensional shower equations in *Approximation B* to obtain the lateral distribution of electrons propagating in a medium of constant density. The results obtained on lateral density distribution of cascade particles by Nishimura and Kamata can be approximated by the well known Nishimura-Kamata-Greisen (NKG) structure function proposed by Greisen (Greisen 1956, Greisen 1960 & Snyder 1989) that has been written through the *equation* (**3.4**) in **Chapter 3**. Using that equation, the electron density can be given by:

$$\rho(r, s_\perp) = N_e C(s_\perp)(\frac{r}{r_m})^{s_\perp - 2}(1 + \frac{r}{r_m})^{s_\perp - 4.5}, \qquad (4.1)$$

The symbols have their usual meaning as discussed in the preceding chapter. But such a widely used relation in (**4.1**) does not hold if $s_\perp$ varies with r, as noted in Akeno (Nagano et al. 1984[a] & 1984[b]), NBU (Sanyal et al. 1993) and some other observations (Capdevielle & Gawin 1982, Bourdeau et al. 1980 & Capdevielle et al. 1990). An improvement of the NKG function was proposed by adopting a modulated, longitudinal age parameter $s_\parallel / s_L$ dependent effective Moliere radius

(Lagutin et al. 1979 & Uchaikin 1979) by the relation (**3.6**) but the lateral shower age is still found to vary with radial distance experimentally. To tackle the situation a method was developed by Capdevielle *et al* introducing the concept of *local age parameter* (LAP) (Capdevielle & Gawin 1982, Bourdeau et al. 1980 & Capdevielle et al. 1990). The formula for the LAP estimated in a small radial distance band $\{x_i, x_j\}$ from the shower core is given by the following relation.

$$s_{local}(i,j) = \frac{\ln\left(F_{ij}X_{ij}^{2}Y_{ij}^{4.5}\right)}{\ln\left(X_{ij}Y_{ij}\right)} \qquad (4.2)$$

The different notations used in the above equation (**4.2**) have been pointed out previously in the equation (**3.7**). The identification $s_{local}(r) \equiv s_{local}(i,j)$ for $r = \frac{r_i + r_j}{2}$ remains valid for the experimental distributions as far as they are approximated by monotonic decreasing functions versus radial distance (note that, $s_{local}(r) \equiv s_{local}(i,j) \equiv s_{\perp}^{local}(r) \equiv s_{ij}^{local}$).

In the present work, we have given emphasis on the estimation of the LAP and on its average using $s_{local}(r)$ values, taken between first minimum and the subsequent maximum from the radial variation of LAP. The estimation of $s_{\perp}$ would also be made through the traditional shower reconstruction method.

4.5.2 BACKGROUND REJECTION: THE QUALITY FACTOR

In the present work the LAP has been proposed to separate γ-ray showers from hadronic ones. In order to understand how LAP and $N_e$work together to optimise their functioning, the general expression for the γ-*ray*-to-background (likewise signal-to-noise ratio is used for detectors performance) shower ratio as a linear function of a parameter Q:

$$\frac{signal}{noise} \equiv \frac{desired\ events}{undesired\ events} \propto Q(E, N_e, s_{local}, \theta) \qquad (4.3)$$

where Q is the γ-ray or hadron identification efficiency and is known as the quality factor. The background rejection or γ-ray acceptance is usually made by numerical maximization of the parameter Q within an appropriate zenith angle, primary energy and N_e ranges corresponding to appropriate cut applied on s_{local}. The quality factor Q essentially quantifies the gain of significance of the applied cut achieved by the separation algorithm. It is defined as

$$Q = \frac{\epsilon_\gamma}{\sqrt{\epsilon_{bkg}}} = \frac{\epsilon_\gamma}{\sqrt{(1-\xi_{bkg})}} \qquad (4.4)$$

, where ϵ_γ and ϵ_{bkg} are respectively the γ-ray and background acceptances from the sample using a cut value of s_{local} while ξ_{bkg} stands for the rejection of background. Here, $\epsilon_\gamma = \frac{n_{\gamma(cut)}}{n_\gamma}$ and $\epsilon_{bkg} = \frac{n_{bkg(cut)}}{n_{bkg}}$, with $n_{\gamma(cut)}$ and $n_{bkg(cut)}$ represent number of showers of either kind passing a particular cut value of s_{local} whereas n_γ and n_{bkg} are the number of all triggered events (before cuts).

The significance of the selection enhancement can also be evaluated with the so-called sensitivity parameter as well and it is defined by the following,

$$S = \frac{n_{\gamma(cut)}}{\sqrt{n_{bkg(cut)}}} \qquad (4.5)$$

where the denominator is the fluctuation of the background showers which actually measures the hadron contamination present in the selected γ-ray (signal) showers.

4.6 ESTIMATION OF SHOWER AGE PARAMETERS

The simulated electron density data have been analyzed in two different methods to obtain shower age parameters $s_\perp$ and $s_{local}(r)$. First, following the traditional approach we estimate $s_\perp$ (along with other shower parameters) by fitting the density data with the NKG structure function using our own reconstruction algorithm. In this approach, the simulated electron densities at different radial distances have been fitted by the method of chi-square minimization through an iterative procedure based on the method of steepest decent to the NKG lateral distribution function of electrons. Here it is to be noted that majority of the EAS groups generally estimate basic shower parameters based on the NKG function. In order to check the goodness of the NKG function in describing the simulated radial density distribution of electrons, we firstly fitted the simulated density data at various radial distances with the NKG function and compared radial density distribution of electrons for simulated events with the fitted curve. Fitted showers with reduced χ^2 less than 5 are only accepted for results involving $s_\perp$. The error in estimating $s_\perp$ in the N_e range $1.5 \times 10^4 - 4.25 \times 10^5$ has been found as ± 0.03.

We directly estimated LAP for each individual shower exploiting equation (4.2). We noted that the description of the data by the NKG function is improved when the Moliere radius is treated as a variable rather than a fixed parameter (Dey

et al. 2012). But this description comes at the expense of very high shower age value which somewhat obscures the physical meaning of the age parameter as assigned in the cascade theory. In this analysis, the error of the LAP for EAS with the primary energy in the PeV range remains within 0.05 for $10m < r < 250m$, whereas for $r < 10m$ or when $r > 300m$ the error of the LAP is found to be higher, about 0.1.

It has shown recently (Dey et al. 2012) that LAP initially decreases with radial distance, reaches a minimum around 50 m, then starts increasing with radial distance, attains a local maximum around 300 m and decreases again thereafter. The nature of such a variation of LAP with radial distance was found independent of energy of the shower initiating particles (Dey et al. 2012). We observed such a characteristic variation of LAP with radial distance at ARGO-YBJ location as shown in **Fig.4.1a** for protons, irons and γ-rays. It is seen from the figure that the nature of variation is nearly the same for both QGSJet and EPOS. Here, it is worthwhile to main that up to 50 TeV or so, the density of electrons in EAS beyond 50 m from the shower core is extremely small even at ARGO-YBJ level and is almost impossible to measure it in practical situation. Hence, we have chosen primary energy from 100 TeV and above for results.

As already mentioned, Akeno group studied the radial variation of LAP (Nagano et al. 1984[a] & Nagano et al. 1984[b]). We compared our simulation results with Akeno observations in **Fig.4.1b** for proton and iron primaries. The single lateral shower age $s_{\perp}$for proton and iron are also given (solid and dashed lines parallel to the x-axis) in the figure for comparison. We also estimated LAP from the lateral density distribution of electrons obtained by the KASCADE experiment (Antoni et al. 2001, Apel et al. 2006 & Ulrich et al. 2008 & 2009[a]) and we compared with our simulation results in **Fig.4.1c**. The errors in the extracted experimental points are quite large but it is at least clear that a constant single lateral shower age is insufficient to describe the experimental findings.

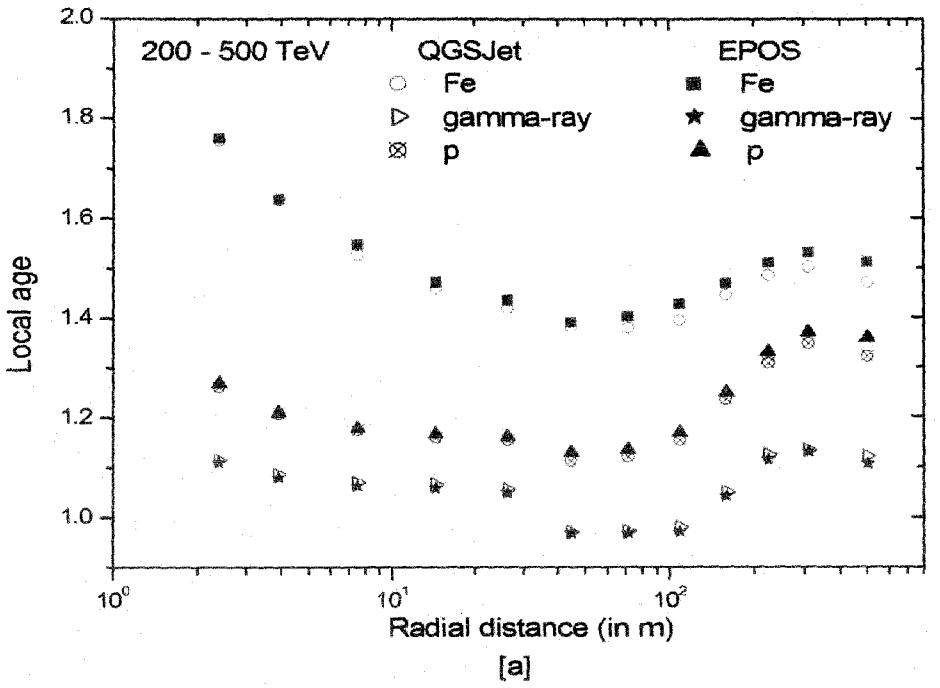
200 - 500 TeV
QGSJet
Fe
gamma-ray
p
EPOS
Fe
gamma-ray
p
Local age
Radial distance (in m)

[a]

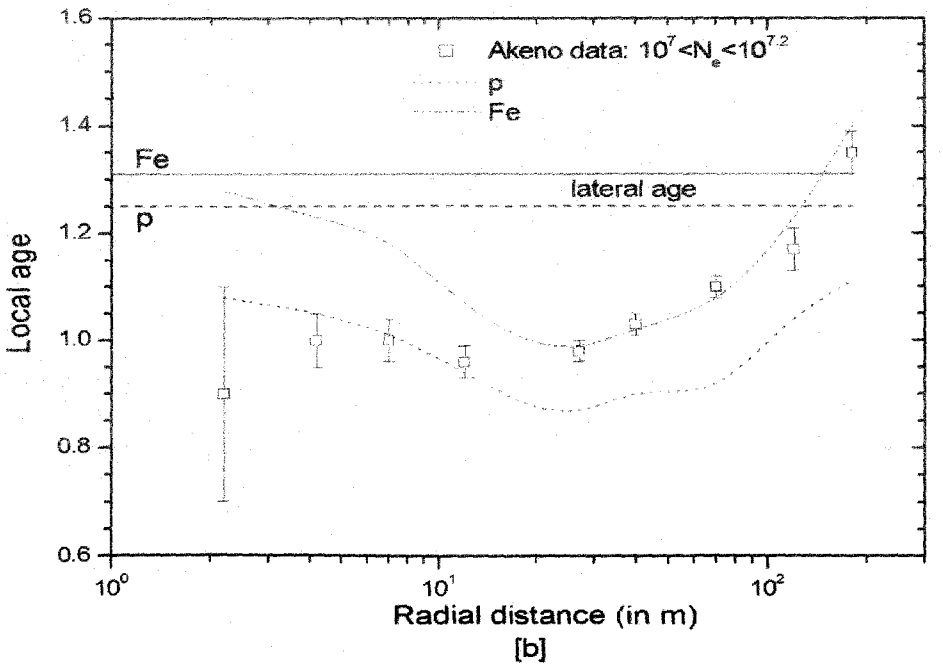
Akeno data: $10^7 < N_e < 10^{7.2}$
p
Fe
Fe
lateral age
p
Local age
Radial distance (in m)

[b]

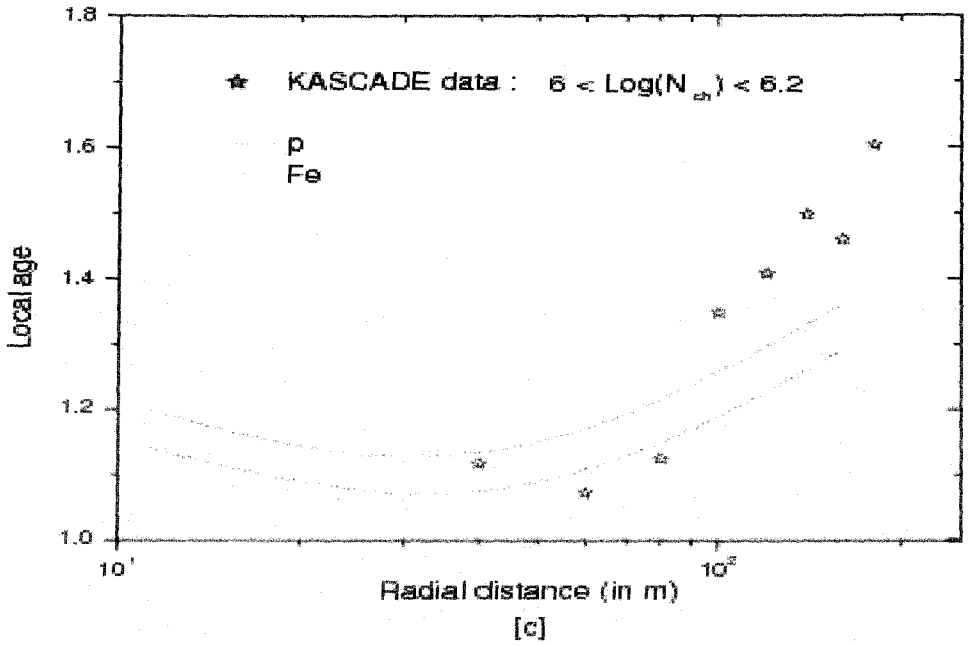

Fig.4.1: [a] The radial variation of LAP obtained at the ARGO-YBJ altitude for p, Fe and γ-ray with hadronic interaction models QGSJet and EPOS. [b] Same as Fig.4.1a at the Akeno level with QGSJet model, compared with experimental data. The solid and dashed lines parallel to the x-axis indicate $s_{\perp}$ for Fe and p. [c] The radial variation of LAP estimated from the KASCADE observed lateral distribution data. Lines indicate the mean values of a sample of simulated EAS events with QGSJet model (the errors in experimental data are not included here).

Since air shower measurements are subjected to large fluctuations, instead of LAP at a particular radial distance we consider for each event a mean LAP ($< s_{local} >$), which is the average of all LAPs for various distance bands (r_i, r_j) over the radial distance taken from 50 m to 300 m. For the purpose of averaging, distance bands are taken in constant steps on the logarithmic scale. The radial distance band from 50 m to 300 m is chosen because the positions of local minimum and maximum at 50 m and 300 m are nearly universal, independently of primary energy and species (Dey et al. 2012).

4.7 RESULTS ON GAMMA-HADRON SEPARATION: METHOD I

The simulated EAS events so generated have been analyzed by employing **method I** at NBU and KASCADE locations (both at sea level) to investigate some important distinguishing features of γ-ray and hadron induced air showers. The observable parameters like $s_{\perp}$, N_e, N_{μ} and N_h are being used. Results obtained

from these studies have been compared with some of the published results of NBU (Bhadra 1999) and KASCADE (Antoni et al. 2001) respectively. In this section, the gamma-hadron separation has also been performed with the help of local electron densities (i.e. ρ_1 and ρ_2), N_e and N_μ at the ARGO-YBJ location.

4.7.1 N_e AND N_μ DEPENDENCIES OF $< s_\perp >$

The correlation between the mean lateral shower age $< s_\perp >$ over a small shower size bin in the range $10^3 - 1.5 \times 10^6$, with the zenith angle interval $0^0 - 45^0$ for p, Fe, γ-ray and mixed composition (mixture-I) using QGSJet model and corresponding NBU results (Bhadra 1999) are put on view in **Fig.4.2a**. The NBU EAS experiment reported the total uncertainties (including instrumental uncertainty) in estimating $s_\perp$ and $N_e$as $\pm 9\%$ and $\pm 0.14 N_e$ (Bhadra et al. 1998). It is important to perceive that the lateral shower age takes higher values for heavy nuclei compared to that of light and γ-ray primaries clearly indicating relatively flatter lateral distribution of electrons as one move from γ-ray to Fe via p.

The variation of $< s_\perp >$ with muon size in the primary energy range $10^2 - 3 \times 10^4$ TeV and zenith angle interval $0^0 - 45^0$ for p, Fe, γ-ray primaries is presented in **Fig.4.2b** with KASCADE experiment using NKG fitting for muons with slightly higher muon threshold energy. The **Fig.4.2b** exhibits the fact that γ-ray initiated showers can be separated out from the background using $< s_\perp >$ and N_μ. It was also concluded in one of our previous work that EASs due to light primary components are younger on the average (Dey et al. 2012).

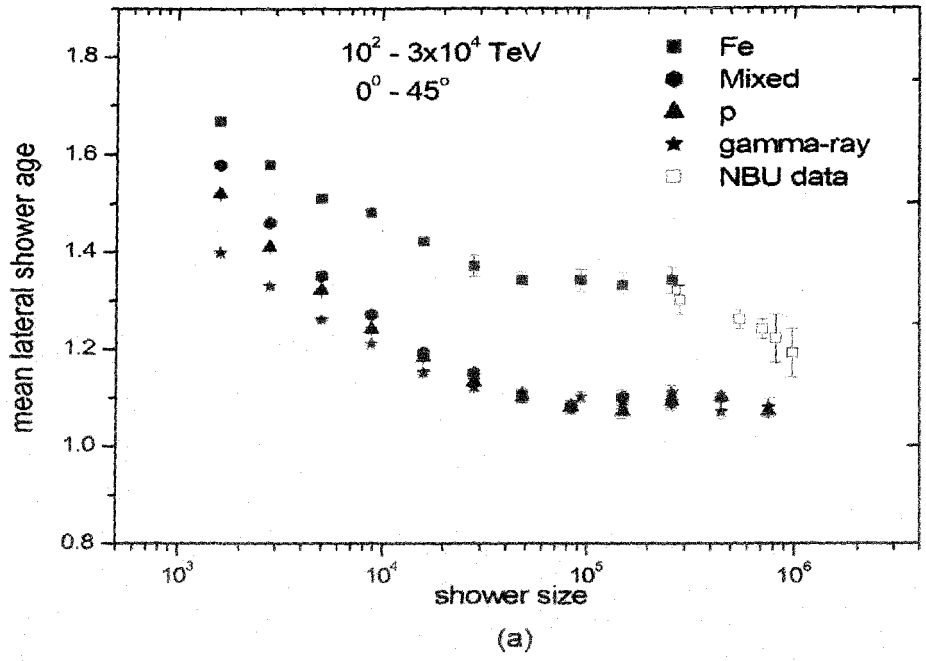

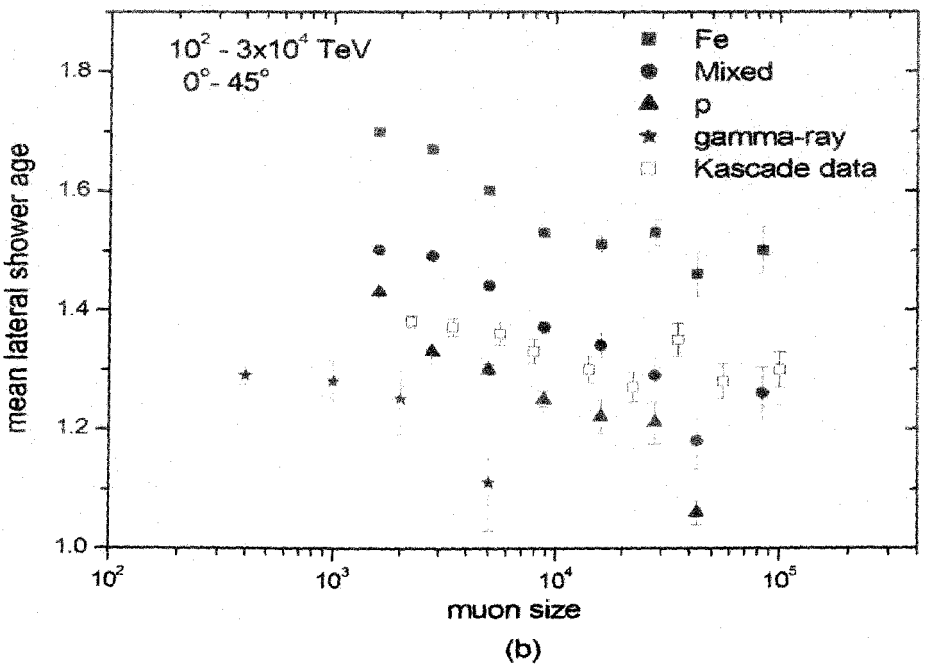

Fig.4.2: [a] Variation of mean lateral shower age with shower size along with NBU data; [b] Variation of mean lateral shower age with muon size. For comparison with KASCADE data in Fig.4.2b, where the age parameter was estimated by NKG fits with r_μ as 420 m and also used truncated muon sizes N_μ^{tr}. The QGSJet model has been used for simulation.

The KASCADE data points indicate that the composition changes slowly from predominantly proton at around 10^{14} eV to heavier primaries with the increase of energy. The NBU data are available only over a small energy window and though both the NBU and the KASCADE data suggest for a mixed composition in the common energy range of study, the NBU data favour for a relatively heavier composition. However, being a small EAS array the NBU experiment could measure electron density only up to 80 m from the shower core and its resolution power for primary composition is thus limited.

4.7.2 VARIATION OF f WITH g

The lateral structure of EAS from different primaries attributes some power of identification and rejection hadron primaries from γ-ray with the same primary energy and size (Sciascio et al. 2005). From the lateral profile of each simulated EAS event, we have estimated electron densities at five adjacent radial points in each of the two arbitrarily chosen distance bands $5-15$ m and $35-45$ m. Next by employing the reconstruction procedure for the determination of local electron density (LED), we obtained two average reconstructed LEDs $\rho_1$and ρ_2 from the shower core.

The selection of γ-ray showers from hadrons becomes visible when one plots the parameter f against g where $g \equiv \frac{N_\mu}{N_e}$ as presented in a $2-$dimensional **Fig.4.3a** using the high-energy interaction model QGSJet. The same study has been repeated for another pair of radial bands $20-30$ m and $50-60$ m, using the same sample of mixture-II and it is depicted in **Fig.4.3b**. The rate of absorption of electrons decreases with increasing radial distance from the core and this feature is revealed from the comparison of **Fig.4.3a** and **Fig.4.3b**. We have checked through the **Fig.4.3c** that the characteristic feature of the $g-f$ distribution does not change appreciably for the high energy interaction model EPOS. Even for a different primary energy range such as 100 - 200 TeV we have found the similar behaviour in $f$against$g$.

It appears from **Figs. 4.3** that this technique essentially exploits the total muon content in an EAS. The EAS events are classified according to their primaries along x-axis (the ratio of muon size to electron size is plotted along x-axis); there is no notable separation along y-axis between events generated by photons and protons.

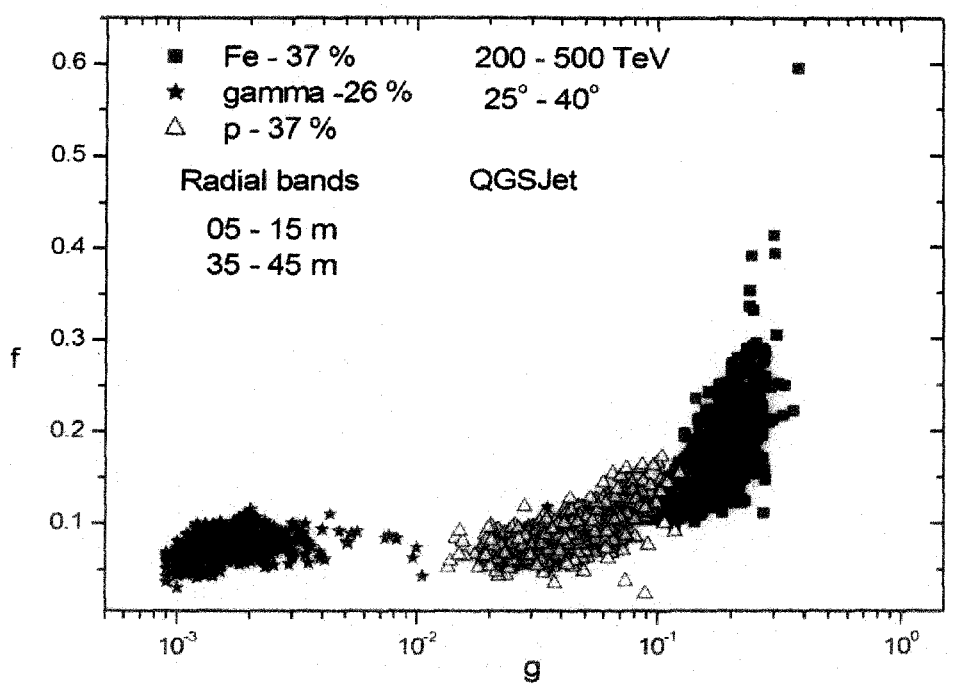
Fe - 37 %
gamma -26 %
p - 37 %
200 - 500 TeV
25° - 40°
Radial bands
QGSJet
05 - 15 m
35 - 45 m
f
g
0.6
0.5
0.4
0.3
0.2
0.1
10^-3
10^-2
10^-1
10^0

[a]

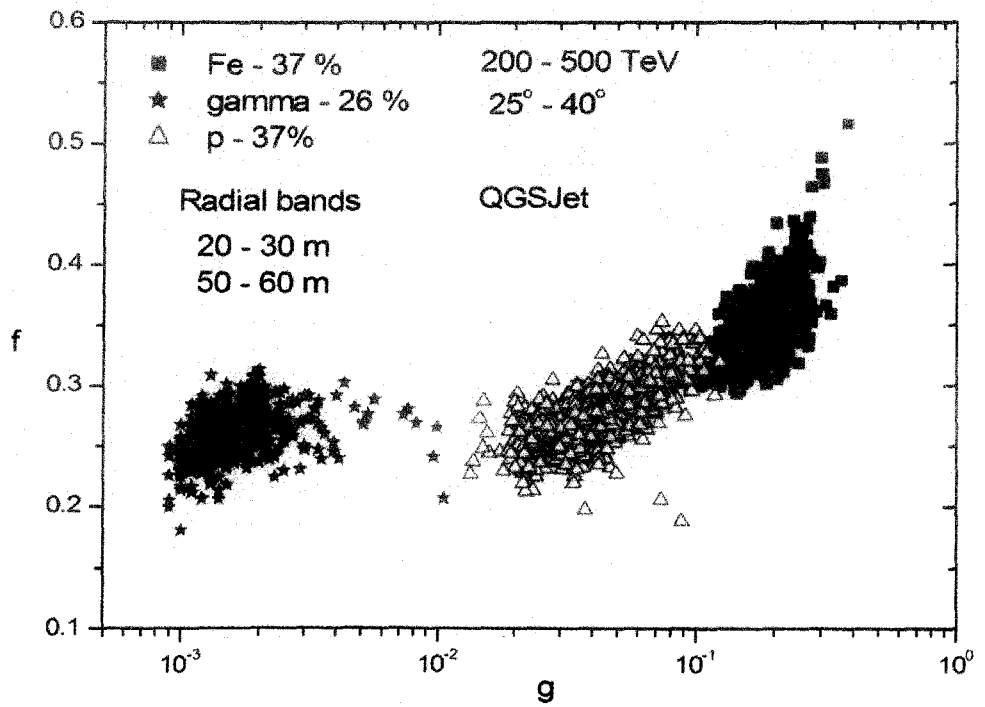
Fe - 37 %
gamma - 26 %
p - 37%
200 - 500 TeV
25° - 40°
Radial bands
QGSJet
20 - 30 m
50 - 60 m
f
g
0.6
0.5
0.4
0.3
0.2
0.1
10^-3
10^-2
10^-1
10^0

[b]

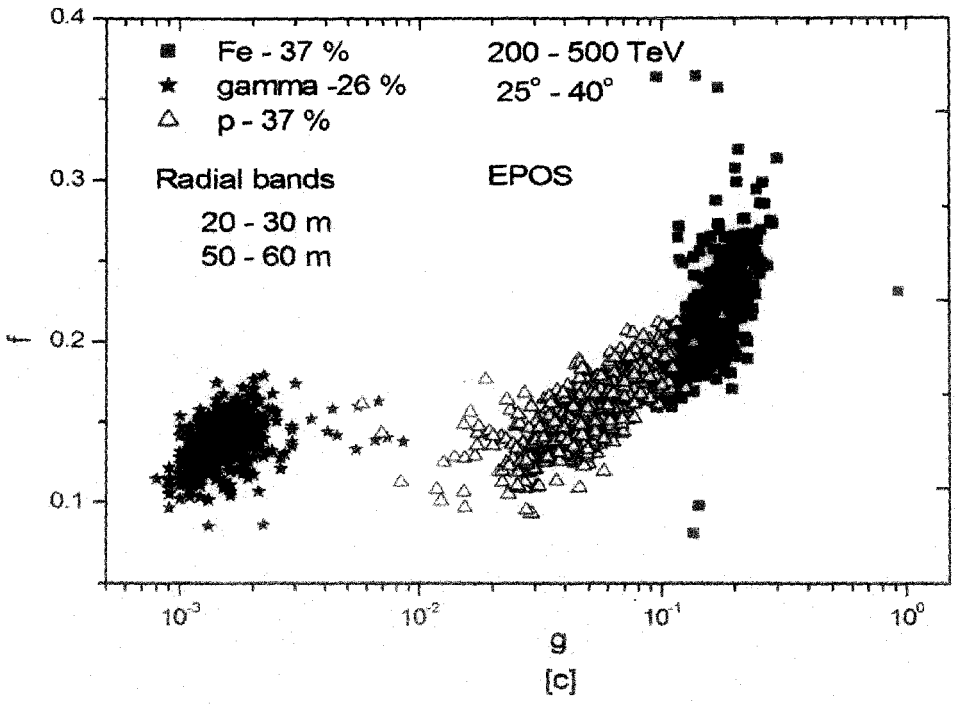

Fig.4.3: Distribution of EAS events generated in the zenith angle interval 25^0 – 45^0 in the $g-f$ plane at ARGO-YBJ level: [a] The ratio (f) for two electron densities are taken between distance bands $5-15$ m and $35-45$ m using the interaction model QGSJet; [b] Same as Fig.4.3a but distance bands are taken at $20-30$ m and $50-60$ m respectively; [c] Same as Fig.4.3b but with the hadronic interaction model EPOS. A negligible percentage of γ-ray primaries are found behind hadron (proton) showers.

4.8 GAMMA-RAY SEPARATION POWER OF METHOD I AND METHOD II

Attempts have been made to discriminate γ-ray showers from hadron initiated showers through method I without taking muon number as an observable. In method I, the r-independent age parameter $s_\perp$ itself is not capable of separating γ-ray showers from the background. This is already revealed in **Fig.4.2a**. The variations of $s_\perp$ and $< s_{local} >$ with N_e in **Fig.4.4a** and **Fig.4.4b** also reaffirm the inability of method **I** over method **II** for the purpose of hadron rejection. From **Fig.4.4a** (also **Fig.4.2a**), it is clear that $s_\perp$values are much nearer to one another corresponding to any N_e-values for both γ-ray and p showers. This ambiguity of method **I** could be well understood if one studies the frequency distribution of $< s_\perp >$ and $< s_{local} >$ for p, Fe and γ-ray showers. Such a study is presented through **Fig.4.4c** and **Fig.4.4d** with the interaction model EPOS at ARGO-YBJ

location. This feature remains unaltered even with the QGSJet model. In **Fig.4.4c**, a major part of the area under the curve of p induced showers is superimposed by the area of γ-ray showers. But from the **Fig.4.4d**, the results seem to be very promising, hinting the possible usefulness of the parameter s_{local} in contrast to $s_{\perp}$ for hadron rejection.

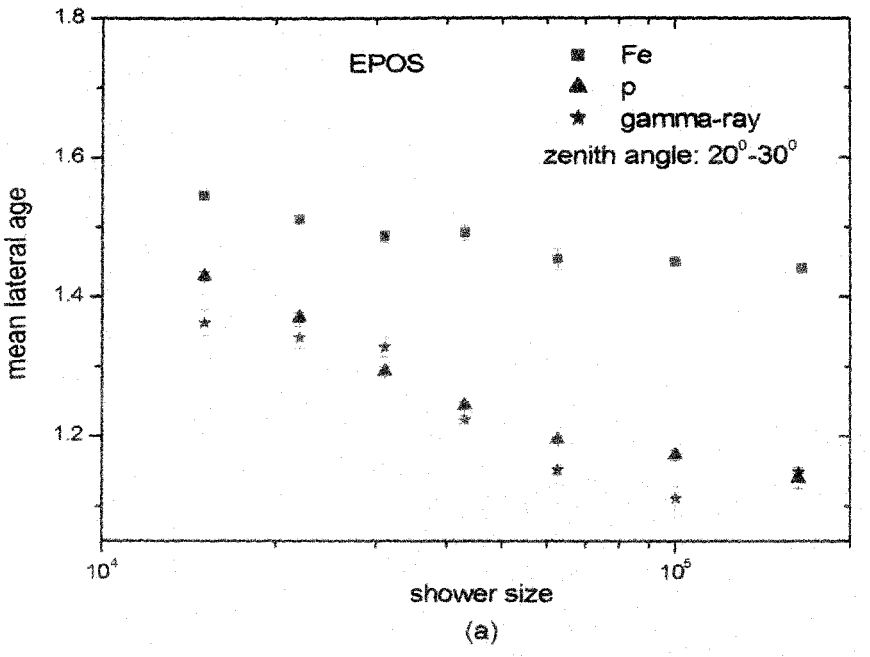

(a)

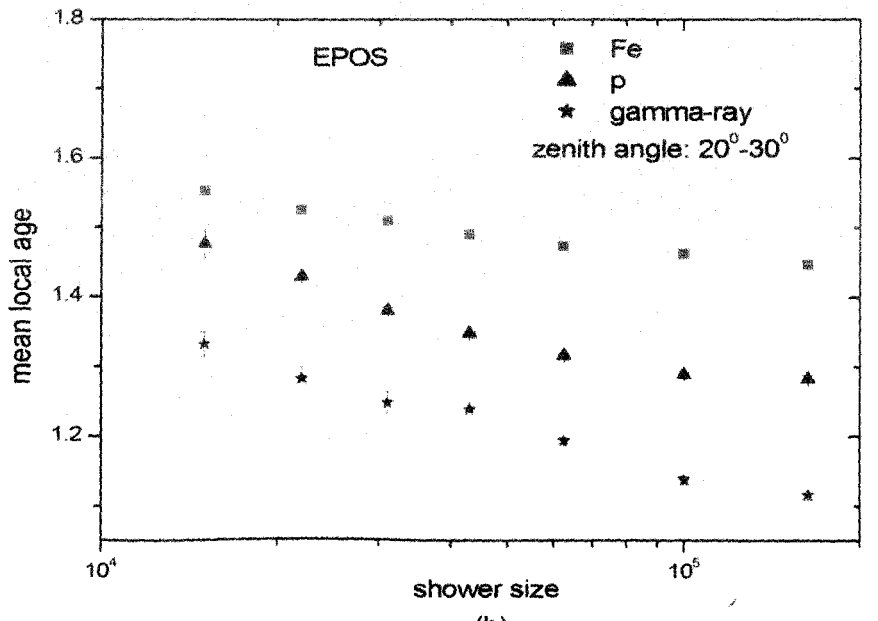

(b)

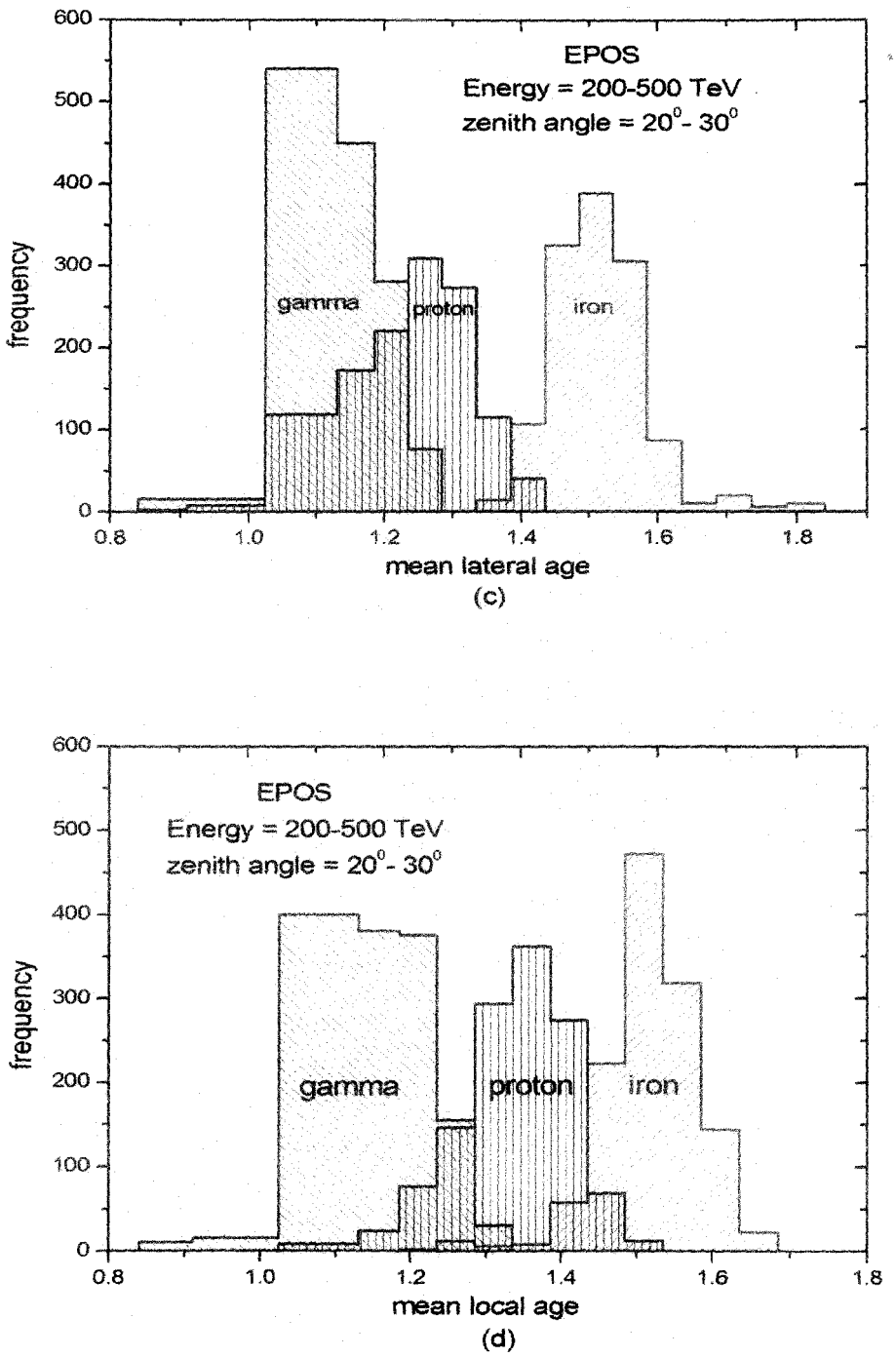

Fig.4.4: [a] Variation of $< s_{\perp} >$ employing method I with N_e at ARGO-YBJ level; [b] Same as Fig.4.4a but with method II; [c] Frequency distribution of $< s_{\perp} >$ and [d] Frequency distribution of $< s_{local} >$.

We would therefore explore through MC simulation study whether LAP is sensitive on primary mass and consequently the possible role that the parameter may play for separating γ-ray showers from a huge background of hadronic showers in primary CRs. One major challenge in this context, however, is the

reliable and unambiguous estimation of the parameter from the experimentally measured electron densities. Since the LAP is found to vary with radial distance, comparison of LAPs obtained by different EAS experimental groups is difficult as the radius of the shower disc differ from experiment to experiment.

4.9 RESULTS ON GAMMA-HADRON SEPARATION: METHOD II

Due to overwhelming background caused by hadron induced EASs, the discrimination of the rare gamma-like events is vital. The background can be rejected by exploiting the LAP between γ-ray-initiated showers and hadron-initiated ones. Here, we noticed that EAS events those are simulated in the same primary energy range initiated by different primaries may produce different N_e. This feature is manifested in the variation of LAP against N_e. The scatter plots of $< s_{local} >$ versus N_e are shown in **Figs. 4.5a**, **4.5b** and **4.5c** respectively where distribution of different primary masses based on s_{local} and N_e data from the mixture-II corresponding to different primary energies and interaction models are presented.

In the primary CR flux, the percentage of γ-ray flux is very small, of the order of 0.001%. To separate such a small fraction of γ-ray component from primary CRs in a real experiment employing method II, it would be nice if we could prepare a mixture with such a small percent of γ-rays and see whether the γ-ray events can be extracted out or not. But due to limited statistics we could not do that. Instead, we made three sub-mixtures of type II maintaining the ratio of primaries as 37% p, 37% Fe and 26% γ-ray for three different combinations of zenith angle, primary energy and shower size ranges. These exercises are worked out for both the high energy interaction models QGSJet and EPOS. From each sub-mixture, we tried to separate γ-ray showers out exploiting s_{local} corresponding to different N_e.

For a small enough cut value of s_{local} we have found poor acceptance for γ-ray induced EAS and very good rejection of background, whereas for a large enough cut value of s_{local} the selection or rejection ability is found to be completely reversed. Cut values of s_{local} lie between the two extremes offered different acceptances and rejections of γ-ray and background respectively. Similarly an appropriate cut on N_e is also needed for the selection/rejection purpose. In astronomical signal selection, optimal cut to selection parameters is

generally set by numerical maximization of the quality factor Q whose formula is already given by the equation **4.4** in the sub-section **4.5.2**.

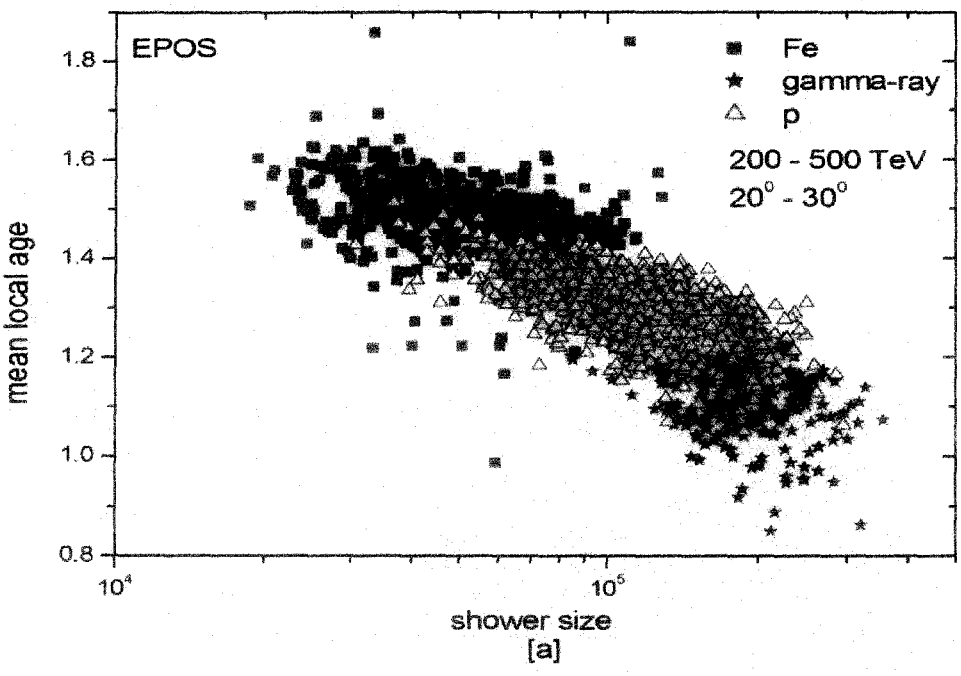

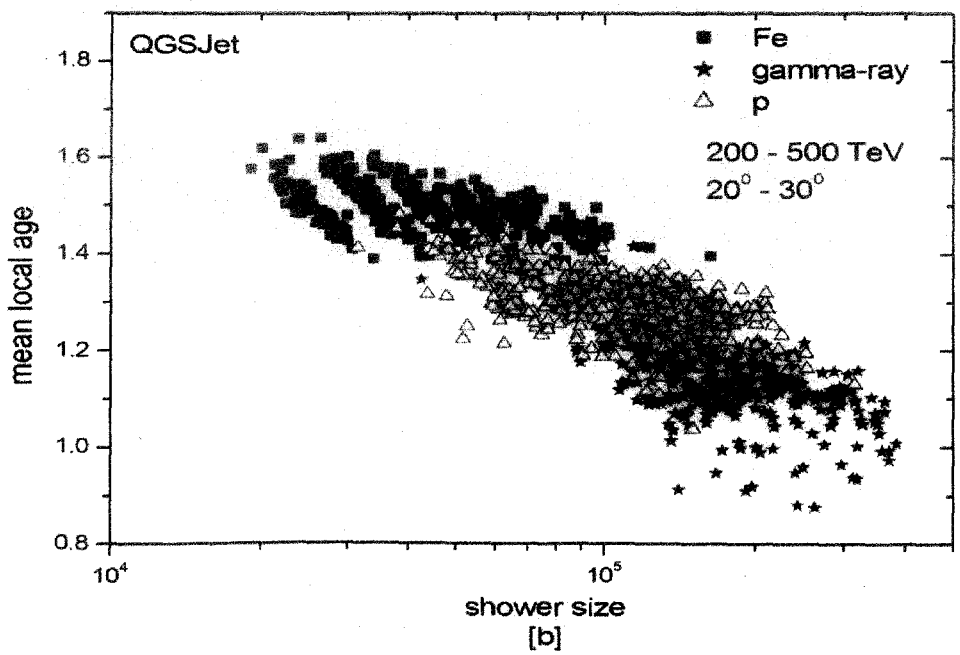

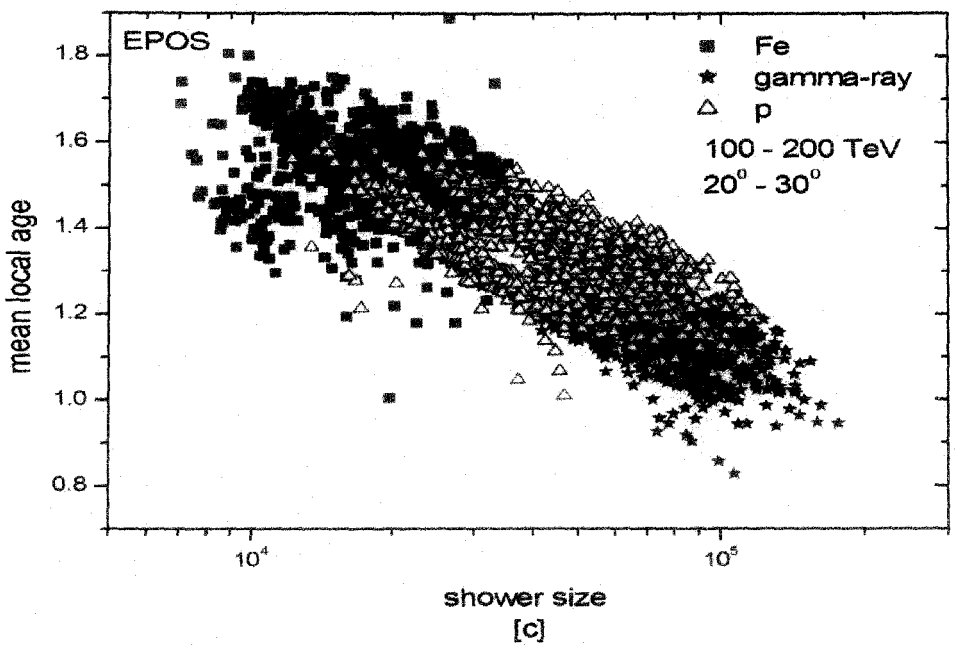

Fig.4.5: [a]-[c] Distribution of simulated showers in mixture II in two primary energy ranges based on s_{local} and N_e at ARGO-YBJ. Dependence on interaction models is also shown through the figures.

The quality factor Q which measures the discrimination power has been estimated as functions of primary energy, zenith angle and shower size, for different cut values of s_{local} utilized to identify γ-ray-initiated air showers against hadron-initiated ones is shown in **table 4.1**. In **table 4.2**, we have given a chart for quality factors estimated at optimal conditions under three different selection criteria.

Another background rejection technique to evaluate the performance of selection algorithm is the application of advanced technique like Principal Component Analysis (PCA) or a Fisher Analysis that allows combining s_{local} and N_e in a single optimized observable.

s_{local}	1.05	1.08	1.10	1.12	1.14	1.15	1.16	1.18	1.20
ϵ_γ	0.146	0.237	0.348	0.510	0.657	0.707	0.778	0.864	0.934
ϵ_{bkg}	0.007	0.022	0.029	0.036	0.058	0.065	0.109	0.145	0.254
Q	1.74	1.61	2.05	2.69	2.73	2.77	2.36	2.27	1.86

Table 4.1: The quality factors at various s_{local} cuts using the interaction model QGSJet. The primary energy, zenith angle and shower size intervals are $200-500$ TeV, $20^0 - 30^0$ and $(1.5-4.0)\times 10^5$ respectively.

Model	E (TeV)	θ (deg.)	$N_e \times 10^5$	s_{local}	ϵ_γ	ϵ_{bkg}	Q
EPOS	100-200	5-15	0.6-2.0	1.14	0.691	0.072	2.57
EPOS	200-500	20-30	1.5-4.0	1.15	0.734	0.048	3.35
QGSJet	200-500	20-30	1.5-4.0	1.15	0.707	0.065	2.77

Table 4.2:The different signal selection parameters at optimal conditions.

4.10 DISCUSSION AND CONCLUSIONS

In this chapter, attempts have been made to discriminate γ-ray induced EAS from hadron initiated shower on the basis of shape of electron density distribution in EAS characterized by lateral shower age parameter that essentially reflects the stage of EAS development in atmosphere. Generally muon content of an EAS is treated as a good estimator for gamma-hadron discrimination. However, a precise measurement of total muons in an EAS requires muon detectors covering large area which is quite expensive. So, we explored whether lateral shower age could be used for the purpose.

We first explored traditional lateral shower age parameter i.e. single (r-independent) shower age as the distinguishing parameter. Later, we attempted to separate out γ-ray initiated EAS on the basis of mean LAP. It is found from the simulation results that γ-ray induced EASs are younger in terms of the mean LAP (i.e. having lower mean LAP) and hence this parameter can effectively separate out γ-ray induced showers from hadronic EAS unlike the case of single lateral shower age. This is probably because of the inadequacy of a single (constant) lateral age parameter to describe the experimental lateral distribution of EAS electrons properly at all distances as noted in several experimental observations. So when a single constant age is assigned (from fitting of the electron density data at different radial distances) to an EAS event, the discriminating power of that parameter on primary masses somewhat becomes dull; it still can distinguish iron initiated showers from proton induced showers but can't effectively separate out γ-ray showers from EASs generated by primary protons. **Fig.4.4a** and **Fig.4.4c** are indicative ones in favour of the inadequacy of $s_{\perp}$ for gamma-hadron discrimination. It is clear from these figures that $< s_{\perp} >$ values for γ-ray and proton induced showers are very much nearer to each other. Lateral distribution of electrons in EAS exhibits universal (primary energy and mass independent) behaviour in terms of LAP (Dey et al. 2012). The present conclusion appears independent on the choice of high energy interaction models, or at least does not have strong interaction model dependence as both the QGSJet and EPOS give similar results.

An important question is the experimental realization of the adopted technique involving LAP. The uncertainty in estimating LAP is usually large in normal circumstance in comparison to that in lateral shower age as the LAP depends on the logarithmic derivative of the electron density versus radial distance. Thus, uncertainty in estimating LAP from experimental data arises mainly from the uncertainties in electron densities and those in radial distance measurements due to erroneous determination of shower core position. These uncertainties should be small for a closely packed air shower array like GRAPES III at Ooty (Gupta et al. 2005) or for a full coverage EAS array like ARGO-YBJ (Sciascio et al. 2007 & Aloisio et al. 2001) and hence the proposed method may successfully work in such kind of experiment. However, at present the ARGO-YBJ carpet provides a full coverage area of about $80m \times 80m$. For successful implementation of the proposed method, a slightly larger coverage area of the carpet would be desirable.

We also tried to identify γ-ray generated EAS by the use of f parameter that describes the ratio of reconstructed average LEDs at two arbitrary distance bands from the shower core as proposed in (Sciascio & Girolamo 2007, Aloisio et al. 2001, Gaisser & Stanev 1991). It is found from the scatter plot of f (as $\boldsymbol{y}$ variable) with the ratio of total muon content to total electron number ($\boldsymbol{x}$ variable) that EAS events are classified according to their respective primaries but the separation occurs not along $\boldsymbol{y}$-axis rather along $\boldsymbol{x}$-axis. This means that essentially the separation is due to the total muon content in EAS, a well studied mass sensitive observable.

CHAPTER 5

GEOMAGNETIC SPECTROSCOPY AND PRIMARY COMPOSITION

5.1 INTRODUCTION

One of the most challenging topics in contemporary astrophysics is the understanding of the origin and nature of high-energy CRs. Several projects across the globe have been envisioned to determine these characteristics of primary CRs. When penetrating from the outer space into the Earth's atmosphere they initiate the development of a phenomenon called EAS by multiple productions of particles in cascading interactions of the primary particles with atmospheric nuclei. The EAS particles can undergo the following processes: (**a**) hadronic interactions, (**b**) electromagnetic interactions, (**c**) unstable particle decays and (**d**) particle propagation (mainly ionization and scattering). Apart from all important processes mentioned above the influence of the Earth's geomagnetic field (GF) on the development of the showers causing asymmetric distribution of shower particles is crucial especially at zenith angles larger than $\sim 50^0$ (Edge et al. 1973, Ave et al. 2000 & Dembinski et al. 2010). However, the effect is commonly ignored at smaller zenith angles where the lateral distribution of secondary particles is well described by analytic function (Greisen 1960) based on a radial symmetry of the distribution of particles in the plane perpendicular to the shower axis.

It is well known that the GF causes the East-West asymmetry on the primary CRs. We have come to realize from the literature that the GF also acts on the charged particles of the EAS during their propagation in the Earth's atmosphere. During the development of a CR cascade in the atmosphere, the secondary charged particles in the shower are influenced by the GF: the perpendicular component of this field causes the trajectories of secondary charged particles to become curved, resulting in a broadening of the spatial distribution of charged particles in the direction of the Lorentz force (see **Fig.5.1**). Finally, this broadening separates positive and negative charged particles to constitute an *electric dipole moment* (Gupta 2011). The possibility of estimating mass composition of CRs by employing such a parameter has been reported in the *rapporteur* of ICRC 2011 (Gupta 2011). However, this aspect was first pointed out by Cocconi nearly sixty years back (Cocconi 1954).

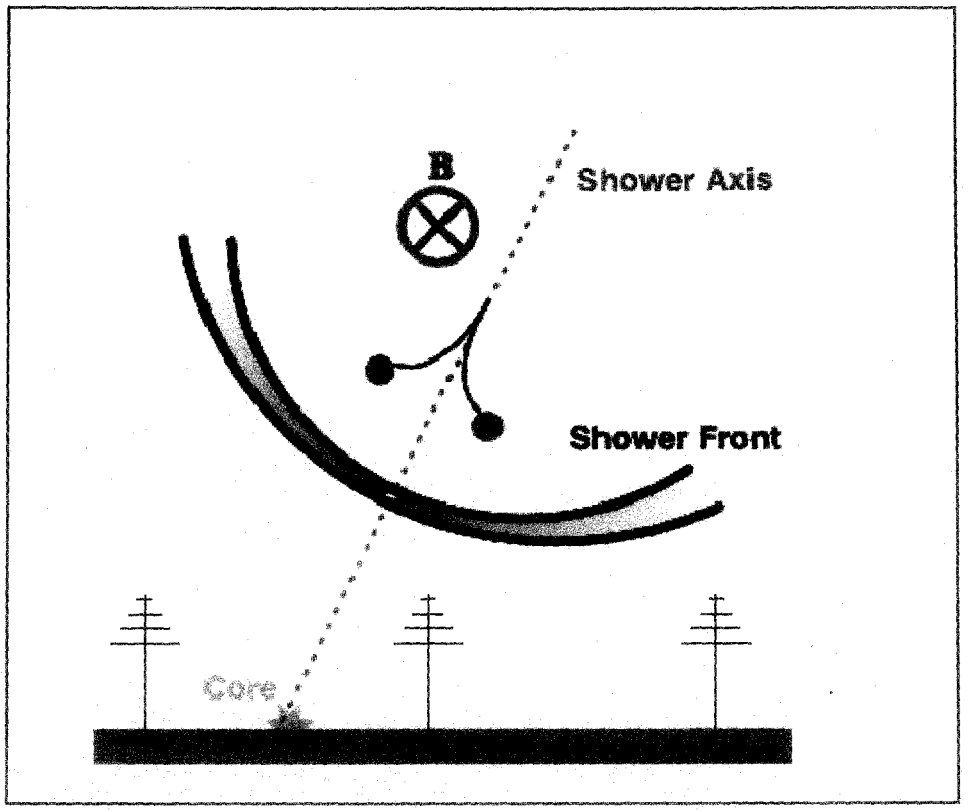

Fig.5.1: Schematic overview of the geomagnetic mechanism.

He further suggested that the geomagnetic broadening effect can be non-negligible in compare to the Coulomb scattering, particularly for the young showers (Cocconi 1954). Since then several studies have been carried out to address the influence of GF on CR EAS (Allan 1970, Colgate 1967, Hillas 1985, Bowden et al. 1992, Lang et al. 1994, Chadwick et al. 1999, Porter 1973, Hough 1973, Browning et al. 1977, Allkofer et al. 1985, Rebel et al. 2008, Mitrica et al. 2009, Sima et al. 2011 & Bernardint 2011) and some important effects arising out of it are also reported. For instance, the separation of electrons and positrons in an EAS by the GF is believed to lead the radio emission in EAS (Allan 1970 & Colgate 1967). The Earth's GF also affects the performance of ground-based gamma ray telescope (Hillas 1985, Bowden et al. 1992, Lang et al. 1994 & Chadwick 1999). The geomagnetic separation of muons can be used to estimate the height of the origin of showers (Earnshaw et al. 1971). The GF induces an azimuthal modulation of the densities of air shower particles, particularly for large angle of incidence (Hillas 1985, Bowden et al. 1992 & Allkofer et al. 1985). If not taken into consideration, the estimated energy of primary CRs may deviate from the true value up to ~2% level at large zenith angles of incidence due to such azimuthal modulation (The Pierre

Auger Coll. 2011). It could also affect the results of large scale anisotropy search by an EAS array if the effect is not accounted correctly (The Pierre Auger Coll. 2011). For the soft component the radiation lengths in atmosphere are very short and electrons/positrons suffer many scatterings thereby frequent changing the directions relative to the GF. As a result the lateral spread of the electrons is mainly due to the multiple Coulomb scattering and the effect of the GF is less pronounced. In contrast after their generation from pion and kaon decays muons travel much longer path without scattering and hence come under the influence of GF. Consequent upon the GF effect should be more pronounced in muon component, particularly for large zenith angles of incidence. The decay schemes of hadonic secondary pions and kaons which produce muons are the following:

$$\pi^{\pm} \rightarrow \mu^{\pm} + \nu_{\mu}(\bar{\nu}_{\mu}) \qquad (5.1)$$

$$K^{\pm} \rightarrow \mu^{\pm} + \nu_{\mu}(\bar{\nu}_{\mu}) \qquad (5.2)$$

Exploiting this feature Capdevielle and his collaborators earlier showed from a MC simulation study that (Capdevielle et al. 2000) heavy nuclei and proton induced showers may be discriminated from the ellipticity of lateral muon distribution and the muon charge ratio (the ratio of positive to negative muons) at convenient distances from the shower core. The so-called ratio of positive to negative muons is a significant quantity which reflects important features of the hadronic meson production in CR collisions and to distinguish the primary mass composition (Wentz et al. 2003 & Vulpescu et al. 2001). In the present work we extend the investigation and from a detailed MC simulation study we would show that the length of the muonic dipole which is formed by the separation of positive and negative muons is found quite sensitive to the mass of shower initiating particles, particularly for inclined showers and hence in principle the parameter can be exploited to estimate primary mass. We would also discuss the practical realization of the method in a real experiment.

5.2 SIMULATION PROCEDURE

For generating EAS events, we employ the air shower simulation program CORSIKA (Cosmic Ray Simulation for KAscade) version 6.600/6.970 (Heck et al. 1998 & Capdevielle 1992). The high energy (above 80GeV/n) hadronic interaction models QGSJET **01** version **1c** (Kalmykov et al. 1997) and EPOS **1.99** (Werner et al. 2006, Pierog & Wener 2008[a]) have been used in combination with

the low energy (below 80GeV/n) hadronic interaction model UrQMD (Bass et al. 1998 & Bleicher et al. 1999). The EGS4 is opted for simulation of the electromagnetic component of shower that incorporates all the major interactions of electrons and photons (Nelson et al. 1985). We consider the US-standard atmospheric model (NASA report 1976) with planar approximation which works for the zenith angle of the primary particles being less than 70^0. The EAS events have been simulated at geographical position corresponds to the experimental site of KASCADE. The geomagnetic field with a homogeneous field approximation is considered. In order to examine the effect of the GF, EAS events are also simulated by switching off the Earth's magnetic field. On the observation level the detection kinetic energy thresholds are chosen as 3 MeV for electrons (e^+ and e^-) and 300 MeV for muons irrespective of primary primary species and energies. The EAS events have been generated for Proton and Iron primaries at fixed primary energy 10^{15} eV taking two zenith angles of incidence, 0^0 and 50^0 and arriving from different geographical directions: North, East, South and West. About 200 EAS events have been generated for each case.

5.3 DATA ANALYSIS

Secondary particles in an EAS are generated maintaining a cylindrical symmetry around the shower axis, which is along the arrival direction of EAS initiating particle. As a result in the absence of the earth's GF, lateral distribution of secondary particles should possesses such a symmetry for all radial distances from the axis in a plane normal to the shower axis. In the observational plane, however, such cylindrical symmetry is distorted for inclined EAS due to geometrical and atmospheric attenuation effects. Since the azimuthal asymmetry in charged particle distribution causes by the GF is superimposed with those caused by geometric and attenuation effect, it is convenient to transform the density information of charge particles of EAS in the observational plane to normal plane so that the sole effect of the GF can be segregated out. Let Z and A are the zenith and azimuthal angles respectively. If (r_0, A) and (r_n, A_n) are the polar coordinates of a point (radial distances are measured from the shower axis) in the observation plane and normal plane respectively as depicted schematically in **Fig.5.2**. From the figure we can easily show that

$$r_n = r_0\sqrt{1 - sin^2 Z cos^2(A - Z)} \qquad (5.3)$$

and

$$tanA_n = \frac{\tan(A - Z)}{cosZ}. \qquad (5.4)$$

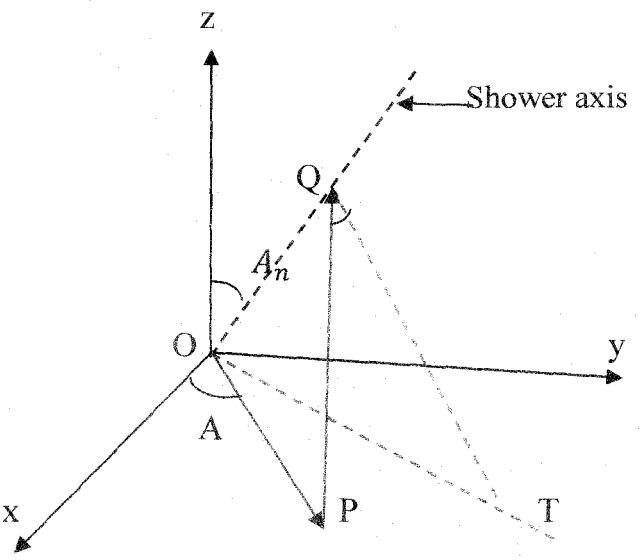

Fig.5.2: Schematic representation of the polar coordinates of the point P. In the observation plane (xy-plane) the polar coordinates of P are (r_0, A), where r_0 corresponds to the segment OP and A is the angle between OP and the x-axis. In the shower front plane (plane $\perp^r$ to the shower axis containing the points P, Q and T) the polar coordinates of P are (r_n, A_n) where r_n corresponds to the segment PQ and A_n is the angle PQT. Notice also that Z represents the zenith angle of the shower.

If the density of a given type of CR secondary at observational plane is denoted as (ρ_0), which is a function of r_0 and A in general, and that in normal plane is denoted by $\rho_n(\equiv \rho_n(r_n))$, in the absence of GF and neglecting the effect of attenuation they are related by the transformation:

$$\rho_n = \frac{\rho_0}{cosZ} \qquad (5.5)$$

We first consider a hypothetical horizontal full coverage air shower array of area $300\,m \times 300\,m$ taking the shower core as the centre of the array. Employing the equations **(5.3)** - **(5.5)** we then transform the simulated density data at observation plane to normal plane.

5.4 GEOMAGNETIC DISTORTIONS OF THE CHARGED PARTICLE DISTRIBUTION: A TOPOLOGICAL ANALYSIS

A basic feature found in the EAS Monte Carlo simulations is the cylindrical symmetry of charged particles in EAS and such symmetry is normally noticed in the simulated data on average basis. In contrast the present analysis revealed an asymmetry in charged particle distribution due to GF, particularly at higher zenith angles as stated above. To get an idea about the magnitude of the asymmetric charged particle distribution due to GF, we introduce a procedure of scanning of charged particle density and barycentre of positive/negative muons with the butterfly (BF) treatment in order to point out ultimately typical signatures relevant to the nature of primaries. The BF structure is shown in the **Fig.5.3**, consisting of two opposite wings around the shower core limited by a pair of symmetric arcs at distances which may be enlarged above 200 m for very large EAS.

The internal angle of the wing is taken as 90^0(quadrant) which can be reduced to emphasize some particular effects. The density of muons inside a wing is compared with that in different wings and the centre of gravity (barycentre) of charged muons (positive and negative separately) are computed from the simulated data. It is possible to rotate the BF around the axis and the corresponding centre of gravities (barycentre) for positive and negative muons successively in each configuration of the BF are computed. The rotation of the BF is measured by the same angle $\psi = 10^0$ (angle between the central axis of each BF's configuration and the x-axis i.e. north in the CORSIKA coordinate system).

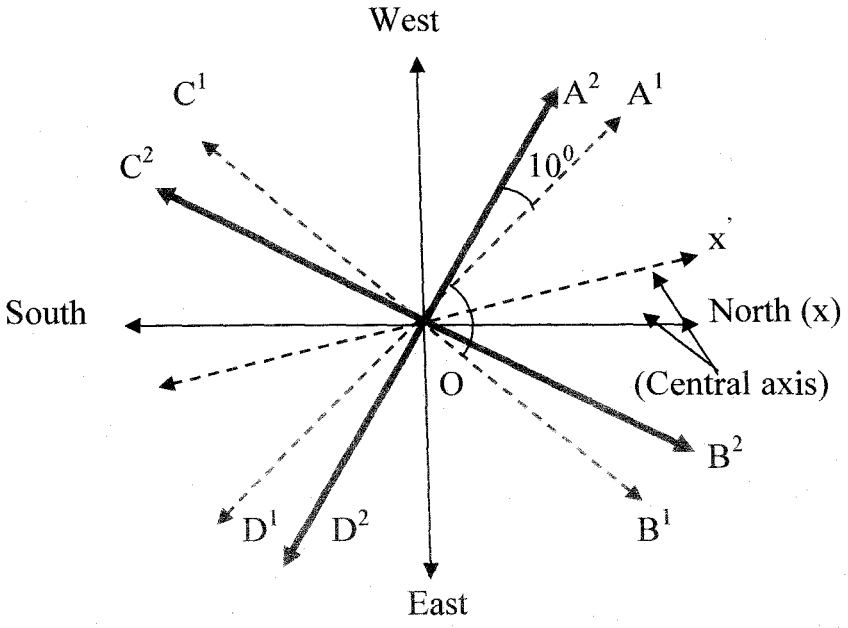

Fig.5.3: Schematic representation of a butterfly (BF) with four wings (viz. A^1-O-B^1, C^1-O-D^1, A^1-O-C^1 and B^1-O-D^1 and then A^2-O-B^2, C^2-O-D^2, A^2-O-C^2 and B^2-O-D^2 etc.). The angle within each wing is 90^0 and rotation of the BF by an amount 10^0 in each case by allowing the rotation of the central axis i.e. North-South by 10^0 in every occasion in counter clockwise direction. The central axis is made to rotate from 0^0 to 180^0 (For some studies the BF is allowed to rotate even from 0^0 to 360^0).

Just to understand about the magnitude of distortions originating from the GF on charged muons we have plotted the coordinates of all barycentres estimated in all successive wings of the BF through the **Fig.5.4**. These barycentres for positive and negative muons are computed separately with and without magnetic field at KASCADE level (nearly no magnetic field is provided by suppressing the KASCADE magnetic field components to 10^{-4} times to their usual values in CORSiKA simulation). The **Fig.5.4** reveals that the imprint of GF on charged muons is clearly visible even for EAS with 0^0 zenith angle from any geographical direction. It has been found that the GF effect is more pronounced for EAS with higher zenith angles.

For these vertical showers with $B \sim 0$ the barycentres are highly concentrated within a small region near the origin (shower core) of the CORSIKA plane. But switching on the KASCADE magnetic field the barycentres get spreading out from the core region for both types of muons.

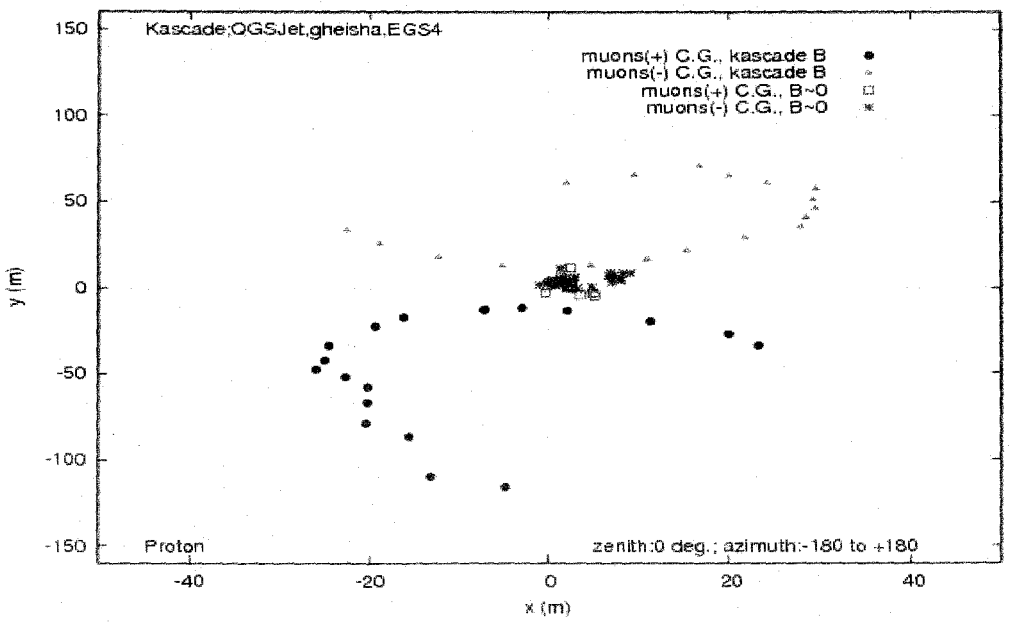

Fig.5.4: The coordinates of different barycentres in successive wings of BF (i.e. B^1-O-A^1, B^2-O-A^2 etc.) at KASCADE level with and without (nearly zero) magnetic fields for $\mu^+$and μ^-separately.

5.5 RESULTS AND DISCUSSION

To examine the azimuthal asymmetric characteristics of the charged particle distribution due to GF, we estimated density/total number of each variety of particles over a small azimuthal angle bin. The azimuthal variation of total (truncated) muon content at observational plane and at normal plane are shown in **Fig.5.5** and **Fig.5.6** respectively for proton and iron initiated EAS of zenith angle of incidence $50^0$and arriving from the (geographical) north. These figures imply that the azimuthal asymmetry in the observational plane is mainly due to geometric effect while in normal plane the observed small azimuthal asymmetry seems to be due to attenuation effect. It appears that the attenuation effect is small, at least when the zenith angle of incidence is within 50^0.

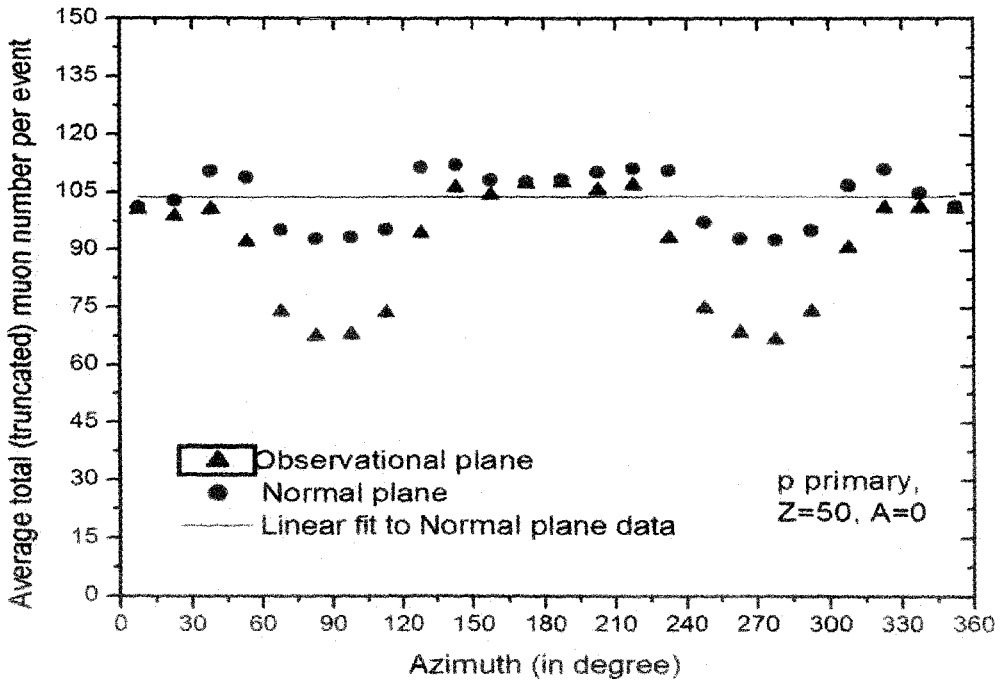

Fig.5.5: Correction for inclination for proton primary.

Since positive and negative particles behave in an opposite way under magnetic field, the geomagnetic effect is not revealed from the azimuthal variation of the total muon content. To examine geomagnetic effect we draw the angular variation of charged muons in inclined air showers which are shown in **Fig.5.7** and **Fig.5.8** for proton primary arriving from the north direction. To understand the influence of GF clearly, we also studied azimuthal variation of charged muons by turning off the GF, which is accomplished in CORSiKA simulation by dividing the components of the GF by a factor of 10^4. Such variations are also included in **Figs.5.7–5.8**. Azimuthal variation of charged muons for iron primary arriving from north and east directions are displayed in **Fig.5.9** and **Fig.5.10**.

The azimuthal variation of electron and positron are shown in **Fig.5.11** for both by turning off and on the GF. As expected it is found that electrons and positrons are much influenced by the GF.

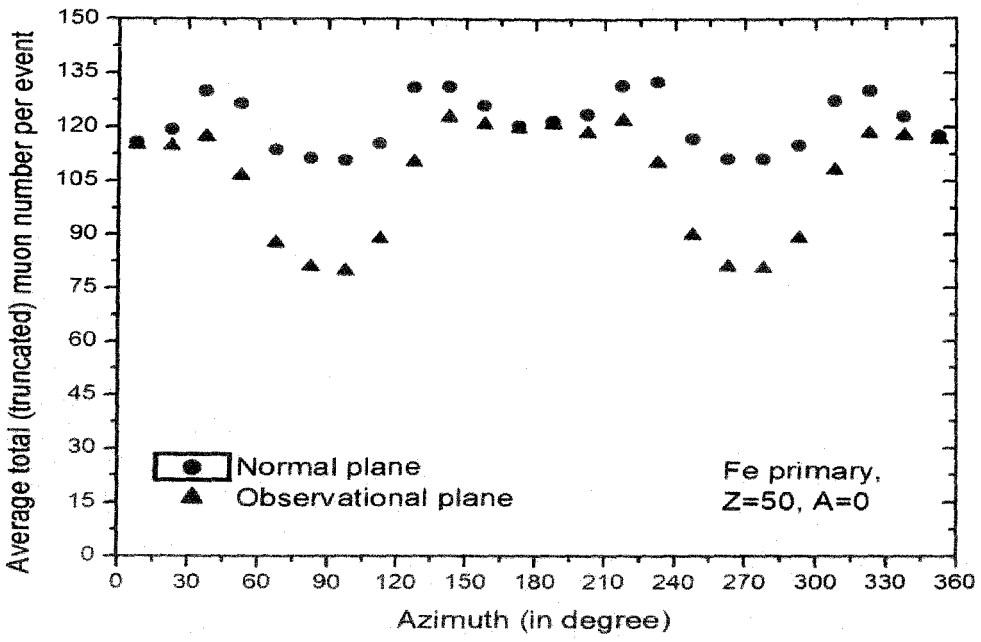

Fig.5.6: Correction for inclination for iron primary.

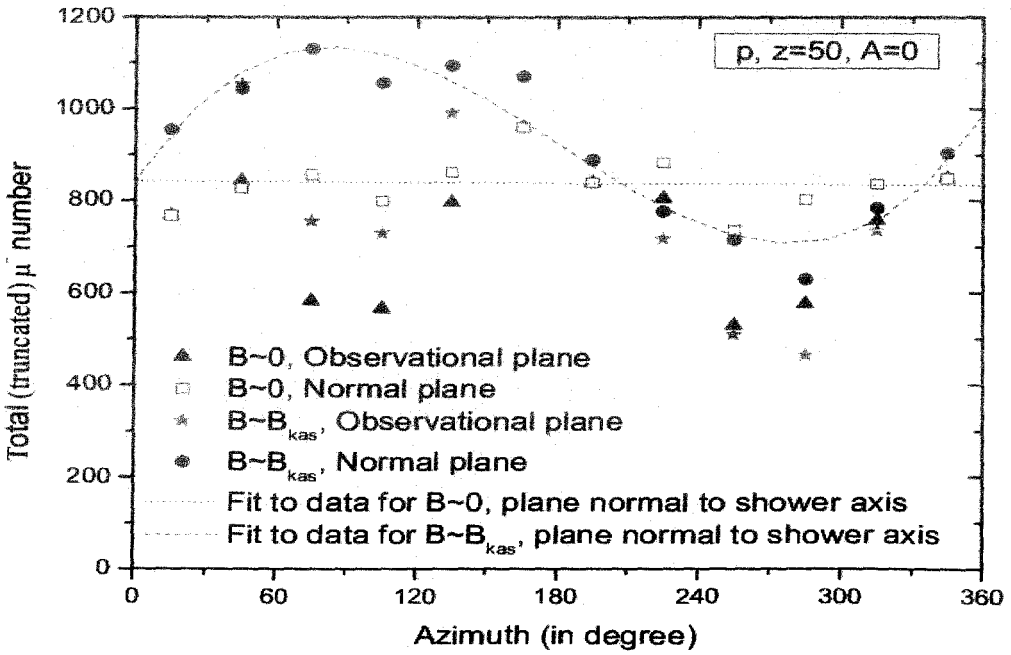

Fig.5.7: Azimuthal variation of μ^- for proton primary.

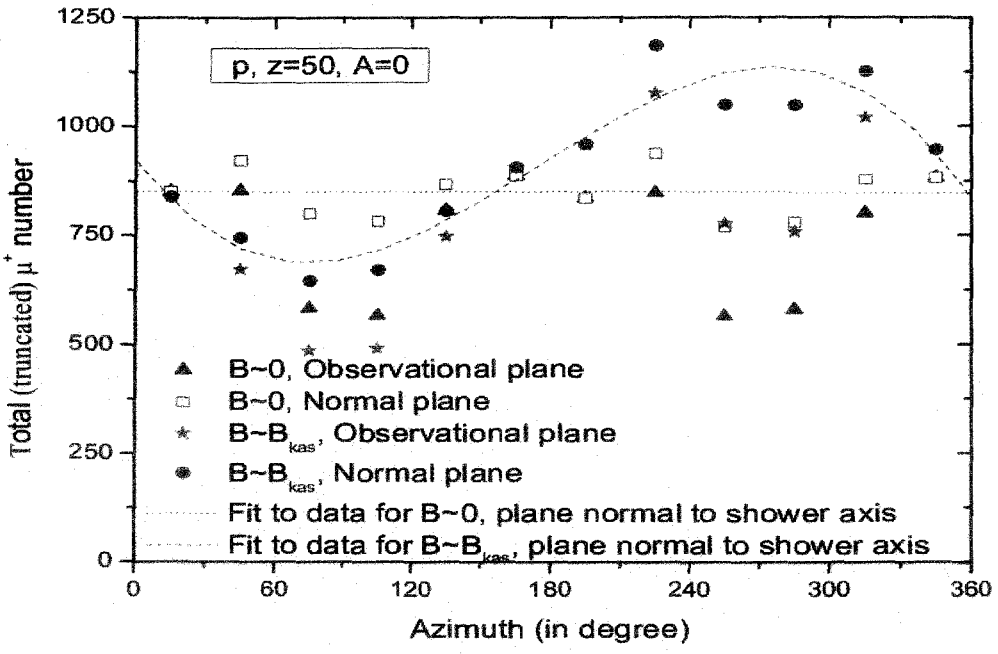

Fig.5.8: Azimuthal variation of μ^+ for proton primary.

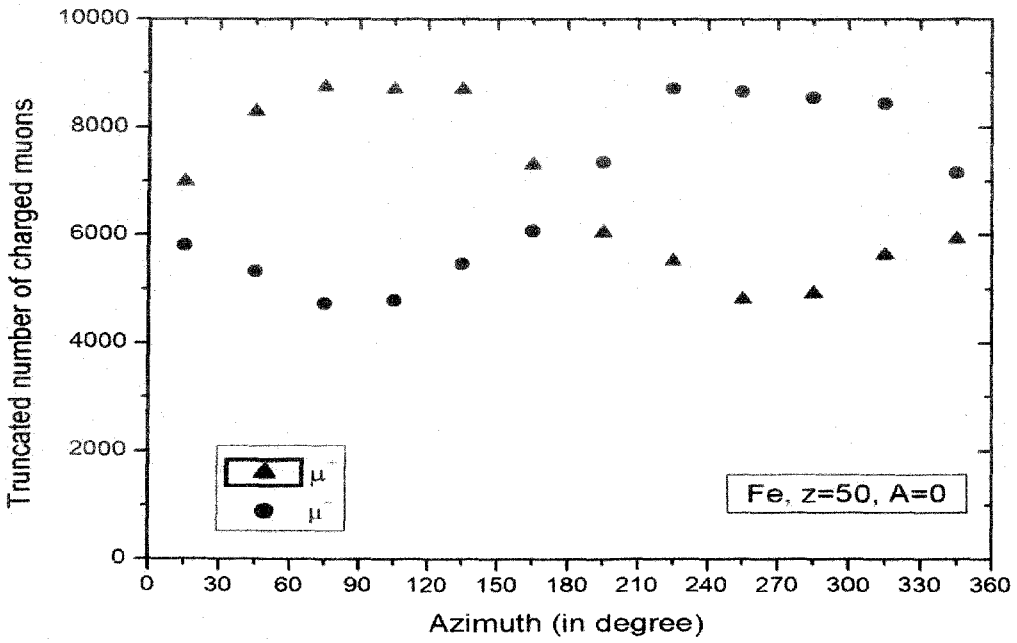

Fig.5.9: Azimuthal variation of charged muons for Fe primary arriving from North direction.

To quantify the influence of GF as well to identify some typical signatures of the shower initiating primary particle we have calculated in each shower the coordinates of positive and negative particles barycentres and thereby estimated the

muon dipole length (l_μ), which is the separation of centre of gravity of negative and positive charged muons. For this purpose we have employed the butterfly (BF) treatment: as stated the BF consists of two opposite wings around the shower core limited by a pair of symmetric arcs. The variation of *muon dipole length* with azimuthal angle for proton and iron initiated EAS of zenith angle of incidence 50^0 and arriving from (geographical) north and east directions are shown in **Fig.5.12**. In this figure the azimuthal variation of *muon dipole length* are also shown when the GF is switched off. In **Fig.5.13** we compare the azimuthal variation of *muon dipole length* for proton and iron primaries.

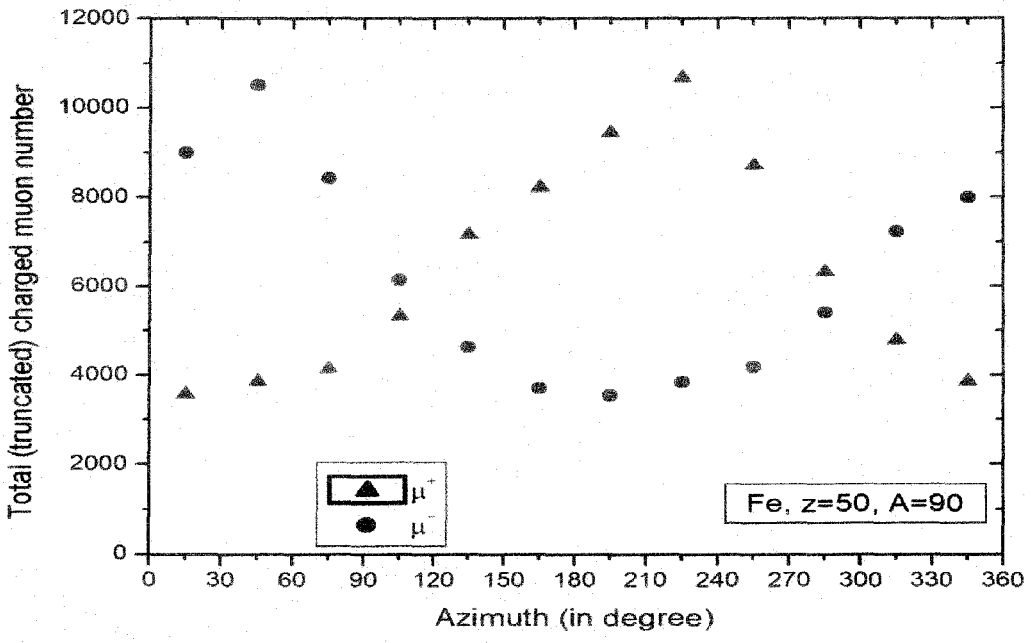

Fig.5.10: Azimuthal variation of charged muons for Fe primary arriving from East direction.

It is found from the **Figs. 5.12-5.13** that the length of the muon dipole increases due to GF. Also the *muon dipole length* is found sensitive to primary mass; it is larger for iron primary in compare to that for proton primary. So the parameter can be used, at least in principle for extracting the nature of primary particles.

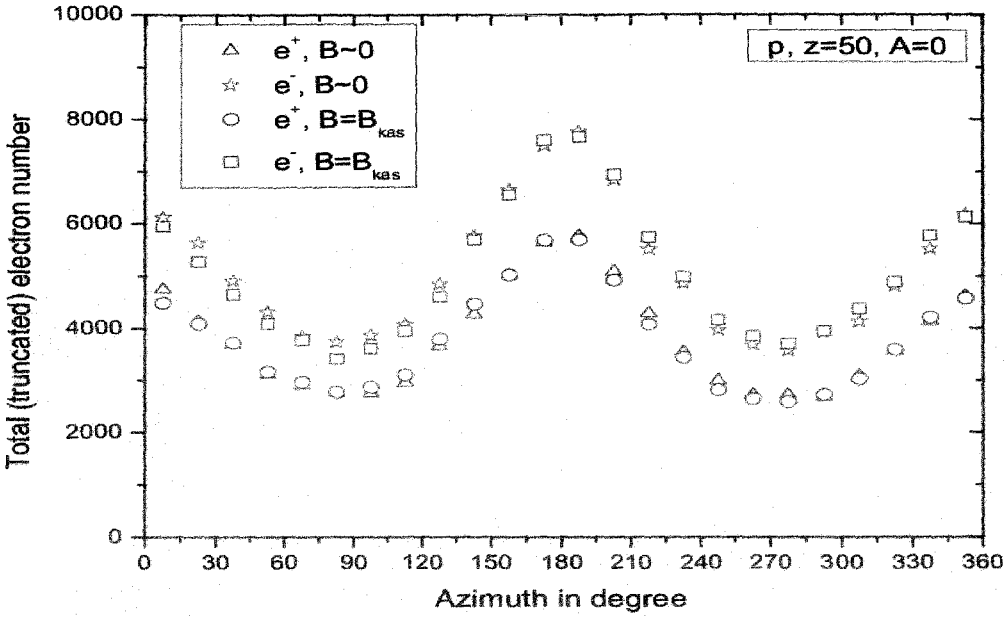

Fig.5.11: Azimuthal variation of charged electrons for p primary arriving from North direction.

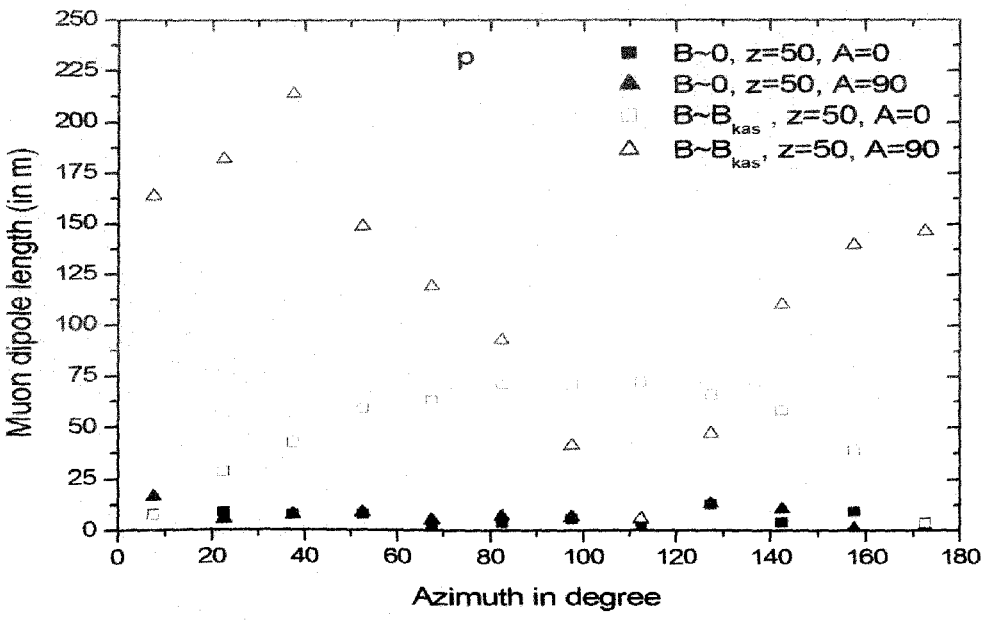

Fig.5.12: Azimuthal variation of muon dipole length for p primary arriving from North and East directions.

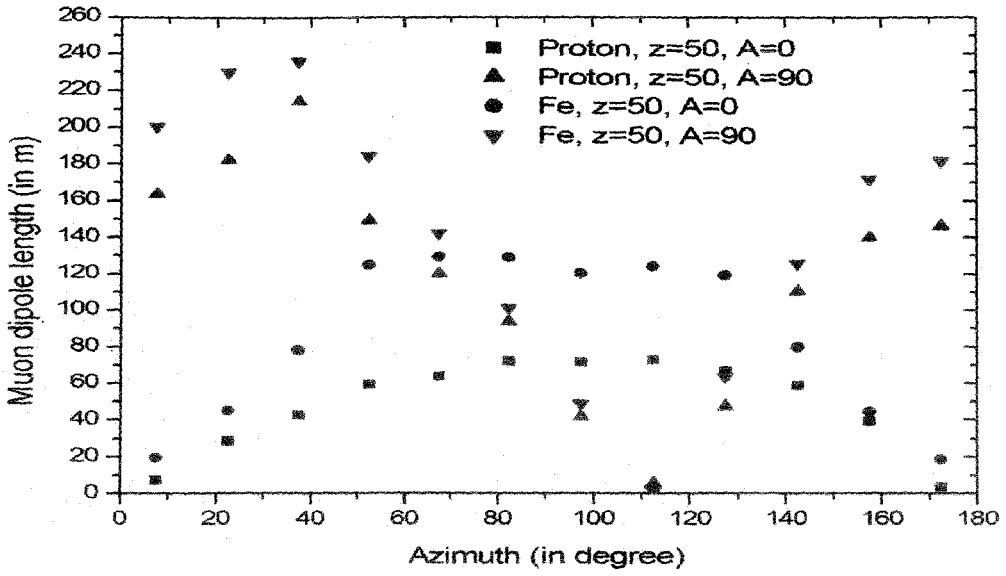

Fig.5.13: Comparison of azimuthal variation of muon dipole length for p and Fe primaries arriving from North and East directions.

5.6 CONCLUSIONS

Our analysis concerning the effects of the GF on positive and negative muon and electron components of inclined EAS reveals several interesting features such as azimuthal asymmetries, sectorial muon-electron relative abundances, amplitude of fluctuations between proton and iron induced showers. Such effects are found to persist and are of comparable magnitude if we replace the UrQMD code in the simulation by the Fluka code in the treatment of low energy hadron collisions.

There are some recent proposals of studying positive and negative muons separately in individual EAS event. In fact few ongoing experiments, such as the WILLI detector (Wentz et al. 2001, Brancus et al. 2003 & Agostinelli et al. 2003) or the Okayama University, Japan EAS installation, have the capability to extract charge information of high energy muons but these experiments do not have large muon detection area, which is needed to extract information about the nature of primaries from the study of geomagnetic influence on EAS muons. If in future these experiments are extended in order to cover larger detection area or new installation of large muon detection area with capability of charge identification come up, the present proposal can be exploited to extract the nature of shower initiating primaries.

CHAPTER 6

ROLE OF AIR SHOWER FLUCTUATIONS ON ESTIMATION OF HADRONIC CROSS SECTIONS

6.1 INTRODUCTION

The study of cosmic ray (CR) extensive air showers (EASs) offers a unique opportunity to extract p-air interaction cross-section at energies well beyond the LHC region at CERN (Abraham et al. 2008). Generally, EAS experiments map the depth of first interaction of the CR particle on an average basis by exploiting its relationship to some air shower observables. The absorption of EAS flux having the same kind of CR particles, the same primary energy and stage of their development at different atmospheric depths is linked with the average mean free path of shower induced particle and this property is often exploited to estimate proton-air cross-section (Hara et al. 1983, Baltrusaitis et al. 1984, Honda et al. 1993 & Aglietta et al. 2009). While estimating p-air cross section from experimental data, the selection of showers of constant energy and stage is usually done by considering simultaneously constant muon size and shower size ranges of small widths at the observation level whereas to ensure the primaries of the selected showers are of the same type, additionally the magnitude of shower size is chosen suitably. This technique is usually called the constant N_e- N_μ method which is being applied in arrays of particle detector experiments. The stated method of estimating hadronic cross section is, however affected mainly by the intrinsic shower fluctuations in the EAS longitudinal development (Alvarez-Muniz et al. 2002 & Ulrich et al. 2009[b]). Besides, the method is found to depend strongly on the choice of high energy interaction models (Alvarez-Muniz et al. 2002 & Ulrich et al. 2009[b]). To disentangle these fluctuations from those of the first interaction point is not an easy task.

The rate of shower numbers $f(\theta)$ of a given primary energy interval selected through their muon size bin and shower size bin corresponding to the maximum development (choosing a common tail from the frequency distribution of the shower size for different zenith angles) is expected to attenuate with increasing atmospheric depth ($sec\theta$). Utilizing this fact the experimental absorption length Λ_{obs}, is obtained from the following equation:

$$f(\theta) = G(\theta)f(0)\exp\left[-\frac{X_0(sec\theta-1)}{\Lambda_{obs}}\right] \qquad (6.1)$$

In equation (**6.1**), X_0 denotes the vertical atmospheric depth of the location while $G(\theta)$ measures its geometrical acceptance in a particular angular bin.

The absorption length of EAS (Λ_{obs}) and the interaction mean free path (λ_{obs}) are, however, not the same but Monte Carlo simulation results suggest that they are connected through the relation (Ellsworth et al. 1982)

$$\Lambda_{obs} = k \times \lambda_{obs}, \qquad (6.2)$$

where k is a constant parameter; the numerical value of k has been found to depend on the primary energy range, the observation level of the experiment and the hadronic interaction model adopted and has to be obtained from Monte Carlo simulations for a particular EAS observation. The common perception is that the deviation of k from unity is originated mainly by fluctuations in air shower development. Besides, different features of the hadronic interaction models also could be partly responsible for $k \neq 1$.

The purpose of the present work is to critically examine whether fluctuations in air shower development is the prime cause for the deviation of the value of k from unity or not. For this purpose a detailed Monte Carlo simulation study has been conducted.

6.2 THE SIMULATION

The EAS simulations are performed utilizing the CORSiKA code (Heck et al. 1998 & Capdevielle 1992) with QGSJET **01** v **1c** (Kalmykov et al. 1997) high energy hadronic interaction model. Hadrons with energies below 80 GeV/n are treated with the GHEISHA **2002d** (Fesefeldt 1985) interaction model. The shower size (N_e) is obtained directly by adding all $e^+$and e^- from the produced γ-rays involving electromagnetic interactions with the EGS**4** option (Nelson et al. 1985). The zenith angle was restricted to events with $\leq 50^0$. The EAS events were generated mainly for proton and iron nuclei as primaries. Showers have been simulated with a particular energy of 2×10^{14} eV, spectral index -2.7. The EAS events were simulated at the geographical position to the experimental site of ARGO-YBJ (Sciascio et al. 2007) (latitude 30.11^0 N, longitude 90.53^0 E, $607\ gm - cm^{-2}$ a.s.l). The magnetic fields are provided accordingly. On the observation level, the kinetic energy thresholds were chosen as 3 MeV for

electrons (e^+ and e^-) irrespective of the primary species. About 2×10^4 EAS events were generated for each primary.

6.3 THE ANALYSIS METHOD

Most of the observables required for the analysis are obtained directly from the simulated data. The absorption length Λ_{sim}, evaluated from equation (**6.1**) is supposed to be combined the effects of the first interaction length λ_{sim} and fluctuations of the EAS development. In experimental evaluation of cross section by air shower method a fixed primary energy is usually chosen by selecting EAS of same muon size. Since our prime motivation is to judge the effect of air shower fluctuations on measurement of cross sections we generated EAS at fixed primary energy. While taking a fixed shower size bin we have chosen showers of the same depth between the first interaction point and the observation level, under the assumption of no fluctuations in the successive interactions (Fukui et al. 1960). The shower size bin is selected from the tail portion of the shower size distributions corresponding to different small zenith angle bins ($\Delta\theta = 3^0 - 7^0, 8^0 - 12^0$etc.) at a particular primary energy. Finally measuring the attenuation of frequencies (event rate) of showers with fixed energy and shower size at different atmospheric depths ($sec\theta$), we have estimated the absorption length Λ_{sim}. The detection efficiencies at different inclinations have to be taken carefully for estimating Λ_{sim}. Due to the imposed full detection efficiency for simulated data, the geometrical acceptance in each individual $sec\theta$ bin is simply given by $\Delta sec\theta = sec7^0 - sec3^0, sec12^0 - sec8^0, \ldots\ldots$ etc. and has been taken carefully for estimating Λ_{sim}.

The Monte Carlo simulation directly gives the value of the hadronic mean free path λ_{sim} for each air shower event which has been noted and a frequency distribution of directly observed λ_{sim} for a common shower size bin is formed. The mean value of λ_{sim} is obtained from the Gaussian fit of the λ_{sim} distribution. The k-parameter is finally obtained by taking the ratio of Λ_{sim} to λ_{sim}.

In order to compare the effects of the intrinsic fluctuations on k with other EAS observables sensitive to air shower fluctuations we have considered the depth of shower maximum and EAS slope parameter i.e. LAP. The method of estimating the LAP has been described in chapter **3** in detail.

The depth of shower maximum is estimated for each EAS event from the longitudinal profile of EAS. The mean LAP, the depth of shower maximum and the k-parameter have been studied at a particular energy for both proton and iron induced showers.

6.4 RESULTS AND DISCUSSION

6.4.1 THE k –PARAMETER FOR PROTON AND IRON INITIATED EASs

Our program is to examine critically the physical meaning of the parameter k related with EAS fluctuations. Simulated EAS events for p and Fe at several small zenith angle intervals are generated and study the shower size spectra at a fixed primary energy of 2×10^{14} eV. We have selected showers which have N_e between 7.5×10^4 and 1.15×10^5 for protons and between 3.5×10^4 and 5.5×10^4 for irons respectively. Such selections of N_e are shown in **Fig.6.1a** and **Fig.6.1b**.

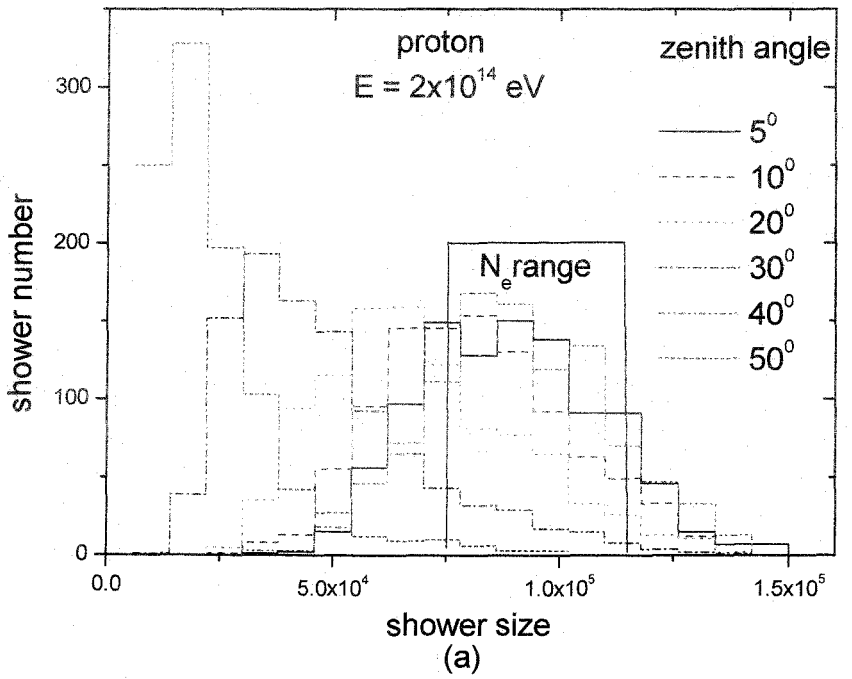

(a)

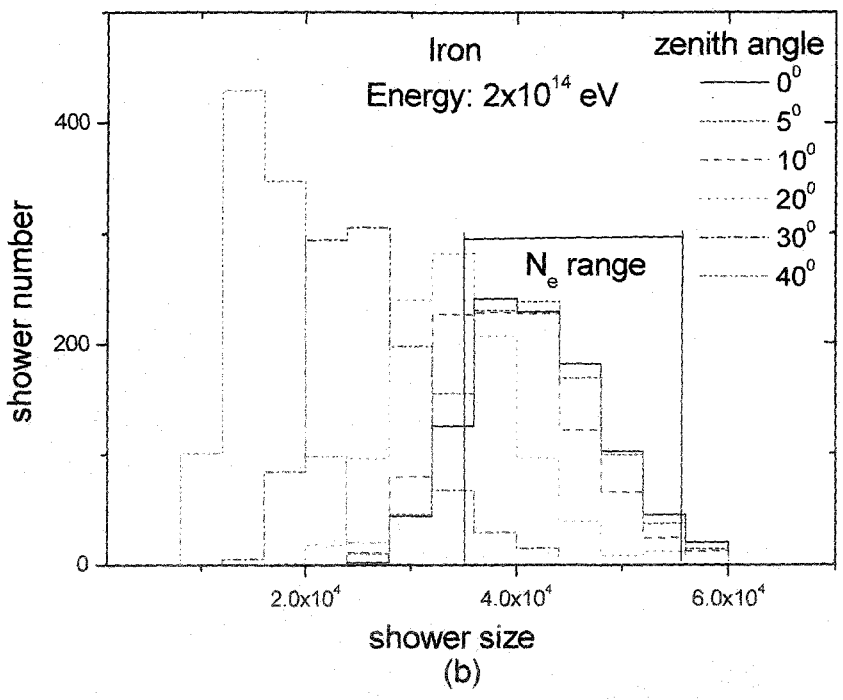

Fig.6.1: [a]-[b] Distributions of shower size for p and Fe induced showers at different mean zenith angles having energy 2×10^{14}eV. The selected showers have $log_{10}N_e = 4.87 - 5.06$ and $4.54 - 4.74$ for p and Fe respectively.

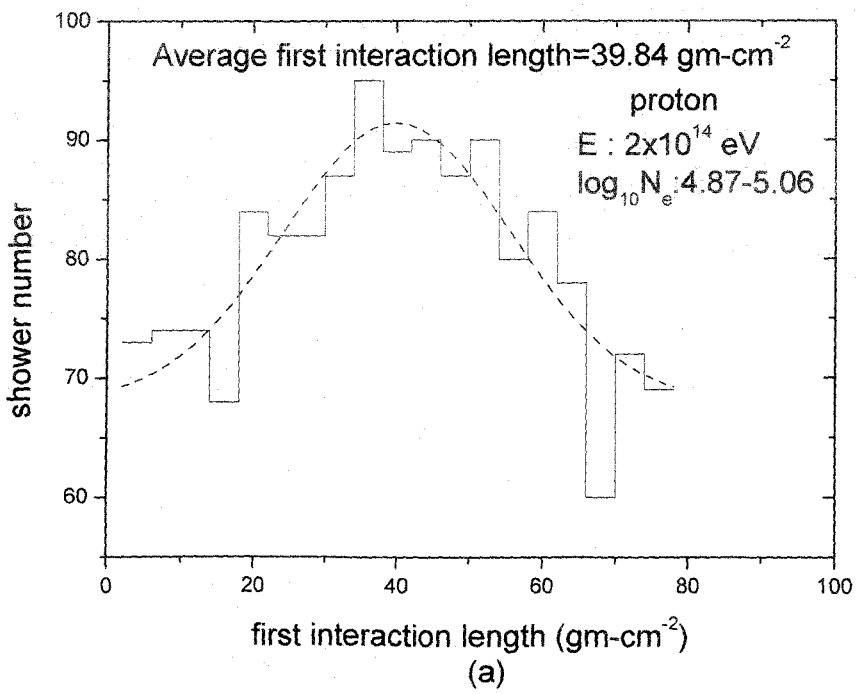

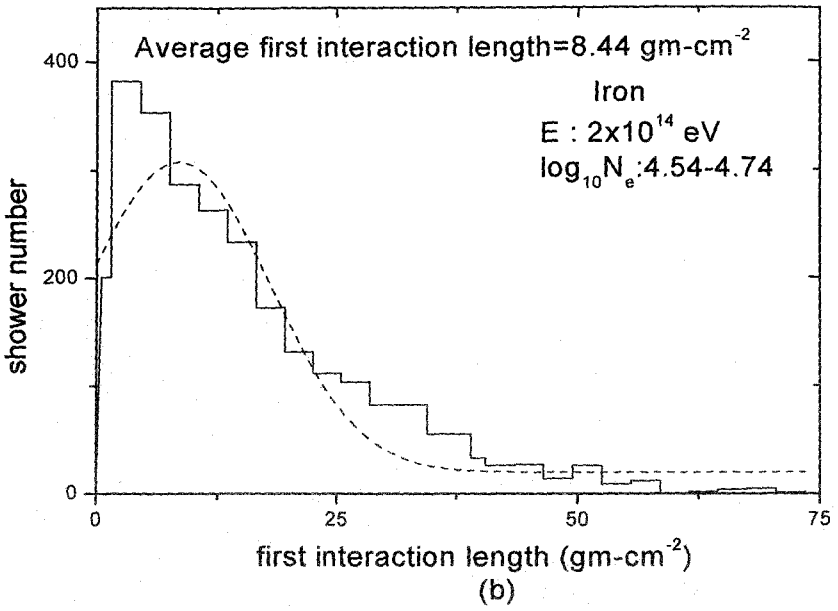

Fig.6.2: [a] Distributions of depth of first interaction for proton and [b] Same as figure 6.2a but for iron with different $log_{10}N_e$ bins. Gaussian fits (---- fit) are made.

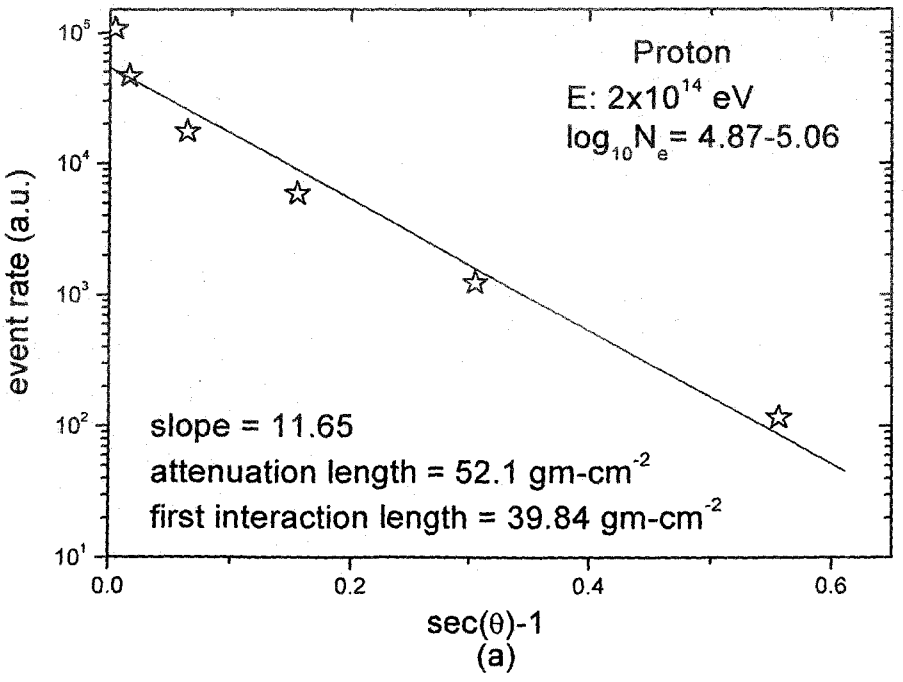

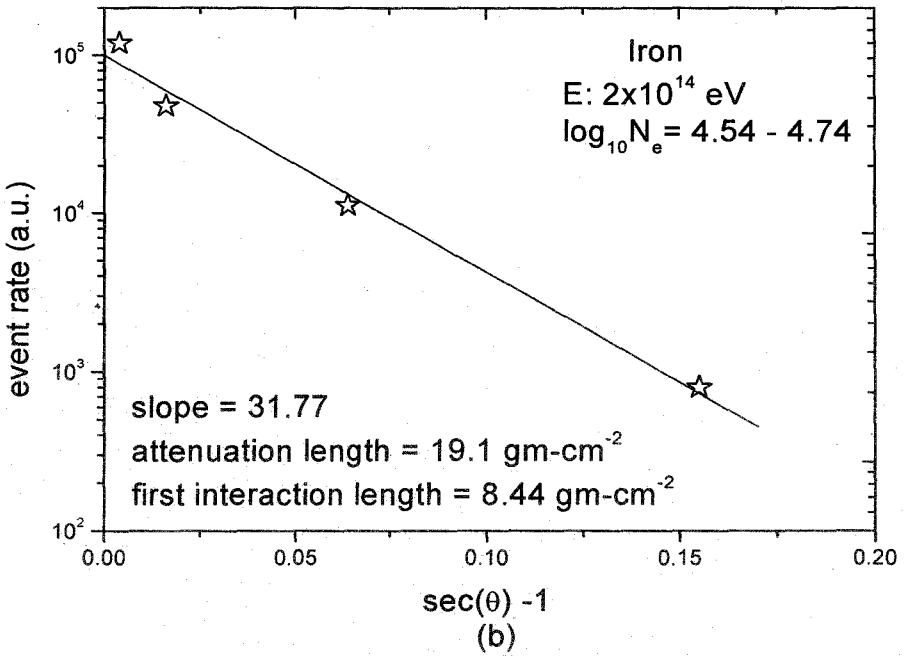

Fig.6.3: [a] Distributions of $sec\theta$ for proton and [b] iron initiated showers including the correction for the geometrical acceptance in each angular bin.

Primary	$log_{10}N_e$	Λ_{sim}	λ_{sim}	k
p	$4.87 - 5.06$	52.1 ± 3.9	39.84 ± 4.3	1.31 ± 0.04
Fe	$4.54 - 4.74$	19.1 ± 1.4	8.44 ± 0.87	2.26 ± 0.09

Table 6.1: Summary of the results obtained from attenuation studies using constant N_e-N_μ method for p and Fe at energy 2×10^{14}eV.

The whole selection procedure discussed is now applied to evaluate Λ_{sim} and then k for both the proton and iron showers. Event numbers as a function of $sec < \theta >$ after correction for the geometrical acceptance of each angular bin are shown in **Fig.6.3a** and **Fig.6.3b** for proton and iron.

The parameter $< \theta >$ denotes the mean zenith angle, obtained from each angular bin. It should be noted that for iron showers we have gone up to only $sec < 30^0 >$ for evaluating the attenuation length due to higher rate of absorption of EAS electrons with increasing depth. The mean depths of first hadronic interaction corresponding to $log_{10}N_e = 4.87 - 5.06$ and $4.54 - 4.74$ for p and Fe primaries could be obtained from the fitting of their frequency distributions and are shown in **Fig.6.2a and Fig.6.2b**. The absorption lengths and resulting fluctuation parameters are summed up in **table 6.1**. The given uncertainties are the statistical ones.

6.4.2 EAS FLUCTUATIONS REFLECTED IN COMPOSITION SENSITIVE OBSERVABLES

The observable parameters the depth of shower maximum (X_m) and its fluctuations $(\sigma(X_m))$ were used widely for CR composition analyses in ultra-high energy region (Auger Coll. 2010). The fluctuations are larger for proton than for iron initiated showers, as expected. Since X_m distribution contains the imprint of the effect of first interaction (λ_{int}) distribution therefore fluctuations of λ_{int} should be larger for proton than iron. Since all these effects in the initial stage of shower development have an impact on the later stage of EAS so the fluctuations in the slope of lateral electron distribution (in terms of LAP) would also obey the similar behaviour.

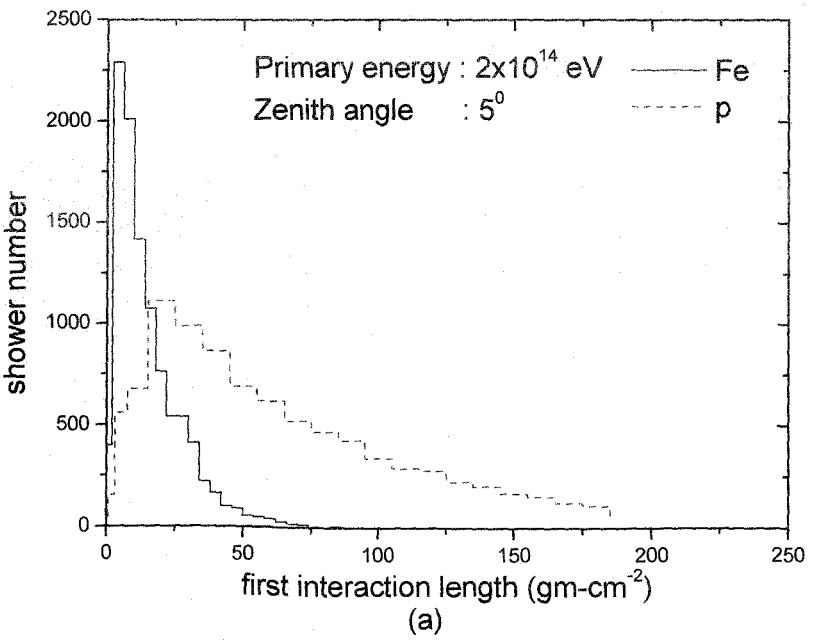

(a)

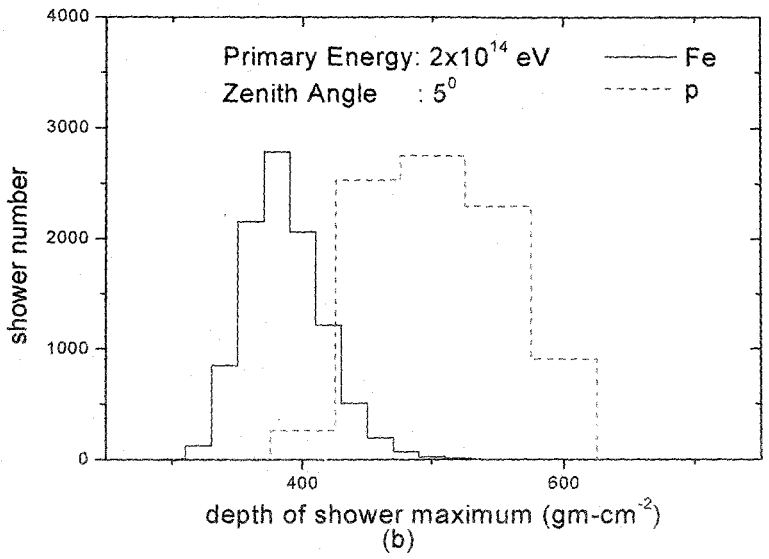

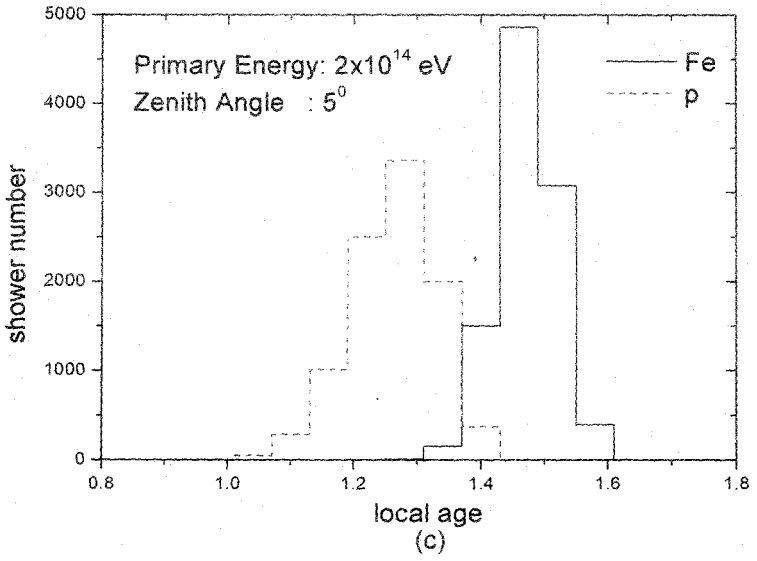

Fig.6.4: [a] Distributions of depth of first interaction; [b] depth of shower maximum and [c] local age for p and Fe primaries at 2×10^{14}eV.

Figs. **6.4a, 6.4b** and **6.4c** show the distributions of the event-by-event values of λ_{int}, X_m and s_{local} in simulated samples of proton and iron primaries at 2×10^{14} eV. The fluctuations of proton and iron initiated showers are clearly visible in the above figures and these magnitudes are the expected ones in the concerned primary energy.

Meaningful information about EAS fluctuations can be extracted from the results of fits for the simulated samples of proton and iron initiated showers is shown in **table 6.2**.

Primary	$< \lambda_{int} >$	$\Delta\lambda_{int}$	$< X_m >$	ΔX_m	$< s_{local} >$	Δs_{local}
p	31.2	42.5	503.5	139.0	1.27	0.15
Fe	8.64	9.10	382.5	60.7	1.47	0.12

Table 6.2: The different columns show the results of the fits to the average distributions constructed from the simulated events. The widths in all three parameters are larger for proton than iron showers.

The magnitudes of fluctuations obtained from all standard measurements in this section clearly contradict the results obtained in the section **6.4.1** in terms of k listed in **table 6.1** on EAS fluctuations.

6.5 DISCUSSION AND CONCLUSIONS

The absorption lengths of proton and iron induced showers at their maximum development in air are estimated at a fixed energy 2×10^{14}eV at the ARGO-YBJ level from Monte Carlo simulation results. The technique involving absorption of CR events for a fixed primary energy has been applied for estimating Λ_{sim}. The mean free path λ_{sim} is related to Λ_{sim} via the k-factor as given in equation **6.2** for simulated data. We evaluated the k parameter for both proton and Fe initiated showers. While measuring cross section by absorption technique muon size is usually considered in EAS experiments to fix the primary energy. In the present study we simulated events for a fixed primary energy. Thereby our results are not affected by the uncertainty of energy estimation.

It is found that the mean value of k for iron induced showers exceeds that for the proton initiated showers. The deviation of k from unity is believed to be mainly due to the fluctuations in cascade development. However, in such a case k for iron induced showers is expected to be smaller than that for proton showers. Note that the fluctuation in the first interaction length is the main source of fluctuation which is higher in proton shower. In the absorption length technique of measuring cross section we essentially study the distribution of first interaction

length and hence the technique is unaffected by the fluctuation of the first interaction length. In the development of air shower after the first interaction, the fluctuations of initial few stages are also important. This is because the leading particle carries about 50% of interaction energy. Hence the effect of fluctuation in proton initiated air showers should be higher than in a Fe induced shower (which has much more secondaries and hence the net effect of fluctuation is reduced when sum of the fluctuations of all secondaries are taken into account) even when cascade development after the first interaction is considered. Such a feature is revealed from the fluctuations of shower age as shown in **Fig.6.4c**. So if fluctuation is the main cause of non-unity of k, the parameter should be smaller for Fe shower than proton shower which is in contradiction to our findings. Hence the physical meaning usually attached to the k-parameter is questionable.

Usually k is assumed from an EAS model, which biases the final results for all the experimental cross-sections. The characteristics of hadronic interactions may be responsible for the deviation of k from unity. The parameter k strongly depends on the average inelasticity and the inelasticity distribution of p and π reactions. Particularly on which other important features of hadronic interactions are responsible for the k-factor will be a subject of future investigation. In addition, a systematic study of the energy dependence of the k-factor is also needed.

CHAPTER 7

NEUTRINO AND GAMMA-RAY SIGNATURES OF PeV COSMIC RAYS ACCELERATED BY PULSARS

7.1 INTRODUCTION

For studying fundamental physical issues in some extreme conditions like strong gravity, strong magnetic fields and high densities, rotation-powered pulsars and pulsar wind nebulae (PWNe) offer fascinating galactic sources next to supernovae remnants and excellent laboratories (Link & Burgio 2005, 2006). On the other hand, the probable candidates of extra-galactic origin for high-energy neutrino/gamma-ray radiation include gamma-ray bursts, active galactic nuclei etc. (Halzen & Hooper 2002). Pulsars are rotating neutron stars and it is known to us that they derive their power at the expense of their rotational energy. The major challenge in this field is however, for clear understanding of the energy conversion mechanisms of rotational power into observed electromagnetic radiation like gamma-rays and neutrinos. It is generally agreed that this occurs through acceleration of charged particles to extremely relativistic energies, using the rotating magnetic field as a unipolar inductor to create very high electric potential difference. Besides this feature, there is a divergence of thoughts regarding acceleration regions: whether the acceleration takes place in the intense field zone near the neutron star surface or in the outer magnetosphere near the speed of light cylinder, or even beyond the light cylinder in the wind zone. The particle acceleration may well be occurring in all of these regions, either in the same pulsar or in pulsars of different ages.

New detection methods and theoretical studies of rotation-powered and magnetically feeds compact objects are current subjects in TeV astrophysics. In recent years, many galactic pulsars and PWNe have been discovered to be gamma-ray emitters (da Oña 2011). These galactic sources can also potentially produce interesting event rates in neutrino telescopes. Since they are at shorter distances to the Earth ($\sim 1 \div 10$ kpc) compared to extra-galactic sources, the source luminosity required for a galactic source to produce the same event rate as an extra-galactic one, is few orders of magnitude smaller. In order to produce high energy neutrino fluxes, galactic sources must accelerate particles at sufficiently high energies. In

this regard, Hillas derived the maximum energy E at which a particle of charge Z can be accelerated, from the simple argument that the Larmour radius of the particle should be smaller than the size of the acceleration region (Hillas 1984).

Recent results of Link and Burgio's (LB) (Link & Burgio 2005, 2006) calculations revealed that young ($t_{age} \lesssim 10^5$ yrs.) and rapidly rotating neutron stars having a stellar magnetic moment with a component anti-parallel to the spin axis, (as we expect in half of the neutron stars), could emit TeV muon neutrinos with fluxes observable by operating or planned large area neutrino telescopes such as *AMANDA-II*, and *Ice-Cube* (Halzen 1990) and *ANTARES*, *NEMO* and *NESTOR* (Carr 2003). As a conjecture to be verified by observations, Link and Burgio considered that protons or heavier ions are accelerated near the surface by the polar caps to PeV energies. When these accelerated ions interact with the thermal radiation field of pulsar, the Δ-resonance state (Δ^+ is an excited state of the proton, with a mass of 1232 MeV) may occur provided their energies exceed the threshold energy for the process. Though radiation losses limit the maximum energy that can be attained by the nuclei in the acceleration process, such an energy condition is expected to satisfy for several pulsars. Subsequently, the Δ^+ particles quickly decay to π^+, and finally muon neutrinos are produced.

The presence of a hadronic component in the flux of pulsar accelerated particles should result in the emission of high-energy neutrinos and gamma-rays simultaneously as both charged and neutral pions are produced in the interactions of energetic hadrons with the ambient photon fields surrounding the acceleration region. Here, we would show that for the model adopted by LB the estimated TeV gamma-ray fluxes from several nearby pulsars are higher than the observed upper limits of fluxes. In the quest for reasons of such inconsistency, we note that an implicit assumption in the Link and Burgio estimation of neutrino flux is that the polar cap area is equal to the neutron star surface area. Such an assumption seems unreasonable in view of the polar cap geometry (Beskin et al. 1993).

A young neutron star is generally encircled by PWN. In recent years, many Galactic PWNe have been discovered to be gamma-ray emitters (da Oña 2011). It was predicted that the gamma-ray luminosity of these nebulae is connected to the spin-down power i.e. the loss rate of rotational energy of the pulsar, and that pulsars with $\dot{E} > 10^{34-35}(\frac{d}{1kpc})^2$ erg-s^{-1} power nebulae that are detectable in gamma-rays (Aharonian et al. 1997). Positive ions, after gaining energy from

pulsar gaps, will move away from the pulsar practically along the open field lines and will finally inject into the nebula. It was very likely that these energetic ions would be trapped by the magnetic field of the nebula for a long period, and consequently they should produce high-energy gamma-rays and neutrinos by interacting with the dense matter of the nebula's environment. We therefore estimate the expected flux of TeV gamma-rays from pulsar nebulae, and by comparing with the observation for a couple of well-known nebulae we checked the consistency of the polar cap model. We also calculate the flux of TeV neutrinos from a couple of PWNe.

Here, we first describe the production mechanism of the TeV gamma-rays and neutrinos in a pulsar environment, estimated the expected flux of gamma-rays from a pulsar for the *polar cap model* of hadrons acceleration as used by (LB). By comparing the *polar cap model* predicted gamma-ray fluxes from some potential young pulsars with the observations, the importance of the inclusion of polar cap area instead of neutron star surface area in the calculation has been emphasized. Incorporating such a feature in the model calculation of fluxes, the revised event rates in a neutrino telescope located at different observation sites on the Earth due to a few potential pulsars are obtained. Adopting the same featured model, fluxes of TeV gamma-rays and neutrinos from pulsar nebulae are found out.

7.2 TeV GAMMA-RAYS AND NEUTRINOS FROM PULSARS

In general, the acceleration of charged particles by astrophysical sources is described by two different kinds of models. The model which describes acceleration of electrons is the so-called *leptonic model* (Aharonian et al. 2008). On the other hand acceleration of heavier ions including protons is described by the so-called *hadronic model* (Halzen & Hooper 2002). Neutrinos are produced only in the *hadronic model* while gamma-ray production can be provided by both the models. Several detailed mechanisms have so far been suggested for acceleration of particles by pulsars that include the popular polar gap (Rudemann & Sutherland 1975, Arons & Scharlemann 1979, Daugherty & Harding 1996, Harding & Muslinov 1998) and the outer-gap models (Cheng et al. 1986).

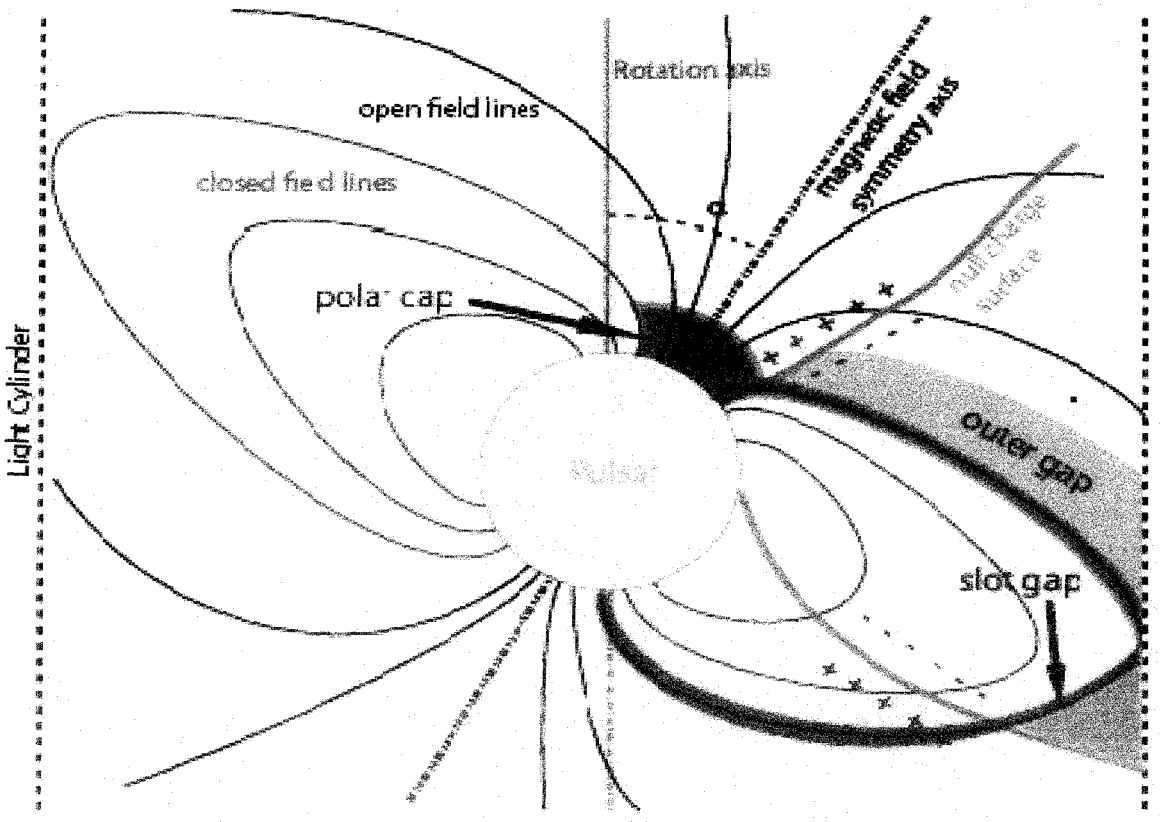

Fig.7.1: The polar cap region is possible candidate for locations within the pulsar's magnetosphere where the acceleration of particles and emission of γ-rays and neutrinos might take place.

In the polar gap model, acceleration of particles takes place in the open field line region above the magnetic pole of the neutron star. In contrast to that, in the case of outer-gap model acceleration occurs in the vacuum gaps between the neutral line and the last open line in the magnetosphere. Thus, the region of acceleration in the polar-gap model is close to the pulsar surface, while the same in the outer-gap model is close to the light cylinder as has been depicted clearly in **Fig.7.1**.

In the polar cap acceleration model, particles are extracted from the polar cap and accelerated by large rotation-induced electric fields, forming the primary beam. A region above the polar cap of a neutron star was proposed by several authors as location of particle acceleration (Rudermann & Sutherland 1975, Arons & Scharlemann 1979).

Electrons are released from the surface of the neutron star when the electron thermal emission temperatures are well below the neutron star surface temperature. Electrons are accelerated by the electric field induced by the rotating axial magnetic dipole. In the case of Crab, potential drops up to 10^{14} eV are induced in the polar cap region, accelerating electrons up to Γ-factors $\approx 10^8$. In this model the charge density at the surface of the pulsar even equals the Goldreich-Julian density (Goldreich & Julian 1969). The charge density $\rho(r)$ decreases as r^{-3}. Thus, magnitude of the parallel component of the electric field goes down to zero at the surface, but increases at much farther radii.

If the surface temperature is below the thermal emission temperature, a vacuum gap will be also formed. Thus, the parallel component of the electric field is not short out in the plasma. Accelerated charged particles will start an electromagnetic pair cascade as shown in **Fig.7.2**. Absorption mechanisms like magnetic pair creation and photon splitting (description was made in the domain of the QED and pronounced in magnetars) restrain gamma-rays with high energies to leave the polar cap area.

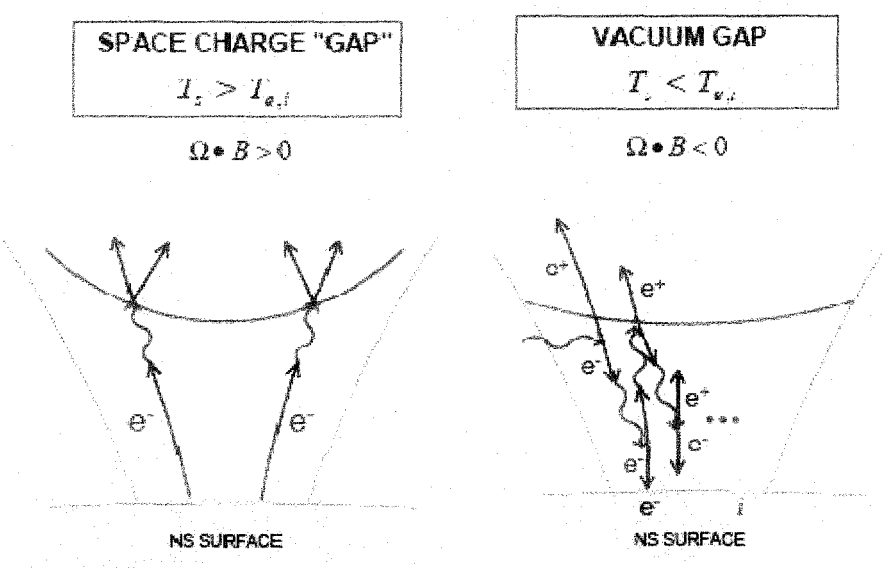

Fig.7.2: Space-charge limited flow and vacuum gap above a neutron star polar cap. T_S is the neutron star surface temperature while $T_{e,i}$ represents the electron or thermal temperature.

The maximum potential drop that may be induced across the magnetic field lines between the magnetic pole and the last field lines that opens to infinity is given by (Goldreich & Julian 1969)

$$\phi = \frac{B_S R^3 \Omega^2}{2c^2} \qquad (7.1)$$

, where R is the stellar radius (neutron star) , B_s is the strength of magnetic field at neutron star surface, $\Omega = \frac{2\pi}{P}$ represents the rotational frequency and c is the speed of light. Accordingly, for young millisecond pulsar with high magnetic fields ($B_S \sim 10^{12}$ G), the magnitude of the potential could be as large as

$$\phi = 7 \times 10^{18} B_{12} P_{ms}^{-2} \; volts \qquad (7.2)$$

,with $B_S \equiv B_{12} \times 10^{12}\, G$. But, in young pulsars the electric field along magnetic field lines is likely to be screened well below the vacuum potentials by the onset of electron – positron pair cascades in the strong magnetic field (Cheng & Rudermann 1977), and this would limit the potential to about 10^{12} eV. Though the flux of synchrotron radiation observed from the Crab and other PWN indicates such a possibility, questions like where in the magnetosphere are pairs created and how many are created, still not settled and one cannot rule out the possibility that ions can reach energies equal to a significant part of the total potentials drop through polar cap acceleration, particularly in view of the observed of gamma radiation of energies above tens and even hundreds of TeV from Crab and other PWN.

LB (Link & Burgio 2005, 2006) conjectured that protons or heavier nuclei are accelerated near the surface of a pulsar by the polar caps to PeV energies (corresponding to no/little screening) when the scalar product of the magnetic dipole moment and magnetic field vector i.e. $\mu.B < 0$ (such a condition is expected to hold for half of the total pulsars). When pulsar-accelerated ions interact with the ambient radiation field of pulsar, the Δ-resonance state may occur provided their energies exceed the threshold energy for the process. The important threshold condition for the creation of Δ-resonance state in proton-photon interaction is given by

$$\epsilon_p \epsilon_\gamma \left(1 - cos\theta_{p\gamma}\right) \geq 0.3 \; GeV^2, \qquad (7.3)$$

where ϵ_p and ϵ_γ stand for proton and photon energies, respectively, and $\theta_{p\gamma}$ is the incident angle between the proton and photon in the laboratory frame. In a young

neutron star with surface temperature, T_∞, the energy of a thermal photon near the surface of the neutron star is $2.8kT_\infty(1+z_g)$, $z_g(\sim 0.4)$ being the gravitational redshift. This implies that in a young pulsar atmosphere, the condition for the production of the Δ-resonance is $B_{12}P_{ms}^{-2}T_{0.1keV} \geq 3\times 10^{-4}$ (Link & Burgio 2005, 2006), where $T_{0.1keV} \equiv \left(\frac{kT_\infty}{0.1keV}\right), T_\infty \sim 0.1\, keV$ being the typical surface temperature of young pulsars. The surface of the young pulsar will emit brightly in soft X-rays, and the protons in accelerated nuclei will scatter with this radiation field. If the protons are sufficiently energetic, they will exceed the threshold for photo-meson production through the Δ-resonance (the Δ^+ is an excited state of the proton, with a mass of 1232 MeV). The Δ-resonance quickly decays into gamma-rays and neutrinos through the following channels

$$p+\gamma \rightarrow \Delta^+ \rightarrow p+\pi^0 \rightarrow p+2\gamma$$

$$p+\gamma \rightarrow \Delta^+ \rightarrow n+\pi^+ \rightarrow n+e^+ + \upsilon_e + \upsilon_\mu + \tilde{\upsilon}_\mu$$

This idea for υ_μ production was explored by (Zhang et al. 2003) in the context of magnetars. It can be shown that young pulsars could be strong sources of muon neutrinos with several tens of TeV energies and with fluxes observable by large-area neutrino observatories.

Since the charge-changing reaction takes place just one-third of the time, on the average four high-energy gamma-rays are produced for every three high-energy neutrinos (or for a muon neutrino antineutrino pair) when a large number of such reactions occur.

7.3 GAMMA-RAY AND NEUTRINO FLUXES FROM PULSARS

Fluxes for gamma-rays and muon neutrinos from pulsars can be estimated in the polar cap model. The charge density of ions near the pulsar surface is $\rho_q \simeq eZn_0$, where $n_0(r) \equiv B_S R^3\Omega/(4\pi Zecr^3)$ is the Goldreich-Julian density (Goldreich & Julian 1969) of ions at a radial distance r. For acceleration to take place, there must be a charge-depleted gap (here the polar gap), and the density in the gap may be written as $f_d(1-f_d)n_0$, where $f_d < 1$ is the depletion factor which is a model-dependent quantity ($f_d = 0$ corresponds to zero depletion). The flux of protons accelerated by a polar cap is therefore

$$I_{pc} = cf_d(1-f_d)n_0 A_{pc}, \qquad (7.4)$$

where $A_{pc} = \eta\, 4\pi R^2$ is the area of the polar cap, η is the ratio of the polar cap area to the neutron star surface area, which is taken as unity by LB in their work. This means that A_{pc} was considered to be equal to the surface area of the whole neutron star in the original calculation by LB. The canonical polar cap radius is given by $r_{pc} = R(\frac{\Omega R}{c})^{1/2}$ (Beskin et al. 1993), and thus the parameter η can be rewritten as

$$\eta = \frac{\Omega R}{4c}. \tag{7.5}$$

The protons accelerated by a polar cap will interact with the thermal radiation field of the neutron star. The temperature of polar caps is expectedly higher than the neutron star's surface temperature, but the contribution of polar caps on the thermal radiation field of a neutron star should be negligible because of their small surface area in comparison with the surface area of the whole neutron star. For a young neutron star with surface temperature T_∞, the photon density close to the neutron star's surface is

$$n_\gamma(R) = \frac{a}{2.8k}[(1 + z_g)T_\infty]^3, \tag{7.6}$$

a, being the Stefan-Boltzmann constant. Numerically, $n_\gamma(R) \simeq 9 \times 10^{19} T_{0.1\,keV}^3\ cm^{-3}$. At a particular radial distance r, the photon density will be $n_\gamma(r) = n_\gamma(R)\left(\frac{R}{r}\right)^2$. The probability that a PeV energy proton starting from pulsar surface will produce Δ-resonance sate by interacting with thermal radiation field is given by (Link & Burgio 2005, 2006)

$$P_c = 1 - P(r) \tag{7.7}$$

with, $\frac{dP}{P(r)} = -n_\gamma(r)\sigma_{p\gamma}dr$. The threshold energy for the production of Δ-resonance state in $p\gamma$ interaction as given by equation (**7.3**) increases rapidly with distance from the surface of neutron star because of the $(1 - cos\theta_{p\gamma})^{-1}$ factor (Link & Burgio 2005, 2006). Requiring conversion to take place in the range $R \leq r \leq 1.2R$ [at $r = 1.2R$, the value of $(1 - cos\theta_{p\gamma})^{-1}$averaged over surface becomes double], P_c has been found as $\simeq 0.02 T_{0.1keV}^3$ (Link & Burgio 2005, 2006). From a follow up calculation by LB, it is found that conversion probability is slightly lower than that mentioned above and can be parameterized as $P_c \simeq T_{0.1keV}^3$. Thus, the total flux of neutrino or gamma-ray generated in pulsar from the decay of Δ^+resonance is

$$I = 2c\xi A_{pc} f_d (1 - f_d) n_0 P_c \,, \tag{7.8}$$

where ξ is $4/3$ and $2/3$ for gamma-rays and muon neutrinos, respectively. Denoting the duty cycle of the gamma-ray/neutrino beam as f_b which has a typical value $f_b \sim 0.1 - 0.3$, the phase-averaged gamma-ray/neutrino flux at the Earth from a pulsar of distance d is given by

$$\phi \simeq 2c\xi\zeta\eta f_b f_d (1 - f_d) n_0 \left(\frac{R}{d}\right)^2 P_c \tag{7.9}$$

where ζ represents the effect due to neutrino oscillation. The decays of pions and their muon daughters result in initial flavour ratios $\phi_{\upsilon_e} : \phi_{\upsilon_\mu} : \phi_{\upsilon_\tau}$ of nearly $1:2:0$ but at large distance from the source the flavour ratio is expected to become $1:1:1$ due to maximal mixing of υ_μ and υ_τ. $\zeta = 1$ and ½ for gamma-rays and muon neutrinos, respectively.

7.4 AVERAGE NEUTRINO AND GAMMA-RAY ENERGIES

The average fraction of energy transferred from the proton to the pion is ~ 0.2, or $200 T_{0.1keV}^{-1}$, corresponding to a Lorentz factor of $\gamma_\pi = 1.4 \times 10^6 T_{0.1keV}^{-1}$. The pion decays in a time $\tau_d = \gamma_\pi \tau_\pi$, where $\tau_\pi = 2.6 \times 10^{-8} s$, and thus moves to $r \sim 10^3 R$ before decaying. The pion is in the densest part of the radiation field for only a short time, of order $R/c \simeq 3 \times 10^{-5} s$, and suffers negligible energy loss to inverse-Compton scattering. When the pion decays, it gives one-fourth of its energy to the muon neutrino, the rest going to the other three leptons. The resulting neutrino energy is then

$$E_{\nu_\mu} \simeq 50 T_{0.1keV}^{-1} \, TeV \tag{7.10}$$

As the parameter ξ is $4/3$ for gamma-ray compared to its $2/3$ value for muon neutrinos. Hence, it is expected that the average energy of the produced gamma-rays would be double to that for muon neutrinos, given by

$$E_\gamma \simeq 100 T_{0.1keV}^{-1} \, TeV \tag{7.11}$$

7.5 TeV GAMMA-RAYS FROM FEW POTENTIAL PULSARS

Though there are about more than 1800 pulsars known through radio detection, only a few have been detected in the gamma-rays. From observations made with gamma-ray telescopes on satellites so far, only *seven* high-confidence

gamma-ray pulsars are known in the energy range up to a few GeV (Thompson 2003). Besides, three other pulsars namely $PSR\ B1046-58$, $B0656+14$ and $J0218+4232$ are considered to be gamma-ray emitters with a lower confidence level (Thompson 2003) in the same energy region. Some basic characteristic properties of the high-confidence *young* gamma-ray pulsars, namely distance (D), spin-down age (τ), period (P), the calculated magnetic field strength (B_S) at the neutron star surface, surface temperature (T_S) and pulsar duty cycle (f_b), are listed in **table 7.1.**

7.5.1 DETECTABILITY

None of the listed pulsars in **table 7.1** is, however, detected at TeV energies despite recent improvement in the knowledge of Galactic gamma-ray sky above 100 GeV, mostly by means of ground-based Imaging Atmospheric Cherenkov telescope systems such as the Collaboration of Australia and Nippon for a Gamma Ray Observatory in the Outback (CANGAROO), High Energy Gamma Ray Astronomy (HEGRA), High-Energy Stereoscopic System (HESS) or the Major Atmospheric Gamma-ray Imaging Cherenkov Observatory (MAGIC). Up to now, no evidence for pulsed emission from any other pulsar has been found from the observations (Chadwick et al. 2000 & Lessard et al. 2000), and only upper limits on the pulsed very high energy gamma-ray flux are derived under various assumptions on the characteristics of the pulsed emission. For the pulsars listed in **table 7.1**, the observed upper limits of integral fluxes are given in **table 7.2**. The upper limits are obtained from the differential spectra assuming a power-law differential spectrum with index -2.4. The upper limits of integral fluxes of gamma-rays from pulsars at around 100 TeV as obtained by the extensive air shower experiments such the Tibet (Amenomori et al. 2008[a] & Wang et al. 2008) are found less restrictive.

Assuming that pulsar-accelerated ions are protons, numerical values of the integral TeV gamma-ray fluxes are obtained for the pulsars listed in **table 7.2** from equation (**7.9**) and are also shown in the same table. It should be mentioned here that for the numerical estimation of flux, we take $Z=1$ and $f_d=1/2$ throughout the present work.

Source	d (kpc)	age (yr)	p (ms)	B_{12}	$T_{0.1keV}$	f_b
Crab	2	10^3	33	3.8	~1.7	0.14
Vela	0.29	$10^{4.2}$	89	3.4	0.6	0.04
B 1706-44	1.8	$10^{4.3}$	102	3.1	1	0.13
B 1509-58	4.4	$10^{3.2}$	151	0.26	1	0.26
J 0205+64	3.2	$10^{2.9}$	65	3.8	0.04	0.9

Table 7.1: The characteristics of high-confidence young low-energy gamma-ray pulsars.

Source	Expected integral flux $(10^{-15}cm^{-2}s^{-1})$		Observed upper limit of integral flux $(10^{-15}cm^{-2}s^{-1})$
	$\eta = 1$	η as eqn. (7.5)	
Crab	1012	1.65	8(56)
Vela	208	0.123	10(20)
B 1509-58	67	0.0034	10(20)
B 1706-44	71	0.0025	10(20)

Table 7.2: Comparison of predicted versus observed integral TeV gamma-ray fluxes from some nearby young gamma-ray pulsars. The numbers in parentheses are the energy thresholds in TeV for which upper limits are determined. The observed upper limits for Crab pulsar are due to (Aharonian et al. 2006[b]) whereas for the rest of the pulsars the observed upper limits are due to (Aharonian et al. 2007[b]).

Source	Expected event rates $(km^{-2}yr^{-1})$
Crab	0.009
Vela	0.0007
B 1509-58	0.00003
B 1706-44	0.00003

Table 7.3: Expected event rates in a neutrino telescope due to some nearby young gamma-ray pulsars.

It is clear from **table 7.2** that the model with $\eta = 1$ is not consistent with the observed upper limits; the observed limits are substantially lower than the

predicted fluxes. The observations made so far, however, do not rule out the model with η given by equation (**7.5**).

7.6 TeV NEUTRINOS FROM PULSARS

When η is given by equation (**7.5**), neutrino fluxes from nearby young gamma-ray pulsars would be much lower than estimated by LB (Link & Burgio 2005, 2006). A high-energy muon neutrino is usually detected indirectly through the observation of the secondary high-energy muon produced by the muon neutrino on interaction with the ice or rock in the vicinity of a neutrino telescope via charged current interactions. Large-area neutrino detectors use the Earth as medium for conversion of a muon neutrino to a muon, which then produces Cherenkov light in the detector. The track of the produced muon is usually reconstructed by detecting the produced Cherenkov light. The probability of the detection of muon neutrinos is the product of the interaction probability of neutrinos and the range of the muon and is $p_{\nu\to\mu} \simeq 1.3\times10^{-6}(\frac{\epsilon_{\nu\mu}}{1\,TeV})$ (Gaisser et al. 1995), where $\epsilon_{\nu\mu}$ is the energy of the incident neutrino. Combining (**7.9**) and $p_{\nu\to\mu}$ gives a muon event rate of

$$\frac{dN}{dAdt} = \phi_\upsilon p_{\nu\to\mu} = \int_{\epsilon_T}^{10\epsilon_T} d\epsilon_\nu \frac{d\phi_\upsilon}{d\epsilon_\nu}\, p_{\nu\to\mu}. \qquad (7.12)$$

The choice of the upper limit of integration is not very important, because the spectrum is steep. The expected event rates in a neutrino telescope due to potential young pulsars are given in **table 7.3**.

The event rates are clearly very low and thus possibility of observing pulsars by a kilometre-scale neutrino detector does not look bright.

7.7 GAMMA-RAYS AND NEUTRINOS FROM PULSAR WIND NEBULAE

A number of nebulae (plerions) have been discovered in radio, optical and X-ray bands such as Crab, the youngest one and most energetic source. Continuous injection of pulsar electrons into the nebula resulting from a statistical acceleration process is inevitable. The radio, optical and *X*-ray emission observed from plerions is believed to be due to synchrotron and ICs emissions (*leptonic origin*). It is likely that positive ions, after gaining energy from polar gaps, will move away from the pulsar practically along the open field lines and will finally inject into the nebula. It

is very likely that these energetic ions would be trapped by the magnetic field of the nebula for a long period and consequently they should produce appreciable high-energy gamma-rays/neutrinos by interacting with the matter of the nebulae (*hadronic origin*).

7.7.1 MAGNETIC TRAPING OF PULSAR-ACCELERATED PeV IONS IN NEBULAE

Conservation of magnetic flux across the light cylinder entails that outside the light cylinder $B \sim r^{-1}$whereas far from the light cylinder the radial component of magnetic field varies as $B_r \sim r^{-2}$. Thus, far outside the light cylinder the azimuthal component of the magnetic field dominates over the radial field. Therefore, accelerated protons while moving away from the pulsar have to cross the field lines (e.g. magnetic field lines at wind shock). The Larmour radius of particles (even for proton) of energy about 1 PeV is expected to be smaller than the radius of nebula during most of the time of the evolution of nebula (Bednarek & Protheroe 2002, Bhadra 2006). Thus, it is very likely that energetic particles of PeV energies would be trapped by the magnetic field of the nebula. The energetic particles propagate diffusively in the envelope, and they escape from nebula when the mean radial distance travelled by the particles becomes comparable with the radius of nebula at the time escaping. This time is somewhat uncertain due to the uncertainty of the value of diffusion coefficient, but is estimated to be at least a few thousand years (Bednarek & Protheroe 2002, Bhadra 2006).

7.7.2 GAMMA-RAYS AND NEUTRINOS FROM NEBULAE OF YOUNG PULSARS

As pointed out in the preceding section, the pulsar-injected ions of PeV energies should be trapped by the magnetic field of the nebula for a long period, and consequently there would be an accumulation of energetic ions in the nebula. These energetic ions will interact with the matter of the nebula. The rate of interactions (ξ) would be $nc\sigma_{pA}$, where n is the number density of protons in nebula and σ_{pA} is the interaction cross-section. In each such interaction, charged and neutral pions will be produced copiously. Subsequently, the decays of neutral pions will produce gamma-rays whereas charged pions and their muon daughters will give rise to neutrinos.

If m is the mean multiplicity of charged particles in proton-ion interaction, then the flux of gamma-rays at a distance d from the source would roughly be

$$\phi_\gamma \approx 2c\beta\eta f_d(1-f_d)n_0(\frac{R}{d})^2\xi mt, \qquad (7.13)$$

where β represents the fraction of pulsar-accelerated protons trapped in the nebula and t is the age of the pulsar. Note that there should not be any reduction of flux due to pulsar duty cycle in the case of emission to nebula. Though n_0 is taken as constant, but actually at the early stages of pulsar, n_0 should be larger owing to the smaller pulsar period. So, the above expression gives only a lower limit of flux. Typical energy of these resultant gamma-rays would be $\sim 10^3/(6m)$ TeV where for (laboratory) collision energy of 1 PeV, m is about 32 (Alner et al. 1987).

Numerical values of the integral TeV gamma-ray fluxes from two nearby nebulae, Crab nebula and Vela nebula, have been estimated for perfect trapping of pulsar-accelerated protons in nebulae and are shown in **table 7.4**. The observed integral gamma-ray fluxes above 1 TeV from Crab nebula (Aharonian et al. 2006[b]) and Vela nebula (Aharonian et al. 2006[c]) are also given in **table 7.4** for comparison.

PWNe	n (cm^{-3})	Expected flux ($\times 10^{-12} cm^{-2} s^{-1}$)	Observed flux ($\times 10^{-12} cm^{-2} s^{-1}$)
Crab nebula	150	0.6	22.6
Vela nebula	1	0.4	12.8

Table 7.4: Comparison of predicted versus observed integral gamma-ray fluxes from two nearby PWN.

The neutrino fluxes from the nebulae would be of nearly the same to those of gamma-rays. Incorporating the neutrino oscillation effect, the expected event rates in a neutrino telescope due to TeV muon neutrinos from Nebulae of Crab and Vela are 0.2 and 0.1 $km^{-2}yr^{-1}$, respectively. Note that the event rates obtained here are rough numerical values. The flux will be higher if the accelerated ion is heavier than proton.

7.8 DISCUSSION AND CONCLUSIONS

The neutrino telescopes currently taking data have not detected any excess from discrete sources yet, although some models could already be constrained by the limits they are providing. Results from neutrino telescopes such as Antartic Muon and Neutrino Detector Array (AMANDA-II) and ANTARES with long exposure time are available. Crab pulsar was not detected as neutrino source. The Crab pulsar would be a strong source, but only if $\boldsymbol{\mu}.\boldsymbol{B} < 0$. If the Crab is a neutrino pulsar, and the temperature is close to the observational upper limit, lack of detection by AMANDA-II requires, $f_d \lesssim 0.01$, which seems surprisingly low in the face of current models of charge-depleted gaps.

Our present work suggests that pulsars (within 10 kpc of Earth and younger than 10^5 yrs.) are unlikely to be strong sources of TeV neutrinos. The non-detection of any statistically significant excess from the direction of any pulsar by the AMANDA-II is thus as per expectations.

If protons are accelerated to PeV energies by the pulsar, then pulsar nebulae are more probable sites of energetic neutrinos provided energetic particles of PeV energies are efficiently trapped by the magnetic field of the nebulae. But, even for pulsar nebulae the expected event rates are small and the detection of pulsar nebulae by the ongoing neutrino telescopes, such as the Ice Cube (Halzen 2006), is very low. We expect that experiments with the proposed High Altitude Water Cherenkov (HAWC) detector will be constantly used to survey large regions of the sky in particular the galactic plane, at gamma-ray energies up to 100 TeV with 10 to 15 times the sensitivity of Milagro (Li 2013).

CHAPTER 8

DISCUSSION

A major issue concerning the study of CRs at PeV energies is the understanding of the *knee* of the CR energy spectrum which is likely to provide key information about the origin of galactic CRs. If the *knee* in the primary CR spectra is due to a mechanism that depends on magnetic rigidity, one expects systematic changes in CR composition through this region. But due to the limited knowledge of particle interactions at high energies and the large fluctuations, which are intrinsic to any EAS, the conclusions on primary CRs deduced from EAS measurements remain somewhat uncertain; sometimes even there are divergences of conclusions from experiment to experiment. To overcome the limitations recent strategies include consideration of several EAS observables simultaneously in extracting information on primary CRs from EAS observations.

From a detailed MC simulation we find that the lateral shower age that describes the slope of the radial distribution of electrons in EAS is a primary mass sensitive parameter. However, a major problem is the reliable and unambiguous estimate of lateral shower age from experimentally measured electron densities owing to its radial variation. In this regard our investigation suggests that the local age offers a good solution towards an unambiguous estimation of the shower age. It is also noticed that the lateral distribution of electrons in EAS exhibits some sort of *scaling* (energy independent) behaviour in terms of this local age parameter. Hence the local age can be employed to extract information about the nature of the primary particle through a multi-parameter approach of studying EAS. It has been found from our analysis that the *3-dimensional* plot of shower size versus muon size and shower age seems to offer better accuracy in compare to the more conventional approach of implementing it through the shower size versus muon size curve.

It is further noticed from a detailed MC simulation study that LAP can be used to separate out gamma ray initiated EAS from the large background of hadron induced EAS. If LAP can be estimated experimentally with good precision the proposed observable might be particularly useful for surface detector experiments those have no reliable muon measurement facilities.

An important question is the experimental realization of the adopted techniques involving LAP. The local age at a particular distance is not always practical owing to the large fluctuation in the electron density data in a real measurement. A rational idea could be to take some sort of average local age between the first minimum, at around a core distance of 50 m, and the subsequent local maximum, at around 300 m. The uncertainty in estimating LAP is usually large in normal circumstances as the parameter depends on the logarithmic derivative of the density versus radial distance. Thus, uncertainty in estimating LAP from experimental data arises mainly from the uncertainties in electron densities and those in radial distance measurements due to uncertainty in determination of shower core position. These uncertainties, however, should be small for a closely packed air shower array like GRAPES-III at Ooty (Gupta et al. 2005) or for a full coverage EAS array like ARGO - YBJ (Sciascio & Girolamo 2007) and thus it would be an interesting task to study the characteristics of LAP experimentally using observed EAS data from such EAS installations.

During the development of a CR cascade in the atmosphere, the secondary charged particles in the shower are influenced by the geomagnetic field; positive and negative charged particles get separated out and constitute an *electric dipole moment*. We found from a MC simulation study that muon dipole length due to geomagnetic field is a primary mass sensitive parameter, particularly for inclined EAS those offer a larger path for the charged particles to move in the atmosphere. The important point is that whether muon dipole length can be realized experimentally. The ongoing experiments, such as the WILLI detector (Wentz et al. 2001, Brancus et al. 2003 & Agostinelli et al. 2003) or the Okayama University, Japan EAS installation have the capability to extract charge information of high energy muons but these experiments do not have large muon detection area, which is needed to estimate muon dipole length precisely. If in future these experiments are extended in order to cover larger detection area or new installation of large muon detection area with capability of charge identification come up, the muon dipole length can be exploited to extract the nature of shower initiating primaries.

The study of EAS offers an opportunity to estimate the total p-air cross section at energies well beyond the accelerator/collider energies. Also note that even at accelerator energies total cross section is very difficult to evaluate from collider experiment. It is found from experiment as well as from MC simulation that the frequency absorption length of EAS with particular muon and electron

sizes is not the same to the mean free path. The intrinsic fluctuations associated with EASs are generally believed to be responsible for such inequality. We examine this point critically and found that shower fluctuation does not have much effect.

Besides the supernova remnants, pulsars are potential candidates for the sources of galactic CRs. Observation of electromagnetic radiation from radio to TeV gamma-rays from pulsars decisively suggest that charge particles get accelerated in the pulsar environment. However, a big question is that whether hadron/nuclei are accelerated at pulsars? So far bearing one or two exceptional cases, the observed electromagnetic radiation from pulsars can well be interpreted in terms of presence of energetic leptons in pulsars. Observation of appropriate flux of neutrinos can give definitive conclusion about the presence of energised hadrons in the pulsar atmosphere. An investigation reported in this thesis, however, suggests that pulsars (within 10 kpc of Earth and younger than 10^5 yrs.) are unlikely to be strong sources of TeV neutrinos if hadrons are accelerated by polar caps of pulsars and the non-detection of any statistically significant excess from the direction of any pulsar by the AMANDA-II is thus as per the expectations. If protons are accelerated to PeV energies by the pulsar, then pulsar nebulae are more probable sites of energetic neutrinos provided energetic particles of PeV energies are efficiently trapped by the magnetic field of the nebulae. But, even for pulsar nebulae the expected event rates are small and the detection of pulsar nebulae by the ongoing neutrino telescopes, such as the Ice Cube (Halzen 2006), is very low. Hence testing pulsars as sources of hadronic cosmic-rays through neutrino astronomy requires at least an order more sensitive neutrino telescope than Ice Cube.

BIBLIOGRAPHY

Abbasi R, *et al.*, HiRes Collab., *Phys. Rev. Lett.* **100 101101** (2008).

Abbasi R *et al.*, (IceCube), *Astrophys. J.* **701, L47** (2009).

Abraham J, *et al.*, Pierre Auger Collab., *Phys. Rev. Lett.* **101 061101** (2008).

Abu-Zayyad, *et al.*, HiRes-MIA Collab., *Phys. Rev. Lett.* **84 4276** (2000).

Abu-Zayyad, *et al.*, HiRes-MIA Collab., *Astrophys. J.* **557 686-699** (2001).

Acharya B S *et al.*, *Proc. 31st ICRC*, Lodz, **1** (2009).

Actis M *et al.*, *Experimental Astronomy*, **32**: **193-316** (2011).

Afanasiev B N *et al.*, in: Nagano M (Ed.), *Proceedings of the Tokyo Workshop on Techniques for the Study of Extremely High Energy Cosmic Rays*, (Institute for Cosmic Ray Research, University of Tokyo, Tokyo, Japan), p. **35**, (2003).

Aglietta M *et al.*, *Phys. Rev. D* **79** 032004 (2009).

Agostinelli S *et al.*, *Nucl. Instr. Meth. A* **506 250-303** (2003).

Aharonian F A *et al.*, *Mon. Not. Roy. Astron. Soc.*, **291, 162** (1997).

Aharonian F A *et al.*, *Nature*, **432**: **75-77**, (2004).

Aharonian F A *et al.*, *APJ* **636**: 777-797 (2006)[a].

Aharonian F A *et al.*, (H.E.S.S. Collaboration) *Astron. Astrophys.* **457 889** (2006)[b].

Aharonian F A *et al.*, (HESS Collaboration), *Astron. Astrophys.*, **448, 206** (2006)[c].

Aharonian F A *et al.*, *Phys. Rev.D*, **75 042004-2** (2007)[a].

Aharonian F A *et al.*, (HESS collaboration), 2007 *Astron. Astrophys.*, **466, 543** (2007)[b].

Aharonian F A *et al.*, *Rep. Prog. Phys.* **71, 096001**, (2008).

Aliu E *et al.*, *Science* **334**: **69-72** (2011).

Aloisio A, *et al.*, *Nuovo Cimento C* **24 739** (2001).

Allan H R, *Acta Phys. Hung. Suppl.* **29 699** (1970).

Allan H R *et al., Proc. 14th Int. Cosmic Ray Conf.* (Munich) vol **8** p **2131** (1975).

Allkofer O C *et al.*, *J. Geophys. Res.* **90 3537** (1985).

Alner G J *et al.*, *Phys. Rep.*, **154, 247** (1987).

Alvarez-Muniz *et al.*, *Phys. Rev. D* **66** 123004 (2002).

Ahn H S *et al.*, ATIC-2 Collab., in: *Proc. of 28th Int. Cosmic Ray Conf.*, Hobart **2**, p. **206**, (1971).

Amenomori M *et al.*, *Science*, **314, 439-442** (2006)[a].

Amenomori M *et al.*, *Phys. Lett. B*, **632, 58-64** (2006)[b].

Amenomori M *et al*, *Nucl. Phys. B, Proc. Suppl.*, **175-176**, 431 (2008)[a].

Amenomori M, *et al.*, Tibet ASγ Collab., *Astrophys. J.* **678 1165-1179** (2008)[b].

Amsler C *et al.*, *Physics Letters B***667, 1** (2008).

Antoni T *et al.*, *Astropart. Phys.***14 245** (2001).

Antoni T *et al.*, *Astropart. Phys.* **6 245** (2002).

Antoni T, *et al.*, KASCADE Collab., *Astropart. Phys.* **24 1-25** (2005).

Apel W D *et al., Astropart. Phys.* **24 467-483** (2006).

Apel W D *et al., Astropart. Phys.* **29 412** (2008).

Apel W D *et al.*, and KASCADE Coll., *Astropart. Phys.* **31**, p.**86** (2009).

Arons J and Scharlemann E T, *ApJ*, **231, 854** (1979).

Arqueros F *et al., Astron. Astrophys.* **359** 682 (2000).

Arteaga-Velazques J C *et al.*, KASCADE-Grande Collab., in: *Proc. of 15th ISVHECRI*, Paris, (2008).

Asakimori K *et al., ApJ*, **502, 278** (1998).

Atwood W B *et al., ApJ* **697 1071** (2009).

Auger P *et al.*, Grandes grebes' cosmiques atmospheriques contenant des corpuscles ultrapenetrants. *C. R. Acad. Sci.*, **206:1721-1723**, (1938).

Auger Collab., *Phys. Rev. Lett.* **104** (2010).

Ave M, Vasquez R A and Zas E, *Astropart. Phys.* **14 91** (2000).

Ave M *et al., Astropart. Phys.* **14 109** (2000).

Baade W, Zwicky F, *Phys. Rev.* **46 76** (1934).

Badran H M and Neekes T C, *Astropart. Phys.* 7 **307-314** (1997).

Baixeras, Carmen, *et al., Nuclear Physics B (Proceedings Supplement)* **114** (2003).

Baltrusaitis *et al., Phys. Rev. Lett. 52* 1380 (1984).

Baltrusaitis R M, *et al.*, Fly's Eye Collab., *Nucl. Instrum. Methods A* **240 410-428** (1985).

Bartoli B *et al., Phys. Rev. D* **85, 092005** (2012).

Bass S A *et al., Prog. Part. Nucl. Phys.* **41 225** (1998).

Bassi P *et al., Phy. Rev.* **A 92** 441 (1953).

Bednarek W and Protheroe R J, *Astropart. Phys.* **16, 397** (2002).

Bell C J, *et al., J. Phys. A* **12 990** (1974).

Bergmann T, *et al., Astropart. Phys.* **26** 420 (2007).

Beillicke M and *VERITAS Collaboration, AIP Conf. Proc.* **1112** pp.**33** (2008).

Bernardint P *et al.*, (ARGO YBJ Collab.), Preprint *arXiv* **1110.0670v1** (2011).

Bernlohr K, *Astropart. Phys.* 5 139 (1999).

Beskin V. S., Gurevich A., Istomin N. Ya, *Physics of the Pulsar Magnetosphere, Cambridge Univ. Press, Cambridge*, p. **117** (1993).

Bird D J, *et al.*, Fly's Eye Collab., *Phys. Rev. Lett.* **71 3401-3404** (1993).

Bhadra A *et al., Nucl. Instrum. Methods* A **414 233** (1998).

Bhadra A, *Pramana J. Phys.* **52 133** (1999).

Bhadra A, *Astropart. Phys.*, **25, 226** (2006).

Bhadra A and Dey R K, *Mon. Not. Roy. Astron. Soc.*, **395 1371-1375** (2009).

Bhadra A *et al., Phys. Rev. D* **79 114027** (2009).

Blandford R, Eichler D, *Phys. Rep.* **154 1-75** (1987).

Bleicher M *et al., J. Phys. G: Nucl. Part. Phys.* **25 1859** (1999).

Blümer J, Engel R and Hörandel J R, *Astropart. Phys.*, **63** (2) **293-338** (2009).

Boothby *et al., Astrophys. J* **491** L35 (1997).

Bothe W, Kolhörster W, *Zeitschr. f. Phys.* **56 751** (1929).

Bourdeau M F, Capdevielle J N and Procureur J, *J. Phys. G: Nucl. Phys.* **6 901** (1980).

Bowden C C G *et al., J. Phys. G: Nucl. Part. Phys.* **18 L55** (1992).

Brancus I M *et al., Nucl. Phys. A* **721 1044c – 1047c** (2003).

Brandt H and Peters B, *Phys. Rev.* **74 1828** (1948).

Browning R and Turver K E, *Nuovo Cimento A* **38 223** (1977).

Budnev N *et al., Nucl. Phys. (Proc. Suppl.)* **190** 247 (2009).

Calabrese A K *et al., ICRC*, **0424** (2009).

Cao Z *et al., IJMPD* **20:1713-1721,** (2011).

Capdevielle J N *et al., Proc. 15th Int. Cosmic Ray Conf.*, Plovdiv, **8, 341** (1977).

Capdevielle J N and Gawin J, *J. Phys. G: Nucl. Phys.* **8 1317** (1982).

Capdevielle J N and Gabinski, P *J. Phys. G: Nucl. Part. Phys.* **16 769** (1990).

Capdevielle J N, The Karlsruhe Extensive Air Shower Simulation Code CORSIKA *KfK Report* **4998** (Karlsruhe) (1992).

Capdevielle J N, Gall C Le, Sanosyan Kh N, *Astropart. Phys.* **13 259** (2000).

Capdevielle J N and Cohen F, *J. Phys. G: Nucl. Part. Phys.* **31 507** (2006)[a].

Capdevielle J N and Cohen F, *J. Phys. G: Nucl. Part. Phys.* **31 1413** (2006)[b].

Capdevielle J N *et al., J. Phys. G: Nucl. Part. Phys.* **36 075203** (2009).

Capdevielle J N, *arXiv*:**1010.0916v1** (2010).

Carr J, *Nucl. Phys. (Proc. Suppl.)* **118**, 383 (2003).

Castellina A and Donato F, To appear in *Planets, Stars and Stellar Systems*, vol.**5**, Springer, arXiv:**1110.2981** (2012).

Catz Ph *et al., Proc. of the Int. Cosmic Ray Conf.* (Denver, USA) vol **4** p **2495** (1973).

Chadwick P M *et al., J. Phys. G: Nucl. Part. Phys.* **25 1223** (1999).

Chadwick P M, Lyons K, McComb T J L, Orford K J, Osborne J L, Rayner S M, Shaw S E and Turver K E, *ApJ*, **537, 414.** (2000).

Cheng K S and Ruderman M, *ApJ*, **214, 598** (1977).

Cheng K S *et al., Astrophys. J,* **300:500-539**, (1986).

Cherev D V *et al., Int. J. Mod. Phys.* A 20 6799 (2005).

Chiba N, *et al., AGASA* Collab., *Nucl. Instrum. Methods A* **311 338-349** (1992).

Chilingarian A *et al., Astropart. Phys.* **28** 58 (2007).

Clay R W, *Proc. 19th Int. Cosmic Ray Conf. (La Jolla)* vol **9** p **323** (1985).

Clay J, *Amsterdam Proc.* **33 711** (1930).

Cocconi G, *Phys. Rev.* **93 646** (1954).

Cocconi G, *Handbuch der Physik: Cosmic Rays* **I** vol **46/1** (Berlin: Springer) p **1.** (1961).

Colgate S A, *J. Geophys. Res.* **72 4869** (1967).

Collmar W *et al., Astron. and Astrophys.* **354 513-521** (2000).

da Oña Wilhelmi E, *in High-Energy Emission from Pulsars and their Systems*, ed. Torres D F and Rea N, **435 – 452** (2011).

Daugherty J K and Harding A K, *ApJ*, **458, 278.** (1996).

De Beer J F *et al.*, *Can. J. Phys.* **46** S185 (1968).

Dedenko L G *et al*, *Proc. 14th Int. Cosmic Ray Conf.* (Munchen) vol **8**, p. **2731** (1975).

Dembinski H *et al.*, *Astropart. Phys.* **34 128** (2010).

Derbina V, *et al.*, *Astrophys. J.* **628** L**41** (2005).

Dermer Charles D, arXiv:**1206.2899** [astro-ph.HE]. (2012).

Dey R K *et al., Proc. of the Int. Cosmic Ray Conf.* Beijing, vol **1/11**, HE: **1.1-1.2**, **174-177**. (2011).

Dey R K *et al., J. Phys. G: Nucl. Part. Phys.* **39 085201** (2012).

Dickinson J E *et al.*, 26th *ICRC* **3** 136 (1999).

Dixon H E and Turver K E, *Proc. R Soc. Lond.* A **339 171** (1974).

Doll P *et al.*, *Nucl. Instrum. Meth.* **488** 517 (2002).

Drescher H J and Farrar G R, *Phys. Rev. D* **67** 116001 (2003).

Drescher H J *et al., Astropart. Phys.* **21 87** (2004).

Earnshaw J R, Machin A C, Orford K J, Pickersgill D R and Turver K E, *Proc. 12th Int. Cosmic. Ray Conf.* **3 1081** (1971).

Edge D M, Evans A C, Garmston H J, *J. Phys. A* **6 1612** (1973).

Efimov N N *et al.*, *Proc. Int. Symp. Astrophysical aspects*, Ed. Nagano M and Takahara F p 20 (1991).

Elbert J *et al.*, *J. Phys. G***2** 971 (1976).

Ellsworth R W *et al.*, *Phys. Rev. D* **26** 336 (1982).

Enomoto R *et al.*, *Nature*, 416: **823-826**, (2002).

Enomoto, R *et al.*, *ApJ* **638**: **397-408** (2006).

Erlykin A *et al.*, *Astrophys. Space Sci. Trans.* 7, 179-182, (2011).

Fass`o A *et al., Proc. Monte Carlo 2000 Conf. (Lisbon)* (Berlin: Springer) p **955** (2001).

Fenyves J, *Techniques in UHE gamma-ray astronomy* edited by Protheroe R J and Stephens S A (University of Adelaide p **124** (1985).

Ferrari A and Sala P R, *ATLAS Int. Note PHYS-No-086* (Geneva: CERN) (1996).

Fesefeldt H, *Report PITHA-85/02* (RWTH Aachen) (1985).

Fermi E, *Phys. Rev.* **75 1169** (1949).

Fletcher R S, Gaisser T K, Lipari P and Stanev T, *Phys. Rev. D* **50 5710** (1994).

Fomin Y *et al.*, *J. Phys. G:Nucl. Part. Phys.* **22** 1839 (1996).

Fowler J *et al.*, *Astropart. Phys.* **15** 49 (2001).

Fukui S *et al.*, *Prog. Theor. Phys., Suppl.* **16 1** (1960).

Fuhrmann D *et al., Proc. 32nd ICRC* v.1 227 (2011).

Gaisser T K, *Proc. Symp. On Astrophysical Aspects of the Most Energetic Cosmic Rays* (Kofu, Japan) p **146**. (1990).

Gaisser T K and Stanev T, *Phys. Rev. D* **43 2** (1991).

Gaisser T K, Halzen F and Stanev T, *Phys. Rept.*, **258, 173** (1995).

Gaisser T K et al., arXiv:1303.3565v1[astro-ph.HE] (2013).

Gandhi R *et al., Phy. Rev. D* **42 263** (1990).

Giller M, Kacperczyk A, Malinowski J, Tkaczyk W and Wieczorek G, *J. Phys. G: Nucl. Part. Phys.* **31 947** (2005).

Glasmacher M *et al., Astropart. Phys.* **12** 1 (1999).

Goldreich P and Julian W H, *ApJ*, **157, 869** (1969).

Gora D *et al., Astropart. Phys.* **24 484**. (2006).

Greisen K, *Progress in Cosmic Ray Physics* vol **III** (Amsterdam: North Holland) (1956).

Greisen K, *Annu. Rev. Nucl. Part. Sci.* **10** 63 (1960).

Grigorov N L *et al.*, Yad Fiz. **11** 1058 (1970).

Guenter S, *Ann. Phys.* **303:117-141**, (2003).

Gupta S K *et al., Nucl. Instrum. and Methods* A **540 311** (2005).

Gupta S K, *ICRC rapporteur* v.12, 241, DOI: 10.7529/ICRC2011/V12/R05 (2011).

Halzen F, *Proc. of the 10th Int. Work. On Neutrino Telescope*; edited by Baldo M. Ceolin, vol. **2**, p. **345** (1990).

Halzen F, Hooper D, *Prog. Theor. Phys.* **65, 1025-1078** (2002).

Halzen F, *Eur. Phys. J C*, **46, 669** (2006).

Hara T *et al., PICRC* **11** 231 (1981).

Hara T *et al., Phys. Rev. Lett.* **50** 2058 (1983).

Harding A K and Gaisser T K, *Astrophys. J*, **358:561-574**, (1990).

Harding A K and Muslimov A G, *ApJ*, **508, 328**. (1998).

Haungs A, Rebel H and Roth M, *Rep. Prog. Phys.*, **66** (7): **1145-1206**, (2003).

Hayakawa S, Cosmic Ray Physics, Wiley, Interscience, New York (1969).

Hayashi Y *et al., Nucl. Instrum. Meth.* **A 545** 643 (2005).

Heck D, Knapp J, Capdevielle J N, Schatz G and Thouw T, The CORSIKA air shower simulation program *Forschungszentrum Karlsruhe Report* FZK **6019** (Karlsruhe) (1998).

Heck D, *Nucl. Phys. B* **151 127** (2006).

Hess V F, Uber Beobachtungen der durchdringenden Strahlung bei sieben freiballonfahrten. *Phys. Z.*, **13:1084-1091**, (1912).

Hillas M and Lapikens J, *Proc. 15th Int. Cosmic Ray Conf.* (Plovdiv) vol **8** p **460**. (1977).

Hillas, A. M, *Ann. Rev. Astron. Astrophys.* **22, 425**. (1984).

Hillas A M, *Proc. 19th Int. Cosmic Ray Conf.* **3 445** (1985).

Hillas A M, *Proc. 20th Int. Cosmic Ray Conf. Moscow* Vol **2** p **362** (1987).

Hillas A M, *Nucl. Phys. Proc. Suppl.* B **52** 29 (1997).

Hinton J A, *New Astronomy Review* **48 331** (2004).

Honda *et al.*, *Phys. Rev. Lett.* **70** 525 (1993)

Hong-Bo Hu *et al.*, *ApJ*, **700, L170-173** (2009).

Horandel J R, *Astropart. Phys.* 21 241 (2004).

Horandel J R, *J. Phys. Conf. Ser.*, **47, 41-50** (2006).

Hough J H, *J. Phys. A: Math. Nucl. Gen.* **6 892** (1973).

Jokipii J R and Morfill G, *Astrophys. J.* **312:170-177**, (1987).

Kalmykov N N, Ostapchenko S S and Pavlov A I *et al.*, *Nucl. Phys.* B **52 17** (1997).

Kamata K and Nishimura J, *Prog. Theor. Phys. Suppl.* **6, 93** (1958).

Kampert Karl-Heinz and Unger M *arXiv:***1201. 10018v2** (astro-ph.HE) 2012.

Karle A *et al.*, *Astropart. Phys.* **3** 321 (1995).

Khristiansen G *et al.*, *Proc. 8th ICRC* **3** 393 (1963).

Khristiansen G *et al.*, [MSU Coll.], *Astropart. Phys.* **2** 127 (1994).

Knapp J, Heck D, Sciuto S J, Dova M T and Risse M, *Astropart. Phys.* **19** 77 (2003).

Kobal M, *Astropart. Phys.* **15 259** (2001).

Kolhörster W, *Phys. Zeitschr.*, **26 654** (1925).

Kolhörster W *et al.*, Gekoppelte Höhenstrahlen. *Naturwis senschaften*, **26(35)**: **576**, doi: **10.1007/BF01773491** (1938).

Kulikov G V and Khristiansen G B, *Zh. Eksp. Teor. Fiz.*, **35:635-640**, (1958).

Knurenko S P, Ivanov A A, Pravdin M I Sabourov A V and Sleptsov I Ye, *Nuc. Phys. Proc. Suppl.*, **175-176**: **201-206**, (2008).

Knurenko S *et al., Proc. XVI ISVHECRI*, arXiv:**10101.1185** (2010).

Koul R *et al.*, *ICRC*, **5:243-246**, (2005).

Lafebre S, Engel R, Falcke H, Hörandel J, Huege T, Kuijpers J and Ulrich R, *Astropart. Phys.* **31** 243 (2009).

Lagutin A A *et al., Proc. 16th Int. Cosmic Ray Conf. (Kyoto)* vol **1** p **18** (1979).

Lang M J *et al.*, *J. Phys. G: Nucl. Part. Phys.* **20 1841** (1994).

Lawrence M A, Reid R J O, Watson A A, *J. Phys. G* **17 733-757** (1991).

Lessard R W *et al., ApJ*, **531, 942.** (2000).

Li Zhi-Xiong *et al.*, *arXiv*: **1304.3895v1** [*astro-ph.HE*] (2013).

Link B., Burgio F, *Phys. Rev. Lett.* **94 181101** (2005).

Link B., Burgio F, *MNRAS*, **371, 375** (2006).

Linsely J *et al.*, J. Phys. Soc. Japan **17** 91 (1962).

Linsley J, *Phys. Rev. Lett.* **10 146-148** (1963).

Lipari P, *Phys. Rev.* D **79 063001** (2009).

MAGIC Collaboration *Nucl. Phys. B Proc. Suppl.* **175 395** (2008).

Michelson P F *et al., Recent Highlights from FermiLAT Observations 32nd Int. Cos. Ray Conf.* Vol. **12** p. **31-36** (2011).

Mitrica B *et al., Nuclear Phys. B (Proc. Suppl.)* **196 462** (2009).

Miyake S *et al.,PICRC*, **5**, p. 3220 (1973).

Miyake S *et al.,PICRC*, **13**, p. 171 (1979).

Nagano M *et al., J. Phys. G* **10 1295** (1984)[a].

Nagano M *et al., J. Phys. Soc. Japan* **53 1667** (1984)[b].

Nagano M, *et al., J. Phys. G* **18 423-442** (1992).

National Aeronautics and Space Administration (NASA) US standard atmosphere *Technical Report* NASA-TM-X-**74335**. (1976).

Navarra G *et al., Nucl. Phys. B (Proc. Suppl.)* **60** B 105 (1998).

Nelson W R, Hirayama H and Rogers D W O, The EGS4 Code System *Report* SLAC**265** (Stanford Linear Accelerator Center, Stanford, CA) (1985).

Nerling F, Blumer J, Engel R and Risse M *Astropart. Phys.* **24 421** (2006).

Nestnhoff S *et al., Astropart. Phys.* **4 119-132** (1995).

Nishimura J, *Cosmic Rays, Handbuch der Physik*, **46, 2, 114**, Berlin: Springer Verlag (1967).

Paling S *et al.*, 25th *ICRC* **5** 253 (1997).

Peters B, *IL Nuovo Cimento*, **22**(4): **800 – 819**, (1961).

Pierog T and Werner K, *Nucl. Phys. B* **196 102** (2008)[a].

Pierog T and Werner K, *Phys. Rev. Lett.* **101 171101** (2008)[b].

Porter N A, *Nuovo Cimento Lett.* **8 481** (1973).

Protheroe R J, Clay R W and Gerhardy P R, *ApJ Lett.* **280 L47** (1984).

Rachen P J *et al., Astron. Astrophys.*, **272:161-175**, (1993).

Rao M V S *Proc. 18th Int. Cosmic Ray Conf. (Bangalore)* vol **11** p **449** (1983).

Rawlins K *et al.*, 28th *ICRC* **1** 173 (2003).

Rawlins K *et al., ICRC* (2011).

Rebel H *et al., J. Phys. G: Nucl. Part. Phys.* **35 085203** (2008).

Roh Soonyong *et al., Astropart. Phys.* **44** 1-8 (2013).

Rossi B and Greisen K *Rev. Mod. Phys.* **13 240** (1941).

Ruderman M A and Sutherland P G, *ApJ*, **196, 51** (1975).

Saha L *et al., Astropart. Phys.* **42 33-44** (2013).

Salazar H, *ICRC*, Poland, (2009).

Samorski M and Stamm W, *ApJ Lett.* **268 L17** (1983).

Sanyal S *et al., Aust. J Phys.* **46 589** (1993).

Schein M *et al., Phys. Rev.* **74 615** (1941).

Schmidt F, Ave M, Cazon L and Chou A, *Astropart. Phys.* **29 355** (2008).

Sciascio G D *et al., Int. J. of Mod. Phys. A* V. **20** No **29 6805-6807** (2005).

Sciascio G D and Girolamo T Di, *Astrophys. Space Sci.* **309 537-540** (2007).

Sciascio G D *et al., 32nd ICRC* (2011).

Sciutto S J, *arXiv:astro-ph/***0106044** (2001).

Settimo Mariangela *et al.*, *Eur. Phys. J. Plus* **127** 87 (2012).

Sima O *et al.*, *Nucl. Instru. Meth. A*, **638 147** (2011).

Simpson J A, *Ann. Rev.Nucl.Part.Sci.*, **33:323-382**, (1983).

Snyder H S, *Phys. Rev.* **76** 1563 (1989).

Stamenov J N, *Proc. 20th Int. Cosmic Ray Conf.* (Moscow) vol **8**, p. **258** (1987).

Suprun D, Gorham P W and Rosner J L, *Astropart. Phys.* **20 157** (2003).

Swordy S P *et al., Astropart. Phys.* **13** 137 (2001).

The Pierre Auger Collab., *JCAP* **11 022** (2011).

Thompson D J, preprint (astro-ph/0312272) (2003).

Tonwar S, *Proc. 17th Int. Cosmic Ray Conf. (Paris)* vol **13** p **330** (1981).

Uchaikin V V, *Proc. 16th Int. Cosmic Ray Conf. (Kyoto)* vol **1** p **14** (1979).

Ulrich H *et al., Nucl. Phys. B* **175 273** (2008).

Ulrich H *et al., Nucl. Phys. B* **196 80** (2009)[a].

Ulrich H *et al.*, *New J. Phys.* **11 065018** (2009)[b].

Voevodsky A V *et al.*, *Bull. Rus. Acad. Sci. Phys.* **57 685-688** (1993).

Vandenbroucke J, *Bulletin of the American Astronomical Society*, **41:909**, (2010).

Vulpescu B *et al.*, *J. Phys. G: Nucl. Part. Phys.* **27 977** (2001).

Wang Y *et al.*, preprint (astro-ph/08041862) (2008).

Watson A *et al., J. Phys.* A 7 1199 (1974).

Wdowczyk J and Wolfendale A W, *Nature* **305 609** (1983).

Weber J *et al.*, 26th *ICRC* **1**, 341 (1999).

Weeks T C and the *VERITAS Collaboration,* arXiv:**1001.5305** (2010).

Wentz J *et al.*, *J. Phys. G: Nucl. Part. Phys.* **27 1699-708** (2001).

Wentz J *et al.*, *Phys. Rev. D* **67 073020** (2003).

Werner K *et al.*, *Phys. Rev. C* **74 044902** (2006).

Wiedenbeck M E *et al.*, *Proc. 28th ICRC* (2003).

Wissel S *et al.*, *ICRC* **0671** (2009).

Wolfendale A W, Nucl. *Phys. B Proc. Suppl.* **22 80** (1990).

Yanasak N E *et al.*, *Astrophys. J.*, **563**: **768-792**, (2001).

Yoshida S *et al J. Phys. G: Nucl. Part. Phys.* **31 1413** (1994).

Yushkov A *et al., Phys. Rev.* D **81 123004**. (2008).

Zei R *et al.*, 30th *ICRC*, **2, 23-26** (2007).

Zhang B, Dai Z G, Meszaros P, Waxman E and Harding A K, *Astrophys. J.*, **595**, **346** (2003).

Zhang J L *et al.*, 31st *ICRC*, 0814 (2009).

INDEX

Astroparticle Physics 44 (2013) 68–75

Contents lists available at SciVerse ScienceDirect

Astroparticle Physics

journal homepage: www.elsevier.com/locate/astropart

Selecting gamma-ray showers from hadronic background using lateral shower age of EAS

R.K. Dey [a,*], A. Bhadra [b]

[a] Department of Physics, University of North Bengal, Siliguri, WB 734013, India
[b] High Energy and Cosmic Ray Research Centre, University of North Bengal, Siliguri, WB 734013, India

ARTICLE INFO

Article history:
Received 22 June 2012
Received in revised form 15 December 2012
Accepted 5 January 2013
Available online 12 January 2013

Keywords:
Cosmic ray
EAS
Lateral age
Local age
Simulation

ABSTRACT

A Monte Carlo (MC) simulation study has been carried out, aimed at identifying and rejecting the background component, constituted by hadronic cosmic rays, from γ-ray primaries in the multi-TeV region. In this work, our main focus is to discuss the possible role of the *local age parameter* (LAP) of cosmic ray extensive air shower (EAS) for separating γ-ray initiated showers from hadron initiated showers. Assigning a mean LAP to each EAS event, we found that the parameter might be useful for selecting γ-ray showers from hadron initiated showers in ground-based EAS experiments without muon measurement facilities.

1. Introduction

The present astrophysical conjecture of γ-ray astronomy leads to reflect newer concepts all the time in connection with the origin and acceleration mechanisms of cosmic rays (CRs). This becomes a viable branch of main stream astronomy with the advent of the ground-based imaging air Cherenkov telescopes (IACTs) [1]. The IACTs such as MAGIC [2], HESS [3], VERITAS [4] and the onboard Fermi Large area telescopes (FermiLAT) [5] along with the CGRO [6] produce results which agree remarkably well with the astrophysical model predictions. On the other hand, the imaging technique provides a method of effectively discriminating between γ-rays initiated showers and the background CR showers, based on the morphology of their Cherenkov images. To understand the important features of the primary energy spectrum vis-a-vis the chemical composition of the CRs at ultra high energy (UHE) and extremely high energy, a complete study of CR air-shower has been the only feasible way. The direct measurements of primary CR flux nearly 100 TeV and above are impractical because of very low and sharply falling flux, but has to be inferred from observations of extensive air showers.

The EAS measurements include estimation of various observable parameters namely shower size (N_e), muon size (N_μ), lateral shower age ($s_\perp$), local age ($s_{local}(r)$ or LAP), longitudinal age (s_L) of electron and muon distributions, hadron content (N_h), air shower associated Cherenkov photon content (N_{Ch}) and depth of shower maximum (X_{max}) (noticing that s_L and X_{max} measurements are made in air-shower arrays equipped with fluorescence detectors [7,8]) and most of these observables are found to be sensitive to primary masses with different degrees. To extract information about primary cosmic rays from the measurements of various experiments still require detailed MC simulations of the shower development as a basis of the data analysis and interpretation. The MC simulations consider the evolution of EAS in the atmosphere initiated by different energetic particles. Modern air-shower arrays equipped with large area detectors and improved electronics could precisely measure several EAS components simultaneously [9]. Employment of independent methods (or techniques) simultaneously using a hybrid detector set up to study high-energy CRs could help to limit systematic errors that have inundated CR experiments. The Pierre Auger Observatory uses hybrid detector in which those particles arriving at earth are detected through one technique while the other technique tracks the development of air showers by observing ultraviolet light emitted high in the earth's atmosphere [10]. Two or three detecting methods are also employed simultaneously in IceTop experiment in the south pole [11]. The inherently present shower-to-shower fluctuations in longitudinal development of EAS events corresponding to the same primary mass, energy and direction, measurements of EAS observables just providing important statistical information about the primary CRs.

In the field of CR air shower physics, the discrimination of γ-ray induced air showers from hadron-induced air showers is a chal-

* Corresponding author.
E-mail addresses: rkdey2007phy@rediffmail.com (R.K. Dey), aru_bhadra@yahoo.com (A. Bhadra).

0927-6505/$ - see front matter © 2013 Elsevier B.V. All rights reserved.
http://dx.doi.org/10.1016/j.astropartphys.2013.01.003

lenging problem that still needs more attention [12–14]. The high energy γ-rays are considered to be the by-product of hadronic components of primary CRs: a fraction of accelerated hadronic cosmic rays are likely to produce γ-rays through Δ-resonances, bremsstrahlung, inverse Compton etc. processes at or very close to the source site by interacting with the ambient matter [15]. The produced γ-rays will carry information about the origin of primary CRs as they point back at their source engines. The γ-ray detection suffers from the huge background constituted by ordinary CRs (hadrons) in the GeV–TeV energy region. The flux of primary γ-rays amongst the CRs has been estimated to be $\sim 10^{-5}$ of the proton flux at 100 TeV [16]. However, some early works predicted a Galactic plane excess higher than this: $\gamma/p \sim 10^{-3}, 3 \times 10^{-3}$ and 10^{-2} at $10^2, 10^3$ and 10^4 TeV [17]. Even at an energy of 10^7 TeV, this ratio has been predicted to rise up to 10^{-1} [18]. To observe astrophysical sources (emitting undeflected γ-rays and assumed as point-like objects) and to study the anisotropy properties of primary CRs, one has to eliminate isotropically distributed CRs.

Usually poor muon content is considered as the signature of γ-ray initiated EAS. In order to select a γ-ray shower based on such a criterion, an EAS array needs to be equipped with muon detectors covering very large area which is economically very challenging and such a facility is rarely available. So one has to look for some other primary mass sensitive observables based on which γ-ray initiated EASs can be separated out without the need of large area muon detector. In some early works, efforts were made to distinguish γ-ray showers on the basis of developmental stage of EAS in the atmosphere with the idea that γ-ray induced EAS will be younger than the hadron initiated EAS [19]. The lateral shower age ($s_\perp$), which is essentially the slope of the lateral density distribution of electrons in EAS (estimated by fitting the electron density data with the NKG function [20]) reflects the developmental stage of EAS and hence $s_\perp$ was used as distinguishing parameter. However, early MC simulation results regarding youthfulness of γ-ray induced showers in terms of shower age were inconclusive [21]. In those simulation works, authors used their own simulation codes and hence the findings could not be cross-checked. Since, nowadays standard simulation code like CORSIKA (COsmic Ray SImulation for KAscade) [22] is available and our knowledge about the high energy particle interactions is much improved now, it would be imperative to revisit the issue.

In the present work exploiting the CORSIKA MC simulation code, we made a detailed study on discrimination of γ-ray induced EAS from the large background contributed by hadrons in the multi-TeV range. The lateral shower profiles generated by various primaries within a particular primary energy range are being used here, and they provide some discriminatory power for separating γ-ray showers from the background. The selection of γ-ray initiated showers is attempted here by employing two different approaches - the Method I and the Method II. In the former approach (method I), we have taken single (r-independent) lateral age parameter i.e. $s_\perp$ as the γ-ray separation parameter. Besides, it has been argued in the literature that the different masses of primary CRs might also be separated using N_e, N_μ and f parameters [23]. The parameter f is giving out the ratio of reconstructed average electron densities at two arbitrary distance bands from the shower core, measuring roughly the rate of absorption of electrons in their lateral developments from the shower core. We also included this technique in the Method I. Experimentally it is observed that the NKG function with a single lateral age is insufficient to describe the lateral density distribution of EAS electrons properly at all distances, which implies that the lateral age changes with the radial distance. Subsequently, the notion of local lateral shower age parameter (LAP) was introduced [24] which is in essence the lateral age at a point. Since experimental electron density data in EAS may fluctuate considerably at a particular radial distance, instead of taking LAP at any particular point we take an average LAP between 50 m (where LAP is minimum) and 300 m (where LAP attains a local maximum) and in Method II, we employed this average LAP (s_{local}) to select γ-ray showers. It is found that when single constant lateral age ($s_\perp$) is used, the separation power becomes subdued. In contrast, the average LAP appears as a suitable mass sensitive parameter for classifying γ-ray induced showers.

The present study has been performed mainly at the geographical location of ARGO-YBJ (latitude 30.11°N, longitude 90.53°E, 4300 m a.s.l.) [25]. This is because the experiment offers a full coverage array and hence can measure radial density distribution of electrons in EAS with great accuracy, which in turn provides an opportunity to estimate LAP accurately. Moreover, since ARGO-YBJ does not have any muon detector, discrimination of γ-ray showers based on an alternative EAS observable, related to only electromagnetic component should be very useful. Since ARGO-YBJ experiment is located at very high altitude, its energy threshold is sub TeV and hence for this location we simulated EAS events in the energy range from 1 TeV to 3 PeV. However, ARGO-YBJ has not yet studied the radial variation of the lateral shower age while a few other experiments, such as Akeno [26] and NBU [27], successfully tested the predicted radial variation of LAP. We simulated a few events at the geographical location of Akeno and compared with the observations to demonstrate again the importance of considering LAP instead of single shower age. The correlations of $s_\perp$ with N_e and/or N_μ have been considered as a basis for extracting information on the nature of primary CRs. The KASCADE [28] and the NBU [29] experiments provide a few results on these aspects. Accordingly we performed simulations at geographical location of these experiments and compared with experimental findings in order to examine primary mass sensitivity of lateral shower age parameter. The MC simulation for generating EAS events considers interaction mechanisms of energetic particles as input. But due to the limited knowledge of particle interactions at high energies (and the large fluctuations) the results of simulation may become model dependent. To ensure that the conclusion of the present work is robust, we consider two high energy interaction models, QGSJet 01 v.1c [30] and EPOS – 1.99 [31] and found that the present findings do not have any strong dependence on the choice of interaction model.

The organization of the paper is as follows. The theoretical background of EAS age parameters $s_\perp$ and $s_{local}(r)$ described in the cascade theory is given in section 2. In section 3, the important considerations adapted in the simulation procedure are given. Estimation of lateral shower age and LAP is discussed in section 4. In sections 5 and 6, we present the results obtained on gamma-hadron separation employing method-I and method-II respectively. Finally, in section 7 summary and our conclusions are pointed out.

2. Shower age parameters: theoretical aspects

Extensive air showers propagating in the same density profile of the atmosphere essentially have equal lateral distributions around the shower axis. In the cascade theory, the problem of estimating the electron lateral distribution received an important recognition in the past. Nishimura and Kamata [32] solved numerically the 3-dimensional shower equations in *Approximation B* (electrons suffer constant amount of collision loss in a radiation length which is equal to the critical energy) to obtain the lateral distribution of electrons propagating in a medium of constant density. The results obtained on lateral density distribution of cascade particles by Nishimura and Kamata can be approximated by the well known Nishimura–Kamata–Greisen (NKG) structure function proposed by Greisen [20], given by

$$f(r) = C(s_\perp)(r/r_m)^{s_\perp - 2}(1 + r/r_m)^{s_\perp - 4.5}, \quad (1)$$

where the normalization factor C ($s_\perp$) is given by

$$C(s_\perp) = \frac{\Gamma(4.5 - s_\perp)}{2\pi\Gamma(s_\perp)\Gamma(4.5 - 2s_\perp)}. \quad (2)$$

The NKG formula has the advantage of normalization as it is integrable in Euler Beta function. The normalization of $f(r)$ implies for the electron density $\rho(r) = N_e f(r)$. But such a widely used relation does not hold if $s_\perp$ varies with r, as noted in Akeno [26], NBU [27] and some other observations [24]. An improvement of the NKG function was proposed by adopting a modulated, longitudinal age parameter s_L (the developmental stage of a pure electromagnetic cascade) dependent effective Moliere radius [33], so that,

$$\rho_{el}(r) = (mr_m)^{-2}\rho_{NKG}(r/m). \quad (3)$$

where r_m is the Moliere radius and $m = 0.78 - 0.21s_L$ so that mr_m may be referred as lateral age dependent effective Moliere radius. But even with such a modification, lateral shower age is found to vary with radial distance experimentally. To handle the situation a method was developed by Capdevielle et al. introducing the notion of *local age parameter* (LAP) [24]. From two neighboring points, i and j, we can give a LAP for any distribution $f(x)$ (where $x = \frac{r}{r_m}$) which characterizes the best fit by a NKG-type function in $[x_i, x_j]$:

$$s_{local}(i,j) = \frac{\ln(F_{ij}X_{ij}^2Y_{ij}^{4.5})}{\ln(X_{ij}Y_{ij})} \quad (4)$$

Here, $F_{ij} = f(r_i)/f(r_j)$, $X_{ij}=r_i/r_j$, and $Y_{ij}=(x_i+1)/(x_j+1)$. More generally, if $r_i \to r_j$, this suggests the definition of the LAP $s_{local}(x)$ (or $s_{local}(r)$) at each point:

$$s_{local}(x) = \frac{1}{2x+1}\left((x+1)\frac{\partial \ln f}{\partial \ln x} + 6.5x + 2\right) \quad (5)$$

Function $f_{NKG}(r)$ with $s=s_{local}(r)$ can be used to fit $f(r)$ in the neighborhood of r.

The identification $s_{local}(r) \equiv s_{local}(i,j)$ for $r = \frac{r_i+r_j}{2}$ remains valid for the experimental distributions (taking $F_{ij} = \rho(r_i)/\rho(r_j)$) as far as they are approximated by monotonic decreasing functions versus distance.

The behavior of LAP on experimental lateral distributions was found in accordance with the prediction [34] which was reaffirmed by the Akeno observations [26]. The stated method was validated by the rapporteurs of the ICRC from 1981 to 1985 [35]. In the present work, we have given emphasis on the estimation of the LAP and on its average using $s_{local}(r)$ values, taken between first minimum and the subsequent maximum from the radial variation of LAP. The estimation of $s_\perp$ would also be made through the traditional shower reconstruction method (electron density data are fitted with the NKG structure function over the entire radial distance under consideration).

3. Simulation of EAS

The EAS events are simulated by coupling the high energy (above 80 GeV/n) hadronic interaction models QGSJet 01 version 1c [30] and EPOS 1.99 [31], and the low energy (below 80 GeV/n) hadronic interaction model GHEISHA (version 2002d) [36] in the framework of the CORSIKA Monte Carlo program version 6.970 [37]. For the electromagnetic part the EGS4 [38] program library has been used. The US-standard atmospheric model [39] with planar approximation has been considered which works only for the zenith angle of the primary particles less than 70°. The maximum zenith angle of primaries has been restricted to 45° here.

The MC simulation data library consists of over 0.1 million EAS events each for p, Fe and γ-ray at the ARGO-YBJ location (latitude 30.11° N, longitude 90.53°E, 4300 m a.s.l.) in the primary energy range 1 TeV to 3 PeV using both QGSJet and EPOS models. In addition, we have generated 25,000 EAS events for each primary component p, Fe, and γ-ray and about 10,000 He events with the model QGSJet 01 v.1c in the primary energy range from 100 TeV to 30 PeV following a power law with a spectral index of −2.7 below the knee and −3.0 above the knee at the geographical locations of KASCADE (latitude 49.1° N, longitude 8.4° E, 110 m a.s.l.) and NBU (latitude 26.8° N, longitude 88.4° E, (~130 m a.s.l.). Besides, a small sample of events for p and Fe primaries are generated at the location of Akeno (35.78° N, 138.5° E, 900 m a.s.l.). The magnetic fields are set for all three observational levels accordingly.

Two mixed samples have been prepared from the generated showers taking 50% p, 25% He, 25% Fe events (mixture-I) and 37% p, 37% Fe, 26% γ-ray events (mixture-II) respectively for better understanding of EAS observational results.

4. Estimation of lateral shower age

The simulated electron density data have been analyzed in two different methods to obtain shower age parameters $s_\perp$ and $s_{local}(r)$. First, following the traditional approach we estimate $s_\perp$ (along with other shower parameters) by fitting the density data with the NKG structure function. In this approach, the simulated electron densities at different radial distances have been fitted by the method of chi-square minimization through an iterative procedure based on the method of steepest decent to the NKG lateral distribution function of electrons. Here it is to be noted that majority of the EAS groups generally estimate basic shower parameters based on the NKG function. In order to check the goodness of the NKG function in describing the simulated radial density distribution of electrons, we firstly fitted the simulated density data at various radial distances with the NKG function and compared radial density distribution of electrons for simulated events with the fitted curve. Fitted showers with reduced χ^2 less than 5 are only accepted for results involving $s_\perp$. The error in estimating $s_\perp$ in the N_e range $1.5 \times 10^4 - 4.25 \times 10^5$ has been found as ±0.03.

Secondly, exploiting Eq. (4) we directly estimated LAP for each individual event. We noted that the description of the data by the NKG function is improved when the Moliere radius is treated as a variable rather than a fixed parameter [40]. But this better description comes at the expense of very high shower age value which somewhat obscures the physical meaning of the age parameter as assigned in the cascade theory. In this analysis, the error of the LAP for EAS with the primary energy in the PeV range remains within 0.05 for 10 m < r < 250 m, whereas for r < 10 m or when r > 300 m the error of the LAP is found to be higher, about 0.1.

It has been shown recently [40] that LAP initially decreases with radial distance, reaches a minimum around 50 m, then starts increasing with radial distance, attains a local maximum around 300 m and decreases again thereafter. The nature of such a variation of LAP with radial distance was found independent of energy of the shower initiating particles [40]. We observed such a characteristic variation of LAP with radial distance at ARGO-YBJ location as shown in Fig. 1a for proton, iron and γ-ray primaries. It is seen from the Fig. 1a that the nature of variation is nearly the same for both QGSJet and EPOS. Here, it is worthwhile to mention that up to 50 TeV or so, the density of electrons in EAS beyond 50 m from the shower core is extremely small even at ARGO-YBJ level and is almost impossible to measure it in practical situation. Hence, we have chosen the primary energy from 100 TeV and above for results.

As already mentioned, Akeno group studied the radial variation of LAP experimentally [26]. We compared our simulation results with Akeno observations in Fig. 1b for proton and Fe primaries. The single lateral shower age for proton and iron primaries are also given (solid and dashed lines parallel to the x-axis) in the figure for

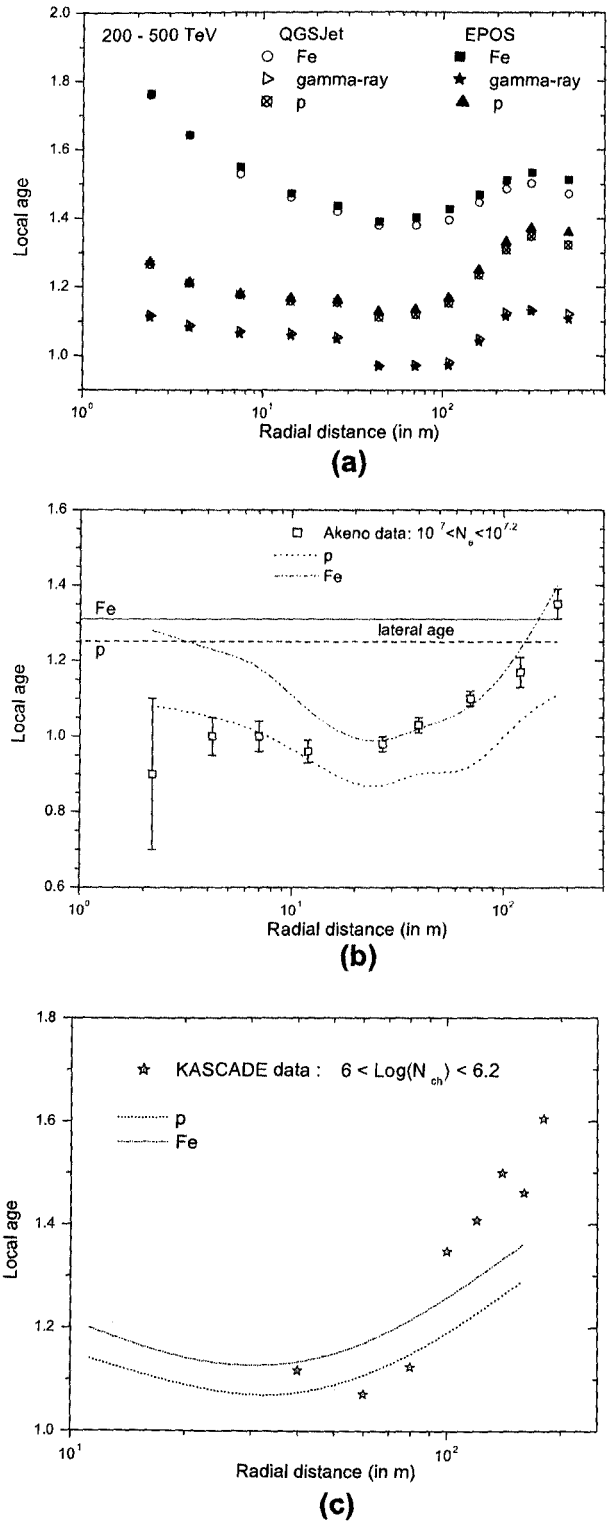

Fig. 1. (a) The radial variation of LAP obtained at the ARGO-YBJ altitude for p, Fe and γ-ray with hadronic interaction models QGSJet and EPOS. (b) Same as Fig. 1a at the Akeno level with QGSJet model, compared with experimental data. The solid and dashed lines parallel to the x-axis indicate $s_\perp$ for Fe and p. (c) The radial variation of LAP estimated from the KASCADE observed lateral distribution data. Lines indicate the mean values of a sample of simulated EAS events with QGSJet model (the errors in experimental data are not included here).

comparison. We also estimated LAP from the lateral density distribution of electrons obtained by the KASCADE experiment [28,41,42] and we compared with our simulation results in Fig. 1c. The errors in the extracted experimental points are quite large but it is at least clear that a constant single lateral shower age is insufficient to describe the experimental findings.

Since air shower measurements are subjected to large fluctuations, instead of LAP at a particular radial distance we consider for each event a mean LAP ($< s_{local} >$), which is the average of LAPs for several small distance bands (r_i, r_j) over the radial distance between 50 m to 300 m. For the purpose of averaging, distance bands are taken in constant steps on the logarithmic scale. The radial distance band from 50 m to 300 m is chosen because the positions of local minimum and maximum at 50 m and 300 m band are nearly universal, independently of primary energy [40].

5. Results on gamma-hadron separation: Method I

First, we analyzed the simulated EAS events generated at NBU and KASCADE locations (both at sea level), obtained $s_\perp$ and other shower parameters and compared with some of the published results of NBU [43] and KASCADE [28] respectively. Secondly, EAS events generated at the geographical location of ARGO-YBJ [25] are analyzed and both $s_\perp$ and $s_{local}(r)$ are estimated.

5.1. N_e & N_μ dependencies of $< s_\perp >$

The correlation between the mean lateral shower age ($< s_\perp >$) over a small shower size bin in the range ($10^3 - 1.5 \times 10^6$), with the zenith angle interval ($0^\circ - 45^\circ$) for p, Fe, γ-ray, mixed composition (mixture-I) using QGSJet model and corresponding NBU results [43] are put on view in Fig. 2a. The NBU EAS experiment reported the total uncertainties (including instrumental uncertainty) in estimating $s_\perp$ and N_e as $\pm 9\%$ and $\pm 0.14 N_e$ [29]. It is important to perceive that the lateral shower age takes higher values for heavy nuclei compared to that of light and γ-ray primaries clearly indicating relatively flatter lateral distribution of electrons as one moves from γ-ray to Fe via p.

The variation of $\langle s_\perp \rangle$ with muon size in the primary energy range ($10^2 - 3 \times 10^4$ TeV) and zenith angle interval ($0^\circ - 45^\circ$) for p, Fe, γ-ray primaries is presented in Fig. 2b with KASCADE data [28]. The variation exhibits the same nature as obtained in the KASCADE experiment using NKG fitting for muons with slightly higher muon threshold energy. The Fig. 2b exhibits the fact that γ-ray initiated showers can be separated out from the background using $\langle s_\perp \rangle$ and N_μ. It was also concluded in one of our previous work that EASs due to light primary components are younger on the average [40].

The KASCADE data points indicate that the composition changes slowly from predominantly proton at around 10^{14} eV to heavier primaries with the increase of energy. The NBU data are available only over a small energy window and though both the NBU and the KASCADE data suggest for a mixed composition in the common energy range of study, the NBU data favor for a relatively heavier composition. However, being a small EAS array the NBU experiment could measure electron density only up to 80 m from the shower core and its resolution power for primary composition is thus limited.

5.2. Variation of f with $\frac{N_\mu}{N_e}$

The lateral structure of EAS from different primaries attributes some power of identification and rejection of hadron primaries from γ-rays with the same primary energy and size [23]. From the lateral profile of each simulated EAS, we have estimated elec-

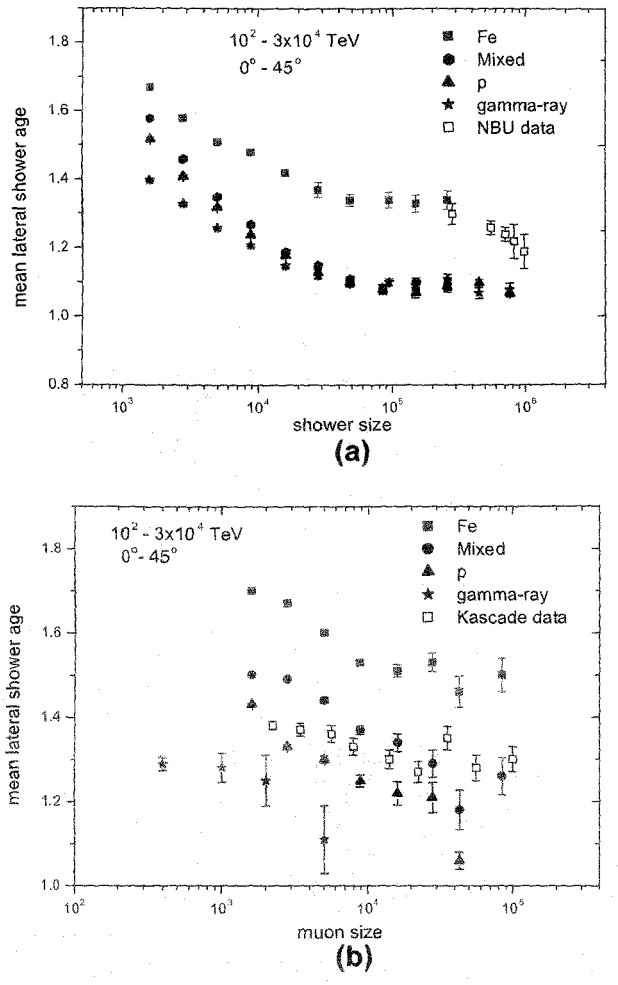

Fig. 2. (a) Variation of mean lateral shower age with shower size along with NBU data; (b) Variation of mean lateral shower age with muon size. For comparison with KASCADE data in Fig. 2b, where the age parameter was estimated by NKG fits with r_μ as 420 m and also used truncated muon sizes N_μ^{tr}. The QGSJet model has been used for simulation.

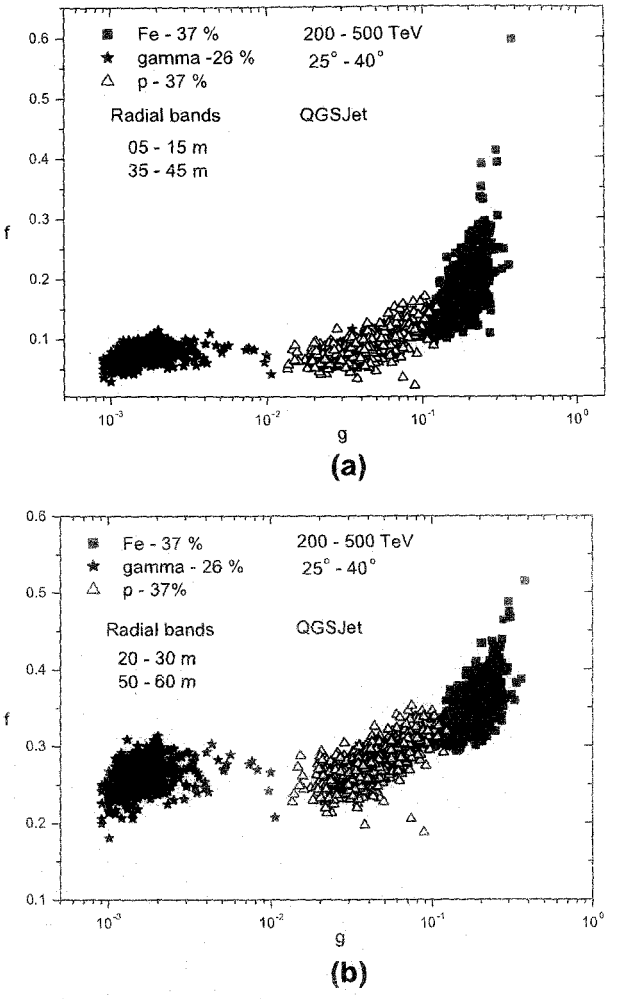

Fig. 3. Distribution of 200–500 TeV EAS events in the g-f plane at ARGO-YBJ level: (a) The ratio (f) for two electron densities are taken between distance bands (5–15) m and (35–45) m; (b) same as Fig. 3a but distance bands are taken at (20–30) and (50–60) m respectively. A negligible percentage of γ-ray primaries are found behind hadron (proton) showers.

tron densities at five adjacent radial points in each of the two arbitrarily chosen distance bands (5–15) m and (35–45) m. Next by employing the reconstruction procedure for the determination of local electron density (LED), we obtained two average reconstructed LEDs ρ_1 and ρ_2 from the shower core.

The selection of γ-ray showers from hadrons becomes visible when one plots the parameter f against g where $g = \frac{N_\mu}{N_e}$ as presented in a 2-dimensional Fig. 3a. The same study has been repeated for another pair of radial bands (20–30) m and (50–60) m, using the same sample of mixture-II and it is depicted in Fig. 3b. The rate of absorption of electrons decreases with increasing radial distance from the core and this feature is revealed from the comparison of Figs. 3a and 3b. We have checked that the characteristic feature of the $g - f$ distribution does not change appreciably for the high energy interaction model EPOS and for a different primary energy range (100–200) TeV.

It appears from the Fig. 3 that this technique essentially exploits the total muon content in an EAS. The events are classified according to their primaries along x-axis (the ratio of muon size to electron size is plotted along x-axis); there is no notable separation along y-axis between events generated by photons and protons.

6. Results on gamma-hadron separation:Method II

In this section we would explore through MC simulation study whether LAP is sensitive on primary mass and consequently the possible role that the parameter may play for separating γ-ray showers from a large background constituted by hadronic showers in primary CRs.

6.1. Variation of LAP with shower size

Due to overwhelming background from hadron induced EAS, the discrimination of the rare gamma-like events is vital. In Fig. 4 we have shown the variation of $< s_{local} >$ as a function of N_e for the primaries p, Fe, and γ-rays from simulated results. Please note that EAS events were simulated for the same fixed primary energy range irrespective of nature of primaries and since different primaries having the same energy may produce different N_e, in Figs. 4a and 4b the starting and ending values of N_e are not always the same for all the primaries. We considered a particular N_e region where data for all the primaries are more or less available with rea-

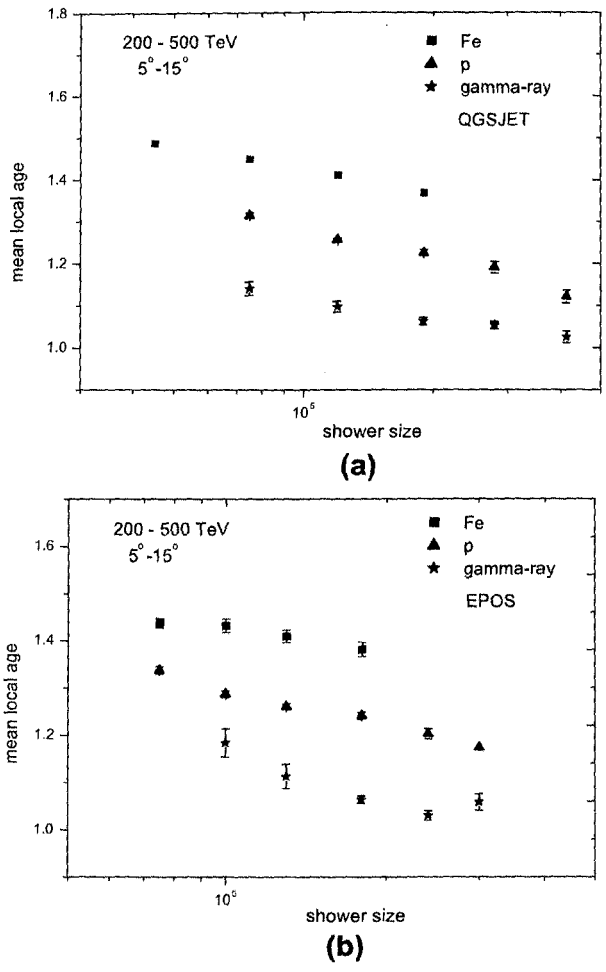

Fig. 4. (a) Variation of $< s_{local} >$ with N_e at ARGO-YBJ with QGSJet model; (b) same as Fig. 4a but for the model EPOS.

sonable statistics. It is clear from the plots that EAS events are classified according to their primaries along y-axis which means that γ-ray induced showers can be separated out on the basis of $< s_{local} >$. The scatter plots for the same variation are shown in Figs. 5a 5b and 5c where distribution of different primary masses based on s_{local} and N_e data from the mixture-II corresponding to different primary energies and interaction models are presented.

6.2. Selection of γ-ray component using LAP

In the primary CR flux, the percentage of γ-ray flux is very very small, of the order of 0.001%. To separate such a small fraction of γ-ray component from primary CRs in a real experiment employing method II, it would be nice if we could prepare a mixture with such a small percent of γ-rays and see whether the γ-ray events can be extracted out or not. But due to limited statistics we could not do that. Instead, we made three sub-mixtures of type II maintaining the ratio of primaries as 37% p, 37% Fe and 26% γ-ray for three different combinations of zenith angle, primary energy and shower size ranges. These exercises are done for both the high energy interaction models QGSJet and EPOS. From each sub-mixture, we tried to separate γ-ray showers out exploiting s_{local} corresponding to different N_e.

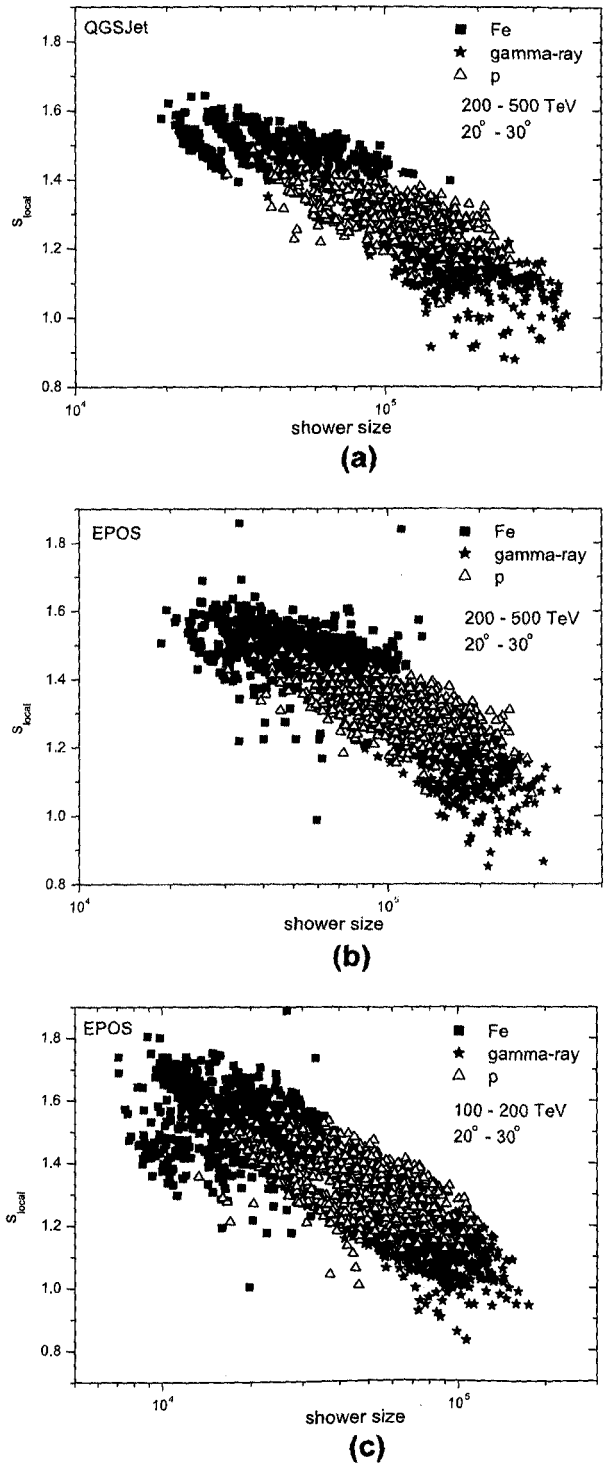

Fig. 5. (a)–(c) Distribution of simulated events in mixture-II in two primary energy ranges based on s_{local} and N_e at ARGO-YBJ. Dependence on interaction models is also shown.

For a small enough cut value of s_{local} we have found poor acceptance for γ-ray induced EAS and very good rejection of background, whereas for a large enough value of s_{local} the situation is found to be completely reversed. Cut values of s_{local} lie between the two ex-

Table I
The quality factor at various s_{local} cuts using QGSJet model. The primary energy, zenith angle and shower size intervals are (200–500) TeV, 20°–30° and (1.5–4.0) × 10^5, respectively.

s_{local}	1.05	1.08	1.10	1.12	1.14	1.15	1.16	1.18	1.20
ϵ_γ	0.146	0.237	0.348	0.510	0.657	0.707	0.778	0.864	0.934
ϵ_{bkg}	0.007	0.022	0.029	0.036	0.058	0.065	0.109	0.145	0.254
Q	1.74	1.61	2.05	2.69	2.73	2.77	2.36	2.27	1.86

Table II
The signal selection parameters at optimal conditions.

Model	E (TeV)	θ (deg.)	$N_e \times 10^5$	s_{local}	ϵ_γ	ϵ_{bkg}	Q
EPOS	100 – 200	5 – 15	0.6 – 2.0	1.14	0.691	0.072	2.57
EPOS	200 – 500	20 – 30	1.5 – 4.0	1.15	0.734	0.048	3.35
QGSJet	200 – 500	20 – 30	1.5 – 4.0	1.15	0.707	0.065	2.77

tremes offered different acceptances and rejections of γ-ray and background respectively. Similarly a proper cut on N_e is also needed for selection of γ-ray induced EAS and the rejection of background. In astronomical signal selection, optimal cut to selection parameters (maximizing the γ-ray efficiency and minimizing the background contamination) is usually set by numerical maximization of the quality factor Q defined by

$$Q = \frac{\epsilon_\gamma}{\sqrt{\epsilon_{bkg}}} = \frac{\epsilon_\gamma}{\sqrt{(1-\xi_{bkg})}} \tag{6}$$

where ϵ_γ and ϵ_{bkg} respectively denote the acceptances of γ-ray and background from the sample using a cut value of s_{local} but ξ_{bkg} stands for the rejection of background. Here, $\epsilon_\gamma = \frac{n_\gamma(cut)}{n_\gamma}$ and $\epsilon_{bkg} = \frac{n_{bkg}(cut)}{n_{bkg}}$, with $n_\gamma(cut)$ and $n_{bkg}(cut)$ represent number of showers of either kind those passed through a particular cut value of s_{local} while n_γ and n_{bkg} are the total number of showers present in the sample before the applied cut. Q essentially quantifies the gain of significance achieved by the separation algorithm. The quality factor is used here to evaluate the selection performance. As for an example the quality factor is evaluated over a shower size and zenith angle bins by varying s_{local} which is shown in Table I. In Table II, we have given a chart for quality factors estimated at optimal conditions in three different situations.

A better option to evaluate the performance of selection algorithm is the application of an advanced technique like Principal Component Analysis or a Fisher analysis that allows to combine s_{local} and shower size in a single optimized observable.

7. Summary and conclusions

In this work, attempts have been made to discriminate γ-ray induced EAS from hadron initiated shower on the basis of shape of electron density distribution in EAS characterized by lateral shower age parameter that essentially reflects the stage of EAS development in atmosphere. Generally muon content of an EAS is treated as a good estimator for gamma-hadron discrimination. However, a precise measurement of total muons in an EAS requires muon detectors covering large area which is quite expensive. So, we explored whether lateral shower age could be used for the purpose.

We first explored traditional lateral shower age parameter i.e. single (r-independent) shower age as the distinguishing parameter. Later, we attempted to separate out γ-ray initiated EAS on the basis of mean LAP. It is found from the simulation results that γ-ray induced EASs are younger in terms of the mean LAP (i.e. having lower mean LAP) and hence this parameter (mean LAP) can effectively separate out γ-ray induced showers from hadronic EAS unlike the case of single lateral shower age. This is probably because of the inadequacy of a single (constant) lateral age parameter to describe the experimental lateral distribution of EAS electrons properly at all distances as noted in several experimental observations. So when a single constant age is assigned (from fitting of the electron density data at different radial distances) to an EAS event, the discriminating power of that parameter on primary masses somewhat becomes dull; it still can distinguish iron initiated showers from proton induced showers but can't effectively separate out γ-ray showers from EASs generated by primary protons. Fig. 2a is an indicative one in favor of the inadequacy of $s_\perp$ for gamma-hadron discrimination. It is clear from the figure that the $< s_\perp >$ values for γ-ray and proton induced showers are very much nearer to each other.

Lateral distribution of electrons in EAS exhibits universal (primary energy and mass independent) behavior in terms of LAP [40]. The present conclusion appears independent on the choice of high energy interaction models, or at least does not have strong interaction model dependence as both the QGSJet and EPOS give similar results.

An important question is the experimental realization of the adopted technique involving LAP. The uncertainty in estimating LAP is usually large in normal circumstances in comparison to that in lateral shower age as the LAP depends on the logarithmic derivative of the density versus radial distance. Thus, uncertainty in estimating LAP from experimental data arises mainly from the uncertainties in electron densities and those in radial distance measurements due to erroneous determination of shower core position. These uncertainties should be small for a closely packed air shower array like GRAPES-III at Ooty [44] or for a full coverage EAS array like ARGO-YBJ [25] and hence the proposed method may successfully work in a such kind of experiment. However, at present, the ARGO-YBJ carpet provides a full coverage area of about (80 m×80 m). For successful implementation of the proposed method, a slightly larger coverage area of the carpet would be desirable.

We also tried to identify γ-ray generated EAS by the use of 'f' parameter that describes the ratio of reconstructed average LEDs at two arbitrary distance bands from the shower core as proposed in [25,45]. It is found from the scatter plot of 'f '(as y variable) with the ratio of total muon content to total electron number (x variable) that EAS events are classified according to their respective primaries but the separation occurs not along y-axis rather along x-axis. This means that essentially the separation is due to the total muon content in EAS, a well studied mass sensitive observable.

Acknowledgments

The authors thank an anonymous referee for constructive comments and suggestions on our original manuscript. We are thankful to Prof. J. N. Capdevielle for many useful suggestions. R.K.D. thanks the UGC (Govt. of India) for support under Grant. No. 41/1407/2012(SR). R.K.D. thanks the USIC (NBU) for providing computational facilities.

References

[1] F. Aharonian et al., H.E.S.S. Collaboration, Astron. Astrophys. 457 (2006) 889.
[2] C. Baixeras, Nucl. Phys. B Proc. Suppl. 114 (2003) 247–252;
C. Baixeras, MAGIC Collaboration, Nucl. Phys. B Proc. Suppl. 175 (2008) 395.
[3] J.A. Hinton, New Astron. Rev. 48 (2004) 331.
[4] T.C. Weeks, The VERITAS Collaboration, 2010. <arXiv:1001.5305[astro-ph]>.;
M. Beilicke, VERITAS Collaboration, in: AIP Conference Proceedings, vol. 1112, 2008, pp. 33.
[5] W.B. Atwood et al., ApJ 697 (2009) 1071. <www-glast.stanford.edu>;
Charles D. Dermer. <arXiv:1206.2899[astro-ph.HE]>.
[6] W. Collmar et al., Astron. Astrophys. 354 (2000) 513–521.

[7] D.J. Bird et al., Fly's Eye collaboration, Phys. Rev. Lett. 71 (1993) 3401.
[8] R.U. Abbasi et al., HIRES collaboration, ApJ 622 (2005) 910.
[9] T. Antoni et al., Astropart. Phys. 24 (2005) 1–25.
[10] J. Abraham et al., Nucl. Instrum. Methods A 50 (2004) 523.
[11] F. Halzen, Pionic photons and neutrinos from cosmic ray accelerators, Astropart. Phys. (2011).
[12] T. Gaisser, Cosmic Rays and Particle Phys, Cambridge University Press, Oxford, 1990.
[13] S. Nestnhoff et al., Astropart. Phys. 4 (1995) 119–132.
[14] H.M. Badran, T.C. Neekes, Astropart. Phys. 7 (1997) 307–314.
[15] A. Bhadra, R.K. Dey, Mon. Not. Roy. Astron. Soc. 395 (2009) 1371–1375.
[16] P.R. Blake, W.F. Nash, J. Phys. G: Nucl. Part. Phys. 26 (2000) 365–375.
[17] A.W. Wolfendale, Nucl. Phys. B Proc. Suppl. 22 (1990) 80.
[18] J. Wdowczyk, A.W. Wolfendale, Nature 305 (1983) 609.
[19] M. Samorski, W. Stamm, ApJ Lett. 268 (1983) L17;
R.J. Protheroe, R.W. Clay, P.R. Gerhardy, ApJ Lett. 280 (1984) L47.
[20] K. Greisen, Progress in Cosmic Ray Physics, NH Publishing Co, Amsterdam, 1956 (vol. III);
H.S. Snyder, Phys. Rev. 76 (1989) 1563.
[21] J. Fenyves Techniques in UHE γ-ray astronomy, R.J. Protheroe, S.A. Stephens (ed.), (University of Adelaide, 1985) pp. 124; A.M. Hillas, in: Proc. 20th Int. Cosmic Ray Conference Moscow, vol. 2, 1987, pp. 362.
[22] D. Heck, et al., FZKA-Report Forschungszentrum Karlshruhe, 1998, pp. 6019.
[23] G. Disciascio et al., Int. J. Mod. Phys. A 20 (29) (2005) 6805–6807.
[24] J.N. Capdevielle, J. Gawin, J. Phys. G: Nucl. Phys. 8 (1982) 1317;
M.F. Bourdeau, J.N. Capdevielle, J. Procureur, J. Phys. G: Nucl. Phys. 6 (1980) 901;
J.N. Capdevielle, P. Gabinski, J. Phys. G: Nucl. Part. Phys. 16 (1990) 769.
[25] G. Disciascio, T.Di Girolamo, Astrophys. Space Sci. 309 (2007) 537–540;
A. Aloisio et al., Nuovo Cimento C24 (2001) 739.
[26] M. Nagano et al., J. Phys. Soc. Japan 53 (1984) 1667;
M. Nagano et al., J. Phys. G 10 (1984) 1295–1310.
[27] S. Sanyal et al., Aust. J. Phys. 46 (1993) 589.
[28] T. Antoni et al., Astropart. Phys. 14 (2001) 245.
[29] A. Bhadra et al., Nucl. Instrum. Methods A 414 (1998) 233.
[30] N.N. Kalmykov, S.S. Ostapchenko, A.I. Pavlov, Nucl. Phys. B (Proc. Suppl.) 5 (1997) 17.
[31] K. Werner et al., Phys. Rev. C 74 (2006) 044902.
[32] P. Lipari, Phys. Rev. D 79 (2009) 063001.
[33] A.A. Lagutin et al., in: Proc. 16th Int. Cosmic Ray Conf. Kyoto, vol. 7, 1979, p. 18
[34] J.N. Capdevielle et al., J. Phys. G: Nucl. Part. Phys. 31 (2005) 507–524.
[35] S. Tonwar, in: Proc. 17th Int. Cosmic Ray Conf., Paris, vol. 13, 1981, p. 330.;
M.V. Rao, in: Proc. 18th Int. Cosmic Ray Conf., Bangalore, vol. 11, 1983.
[36] H. Fesefeldt, Report PITHA-85/02 (RWTH Aachen) 1985.
[37] D. Heck, J. Knapp, J.N. Capdevielle, G. Schatz, T. Thouw, The CORSIKA air shower simulation program, Forschungszentrum Karlsruhe Report FZK 6019 (Karlsruhe), 1998.;
J.N. Capdevielle, The Karlsruhe Extensive Air Shower Simulation Code CORSIKA KfK Report 4998 (Karlsruhe), 1992.
[38] W.R. Nelson, H. Hiramaya, D.W.O. Rogers, Report SLAC, 1985, p. 265
[39] National Aeronautics and Space Administration (NASA) U.S. Standard Atmosphere Tech. Rep. NASA-TM-X-74335, 1976.;
J. Knapp, D. Heck Tech. Rep. 5196B Kernforschungszentrum Karlsruhe, 1993.
[40] R.K. Dey et al., J. Phys. G: Nucl. Part. Phys. 39 (2012) 085201.
[41] H. Ulrich et al., Nucl. Phys. B 175 (2008) 273;
H. Ulrich et al., Nucl. Phys. B 196 (2009) 80.
[42] W.D. Apel et al., Astropart. Phys. 24 (2006) 467.
[43] A. Bhadra, Pramana: J. Phys. 52 (1999) 133–144.
[44] S.K. Gupta et al., Nucl. Instrum. Methods A 540 (2005) 311.
[45] T.K. Gaisser, T. Stanev, Phys. Rev. D 43 (1991) 2.

IOP PUBLISHING JOURNAL OF PHYSICS G: NUCLEAR AND PARTICLE PHYSICS

J. Phys. G: Nucl. Part. Phys. **39** (2012) 085201 (14pp) doi:10.1088/0954-3899/39/8/085201

Scaling behaviour of lateral distribution of electrons in EAS

R K Dey[1], **A Bhadra**[2] **and J N Capdevielle**[3]

[1] Department of Physics, University of North Bengal, Siliguri, WB 734013, India
[2] High Energy and Cosmic Ray Research Centre, University of North Bengal, Siliguri, WB 734013, India
[3] APC, University Paris-Diderot, Bt. Condorcet, 10 rue Alice Domon et Leonie Duquet 75205 Paris Cedex 13 et Académie des Sciences d'Outre mer, 15 rue La Pérouse, 75116, Paris

E-mail: rkdey2007phy@rediffmail.com, aru-bhadra@yahoo.com and capdev@apc.univ-paris7.fr

Received 8 July 2011
Published 4 July 2012
Online at stacks.iop.org/JPhysG/39/085201

Abstract

From a Monte Carlo simulation study of cosmic ray air showers around the knee of the primary energy spectrum it is shown that, despite a strong radial dependence of the lateral shower age parameter, the lateral density distribution of electrons in cosmic ray EAS displays *universality* when expressed in terms of local age parameters. The nature of the radial variation of local age is found to depend on the choice of the effective Moliere radius, particularly for radial distances below about 400 m. The possible use of shower age parameters in a multi-parameter study of EAS for extracting information about the nature of the shower initiating particles, has been re-examined.

(Some figures may appear in colour only in the online journal)

1. Introduction

A number of recent studies indicate that the average shape of several distributions of electrons in very high energy cosmic ray extensive air showers (EAS), such as the energy distribution or angular distribution, primarily exhibits the so called *universality* [1–4]: it depends only on the stage of the longitudinal shower development in the atmosphere or equivalently on the longitudinal shower age parameters ($s_{||}$) (that represents the variation of the total number of EAS electrons with the atmospheric depth and hence describes the longitudinal shower development; details about the parameters are given in the next section) irrespective of the nature of the primary particle and energy. Such a feature was first divulged from the early work by Kamata and Nishimura [5] in the context of the development of cosmic ray cascades in the atmosphere. The experimental data also appear to substantiate this *universality* behaviour on an average basis [6]. The *universality* property is quite advantageous for the analysis of high energy cosmic ray data as it helps to parameterize the electron positron distributions, it seems useful for an accurate estimation of the muon and electromagnetic (EM) contents in an EAS

[7] and also it assists to infer the primary mass composition and the nature of the first few interactions from the observed EAS data [6].

The observed lateral density distribution (LDD) of EAS electrons is, however, usually described in terms of the lateral shower age ($s_\perp$), which essentially describes its slope. Theoretically, the relation $s_{||} = s_\perp$ holds for both EM showers and hadron initiated EAS [2, 5]. In most experiments, however, the estimated $s_\perp$ differs from $s_{||}$ for an EAS with hadrons as primary. Here note that $s_{||}$ can be estimated observationally only if the EAS experiment is equipped with Cherenkov or fluorescence detectors, whereas s_- follows immediately from the lateral distribution of electrons, which is a basic measurement of any conventional EAS array consisting of particle detectors. Hence it is imperative to explore the *universality* of LDD of EAS electrons in terms of the lateral shower age.

A major challenge, however, is the reliable and unambiguous estimate of $s_\perp$ from experimentally measured electron densities. Usually the LDD of electrons in an EAS is approximated by the well known Nishimura–Kamata–Greisen (NKG) structure function [8] and the shower parameters, namely the shower size (N_e) (the total number of electrons in an EAS at an observational level) and $s_\perp$ are evaluated by fitting the measured densities with the NKG function. However, experimentally it is observed that the NKG function with a single $s_\perp$ is insufficient to describe the LDD of EAS electrons properly at all distances, which implies that the lateral age changes with the radial distance. Subsequently some modifications of the NKG structure function [9] were proposed but the radial dependency on the shower age could not be removed totally. Under the circumstances, the notion of *local shower age parameters* (LAP) was introduced [10] which is in essence the lateral age at a point.

In this work, from a detailed Monte Carlo (MC) simulation study, we show that the shape of the radial variation of the LAP (and hence the LDD of the electrons in an EAS) exhibits some sort of *scaling* (energy and mass independent) behaviour. The shape of the radial variation of the LAP is, however, found to depend on the choice of the effective Moliére radius in the NKG function. Such a scaling feature provides a better description of the radial electron distributions in EAS and should help to estimate the electron content in an EAS accurately. We also investigate the characteristics of the LAP and its correlation with other EAS observables and thereby the possible role that the parameters may play in a multi-parameter approach to studying EAS, in order to understand the nature of shower initiating particles.

The plan of this paper is the following. In the next section the shower age parameters of EAS will be introduced. In section 3 the simulation procedure adapted in this work will be described. The estimation of the shower age parameters is given in section 4. The results on the characteristics of the local shower age and its correlation with other EAS observables will be given in section 5. Finally we will conclude in Section 6.

2. Shower age parameters

The average longitudinal profile of an EM cascade, which is developed in a medium through a multiplicative process involving the interactions of electrons and photons when passing through it, was provided by Greisen [8] in the so-called Approximation B (i.e., considering the processes like a pair production by the photons, *bremsstrahlung* by the electrons and the ionization loss suffered by the electrons while neglecting the Compton scattering)

$$N_e = \frac{0.31}{\sqrt{\ln(E_0/\epsilon_0)}} \exp[t(1 - 1.5\ln(s_{||})]. \tag{1}$$

Here E_0 is the energy of the primary photon generating the cascade, ϵ_0 is the critical energy (below which ionization losses predominate over that due to pair production) with a value

of ~82 MeV. Note that t is expressed here in cascade units (the atmospheric depth has been divided by the electron radiation length in air, taken as 37.1 gmcm^{-2}). The longitudinal age $s_{||}$ is defined by the simple relation

$$s_{||} = \frac{3t}{t + 2\ln(E_0/\epsilon_0)} \,. \tag{2}$$

The developmental stage of a pure EM cascade is thus characterized solely by $s_{||}$. Basically this parameter represents the change of the total number of EAS electrons with the atmospheric depth (dN/dt) [11]. Recent MC simulation studies [3, 4] exhibited a possible universality for large EAS with primaries in the EeV energy range in terms of $s_{||}$.

Advancing the preliminary work of Moliére and Bethe on the LDD of an electron near the cascade maximum, Nishimura and Kamata obtained an expression of radial distance dependence of $s_{||}$ by solving the three dimensional diffusion equations in Approximation B and taking into account the hegemony of the multiple Coulomb scattering [5]

$$s_{||}(r) = \frac{3t}{t + 2\ln(E/\epsilon_0) + 2\ln(r/r_m)} \tag{3}$$

where r is the radial distance from the shower core and r_m is the Moliére radius (near 80 m at sea level) which is a characteristic constant of a medium defined as the radius of a cylinder containing on average 90% of the EMS's energy deposition.

In the same theoretical context, the LDD of cascade particles can be approximated by the NKG structure function [8], given by

$$f(r) = C(s_\perp)(r/r_m)^{s_\perp - 2}(1 + r/r_m)^{s_\perp - 4.5} \,, \tag{4}$$

where the normalization factor $C(s_\perp)$ is given by

$$C(s_\perp) = \frac{\Gamma(4.5 - s_\perp)}{2\pi\Gamma(s_\perp)\Gamma(4.5 - 2s_\perp)} \,. \tag{5}$$

The NKG formula has the advantage of normalization as it is integrable in the Euler Beta function provided $s_\perp$ is independent of r. The normalization of $f(r)$ implies that $\rho(r) = N_e f(r)$, $\rho(r)$ being the electron density at r. The relation $s_{||} = s$ was considered to hold for pure EMS [5]. The equations (1), (2) and (4) together provide an attractive and a complete procedure for calculating the 3D development of the EM cascade, as first pointed out by Cocconi [12].

The superposition of many such pure EM cascades build the electron component of a hadron initiated EAS. It was suggested [2, 5] that for hadron initiated EAS, both the longitudinal structure and lateral structure of soft components can be described by that of a resulting single cascade, assigning a suitable value to the age parameter.

The various approximations made in obtaining the solutions, as well as due to an over-simplification of the adopted 3D transport equations, the analytical expressions of EM cascades are of restricted applicability. It was observed that near the shower axis, the NKG predicted densities were somewhat lower than those with the original NK formula [13] for $s \geqslant 1.2$. On the other hand, experimentally observed densities were noted to be larger than those given by the NKG far from the axis [8], which was inferred as a possible contribution from the muon decay. A shorter value of the second momentum of the distribution than in the NKG was observed [14] and a couple of years later a steeper profile was exhibited from an MC calculation near 100 GeV [15]. An improvement of the NKG function was subsequently proposed by adopting a modulated, longitudinal age parameter $s_{||}$ dependent effective Moliére

radius so that

$$\rho_{el}(r) = (mr_m)^{-2}\rho_{\mathrm{NKG}}(r/m) \tag{6}$$

where $m = 0.78 - -0.21s_{||}$.[4]

On the other hand, observing that the experimental LDD of electrons in EAS was steeper than that given by the ρ_{NKG} and was in better agreement with the MC calculations of Hillas [15] at lower energies, Capdevielle *et al* [10] introduced the notion of *local age*. After testifying the behaviour of the LAP on experimental lateral distributions [10] and reaffirming it with the Akeno observations [16], this approach was validated by the *rapporteurs* of the International Cosmic Ray Conferences during the period 1981 to 1985 [17]. The whole procedure was also employed in the calculation of the radio effects of EAS [18].

If electron densities are describing any NKG-like distribution $f(x)$, where $x = \frac{r}{r_m}$, for two neighbouring points, i and j, we have the (local) lateral age

$$s_{ij}^{\mathrm{local}} = \frac{\ln\left(F_{ij}X_{ij}^2Y_{ij}^{4.5}\right)}{\ln(X_{ij}Y_{ij})} \tag{7}$$

where $F_{ij} = f(r_i)/f(r_j)$, $X_{ij} = r_i/r_j$ and $Y_{ij} = (x_i{+}1)/(x_j{+}1)$. More generally, if $r_i \to r_j$, this suggests the definition of the LAP $s_{\perp}^{\mathrm{local}}(r)$ at each point:

$$s_{\perp}^{\mathrm{local}}(r) = \frac{1}{2x+1}\left((x+1)\frac{\partial \ln f}{\partial \ln x} + (2+\beta_0)x + 2\right) \tag{8}$$

If $\beta_0 = 4.5$, $f_{\mathrm{NKG}}(r)$ with $s_{\perp} \equiv s_{\perp}^{\mathrm{local}}(r)$ can be used to fit f in the neighbourhood of r.

Typical behaviour was predicted with a characterized minimum value of $s^{\mathrm{local}}(r)$ near 50 m from the axis, followed by a general increase at a large distance [10]. The relation $s_{\perp}^{\mathrm{local}}(r) = s_{ij}^{\mathrm{local}}$ for $r = \frac{r_i+r_j}{2}$ was found to be valid for the experimental distributions (taking $F_{ij} = \rho(r_i)/\rho(r_j)$ as far as they were approximated by monotonic decreasing functions versus distance).

Such a prediction was substantiated by the Akeno [16], North Bengal University (NBU) EAS experiment [19] and other experiments [10]. The LAP depends mainly on the logarithmic derivative of the density versus the distance as it appears in the relation (9); however, this pure mathematical approach may not be attained in practice at any radial distance, due to the experimental uncertainties arising mainly from the use of a finite number of detectors for the density measurements, triggering conditions and errors in the determination of the shower core position. Therefore, $s_{\perp}^{\mathrm{local}}(r)$ is estimated via relation (7) using physical bands of distance $[r_i, r_j]$; for experiments with very dense grids of detectors, such distance bands may be reduced to 5–10 m, but they may have to enlarge up to about 20 m for arrays with a lower resolution, as well as in the case of individual showers with large fluctuations. For very large and giant EAS, the interval $[r_i, r_j]$ maybe required to exceed 100 m or so. We preferred to conserve the characteristic parameters of EM cascades in relation (7) including the value of the Moliére radius to facilitate the comparison with the experimental data, which is most frequently expressed in NKG formalism.

The dependence of $s_{\perp}(r)$ on r rules out a consistent integration via relation (4) casting some doubt on the accurate relation between density and size; it was shown that such a dependence of $s_{\perp}(r)$ on r is mainly a basic feature of pure EM cascades [10, 20].

[4] ρ_{el}, not just ρ_{NKG}, was implemented in the so called subroutine NKG of CORSIKA (Cosmic Ray Simulation for KAscade).

3. Method of simulation

For generating EAS events, the air shower simulation program CORSIKA [21] is exploited here. Here our discussions are mainly restricted to cosmic rays in the knee region of the primary spectrum. In this work, the high energy (above 80 GeV/n) hadronic interaction model QGSJET 01 version 1c [22] was used in combination with the low energy (below 80 GeV/n) hadronic interaction model GHEISHA (version 2002d) [23] or FLUKA [24], depending on the primary energy in the framework of the CORSIKA MC program version 6.600/6.735 [21] to generate EAS events. Note that the low energy interaction model GHEISHA exhibits a few shortcomings [25, 26] but the LDD of EAS electrons does not depend much on the low energy hadronic models, except at large distances [25]. Hence for very high energy events involving large radial distances we employed FLUKA [24]. A relatively smaller sample was also generated using the high-energy interaction model SIBYLL (version 2.1) [27] to judge the influence of the hadronic interaction models on the results.

The CORSIKA program allows one to choose either of the two options, the EGS4 (electron gamma shower system version 4) [28] and the NKG for obtaining a lateral distribution of the charge particles. The former option facilitates a detailed MC simulation of the EM component of a shower that incorporates all the major interactions of electrons and photons (see [11]), whereas the NKG option relies on an analytical approach rather than a full MC simulation. In the NKG option, the electron density of an EM sub-shower is calculated straightaway using the NKG function with a reduced Moliére radius [9, 10]. One gets better accuracy and more detailed information about the EM component with the EGS4 option, at the expense of long computing time. We underline here that the NKG option (subroutine NKG inside CORSIKA)[5] is dealing mainly with the relations ((6), (7)) and not directly with equation (4).

We have considered the US-standard atmospheric model [31] with a planar approximation. The maximum primary zenith angle was restricted to 50°. The EAS events were generated mainly for proton and iron nuclei as primaries. A few events were also generated for γ as primary. Irrespective of the nature of the primaries, the slope of primary power law spectra was taken as -2.7 below the knee (3×10^{15} eV) and as -3.0 above. The EAS events were simulated at different geographical positions corresponding to the experimental sites of AKENO [16], KASCADE [30] and NBU [32]. The magnetic fields are provided accordingly. On the observational level, the kinetic energy thresholds were chosen as 3 MeV for electrons (e^+ and e^-) irrespective of the primary species and energies.

3.1. Generation of the EAS Monte Carlo library

The simulated shower library consists of more than 30 000 EAS events with the EGS4 option and more than 180 000 events with the NKG option in the primary energy interval of 10^{14} eV to 3×10^{16} eV. In order to appreciate the asymptotic tendencies at ultra high energies, our library has also been enriched by about 1000 events simulated at $E_o = 5 \times 10^{17}$ and 10^{18} eV for proton and iron primaries: apart from the thinning factor which is taken as 10^{-6} with optimum weight limitation [33] (i.e., all particles are followed up to an energy $E_{\rm th}$, where $E_{\rm th}/E_o = 10^{-6}$, after which only one of those particles is tracked giving appropriate weight to it) the simulation conditions are here identical concerning the hadronic interaction models, the zenith angle range, both the EGS4 and the NKG options. Here we would like to specify that the optimized thinning factor 10^{-6} with the optimum weight limitation for the CORSIKA

[5] Reference [29] in the original documentation of CORSIKA was mismatched with the appropriate references [10]; it was unfortunately reproduced in the user's guide and in several papers, as for instance [30], thereby generating a confused interpretation of the NKG option.

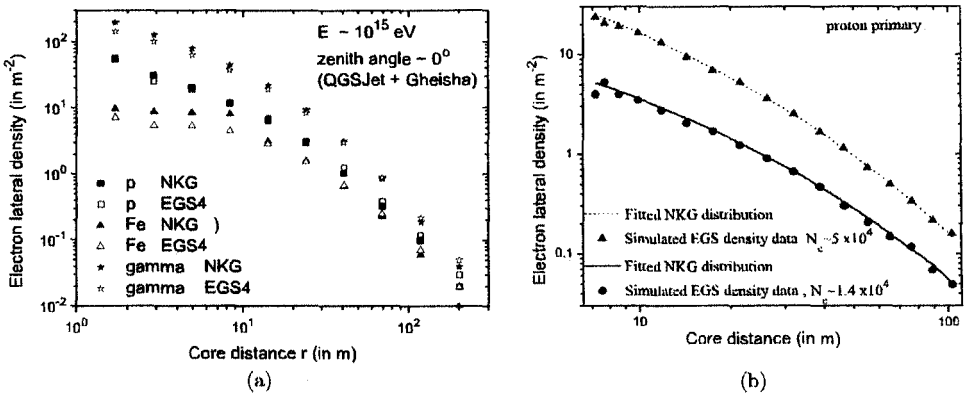

Figure 1. Lateral distribution of electrons from the simulated data. (a) Comparison of the EGS4 and the NKG output for different primary cosmic ray species, (b) NKG fitting of the EGS4 output of electron density at the NBU site with a constant single age restricting radial distance only up to 100 m. The statistical errors are within the dimensions of the symbols used.

version used here is considered as the best compromise between the computing time and the accuracy at ultra high energies [34].

In all cases involving the EGS4 option, the longitudinal development is restored numerically and that $s_{||}$ is computed [35], instead of relation (2), by:

$$s = \exp\left[\frac{2}{3} \times \left\{1 + \frac{\alpha}{t} - \tau\right\}\right] \quad \text{with } \tau = \frac{t_{\max}}{t}, \ \alpha = \ln\frac{N_{\max}}{N_e} \tag{9}$$

where $t_{\max}$, $N_{\max}$ are respectively depth and size read at the cascade maximum.

3.2. The NKG and the EGS options

We used both the EGS4 and the NKG options simultaneously for about 30 000 events. In figure 1(a) we compare the LDD of EAS electrons obtained with the stated two options for proton, iron and gamma primaries. It is noted that the NKG option gives a higher density with a steeper radial distribution compared to the EGS option. A small density excess appears for the pure EM cascades near the axis for the NKG option; such an excess presents also in the proton initiated air showers. However, for the proton showers, a tolerable agreement between the output of the two options was noted over a large band of densities between radial distances of 10–100 m from the shower axis; it reconfirms that for proton and photon initiated showers the NKG option is quite useful to calculate a large number of cascades in a short time.

For Fe primaries, both the options indicate an older profile near the axis. The NKG option was found to give an excess density between 2–10 m distance. The average energy of the positrons was quite a bit lower in the case of iron initiated showers and the cross section of positron annihilation becomes more important for the lower part of the cascade. This effect is probably enhanced by the longer path of the electrons in the geomagnetic field and the larger energy loss by ionization. The NKG option is, therefore, not so accurate for the simulation of heavy nuclei initiated showers with large zenith angles after the shower maximum. For vertical showers, the output of the NKG option is nevertheless acceptable. At larger distances a slight deficit in the densities appears with the NKG option; this probably comes from the different treatment of the multiple Coulomb scattering in the NKG option than in the EGS. Furthermore, Bhaba and Moller scattering are treated in complement with the separated MC

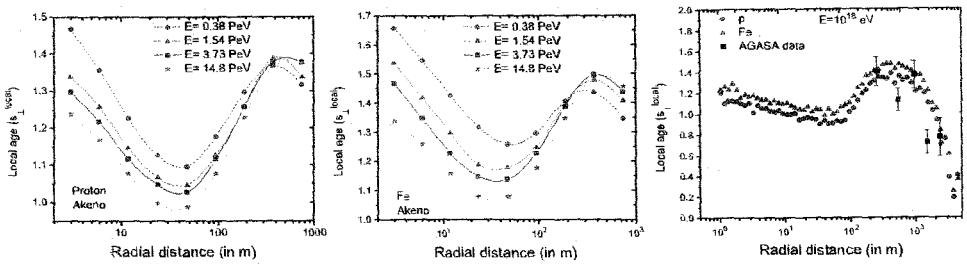

Figure 2. Variation of the LAP (estimated from the simulated data) with radial distance for different primary energies at AKENO site (920 g cm^{-2}) for (a) p (b) Fe (c) for both p and Fe along with the local age obtained from the experimental data. The lines are only a guide for the eye.

procedures. On the other hand, the geomagnetic field of the earth enhances the path of the muons. Consequently their loss by ionization and their decay give more electrons, which is not incorporated in the NKG option. Besides, the NKG option does not accommodate photo-production inside the EM sub-cascades.

4. Estimation of shower age

The simulated data were analysed using the reconstruction algorithms developed to obtain shower size and shower age. We adopted two different methods. First following the traditional approach, we estimated the basic shower parameters by fitting the density data to the NKG function by the method of chi-square minimization through an iterative procedure based on the method of steepest decent. As for example, in figure 1(b) the simulated particle densities at different radial distances are plotted along with the fitted curve obtained with the NKG function. Here it is noted that the majority of the EAS groups traditionally estimate basic shower parameters based on the NKG function. The error in estimating lateral shower age in the shower size interval 10^3–10^5 particles (corresponding to the primary energy range 10^{14}–3×10^{15} eV) was found to be ± 0.03 for the QGSJET model and ± 0.05 for the SIBYLL. The larger error for the SIBYLL model seems solely statistical, due to the generation of a relatively fewer number of EAS events using the later model.

The local age for EAS charged particles was computed for each individual event straightaway, applying equation (7). When estimating the LAP, the main sources of error are the fluctuations in particle density and the uncertainties in radial distance estimation. In simulated data the radial distance of each particle is known with a high accuracy. In this work the error in the LAP, due to uncertainties in radial distance estimation, was kept small by taking small radial bins. For minimizing the statistical fluctuations in particle density at different radial bins, a large number of events need to be considered. In this analysis, the error of the LAP for EAS with the primary energy in the PeV range remains within 0.05 for 10 m $< r <$ 250 m, whereas for $r <$ 10 m or when $r >$ 300 m the error of the LAP is found to be higher, about 0.1. At higher primary energies (5×10^{17}–10^{18} eV) the error of the LAP is found at about 0.12 near the core, which decreases to about the 0.07 level when 20 m $< r <$ 300 m but increases again with the radial distance and reaches to about 0.15 when r approaches 1000 m.

The variation of the LAP with the radial distance from the shower core is shown in figure 2. It is known from previous studies [10] that with an increase of the radial distance, the

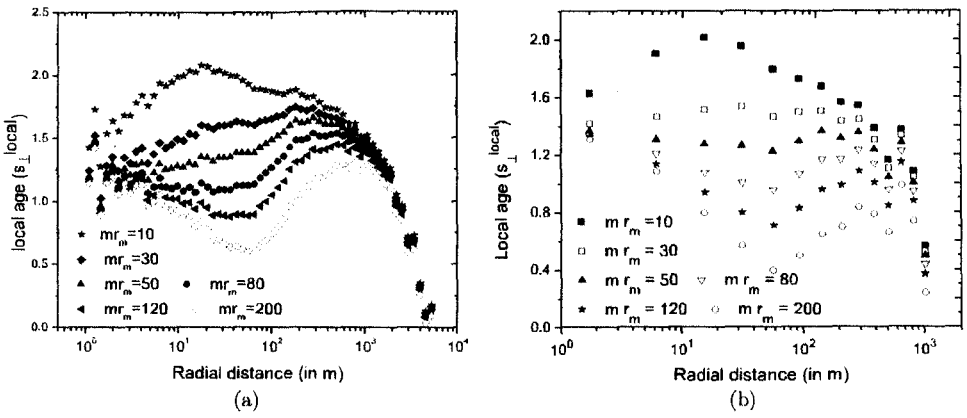

Figure 3. Variation of the LAP (estimated from the simulation data) with the radial distance for different choices of the effective Moliére radius at the KASCADE site (a) for p with a primary energy 5×10^{17} eV (b) for γ with a primary energy 10^{15} eV.

LAP initially decreases, reaching a minimum at around 50 m and then increases, as was also noted from the experimental data [16, 19,10]. Here we noticed two other interesting features (figure 2(a)–(c)): the local age again starts to decrease at around 300–400 m. To examine whether the experimental data also demonstrates a fall in the local age at large radial distances, we compute the local age from the LDD data of total charged particles, as measured by the AGASA experiment [36] for primary energy 2×10^{18} eV and compared these values with our simulation results in figure 2(c). The experimental data clearly support the trend predicted by the simulation results at larger radial distances. The characteristic high–low–high kind of radial variation in the local age at relatively smaller distances (within 300 m or so) could not be substantiated by the AGASA data, due to the large separation of the detectors of the array. It is worthwhile mentioning that there was an indication for such a decrease of $s_\perp^{local}(r)$ at around 300 m in the experimental results obtained by Akeno [19] and KASCADE-Grande [37]. Such behaviour is also depicted in figure 3 of the Kascade report [30], where one may notice a maximal deficit at 50–80 m in the ratio of the measured and the fitted electron densities, as well as an excess at large distances when fitting with the NKG formula. The later feature, however, has not been thoroughly investigated.

These findings are important for an analysis of very large air showers observed/to be observed by the KASCADE-Grande, AGASA, AUGER, Yakutsk, Telescope Array involving large radial distances. The large EAS experiments often treat charged particle densities at large radial distances, such as at 500, 600, 1000 m from the shower core as an estimator of the primary particle energy, though such a technique involves several uncertainties [38]. These findings, of a rapid change in the slope of the radial distribution of electrons at large radial distances, suggest that more controls should be adopted in the estimation of the primary energy of large showers, for instance by taking particle densities at more than one radial distance.

Another important observation is that in general the nature of the variation of the local age with the radial distance appears nearly the same for all of the primary energies, i.e. the nature of the variation is practically independent of the energy of the shower initiating particles, which implies that the local age (or the lateral distribution of electrons in EAS) exhibits some sort of scaling behaviour in respect to the radial dependence from the shower core.

To examine systematically the influence of the effective Moliére radius on the shape of the lateral distribution of charged particles in EAS, we study the radial variation of the LAP for different effective Moliére radii, which is shown in figure 3(a) for a proton primary with a primary energy 5×10^{17} eV.

A string-like feature emerged with two nodes, as seen from the figures, one close to the shower core while the other at around $r \sim 400$ m that increases slowly with the effective Moliére radius; the effective Moliére radius behaves somewhat like the tension in a piece of string. Beyond the second node, however, the LAP is found to decrease monotonically with an increase of the radial distance, irrespective of the choice of the effective Moliére radius.

In order to explore the inherent cause of such a feature of the LDD of electrons in hadron initiated EAS, we studied the radial variation of the local age for γ ray initiated showers, and one such plot at the primary energy 10^{15} eV is shown in figure 3(b). We found the similar nature of radial variation of the LAP as in the hadron initiated showers. As ascertained in previous simulations [10], the behaviour of $s^{\text{local}}(r)$ comes mainly from the discrepancies between the EGS output and the NKG function, i.e. between the rigorous descriptions of the EM cascade adopting the basic EM processes as well as the Moller, Bhabha scattering, positron annihilation, dependence of the cross section on energy on the one hand, Approximation B combined with Landau and small angle approximations in a single description of the multiple Coulomb scattering on the other hand. When the experimental data [30, 35] are superimposed on figure 3, we understand that a reduced Moliere radius (between 20–50 m) is favoured for all primary energies, implying a dramatic reduction in the mean scattering angle connected with the scattering energy of 21 MeV.

5. Characteristics of the shower age parameter

To explore the physical nature associated with the lateral shower parameter, if any, we studied the details of the characteristics of the shower age. For the local age, we considered two different parameters: the minimum value corresponds to the local age at the radial distance, about 40 m, and an average value between 40 to 300 m.

5.1. Distribution of shower age and its fluctuation

The distributions of the LAP and the lateral shower age were studied for the primary energy range 3×10^{14} to 3×10^{16} eV. The fluctuations in the shower age were found to be larger for proton initiated showers compared to those initiated by a heavier primary. If we consider a small primary energy bin instead of a wide one, for instance by selecting the showers inside a small muon size band, we observed that both the distributions of p and Fe could be separated, which in fact becomes very contrasted as shown in figure 4(a); this approach, if adopted with the experimental data, may yield important information on the primary composition around the knee region.

The fluctuations (σ) (variance) in the LAP in different shower age bins are estimated and as a function of the shower size are drawn in figure 4(b) for proton and iron primaries for the interaction model QGSJET. In accordance with expectations [39], the fluctuations in the LAP were found to be larger for the proton initiated showers in comparison to those initiated by the primary Fe, except at lower energies.

5.2. Longitudinal shower age versus lateral shower age

For each simulated event, the longitudinal shower age was also estimated using the relation (9) and the difference between the two age parameters, longitudinal age and average local age,

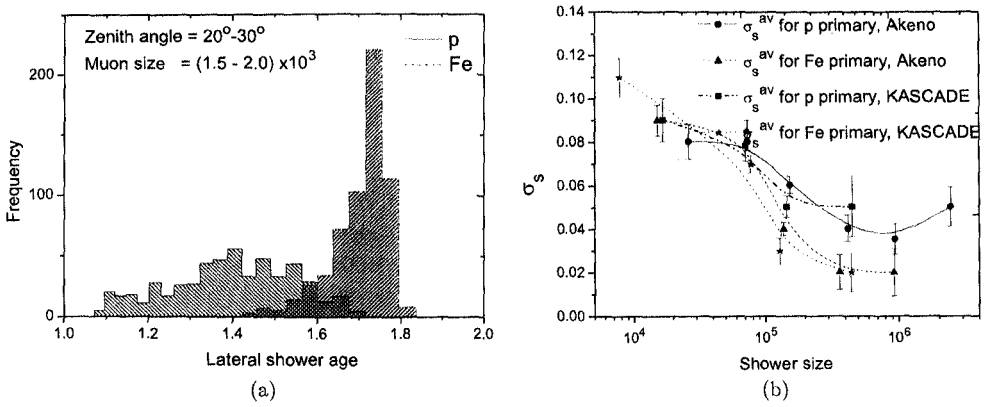

Figure 4. (a) Distribution of the lateral age parameter from simulation at sea level for p and Fe primaries within a small muon size window and (b) the variance (σ) of the distribution of the LAP as a function of shower size. The lines are only a guide for the eye.

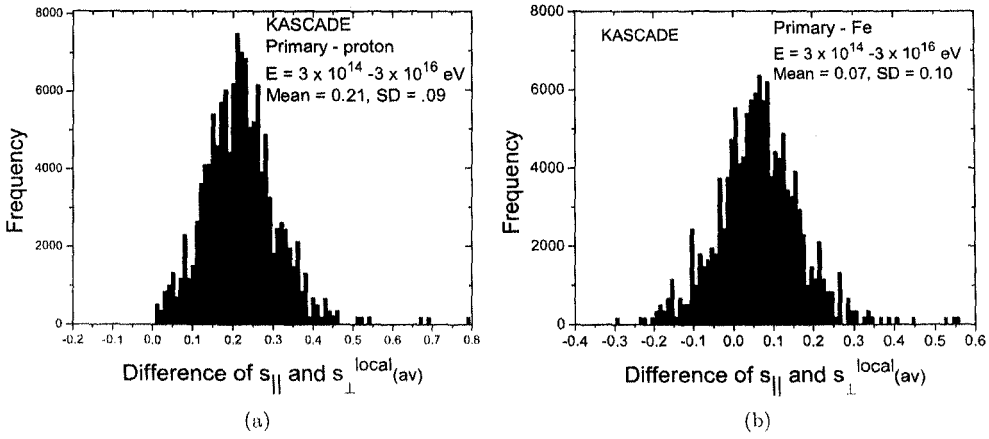

Figure 5. Distribution of the difference between the longitudinal shower age and local shower age from simulated data for (a) p and (b) iron primaries at the KASCADE location.

was obtained. The frequency distributions of the differences between the two age parameters for proton and Fe primaries are given in figure 5. The frequency distribution for where the proton primary peaks, at around 0.2, is consistent with the early observations [40, 10], whereas for Fe initiated showers the peak difference is much lower, at about 0.07. However, for a non-negligible fraction of events, the differences between the two shower age parameters were found to be substantial.

5.3. Variation of the shower age with electron size

In figure 6, we plot the local shower age at a radial distance of about 40 m (minimum value) versus an average shower size, obtained from the simulation results for both proton and iron primaries at the Akeno and KASCADE locations. The corresponding observational results

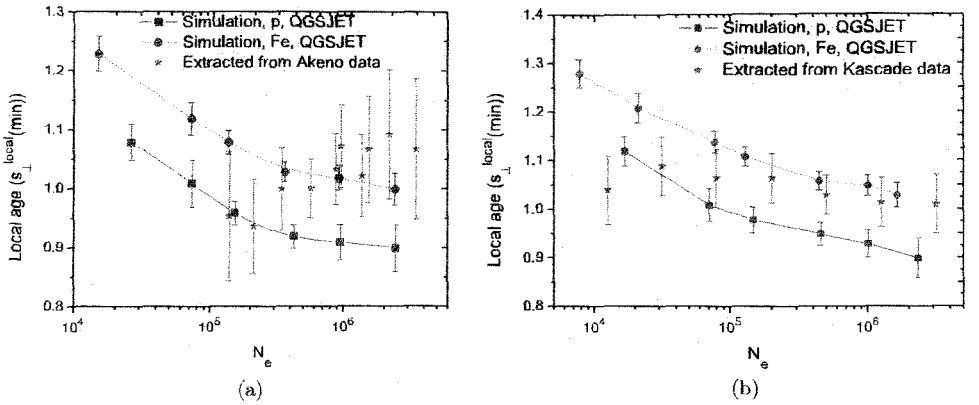

Figure 6. variation of the lateral shower age with shower size for proton and Fe primaries at the (a) Akeno and (b) KASCADE locations. The lines are only a guide for the eye.

extracted from the Akeno and KASCADE experimental data are also given in figure 6. For the Akeno experimental data, we extracted a minimum local age for the different shower sizes from reference [16], whereas for KASCADE we estimated it from their measured lateral distribution [30, 37,42].

The comparison of the simulated results with the experimental observations from both the Akeno and KASCADE EAS experiments (figure 6) indicate a need for a change in the primary composition towards a heavier primary, as the energy increases across the knee of the primary energy spectrum. The KASCADE group also reached a similar conclusion using the shape parameter instead of the shower age [42], as well as from the study of the muon content in EAS [43]. The present data of the LHC, especially the pseudo-rapidity density distributions, suggest larger multiplicities and inelasticities than in the models used in the CORSIKA simulations [44]. However, up to an energy of 2.6×10^7 GeV, this could result in a very small reduction of the reported enhancement of the primary mass with energy.

6. Conclusions

From the present analysis we conclude the following.

(1) The lateral distribution of electrons in EAS exhibits some sort of scaling (energy independent) behaviour in terms of the local age. The characteristic feature of the local age versus the radial distance curve is that with an increase of the radial distance, the local age decreases initially and reaches a minimum, at around 40 m, then it starts increasing, attaining a local maxima, at around 300–400 m, and then starts decreasing again. Such a feature appears to be independent of the energy of the EAS initiating particle, at least there is no strong dependence on the primary energy. Such a characteristic radial variation in the local age is found as a generic feature of EM cascades.

(2) The local age offers a good solution towards an unambiguous estimation of the shower age. Since the shower age varies with the radial distance, even for the modified NKG functions, a comparison of the lateral shower age of different EAS experiments is not meaningful, as the radii of the shower discs naturally differ from experiment to experiment, depending on the experimental set up. Even in a single EAS experiment different events have different

radial extensions and thus a lateral age obtained through fitting with the NKG function seems ambiguous. The local age at a particular distance (say at about 40 m where it takes the minimum value) is, however, not always practical owing to the large fluctuation in the electron density data in a real measurement. A rational idea could be to take some sort of average local age between the first minimum, at around a core distance of 40 m, and the subsequent local maximum, at around 300 m. Experimentally the radial variation of the LAP can be checked properly with a full coverage detector array, like the ARGO-YBJ [45].

(3) The use of a reduced effective Moliére radius in the NKG function leads to a roughly constant age over a radial distance up to about 200 m [41], but the shower age estimated in such a manner is found take quite a higher value than that of the longitudinal age. More importantly, even with a reduced effective Moliére radius, the local age is still found to vary after a radial distance of about 200 m.

(4) The lateral age offers a good estimator of the longitudinal development of an EAS cascade, as already noted in some earlier works [46, 40,10]. However, the parameter correlates with the stage of the shower development on a statistical basis; the average of this parameter increases as air showers traverse an increased thickness of atmosphere. The experimental observations [20] also substantiate such behaviour. The distribution of the differences between the local age and the longitudinal age also indicate the strong correlation between the two ages. Such a feature has been noted for two different hadronic interaction models, the QGSJET and the SIBYLL, and hence appears robust. It is imperative to examine such correlations using EPOS [47], the only model that seems to be providing quite a consistent description of the longitudinal and lateral EAS profiles [48], which would need to be performed in future work.

(5) The fluctuation of the LAP was found to be sensitive to the nature of the primary particle. However, the level of uncertainty in determining the lateral shower age from the experimental data is comparable with the magnitude of fluctuation and hence deriving any firm conclusion on the nature of the primary only from the shower age fluctuation is difficult. If showers within a small bin of the primary energy could be selected, for instance by considering shower events in a small muon size interval, the distribution of shower age was found to be quite sensitive on primary composition; this property may be useful (in conjunction with other primary sensitive parameters) to extract information about primaries.

The comparison of the simulation results with the Akeno and the KASCADE observations in respect to a variation of the shower age with shower size around the knee indicates a change in the primary composition towards heavier primaries across the knee. This finding supports the results obtained from the study of the muon content in EAS. The 3D plot of the shower size versus muon size and shower age may improve accuracy over the conventional approach: deducing the composition through the shower size versus muon size curve. It would be an interesting task to apply such a method for a composition study using observed EAS data from a closely packed air shower array with the facility of concurrent muon measurements, such as the GRAPES experiment at Ooty [49].

Acknowledgments

The authors sincerely thank two anonymous referees and a board member for critical comments and helpful suggestions. AB would like to thank the Department of Science and Technology (Govt. of India) for support under the grant no. SR/S2/HEP-14/2007.

References

[1] Giller M, Kacperczyk A, Malinowski J, Tkaczyk W and Wieczorek G 2005 *J. Phys. G: Nucl. Part. Phys.* **31** 947
Nerling F, Blumer J, Engel R and Risse M 2006 *Astropart. Phys.* **24** 421
[2] Lipari P 2009 *Phys. Rev.* D **79** 063001
[3] Lafebre S, Engel R, Falcke H, Hörandel J, Huege T, Kuijpers J and Ulrich R 2009 *Astropart. Phys.* **31** 243
[4] Schmidt F, Ave M, Cazon L and Chou A 2008 *Astropart. Phys.* **29** 355
Gora D *et al* 2006 *Astropart. Phys.* **24** 484
[5] Kamata K and Nishimura J 1958 *Prog. Theor. Phys. Suppl.* **6** 93
[6] Yushkov A *et al* 2010 *Phys. Rev.* D **81** 123004
[7] Apel W D *et al* 2008 *Astropart. Phys.* **29** 412
[8] Greisen K 1956 *Progress in Cosmic Ray Physics* vol III (Amsterdam: North Holland)
Greisen K 1960 *Annu. Rev. Nucl. Part. Sci.* **10** 63
Snyder H S 1989 *Phys. Rev.* **76** 1563
[9] Lagutin A A *et al* 1979 *Proc. 16th Int. Cosmic Ray Conf. (Kyoto)* vol 1 p 18
Uchaikin V V 1979 *Proc. 16th Int. Cosmic Ray Conf. (Kyoto)* vol 1 p 14
[10] Capdevielle J N and Gawin J 1982 *J. Phys. G: Nucl. Phys.* **8** 1317
Bourdeau M F, Capdevielle J N and Procureur J 1980 *J. Phys. G: Nucl. Phys.* **6** 901
Capdevielle J N and Gabinski P 1990 *J. Phys. G: Nucl. Part. Phys.* **16** 769
[11] Rossi B and Greisen K 1941 *Rev. Mod. Phys.* **13** 240
[12] Cocconi G 1961 *Handbuch der Physik: Cosmic Rays* I vol 46/1 (Berlin: Springer) p 215
[13] Nishimura J 1967 *Handbuch der Physik: Cosmic Rays* II vol 46/2 (Berlin: Springer) p 1
[14] Allan H R *et al* 1975 *Proc. 14th Int. Cosmic Ray Conf. (Munich)* vol 8 p 2131
[15] Hillas M and Lapikens J 1977 *Proc. 15th Int. Cosmic Ray Conf. (Plovdiv)* vol 8 p 460
[16] Nagano M *et al* 1984 *J. Phys. Soc. Japan* **53** 1667
[17] Tonwar S 1981 *Proc. 17th Int. Cosmic Ray Conf. (Paris)* vol 13 p 330
Rao M V S 1983 *Proc. 18th Int. Cosmic Ray Conf. (Bangalore)* vol 11 p 449
Clay R W 1985 *Proc. 19th Int. Cosmic Ray Conf. (La Jolla)* vol 9 p 323
[18] Suprun D, Gorham P W and Rosner J L 2003 *Astropart. Phys.* **20** 157
[19] Sanyal S *et al* 1993 *Aust. J. Phys.* **46** 589
[20] Bhadra A 1999 *Pramana J. Phys.* **52** 133
[21] Heck D, Knapp J, Capdevielle J N, Schatz G and Thouw T 1998 The CORSIKA air shower simulation program *Forschungszentrum Karlsruhe Report* FZK 6019 (Karlsruhe)
Capdevielle J N 1992 The Karlsruhe Extensive Air Shower Simulation Code CORSIKA *KfK Report* 4998 (Karlsruhe)
[22] Kalmykov N N, Ostapchenko S S and Pavlov A I *et al* 1997 *Nucl. Phys.* B **52** 17
[23] Fesefeldt H 1985 *Report PITHA-85/02* (RWTH Aachen)
[24] Fassò A *et al* 2001 *Proc. Monte Carlo 2000 Conf. (Lisbon)* (Berlin: Springer) p 955
[25] Drescher H J *et al* 2004 *Astropart. Phys.* **21** 87
[26] Bhadra A *et al* 2009 *Phys. Rev.* D **79** 114027
Heck D 2006 *Nucl. Phys.* B **151** 127
Ferrari A and Sala P R 1996 *ATLAS Int. Note PHYS-No-086* (Geneva: CERN)
[27] Fletcher R S, Gaisser T K, Lipari P and Stanev T 1994 *Phys. Rev.* D **50** 5710
[28] Nelson W R, Hirayama H and Rogers D W O 1985 The EGS4 Code System *Report* SLAC265 (Stanford Linear Accelerator Center, Stanford, CA)
[29] Capdevielle J N *et al* 1977 *Proc. 15th Int. Cosmic Ray Conf. (Plovdiv)* vol 8 p 341
[30] Antoni T *et al* 2001 *Astropart. Phys.* **14** 245
[31] National Aeronautics and Space Administration (NASA) 1976 US standard atmosphere *Technical Report* NASA-TM-X-74335
Knapp J and Heck D 1993 *KfK Technical Report* 5196B (Kernforschungszentrum Karlsruhe)
[32] Bhadra A *et al* 1998 *Nucl. Instrum. Methods* A **414** 233
[33] Kobal M 2001 *Astropart. Phys.* **15** 259
[34] Knapp J, Heck D, Sciutto S J, Dova M T and Risse M 2003 *Astropart. Phys.* **19** 77
[35] Capdevielle J N and Cohen F 2005 *J. Phys. G: Nucl. Part. Phys.* **31** 507
Capdevielle J N and Cohen F 2005 *J. Phys. G: Nucl. Part. Phys.* **31** 1413
[36] Yoshida S *et al* 1994 *J. Phys. G: Nucl. Part. Phys.* **20** 651
[37] Ulrich H *et al* 2008 *Nucl. Phys.* B **175** 273
Ulrich H *et al* 2009 *Nucl. Phys.* B **196** 80

[38] Capdevielle J N *et al* 2009 *J. Phys. G: Nucl. Part. Phys.* **36** 075203
[39] Catz Ph *et al* 1973 *Proc. of the 13th Int. Cosmic Ray Conf. (Denver, USA)* vol 4 p 2495
[40] Dedenko L G *et al* 1975 *Proc. 14th Int. Cosmic Ray Conf. (Munchen)* vol 8 p 2731
Stamenov J N 1987 *Proc. 20th Int. Cosmic Ray Conf. (Moscow)* vol 8 p 258
[41] Nagano M *et al* 1984 *J. Phys. G: Nucl. Part. Phys.* **10** 1295
[42] Apel W D *et al* 2006 *Astropart. Phys.* **24** 467
[43] Antoni T *et al* 2002 *Astropart. Phys.* **6** 245
[44] Capdevielle J N 2010 arXiv:1010.0916v1
[45] Aloisio A *et al* 2001 *Nuovo Cimento* C **24** 739
[46] Dixon H E and Turver K E 1974 *Proc. R. Soc. Lond.* A **339** 171
[47] Werner K, Liu F-M and Pierog T 2006 *Phys. Rev.* C **74** 044902
Pierog T and Werner K 2009 *Nucl. Phys.* B **196** 102
[48] Pierog T and Werner K 2008 *Phys. Rev. Lett.* **101** 171101
[49] Gupta S K *et al* 2005 *Nucl. Instrum. Methods* A **540** 311

Mon. Not. R. Astron. Soc. 395, 1371–1375 (2009) doi:10.1111/j.1365-2966.2008.14345.x

TeV neutrinos and gamma-rays from pulsars

A. Bhadra[1]★ and R. K. Dey[2]★

[1]*High Energy and Cosmic Ray Research Centre, University of North Bengal, Siliguri, WB 734013, India*
[2]*Department of Physics, University of North Bengal, Siliguri, WB 734013, India*

Accepted 2008 December 9. Received 2008 December 9; in original form 2008 September 27

ABSTRACT

Recent studies suggest that pulsars could be strong sources of TeV muon neutrinos provided positive ions are accelerated by pulsar polar caps to PeV energies. In such a situation, muon neutrinos are produced through the Δ-resonance in interactions of pulsar-accelerated ions with its thermal radiation field. High-energy gamma-rays should also be produced simultaneously in pulsar environment as both charged and neutral pions are generated in the interactions of energetic hadrons with the ambient photon fields. Here, we estimate TeV gamma-ray flux at the Earth from a few nearby young pulsars. When compared with the observations, we find that proper consideration of the effect of polar cap geometry in flux calculation is important. Incorporating such an effect, we obtain the (revised) event rates at the Earth due to a few potential nearby pulsars. The results suggest that pulsars are unlikely to be detected by the upcoming neutrino telescopes. We also estimate TeV gamma-ray and neutrino fluxes from pulsar nebulae for the adopted model of particle acceleration.

Key words: neutrinos – pulsars: general – gamma-rays: theory.

1 INTRODUCTION

Probable candidates of high-energy neutrino radiation include gamma-ray bursts, active galactic nuclei, etc. (Halzen & Hooper 2002). Recently, Link & Burgio (LB) (Link & Burgio 2005, 2006) have shown that pulsars could also be a strong source of high-energy neutrinos. As per their results, pulsars with a magnetic moment component antiparallel to the spin axis, which is expected in half of the total neutron stars, could emit TeV muon neutrinos with fluxes observable by the operating or planned large area neutrino observatories. As a conjecture to be verified by observations, LB considered that protons or heavier ions are accelerated near the surface of the pulsar by the polar caps to PeV energies. When these accelerated ions interact with the thermal radiation field of pulsar, the Δ-resonance state may occur provided their energies exceed the threshold energy for the process. Though radiation losses limit the maximum energy that can be attained by the nuclei in the acceleration process, such an energy condition is expected to satisfy for several pulsars. Muon neutrinos are subsequently produced from the decay of Δ-particles.

The presence of a hadronic component in the flux of pulsar-accelerated particles should result in the emission of high-energy neutrinos and gamma-rays simultaneously as both charged and neutral pions are produced in the interactions of energetic hadrons with the ambient photon fields surrounding the acceleration region. Here, we would show that for the model adopted by LB the estimated TeV gamma-ray fluxes from several nearby pulsars are higher than the observed upper limits of fluxes. In the quest for reasons of such inconsistency, we note that an implicit assumption in the LB estimation of neutrino flux is that the polar cap area is equal to the neutron star surface area. Such an assumption seems unreasonable in view of the polar cap geometry (Beskin, Gurevich & Istomin 1993). When this fact is taken into consideration, the stated inconsistency between the estimated and the observed gamma-ray fluxes is found to disappear. In view of this observation, the revised estimates of the neutrino fluxes from a few known gamma-ray pulsars are obtained by incorporating polar cap geometry.

A young neutron star is generally encircled by pulsar wind nebula (PWN). Positive ions, after gaining energy from polar gaps, will move away from the pulsar practically along the open field lines and will finally inject into the nebula. It is very likely that these energetic ions would be trapped by the magnetic field of the nebula for a long period, and consequently they should produce high-energy gamma-rays and neutrinos by interacting with the matter of the nebula. We therefore estimate the expected flux of TeV gamma-rays from pulsar nebulae, and by comparing with the observation for a couple of well-known nebulae we check the consistency of the model. We also calculate the flux of TeV neutrinos from a couple of pulsar nebulae.

This article is organized as follows. In the next section, after describing the generation of the TeV gamma-rays and neutrinos in a pulsar environment, the expected flux of gamma-rays from a pulsar is estimated for the polar cap model of acceleration as used by LB. By comparing the model-predicted gamma-ray fluxes from

★E-mail: aru_bhadra@yahoo.com (AB); rkdey2007@rediffmail.com (RKD)

some potential young pulsars with the observations, the importance of the inclusion of polar cap area in the calculation has been stressed in Section 3. Incorporating such a feature, (revised) event rates in a neutrino telescope at the Earth due to a few potential pulsars are obtained in Section 4. In Section 5, fluxes of TeV gamma-rays and neutrinos from pulsar nebulae are obtained for the adopted model, and finally the results are concluded in Section 6.

2 TEV GAMMA-RAYS AND NEUTRINOS FROM PULSARS

Several detailed mechanisms have so far been suggested for acceleration of particles by pulsars that include the popular polar gap (Ruderman & Sutherland 1975; Arons & Scharlemann 1979; Daugherty & Harding 1996; Harding & Muslimov 1998) and the outer-gap models (Cheng, Ho & Ruderman 1986). In the former model, acceleration of particles takes place in the open field line region above the magnetic pole of the neutron star whereas in the case of outer-gap model it occurs in the vacuum gaps between the neutral line and the last open line in the magnetosphere. Thus, the region of acceleration in the polar-gap model is close to the pulsar surface, while the same in the outer-gap model is close to the light cylinder.

In the polar cap acceleration model, particles are extracted from the polar cap and accelerated by large rotation-induced electric fields, forming the primary beam. The maximum potential drop that may be induced across the magnetic field lines between the magnetic pole and the last field lines that opens to infinity is $\Delta\phi = B_S R^3 \Omega^2 / 2c^2$ (Goldreich & Julian 1969), where B_S is the strength of magnetic field at neutron star surface, R is the radius of the neutron star, Ω is the angular velocity and c is the speed of light. Accordingly, for young millisecond pulsar with high magnetic fields ($B_S \sim 10^{12}$ G), the magnitude of the potential drop could be as large as $7 \times 10^{18} B_{12} P_{ms}^{-2}$ volts ($B_S \equiv B_{12} \times 10^{12}$ G). But, in young pulsars the electric field along magnetic field lines is likely to be screened well below the vacuum potentials by the onset of electron–positron pair cascades in the strong magnetic field (Cheng & Ruderman 1977), and this would limit the potential to about 10^{12} eV. Though the flux of synchrotron radiation observed from the Crab and other PWN indicates such a possibility, questions like where in the magnetosphere are pairs created and how many are created are still not settled, and one cannot rule out the possibility that ions can reach energies equal to a significant part of the total potential drop through polar cap acceleration, particularly in view of the observation of gamma radiation of energies above tens and even hundreds of TeV from Crab and other PWN.

LB (Link & Burgio 2005, 2006) conjectured that protons or heavier ions are accelerated near the surface of a pulsar by the polar caps to PeV energies (correspond to no/little screening) when $\mu \cdot \boldsymbol{\Omega} < 0$ (such a condition is expected to hold for half of the total pulsars). When pulsar-accelerated ions interact with the thermal radiation field of pulsar, the Δ-resonance state may occur provided their energies exceed the threshold energy for the process. The threshold condition for the production of Δ-resonance state in $p\gamma$ interaction is given by

$$\epsilon_p \epsilon_\gamma (1 - \cos\theta_{p\gamma}) \geq 0.3 \text{ GeV}^2, \quad (1)$$

where ϵ_p and ϵ_γ are the proton and photon energies, respectively, and $\theta_{p\gamma}$ is the incident angle between the proton and photon in the laboratory frame. In a young neutron star with surface temperature T_∞, the energy of a thermal photon near the surface of the neutron star is $2.8\,kT_\infty(1 + z_g)$, $z_g(\sim 0.4)$ being the gravitational redshift. This implies that in a young pulsar atmosphere, the condition for the production of the Δ-resonance is $B_{12} P_{ms}^{-2} T_{0.1\,keV} \geq 3 \times 10^{-4}$ (Link & Burgio 2005, 2006) where $T_{0.1\,keV} \equiv (kT_\infty / 0.1 \text{ keV})$, $T_\infty \sim 0.1$ keV being the typical surface temperature of young pulsars. Such a condition holds for many young pulsars, and thus Δ-resonance should be reached in pulsar atmosphere. Gamma-rays and neutrinos are subsequently produced through the following channels

$$p + \gamma \rightarrow \Delta^+ \rightarrow \begin{cases} p + \pi^o \rightarrow p + 2\gamma \\ n\pi^+ \rightarrow n + e^+ + \nu_e + \nu_\mu + \bar{\nu_\mu} \end{cases}.$$

Since the charge-changing reaction takes place just one-third of the time, on the average four high-energy gamma-rays are produced for every three high-energy neutrinos (or for a muon neutrino antineutrino pair) when a large number of such reactions occur.

The flux of gamma-rays and muon neutrinos from pulsars can be estimated as follows. The charge density of ions near the pulsar surface is $\rho_q \simeq eZn_o$, where $n_o(r) \equiv B_S R^3 \Omega / (4\pi Zecr^3)$ is the Goldreich–Julian density (Goldreich & Julian 1969) of ions at radial distance r. For acceleration to take place, there must be a charge-depleted gap (here polar gap), and the density in the gap may be written as $f_d(1 - f_d)\, n_o$, where $f_d (< 1)$ is the depletion factor which is a model-dependent quantity ($f_d = 0$ corresponds to zero depletion). The flux of protons accelerated by a polar cap is therefore

$$I_{pc} = c f_d (1 - f_d) n_o A_{pc}, \quad (2)$$

where $A_{pc} = \eta\, 4\, \pi\, R^2$ is the area of the polar cap, η is the ratio of the polar cap area to the neutron star surface area, which is taken as unity by LB in their work (i.e. in the original calculation by LB A_{pc} was taken to be equal to the surface area of the whole neutron star). The canonical polar cap radius is given by $r_{pc} = R(\Omega R/c)^{1/2}$ (Beskin et al. 1993), and thus

$$\eta = \Omega R / (4c). \quad (3)$$

The protons accelerated by a polar cap will interact with the thermal radiation field of the neutron star. The temperature of polar caps is expectedly higher than the surface temperature of neutron star, but the contribution of polar caps on the thermal radiation field of a neutron star should be negligible because of their small surface area in comparison with the surface area of the whole neutron star. For a young neutron star with surface temperature T_∞, the photon density close to the neutron star surface is $n_\gamma(R) = (a/2.8k)[(1 + z_g)T_\infty]^3$, a being the Stefan–Boltzmann constant. Numerically, $n_\gamma(R) \simeq 9 \times 10^{19} T_{0.1\,keV}^3$. At radial distance r, the photon density will be $n_\gamma(r) = n_\gamma(R)(R/r)^2$. The probability that a PeV energy proton starting from the pulsar surface will produce Δ particle by interacting with thermal field is given by (Link & Burgio 2005) $P_c = 1 - \int_R^r P(r)$, where $dP/P = -n_\gamma(r)\, \sigma_{p\gamma}\, dr$. The threshold energy for the production of Δ-resonance state in $p\gamma$ interaction as given by equation (1) increases rapidly with distance from the surface of neutron star because of the $(1 - \cos\theta_{p\gamma})^{-1}$ factor (Link & Burgio 2005). Requiring conversion to take place in the range $R \leq r \leq 1.2R$ [at $r = 1.2R$, the value of $(1 - cos\theta_{p\gamma})^{-1}$ averaged over surface becomes double], P_c has been found as $\simeq 0.02\, T_{0.1\,keV}^3$ (Link & Burgio 2005). From a followup calculation by Link & Burgio (2006), it is found that conversion probability is slightly lower than that mentioned above and can be parametrized as $P_c \simeq T_{0.1\,keV}^3$. Thus, the total flux of neutrino/gamma-ray generated in pulsar from the decay of Δ^+ resonance is

$$I = 2c\xi A_{pc} f_d (1 - f_d) n_o P_c, \quad (4)$$

where ξ is 4/3 and 2/3 for gamma-rays and muon neutrinos, respectively. Denoting the duty cycle of the gamma-ray/neutrino beam as

f_b (typically $f_b \sim 0.1-0.3$), the phase-averaged gamma-ray/neutrino flux at the Earth from a pulsar of distance d is given by

$$\phi \simeq 2c\xi\zeta\eta f_b f_d(1-f_d)n_o\left(\frac{R}{d}\right)^2 P_c, \quad (5)$$

where ζ represents the effect due to neutrino oscillation (the decays of pions and their muon daughters result in initial flavour ratios $\phi_{\nu_e}:\phi_{\nu_\mu}:\phi_{\nu_\tau}$ of nearly 1:2:0 but at large distance from the source the flavour ratio is expected to become 1:1:1 due to maximal mixing of ν_μ and ν_τ.). $\zeta = 1$ and 1/2 for gamma-rays and muon neutrinos, respectively.

Average energy of the produced muon neutrinos would be $\epsilon_{\nu_\mu} \sim 50\,T_{0.1\,\mathrm{keV}}^{-1}$ TeV (Link & Burgio 2005, 2006) whereas for gamma-rays it is expected to be $E_\gamma \sim 100\,T_{0.1\,\mathrm{keV}}^{-1}$ TeV.

3 TEV GAMMA-RAYS FROM A FEW POTENTIAL PULSARS: COMPARISON WITH OBSERVATIONS

Though there are about 1800 pulsars known through radio detections, only a few have been detected in the gamma-rays. From observations made with gamma-ray telescopes on satellites so far, only seven high-confidence gamma-ray pulsars are known in the energy range up to a few GeV (Thompson 2003). Besides, three other pulsars (PSR B1046−58, B0656+14 and J0218+4232) are considered to be gamma-ray emitters with a lower confidence level (Thompson 2003) in the same energy region. Some basic properties of the high-confidence *young* gamma-ray pulsars, namely distance (D), spin-down age, period (P), the calculated magnetic field strength at the neutron star surface, surface temperature and pulsar duty cycle (f_b), are listed in Table 1.

None of the listed pulsars is, however, detected at TeV energies despite recent improvement in the knowledge of Galactic gamma-ray sky above 100 GeV, mostly by means of ground-based Imaging Atmospheric Cherenkov telescope systems such as the Collaboration of Australia and Nippon for a Gamma Ray Observatory in the Outback (CANGAROO), High Energy Gamma Ray Astronomy (HEGRA), High-Energy Stereoscopic System (HESS) or the Major Atmospheric Gamma-ray Imaging Cherenkov Observatory (MAGIC). Up to now, no evidence for pulsed emission from any other pulsar has been found from the observations (Chadwick et al. 2000; Lessard et al. 2000; de Naurois et al. 2002; Aharonian et al. 2004, 2007), and only upper limits on the pulsed very high energy gamma-ray flux are derived under various assumptions on the characteristics of the pulsed emission. For the pulsars listed in Table 1, the observed upper limits of integral fluxes are given in Table 2. The upper limits are obtained from the differential spectra assuming a power-law differential spectrum with index −2.4. The upper limits of integral fluxes of gamma-rays from the pulsars at around 100 TeV as obtained by the extensive air shower experiments such as the Tibet (Amenomori et al. 2008; Wang et al. 2008) are found less restrictive.

Table 1. The characteristics of high-confidence young low-energy gamma-ray pulsars.

Source	d (kpc)	age (yr)	p (ms)	B_{12}	$T_{0.1\,\mathrm{keV}}$	f_b
Crab	2	10^3	33	3.8	∼1.7	0.14
Vela	0.29	$10^{4.2}$	89	3.4	0.6	0.04
$B\,1706-44$	1.8	$10^{4.3}$	102	3.1	1	0.13
$B\,1509-58$	4.4	$10^{3.2}$	151	0.26	1	0.26
$J\,0205+64$	3.2	$10^{2.9}$	65	3.8	0.04	0.9

Assuming that pulsar-accelerated ions are protons, numerical values of the integral TeV gamma-ray fluxes are obtained for the pulsars listed in Table 2 from equation (5) and are also shown in the same table (for the numerical estimation of flux, we take $Z = 1$ and $f_d = 1/2$ throughout this work).

It is clear from Table 2 that the model with $\eta = 1$ is not consistent with the observed upper limits; the observed limits are substantially lower than the predicted fluxes. The observations made so far, however, do not rule out the model with η given by equation (3).

4 TEV NEUTRINOS FROM PULSARS

When η is given by equation (3), neutrino fluxes from nearby young gamma-ray pulsars would be much lower than estimated by LB (Link & Burgio 2006). A high-energy muon neutrino is usually detected indirectly through the observation of the secondary high-energy muon produced by the muon neutrino on interaction with the ice or rock in the vicinity of a neutrino telescope via charged current interactions. The track of the produced muon is usually reconstructed by detecting the Cerenkov light emitted by the muon as it propagates through the telescope. The probability of the detection of muon neutrinos is the product of the interaction probability of neutrinos and the range of the muon and is $p_{\nu\to\mu} \simeq 1.3\times10^{-6}(\epsilon_{\nu_\mu}/1\ \mathrm{TeV})$ (Gaisser, Halzen & Stanev 1995). The expected event rates in a neutrino telescope due to potential young pulsars are given in Table 3.

The event rates are clearly very low and thus possibility of observing pulsars by a kilometre-scale neutrino detector does not look bright.

5 GAMMA-RAYS AND NEUTRINOS FROM PULSAR NEBULA

A young neutron star is generally encircled by PWN. Positive ions, after gaining energy from polar gaps, will move away from the pulsar practically along the open field lines and will finally inject into the nebula. It is very likely that these energetic ions would be trapped by the magnetic field of the nebula for a long period and consequently they should produce appreciable high-energy gamma-rays/neutrinos by interacting with the matter of the nebula.

5.1 Magnetic trapping of pulsar-accelerated PeV ions in nebulae

Conservation of magnetic flux across the light cylinder entails that outside the light cylinder $B \sim r^{-1}$ whereas far from the light cylinder the radial component of magnetic field varies as $B_r \sim r^{-2}$. Thus, (far) outside the light cylinder the azimuthal component of the magnetic field dominates over the radial field. Therefore, accelerated protons while moving away from the pulsar have to cross the field lines (e.g. magnetic field lines at wind shock). The Larmor radius of particles (even for proton) of energy about 1 PeV is expected to be smaller than the radius of nebula during most of the time of the evolution of nebula (Bednarek & Protheroe 2002; Bhadra 2006). Thus, it is very likely that energetic particles of PeV energies would be trapped by the magnetic field of the nebula. The energetic particles propagate diffusively in the envelope, and they escape from nebula when the mean radial distance travelled by the particles becomes comparable with the radius of nebula at the time of escaping. This time is somewhat uncertain due to the uncertainty of the value of

Table 2. Comparison of predicted versus observed integral TeV gamma-ray fluxes from some nearby young gamma-ray pulsars. The numbers in parentheses are the energy thresholds in TeV for which upper limits are determined. The observed upper limits for Crab pulsar are due to Aharonian et al. (2006a) whereas for the rest of the pulsars the observed upper limits are due to Aharonian et al. (2007).

Source	Expected integral flux		Observed upper limit of integral flux
	$\eta = 1$ (10^{-15} cm^{-2} s^{-1})	η as given by equation (3) (10^{-15} cm^{-2} s^{-1})	(10^{-15} cm^{-2} s^{-1})
Crab	1012	1.65	8 (56)
Vela	208	0.123	10 (20)
B 1509 − 58	67	0.0034	10 (20)
B 1706 − 44	71	0.0025	10 (20)

Table 3. Expected event rates in a neutrino telescope due to some nearby young gamma-ray pulsars.

Source	Expected event rates (km^{-2} yr^{-1})
Crab	0.009
Vela	0.0007
B 1509 − 58	0.00003
B 1706 − 44	0.00003

diffusion coefficient, but is estimated to be at least a few thousand years (Bednarek & Protheroe 2002; Bhadra 2006).

5.2 Gamma-rays and neutrinos from nebulae of young pulsars

As pointed out in the preceding section, the pulsar-injected ions of PeV energies should be trapped by the magnetic field of the nebula for a long period, and consequently there would be an accumulation of energetic ions in the nebula. These energetic ions will interact with the matter of the nebula. The rate of interactions (ξ) would be $nc\,\sigma_{pA}$, where n is the number density of protons in nebula and σ_{pA} is the interaction cross-section. In each such interaction, charged and neutral pions will be produced copiously. Subsequently, the decays of neutral pions will produce gamma-rays whereas charged pions and their muon daughters will give rise to neutrinos.

If m is the mean multiplicity of charged particles in proton–ion interaction, then the flux of gamma-rays at a distance d from the source would roughly be

$$\phi_\gamma \approx 2c\beta\eta f_d(1 - f_d)n_o \left(\frac{R}{d}\right)^2 \xi m t, \qquad (6)$$

where β represents the fraction of pulsar-accelerated protons trapped in the nebula and t is the age of the pulsar. Note that there should not be any reduction of flux due to pulsar duty cycle in the case of emission to nebula. Though n_o is taken as constant, but actually at the early stages of pulsar n_o should be larger owing to the smaller pulsar period. So, the above expression gives only a lower limit of flux. Typical energy of these resultant gamma-rays would be $\sim 10^3/(6m)$ TeV where for (laboratory) collision energy of 1 PeV m is about 32 (Alner et al. 1987).

Numerical values of the integral TeV gamma-ray fluxes from two nearby nebulae, Crab nebula and Vela nebula, have been estimated for perfect trapping of pulsar-accelerated protons in nebulae and are shown in Table 4. The observed integral gamma-ray fluxes above 1 TeV from Crab nebula (Aharonian et al. 2006a) and Vela nebual (Aharonian et al. 2006b) are also given in Table 4 for comparison.

Table 4. Comparison of predicted versus observed integral gamma-ray fluxes from two nearby PWN.

PWNe	n (cm^{-3})	Expected flux ($\times 10^{-12}$ cm^{-2} s^{-1})	Observed flux (10^{-12} cm^{-2} s^{-1})
Crab nebula	150	0.6	22.6
Vela nebula	1	0.4	12.8

The neutrino fluxes from the nebulae would be of nearly the same to those of gamma-rays. Incorporating the neutrino oscillation effect, the expected event rates in a neutrino telescope due to TeV muon neutrinos from nebulae of Crab and Vela are 0.2 and 0.1 km^{-2} yr^{-1}, respectively. Note that the event rates obtained here are rough numerical values. The flux will be higher if the accelerated ion is heavier than proton.

6 CONCLUSION

To summarize, this work suggests that pulsars are unlikely to be strong sources of TeV neutrinos. The non-detection of any statistically significant excess from the direction of any pulsar by the Antarctic Muon and Neutrino Detector Array (AMANDA)-II telescope (Ahrens et al. 2004; Ackermann et al. 2005, 2008) is thus as per expectations.

If protons are accelerated to PeV energies by the pulsar, then pulsar nebulae are more probable sites of energetic neutrinos provided energetic particles of PeV energies are efficiently trapped by the magnetic field of the nebulae. But, even for pulsar nebulae the expected event rates are small and the detection probability of pulsar nebulae by the upcoming neutrino telescopes, such as the IceCube (Halzen 2006), is very low.

ACKNOWLEDGMENTS

The authors would like to thank an anonymous referee for very useful comments and suggestions.

REFERENCES

Ackermann M. et al., 2005, Phys. Rev. D, 71, 077102
Ackermann M. et al., 2008, ApJ, 675, 1014
Aharonian F., et al. (HEGRA collaboration), 2004, ApJ, 614, 897
Aharonian F. et al. (HESS Collaboration), 2006a, Astron. Astrophys., 457, 899

Aharonian F. et al. (HESS Collaboration), 2006b, Astron. Astrophys., 448, 206
Aharonian F. et al. (HESS collaboration), 2007, Astron. Astrophys., 466, 543
Ahrens J. et al., 2004, Phys. Rev. Lett., 92, 071102
Alner G. J. et al., 1987, Phys. Rep., 154, 247
Amenomori M. et al. (Tibet ASgamma Collaboration), 2008, Nucl. Phys. Proc. Suppl., 175-176, 431
Arons J., Scharlemann E. T., 1979, ApJ, 231, 854
Bednarek W., Protheroe R. J., 2002, Astropart. Phys., 16, 397
Beskin V. S., Gurevich A. V., Istomin N. Ya., 1993, Physics of the Pulsar Magnetosphere. Cambridge Univ. Press, Cambridge, p. 117
Bhadra A., 2006, Astropart. Phys., 25, 226
Chadwick P. M., Lyons K., McComb T. J. L., Orford K. J., Osborne J. L., Rayner S. M., Shaw S. E., Turver K. E., 2000, ApJ, 537, 414
Cheng K. S., Ruderman M., 1977, ApJ, 214, 598
Cheng K. S., Ho C., Ruderman M., 1986, ApJ, 300, 500
Daugherty J. K., Harding A. K., 1996, ApJ, 458, 278
de Naurois M. et al., 2002, ApJ, 566, 343
Gaisser T. K., Halzen F., Stanev T., 1995, Phys. Rept., 258, 173
Goldreich P., Julian W. H., 1969, ApJ, 157, 869
Halzen F., 2006, Eur. Phys. J. C, 46, 669
Halzen F., Hooper D., 2002, Prog. Theor. Phys., 65, 1025
Harding A. K., Muslimov A. G., 1998, ApJ, 508, 328
Lessard R. W. et al., 2000, ApJ, 531, 942
Link B., Burgio F., 2005, Phys. Rev. Lett., 94, 181101
Link B., Burgio F., 2006, MNRAS, 371, 375
Ruderman M. A., Sutherland P. G., 1975, ApJ, 196, 51
Thompson D. J., 2003, preprint (astro-ph/0312272)
Wang Y. et al., 2008, preprint (astro-ph/ 08041862)

This paper has been typeset from a TEX/LATEX file prepared by the author.

Imprint of Geomagnetic field on charged particle distribution in EAS

J.N. CAPDEVIELLE[1,2], R.K. DEY[2], A. BHADRA[3]
[1]*APC, Univ. Paris-Diderot, Bt. Condorcet, 10 rue Alice Domon 75205 Paris Cedex 13 France*
[2]*Dept of Physics, Univ. of North Bengal, Siliguri, WB 734013 India*
[3]*High Energy and Cosmic Ray Research Centre, Univ. of North Bengal, Siliguri, WB 734013 India*
capdev@apc.univ-paris7.fr
DOI: 10.7529/ICRC2011/V01/1127

Abstract: The standard perception is that the muons and othercharged particles in cosmic ray extensive air shower (EAS) are distributed symmetrically about the shower axis. However, from an analysis of Monte Carlo simulation data it is revealed that an asymmetry may develop in both positive and negative muon numbers about the shower axis depending on the geomagnetic field at the location of the observation. Such an asymmetry is particularly pronounced at certain zenith and azimuth angle range. The electron component of EAS also carries such an impression but with a smaller magnitude. Such an effect of geomagnetic field is found to enhance with the mass of the shower initiating particles.

Keywords: geomagnetic field, EAS electron and muon distributions, barycenters of positive and negative particles

1 Muon component and geomagnetic field

An advantageous feature of CORSIKA [1] is that particles and anti-particles can be followed separately and individually. Hence in a Monte Carlo simulation study using CORSIKA one can follow positive and negative muons during propagation in the atmosphere, as well as on arrival at ground level: muons are collected after charged pion double body decay and also after two-body and three-body kaon decays with the different branching ratios. The deflection of muons during their propagation in the atmosphere is caused predominantly by the multiple Coulomb scattering and the curvature of the trajectories, as for all the charged particles of the simulation, in the Earth's magnetic field.

Our first attempt concerning positive and negative muons separately was carried out at high energy for the AUGER Observatory (PAO) and also at relatively lower energies [2, 3]. In the coordinate system of CORSIKA, the magnetic field at PAO is characterized by the two geomagnetic components $B_x = 20.5\mu T$ and $B_z = -14.5\mu T$. In order to point out some typical signature of the nature of primary particle, not on the traditional muon-electron abundance, but on the contrast behavior of positive and negative particles in EAS, we calculated the barycenters of positive and negative muons, $\delta_{\mu+\mu-}$ and the orientation, $\phi_{\mu+\mu-}$ for each shower event at certain azimuthal angles.

For the soft component the radiation lengths are too short and too many scattering deviations occur and as a result the lateral spread is mainly due to the multiple coulomb scattering. Consequently the possibility of sorting out the signature of the geomagnetic field on the soft component is not much. Nethertheless, we shall explore herealso, taking all the advantages of the EGS option, the possible differences between proton and heavy nuclei induced showers revealing in the electron and positron component.

In the case of EAS muons, especially for heavy nuclei initiated showers where the muons start at higher altitude at comparatively lower energies than for proton primaries, a barycenter separation of about 200 m was obtained at UHE for vertical showers (iron primaries) using a thinning factor 10^{-6}. It appears that this separation, which is clearer in the case of nuclei, is also connected with the statistical reduction of the fluctuations of showers initiated by nuclei.

To eliminate any possible bias generated by the thinning technique and to understand more rapidly the benefit of this geomagnetic effect, a sample of few hundred showers without thinning for muons with detection threshold energies exceeding 300 MeV, was simulated and some systematic features have emerged out from the simulated data. For instance, for primary iron induced near vertical showers at 10^6 GeV, the orientation of the dipole towards East-West direction and a net barycenter separation of about 100 m have been noticed irrespective of the azimuthal angle of incidence.

A tremendously large separation of about 500 m (figure1) has been found in the case of very inclined showers ($\Theta = 55°$) at a depth of $860g/cm^2$.

The difference between heavy and light nuclei at UHE can be studied in both directions:

- ratio of μ^+,μ^- at convenient distances
- ellipticity of the muon component

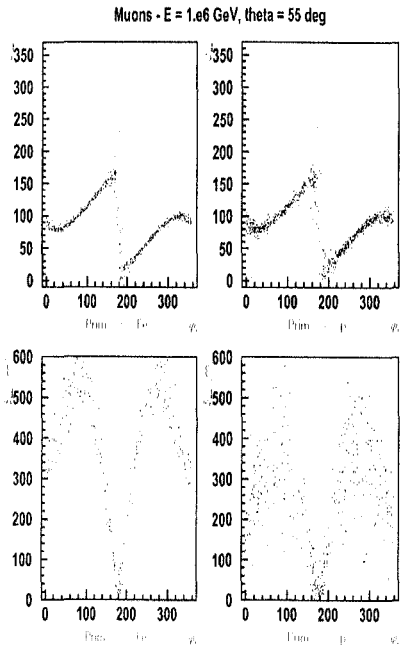

Figure 1: dependences of positive-negative muon dipole orientation $\phi_{\mu+\mu-}$ (upper part), barycenter separation $\delta_{\mu+\mu-}$ (lower part) versus azimuthal incidence ϕ_i with showers zenithal incidence at 55° .
- left side : iron initiated showers
- right side : proton initiated showers

Alternatively, in the absence of detectors for muon charge identification, we introduced the ellipticity factor $\epsilon(r) = \rho_{\mu//}(r)/\rho_{\mu\perp}(r)$, the ratio of total muon densities at the same distance from the shower axis, one on the axis oriented along the muonic dipole and the other on the axis perpendicular to it.

2 Asymmetries in electron and muon distributions

Following the stated preliminary approach, in the present calculations we have considered a sample of simulated EAS events with fixed primary energy 10^6 GeV and try to extract the nature of primaries from the distribution of charged particles (muons and electrons) in different quadrants centered about the shower core and taking the X and Y axes as North and West direction respectively following the convention used in CORSIKA.

We consider both vertical as well as large inclined showers (zenith angle $\Theta = 50°$) to clearly identify the effect of gromagnetic field which should be pronounced along the longer path. In the later case we compare showers initiated with azimutal angles $\phi = 0°$ (figure 2-left) and $\phi = 90°$

	-45 to 45°	45 to 135°	135 to 225°	225 to 315°
$e+$	346	245	503	235
$e-$	514	338	775	374
$\mu+$	916	724	1043	422
$\mu-$	877	404	1010	708

Table 1: Kascade level: number of electrons and muons in quadrants for p primary $\Theta = 50°$, $\phi = 0°$

	-45 to 45°	45 to 135°	135 to 225°	225 to 315°
$e+$	246	184	270	147
$e-$	353	233	393	231
$\mu+$	1225	1117	1387	523
$\mu-$	1211	502	1363	1095

Table 2: Kascade level: number of electrons and muons in quadrants for Fe primary $\Theta = 50°$, $\phi = 0°$

(figure 2-right). The relative muon to electron ratio $\rho(\Phi 1)$ is calculated from the muon /electron size in each quadrant normalized to the total muon/electron content for all the quadrants ($\Phi 1$ is the angle of the central axis of a given quadrant with the X axis) and the differences appearing in the tabulations for p, Fe in each sector have been revealed. This behaviour emerges from the simulation results such as presented in the table 1 at Kascade [4] location for p initiated showers and also for iron induced EAS as given in the table 2. The calculations have been performed at Kascade and Ice Top levels [5] with components of magnetic field, respectively $B_x = 20.52\mu T$, $B_z = 43.57\mu T$ and $B_x = 16.62\mu T$, $B_z = -52.55\mu T$. Note that Ice Top is situated within few meters of the geographic south pole but very far away from the geomagnetic South pole.

The same study has been made by dividing the components of the geomagnetic field by a factor of one thousand to identify the role of the other factors especially the annihilation of the positron and the capture of negative muons of low energy on asymmetries in charged partcle distribution in inclined showers. The results are shown here for muons with energies larger than 230 MeV, whereas the energy threshold for electrons is 5 MeV. We underline that Tables 1 and 2 are just a small sample illustrating general assymmetries in the different quadrant after adding in each sector all muons(positive and negative) as well as all electrons and positrons. Those large anisotropies in inclined EAS can be measured without expensive detectors needing charge separation but with normal detectors sufficient to collect important information in terms of relation between muons and geomagnetic field as well as hints of primary composition.

3 Topological analysis by the BF treatment

A basic assumption of all known hitherto codes used to analyse the data obtained with the CORSIKA and other

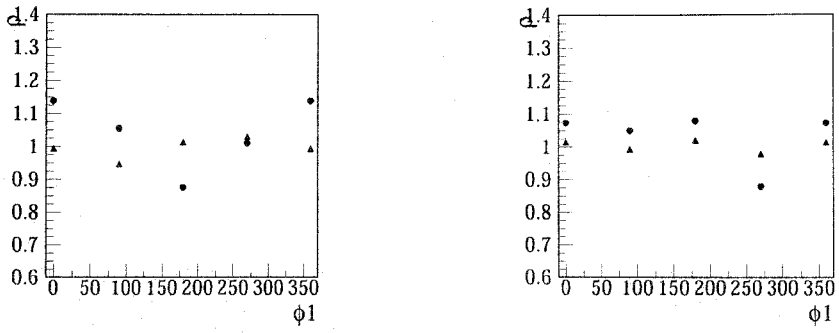

Figure 2: Relative muon electron ratio ρ in different quadrants left: EAS $\phi = 0°$ discs (proton primaries), triangles (iron primaries); right: EAS $\phi = 90°$ discs (proton primaries), triangles (iron primaries)

EAS Monte Carlo simulations is the cylindrical symmetry of charged particles in EAS and such a symmetry is normally noticed on average. In contrast the present analysis revealed an anisotropy in charged particle distribution due to geomagnetic field, particularly at higher zenith angle as stated above. To conserve the asymmetric characteristics of the charged particle distribution due to geomagnetic field, we introduce a procedure of scanning of charged particle density with the butterfly (BF) treatment in order to point out typical signatures relevant to the nature of primaries: the BF consists of two opposite wings around the shower core limited by a pair of symmetric arcs at distances which may be enlarged above $200m$ for very large EAS.

The internal angle of the wing is taken as 90°(quadrant) which can be reduced to emphasize some particular effects. The density of muons inside a wing is compared with that in different wings and the centre of gravity of charged particles (positive and negative separately) are computed from the simulation data. A large separation corresponds to a flatter distribution of the lateral distribution. It is possible to rotate the BF around the axis to identify the areas containing larger differences. The rotation of the BF is measured by the same angle $\Phi 1$ (between the central axis of the BFs and the X axis) to the case of the quadrants. One may notice the contrast between p and iron primaries characterized by a steep decrease of $\Phi 1 = 0.°$ to $\Phi 1 = 180.°$ followed by a fast increase (p primary) against a more modest variation for iron primary as shown in figure 2 . The lateral muon distributions are also calculated separately for positive and negative muons inside the different sectors and compared at both levels of Kascade and Ice Top(figure3), respectively for $\phi = 0.°$ and $\phi = 90.°$

Adopting the BF technique we have also explored the variation of the separating distances of the barycenters of positive and negative muons at both levels of Kascade and Ice Top (figure4), respectively for $\phi = 0.°$ and $\phi = 90.°$

4 Discussion

Our analysis concerning the effects of the geomagnetic field on positive and negative muon and electron components of inclined EAS reveals differences in various features such as asymmetries in sectorial distributions, sectorial muon-electron relative abundances, amplitude of fluctuations between proton and iron induced showers. Such effects are found to persist and are of comparable magnitude if we replace the Gheisha code in the simulation by the Fluka code in the treatment of low energy hadron collisions.

New estimators can be derived from the asymmetries in the profile of muons lateral distributions in different wings of the BF, especially when contrast view in different wings is considered and when the X axis of the BF is superimposed on the axis of the muon dipole : the behavior of the muon electron ratio in different sectors also carries signature discriminating light and heavy primaries. The present calculations will be extended in near future for different primary energies in order to present the results at both fixed electron or muon size.

Furthermore, our method can be implemented experimentally to identify the nature of primary particle with the employment of large muon detectors able to distinguish positive and negative particles at distances of $10 - 50m$ in an EAS array.

References

[1] J. N. Capdevielle et al. KfK report-4998, ed. KfK*The Extensive Air Shower Simulation Code CORSIKA*, Karlsruhe (1992) and report-6019(1998) ed. FZK
[2] J.N. Capdevielle et al., Astrop.Phys., 13, 259(2000)
[3] J.N. Capdevielle, 1st Arctic Workskop on C. R. Muons, Sodankyla, Finland (1999)
[4] W D Apel et al., Astropart. Phys. 24, 467 (2006)
[5] T. Stanev, Nucl.. Phys. B,196,159, 164 (2009)

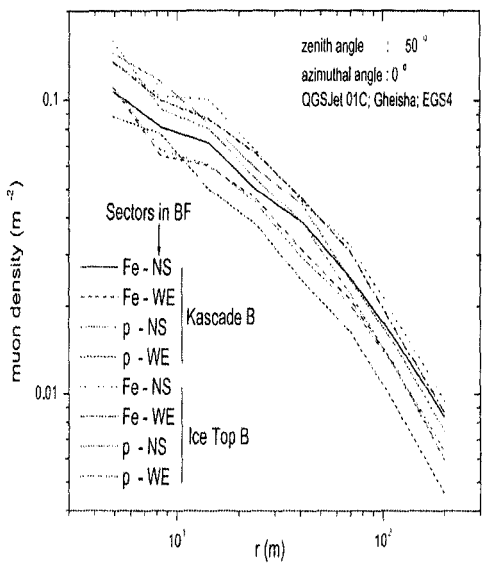

Fig.3

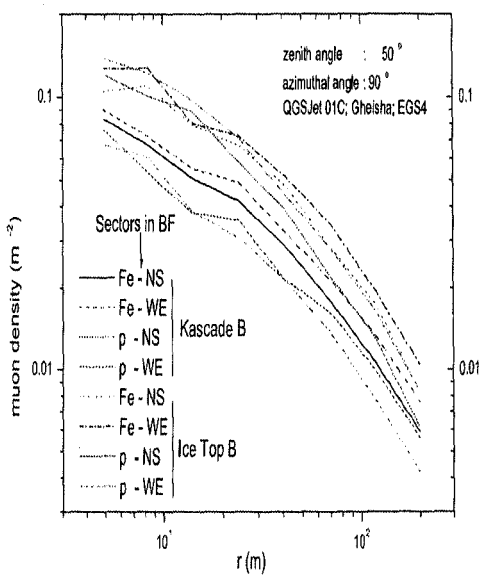

Fig.5

Figure 3: Lateral muon distributions in different sectors.Left: for $\theta = 50°$ and $\phi = 0°$. Upper curves for Ice Top array, lower curves for Kascade level. Right : the same for $\phi = 90°$.

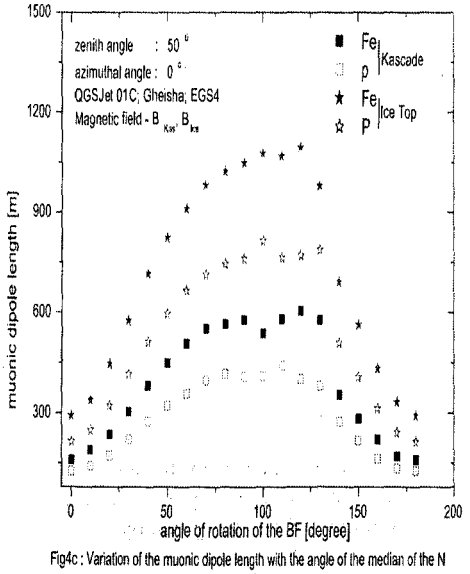

Fig4c : Variation of the muonic dipole length with the angle of the median of the N sector of the BF with OX axis of the CORSIKA coordinate at Kascade & Ice Top sites.

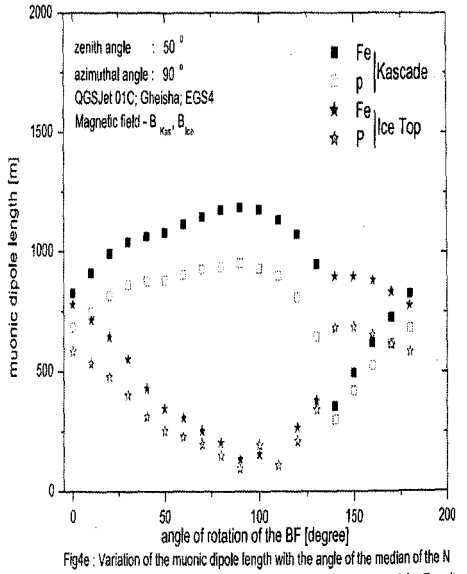

Fig4e : Variation of the muonic dipole length with the angle of the median of the N sector of the BF with OX axis of the CORSIKA coordinate at Kascade & Ice Top sites.

Figure 4: Distance between positive Mu+ and negative Mu- barycenters in different sectors. Left: for $\theta = 50°$ and $\phi = 0°$. Upper curves for Ice Top array, lower curves for Kas cade level. Right : the same for $\phi = 90°$.

Primary mass sensitivity of lateral shower age parameter in EAS

R.K. DEY[1], A. BHADRA[2], J.N. CAPDEVIELLE[3]
[1]*Dept of Physics, Univ. of North Bengal, Siliguri, WB 734013 India*
[2]*High Energy and Cosmic Ray Research Centre, Univ. of North Bengal, Siliguri, WB 734013 India*
[3]*APC, Univ. Paris-Diderot, Bt. Condorcet, 10 rue Alice Domon 75205 Paris Cedex 13 France*
rkdey2007phy@rediffmail.com
DOI: 10.7529/ICRC2011/V01/0107

Abstract: Detailed Monte Carlo simulation studies of cosmic ray extensive air showers in the energy range 0.1 PeV - 1 EeV are made using CORSIKA in order to examine the sensitivity of lateral shower age to primary mass. After proposing an unambiguous way of estimating lateral shower age parameter, a few measurable properties of the lateral shower age and its correlation with other EAS observables are studied for different primaries using the Monte Carlo simulated data, which demonstrate clear mass dependence. The findings from simulation are compared with some experimental results to extract information on average mass composition around the knee region.

Keywords: cosmic ray, EAS, lateral shower age

1 Introduction

The lateral density distribution of electrons in cosmic ray extensive air shower (EAS) is usually approximated by the well known Nishimura-Kamata-Greisen (NKG) structure function [1] and the shower parameters viz. shower size which is the total number of electrons in an EAS and shower age ($s_\perp$) that describes the slope of the radial distribution of electrons in EAS are evaluated by fitting the structure function with the measured densities. While shower size is often related with the energy of the EAS initiating particle but the lateral shower age has not received sufficient importance so far in deducing information on primaries from EAS observations. This is probably because the lateral shower age estimated from experimental data differs from the longitudinal age (s_L) that describes the developmental stage of a cosmic ray cascade in atmosphere. Note that theoretically $s_\perp$ is supposed to be equal to s_L. It is further observed that the NKG function with a single lateral age parameter is insufficient to describe the experimental lateral distribution of EAS electrons properly at all distances implying that the lateral age changes with radial distance.

Some experimental results [2, 3], however, suggests that two age parameters are connected through the approximate relation $s_L \geq s_\perp + \delta$, with $\delta \approx 0.2$. Some early Monte Carlo (MC) simulation studies [4] also indicate that the lateral age has some correlation with longitudinal age and hence the parameter should be sensitive on the nature of the shower initiating particle. In recent years the knowledge of high energy interactions has been improved a lot with the accelerator results. Consequently uncertainties on the results of MC studies of EAS have been reduced significantly at present.

In the present work we would explore through MC study whether lateral age parameter is sensitive on primary mass and consequently the possible role that the parameter may play in a multi-parameter approach of studying EAS to understand the nature of shower initiating particles. One major challenge, however, is the reliable and unambiguous estimation of the lateral shower age from the experimentally measured electron densities. We would address this problem first.

2 Lateral age parameter

The lateral density distribution of cascade particles can be approximated by the well known Nishimura-Kamata-Greisen (NKG) structure function proposed by Greisen [1], which is given by

$$f(r) = C(s_\perp)(r/r_m)^{s_\perp - 2}(1 + r/r_m)^{s_\perp - 4.5}\,, \qquad (1)$$

where r is the radial distance from the shower core, r_m is the Molière radius which is nearly $80m$ at sea level, and the normalization factor $C(s_\perp)$ is given by

$$C(s_\perp) = \frac{\Gamma(4.5 - s_\perp)}{2\pi\Gamma(s_\perp)\Gamma(4.5 - 2s_\perp)}\,. \qquad (2)$$

The NKG formula has the advantage of normalization as it is integrable in Euler Beta function. The normalization of

f(r) implies for the electron density $\rho(r) = N_e f(r)$. But such a handy relation does not hold if $s_\perp$ varies with r, as noted in several observations.

An improvement of the NKG function was proposed by adopting a modulated, longitudinal age parameter s_L dependent effective Moliere radius so that

$$\rho_{el}(r) = (mr_m)^{-2}\rho_{NKG}(r/m) \qquad (3)$$

where $m = 0.78 - 0.21s_L$. But even with such a modification lateral age is found to vary with radial age experimentally. To handle the situation a method was developed by Capdevielle et al. [4] introducing the notion of local age parameter.

From two neighbouring points, i and j, we can give a (local) lateral age parameter for any distribution $f(x)$ (where $x = \frac{r}{r_m}$) which characterizes the best fit by a NKG-type function in $[x_i, x_j]$:

$$s_{ij} = \frac{\ln(F_{ij}X_{ij}^2Y_{ij}^{4.5})}{\ln(X_{ij}Y_{ij})} \qquad (4)$$

where $F_{ij} = f(r_i)/f(r_j)$, $X_{ij}=r_i/r_j$, and $Y_{ij}=(x_i+1)/(x_j+1)$. More generally, if $r_i \to r_j$, this suggests the definition of the LAP $s(x)$ (or $s(r)$) at each point :

$$s(r) = \frac{1}{2x+1}\left((x+1)\frac{\partial \ln f}{\partial \ln x} + 6.5x + 2\right) \qquad (5)$$

Function $f_{NKG}(r)$ with s=$s(r)$ can be used to fit f in the neighbourhood of r.

The identification $s(r) = s_{ij}$ for $r = \frac{r_i+r_j}{2}$ remains valid for the experimental distributions (taking $F_{ij} = \rho(r_i)/\rho(r_j)$ as far as they are approximated by monotonic decreasing functions versus distance.

The behavior of the local age parameter s_{Loc} on experimental lateral distributions was found in accordance with the prediction [4] which was reaffirmed by the Akeno observations [5]. The stated method was validated by the rapporteurs of the ICRC from 1981 to 1985 [6]. The whole procedure was also employed in the calculation of radio effects of EAS.

In the present work we would consider local (lateral) age parameter.

3 Generation of EAS events

For generating EAS events, the air shower simulation program CORSIKA (COsmic Ray SImulation for KAscade) version 6.600 and 6.735 [7] is exploited here in the energy range from 0.1 PeV to 1 EeV. The high energy (above 80GeV/n) hadronic interaction model QGSJET 01 version 1c [8] has been used in combination with the low energy (below 80GeV/n) hadronic interaction model GHEISHA (version 2002d) or FLUKA [9] depending on the primary energy. For the electro-magnetic part both the EGS4 program library and the NKG option are used. We consider the US-standard atmospheric model [10] with planar approximation. The maximum primary zenith angle is restricted to 50°. The EAS events have been generated mainly for Proton and Iron nuclei as primaries. A small number of events have also been simulated for He primaries.

4 Estimation of lateral shower age

The simulated data have been analyzed using the reconstruction algorithms developed to obtain basic shower parameters i.e. shower size (total number of shower electrons) and shower age. We adopt two different methods. First following the traditional approach we estimate basic shower parameters by fitting the density data with the NKG structure function. Secondly, exploiting Eq.(4) we directly estimate local shower age parameter for each individual event.

We noted that the description of the data by the NKG function is improved a lot when the Moliere radius is treated as a variable rather than a fixed parameter. But this better description comes at the expense of very high shower age value which somewhat obscures the physical meaning of the age parameter as assigned in the cascade theory.

The variation of local age parameter with radial distance from the shower core is shown in figure 1(Left) for proton and iron primaries. It is known from previous studies [4] that the local age parameter initially decreases with radial distance, reaches a minimum between 30 to 50 m and then increases with radial distance. Here we have noticed two other interesting features: The local age again starts to decrease around 300 m and more importantly the nature of the variation of local age with radial distance appears nearly the same for all primary energies i.e. the nature of variation is practically independent of energy of the shower initiating particles. This decrease of s(r) around 300 m has been noticed in Akeno [5] and in Kascade-Grande [11].

Such a behaviour is also confirmed experimentally in figure 1(Right) of Kascade report [12]: this figure exhibits a maximal deficit at 50-80m in the ratio of measured and fitted electron densities, as well as an excess at large distances when fitting with NKG formula. Here we have compared the radial variation of local age obtained out of the simulated data for proton and iron primaries with those obtained from the experimentally measured density distribution data of KASCADE in figure 2.

5 The correlation of shower age parameter with other EAS observables

To explore the physical nature associated with lateral shower parameter, if any, we study some characteristics of shower age. We consider local age at two different conditions, the minimum value of local age that corresponds to

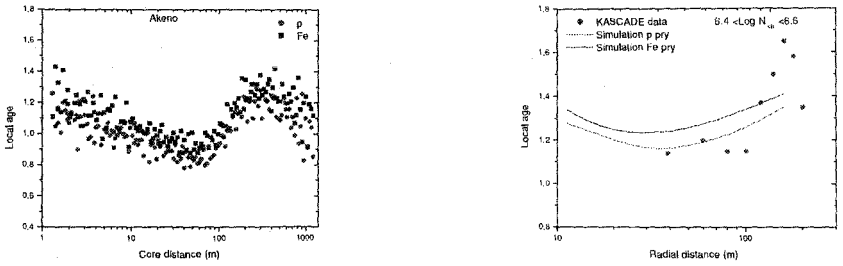

Figure 1: Left: Local age parameter obtained from simulated data as a function of radial distance for proton and Fe primaries at Akeno site at energy 10^{18} eV; Right: The radial variation of local age obtained from the KASCADE observed lateral distribution data.

local age at about radial distance 50 m and a some sort of average between 50 m to 200 m.

The variation of local shower age with shower size for the zenith angle interval (0^o - 45^o) is presented in figure 2 for KASCADE location. It is noticed that the local age decreases with shower size but the rate of decrease slows down at higher shower size. With increasing primary energy i.e. with increasing shower size showers penetrate deeper into the atmosphere resulting in steeper lateral distribution indicated by the smaller lateral shower age parameter. The simulation results show that showers induced by heavier primaries are older compared to those generated by light primaries. When the simulation results are compared with the experimental data, the KASCADE observations indicate for a change in mass composition towards heavier nuclei around the knee.

The fluctuations (variance) of local shower age in different shower size bins are estimated and the shower age fluctuations as a function of shower size are drawn in figure 3 for proton and iron primaries. It is found that at higher energies fluctuations in local shower age is larger for proton initiated showers in compare to those initiated by primary Fe which is in accordance to the predictions of early works [13] but at lower energies a reverse trend has been noticed. In figures 4 we plot the 3-dimensional curve between average local shower age at a radial distance about 40 m (minimum value), average shower size and mean muon size obtained from simulation results for both proton and iron primaries at Akeno and KASCADE location. The corresponding observational results of the Akeno and KASCADE experiments are also shown. For the Akeno experimental data we extract the minimum local age for different shower sizes from a paper [5] whereas the mean muon content corresponding to those shower sizes are obtained from reference. In the case of KASCADE data, we estimated local age from their measured lateral distribution and corresponding muon size are extracted from the $N_e - N_{mu}$ curve.

The comparison of simulated results with experimental observation from both the Akeno and KASCADE EAS experiments (figure 4) indicate for a change in primary composition towards heavier primary as energy increases across

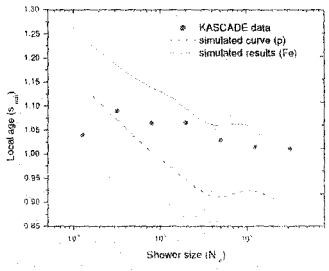

Figure 2: Variation of local age with shower size.

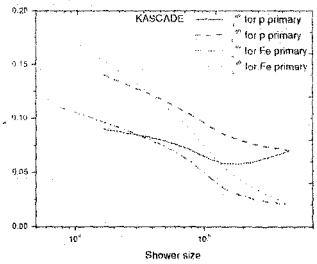

Figure 3: Fluctuation of shower age as a function of shower size.

the knee of the primary energy spectrum. The KASCADE group also reached at the similar conclusion using slope parameter instead of shower age.

6 Conclusions

The present analysis sugests that the local age parameter offers a good solution toward unambiguous estimation of shower age parameter. Since the local age parameter is found to vary with radial distance, comparison of age parameters obtained by different EAS experimental groups is

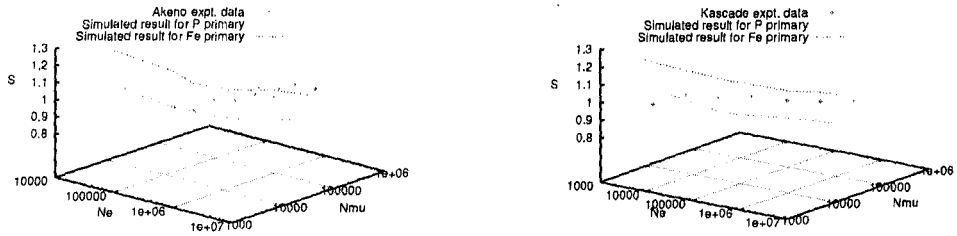

Figure 4: 3-Dimensional plot between shower size, muon size and lateral shower age for proton and Fe primaries at Akeno and KASCADE locations.

difficult as the radius of the shower disc differ from experiment to experiment. Local age at a particular distance (say at the position of minimum i.e. around core distance 40 m) is however, problematic owing to the large fluctuation of electron density data in EAS in a real measurement. We, therefore, propose to take some sort of average local age between the first minimum at around core distance of 40 m and the subsequent local maximum at around 300 m.

The local shower age takes higher value for iron initiated showers in compare to that of proton initiated showers which means that lateral distribution of electrons for iron initiated EAS is flatter relative to that of proton initiated EAS. The slope of lateral shower age versus atmospheric depth curve is, however, more or less the same for proton and iron initiated EAS.

The fluctuation of local/lateral shower age parameter has been found quite sensitive to the nature of primary particle. However, the level uncertainty in determining lateral shower age, particularly in experiments, is comparable with the magnitude of fluctuation and hence deriving any firm conclusion on the nature of primary from the study of fluctuation of lateral shower age alone is difficult.

For the study of primary composition the 3-dimensional plot of shower size versus muon size and shower age seems to offer better accuracy in compare to the more conventional approach of implementing it through the shower size versus muon size curve. It would be an interesting task to apply such 3-dimensional plot to obtain the composition of primary cosmic rays using observed EAS data from a closely packed air shower array with the facility of concurrent muon measurements such as the GRAPES experiment at Ooty [14].

Theoretically the total muon content in an EAS is a strong mass sensitive parameter. However, it is revealed from many experimental studies that it is not always possible to extract proper information on primary mass from the muon content alone. This is mainly due to the limited muon detection area in a real EAS experiment and EAS fluctuations. The present findings suggest that simultaneous study of magnitude of lateral age, its fluctuation and the 3-dimensional variation of the parameter with electron and muon content of EAS may assist to extract the nature of the shower initiating particle with a better accuracy.

References

[1] K Greisen, Progress in Cosmic Ray Physics, Vol.III, Amsterdam, NH publishing Co 1956

[2] L. G. Dedenko *et al.*, Proc. 14th Int. Cosmic Ray Conf. (Munchen) vol 8, p. 2731 (1975)

[3] J N Stamenov, Proc. 20th Int. Cosmic Ray Conf. (Moscow) vol 8, p. 258 (1987).

[4] J.N. Capdevielle and J. Gawin, J. of Physics G,8, 1317 (1982)

[5] M. Nagano et al., Journal of the physical society of Japan, vol. 53, pp.1667-1681 (1984)

[6] S. Tonwar, Proc. 17^{th} ICRC, Paris, 13, 330 (1981); M.V. Rao, Proc. 18^{th} ICRC,Bangalore 11 (1983)

[7] D. Heck et al., FZK A report-6019 ed. FZK *The CORSIKA Air Shower Simulation Program*, Karlsruhe (1998)

[8] N N Kalmykov, S S Ostapchenko et al., Nucl. Phys. B (Proc. Suppl.) 52,17 (1997)

[9] H Fesefeldt Report PITHA-85/02 (RWTH Aachen)(1985); A Ferrari and P R Sala ATLAS int. note PHYS-N0-086(CERN,Geneva)(1996)

[10] NASA, U.S.Standard Atmosphere, Tech.Rep.NASA-TM-X-74335(1976)

[11] J.N. Capdevielle et al., J.Phys. G : Nucl. Part. Phys., 31 , 507-524(2005)

[12] T Antoni, et al., Astropart. Phys. 14, 245 (2001)

[13] M Nagano et al., J. Phys. G, 10(1984), 1295-1310

[14] S K Gupta et al., Nucl. Instrum. and Methods. A 540, 311 (2005)

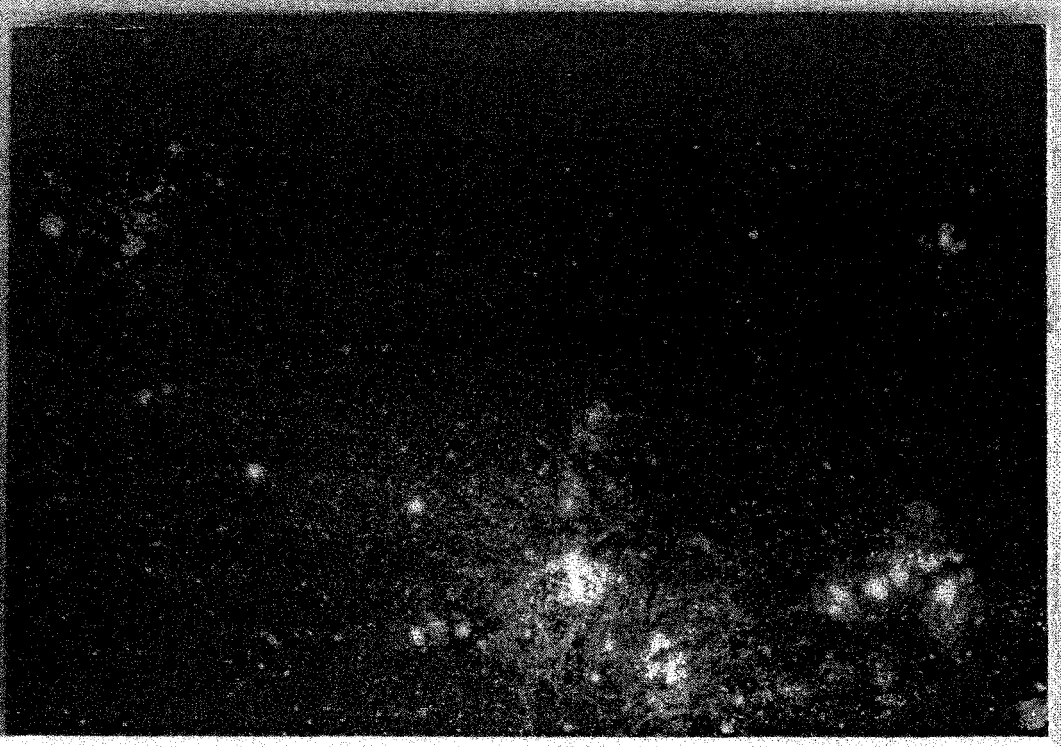

Ed. Arunava Bhadra

Exploring the Cosmos

Proceedings of the Conference on Astrophysics and Astroparticle Physics held at NBU during Jan 27 & 28, 2011

LAP LAMBERT Academic Publishing

Impressum/Imprint (nur für Deutschland/ only for Germany)
Bibliografische Information der Deutschen Nationalbibliothek: Die Deutsche Nationalbibliothek verzeichnet diese Publikation in der Deutschen Nationalbibliografie; detaillierte bibliografische Daten sind im Internet über http://dnb.d-nb.de abrufbar.

Coverbild: www.ingimage.com

Verlag: LAP LAMBERT Academic Publishing GmbH & Co. KG
Dudweiler Landstr. 99, 66123 Saarbrücken, Deutschland
Telefon +49 681 3720-310, Telefax +49 681 3720-3109
Email: info@lap-publishing.com

Herstellung in Deutschland:
Schaltungsdienst Lange o.H.G., Berlin
Books on Demand GmbH, Norderstedt
Reha GmbH, Saarbrücken
Amazon Distribution GmbH, Leipzig
ISBN: 978-3-8443-9165-7

Imprint (only for USA, GB)
Bibliographic information published by the Deutsche Nationalbibliothek: The Deutsche Nationalbibliothek lists this publication in the Deutsche Nationalbibliografie; detailed bibliographic data are available in the Internet at http://dnb.d-nb.de.

Cover image: www.ingimage.com

Publisher: LAP LAMBERT Academic Publishing GmbH & Co. KG
Dudweiler Landstr. 99, 66123 Saarbrücken, Germany
Phone +49 681 3720-310, Fax +49 681 3720-3109
Email: info@lap-publishing.com

Printed in the U.S.A.
Printed in the U.K. by (see last page)
ISBN: 978-3-8443-9165-7

Gamma-Hadron discrimination of primary cosmic rays from EAS observations

R. K. Dey

Department of Physics, University of North Bengal, Siliguri, WB INDIA 734013

rkdey2007phy@rediffmail.com

A. Bhadra

High Energy & Cosmic Ray Research Centre, University of North Bengal, Siliguri WB INDIA 734013

aru_bhadra@yahoo.com

A Monte Carlo simulation study has been carried out, aimed at identifying and rejecting the background component, constituted by hadronic cosmic rays, from γ-ray primaries at energies above 100 TeV. The usual methods for this purpose using muons and secondary hadrons are revisited here. In this work our main focus is to discuss the possible role of longitudinal age, lateral age and local age parameters of EAS for separating γ-ray initiated showers from hadronic showers. Local age parameter may serve as an estimator of gamma-hadron discrimination in ground-based EAS experiments with or without muon measurement facilities.

Pacs: 96.50.sd, 96.50.sb, 95.75.-z, 96.50.S-

Keywords: cosmic ray, EAS, gamma-hadron, Monte Carlo simulations

1. INTRODUCTION

The present astrophysical conjecture of γ-ray astronomy is leading to answer several questions related with the origin and acceleration mechanisms of Cosmic Rays. This becomes a viable branch of main stream astronomy with the advent of the ground-based imaging Cherenkov telescopes. The Cherenkov telescopes HESS, VERITAS and the Fermi γ-ray satellite along with CGRO produce results which agree remarkably well with theoretical predictions [1]. To understand the important

features of the primary energy spectrum vis-a-vis the chemical composition of the cosmic rays at UHE and extremely high energy, a complete study of cosmic ray air-shower has been the only feasible way. The direct measurements of primary cosmic ray flux nearly 10^{14} eV and above are impractical because of very low and sharply falling flux, but has to be inferred from observations of extensive air showers.

The EAS measurements provide various observable parameters namely shower size (N_e), muon size (N_μ), lateral age ($s_\square$), local age (s_{Local}), hadron number (N_{Had}), air shower associated Cherenkov photons (N_{Ch}), shower maximum (X_{max}) and longitudinal age (s_L) (where air-shower arrays are equipped with fluorescence detectors [2,3]) and many of these observables are found to be sensitive to primary masses with different degrees. The measurements from different experiments would still require detailed Monte Carlo simulations of the shower development as a basis of the data analysis and interpretation. The M C simulations consider the evolution of EAS in the atmosphere initiated by different energetic particles. Modern air-shower arrays equipped with large area detectors and improved electronics could precisely measure several EAS components simultaneously [4,5]. Currently simultaneous observations of showers using two distinct detector methods could also help to limit systematic errors that have inundated cosmic ray experiments.

In the field of cosmic ray physics, the discrimination of γ-ray induced air showers from hadron-induced air showers is a long standing problem that still needs more attention [6,7,8]. γ-ray detection suffers from the huge background constituted by ordinary cosmic rays (hadrons), whose flux is about 4 order of magnitude larger than the γ-ray flux. To observe astrophysical sources (assume as point-like objects), one has to eliminate isotropically distributed cosmic rays. In this paper we will discuss some important distinguishing features of γ-ray induced EASs from those induced by the normal cosmic ray nuclei with the help of age parameters & few

other best possible EAS observables. In EAS technique the muon measurements of the two types of showers are important because muon content has been treated beautifully as one of the primary mass sensitive parameters. In KASCADE experiment the secondary hadron content has been used in order to distinguish different primary cosmic ray nuclei but measurements were at variance with the results obtained from electron/muon analysis at sea level [9]. The hadron measurements are usually preferable at mountain altitude because of higher EAS survival energy in the form of hadron component. The three different shape parameters ($s_{\square}$, s_{Local} & s_L) of their lateral and longitudinal profiles of simulated EASs are used in this work to extract important distinguishing features between γ-ray induced showers and protons/nuclei induced showers.

The important considerations adapted in the simulation procedure are given in section **II**. The three different shower age parameters are described briefly in section **III**. In section **IV** we discuss the results obtained on gamma-hadron separation. Finally, section **V** presents our conclusions.

2. SIMULATIONS OF EAS

Results for the present work have been obtained by coupling the high energy (above 80 GeV/n) hadronic interaction model QGSJet 01 version 1c [11] and the low energy (below 80 GeV/n) hadronic interaction model GHEISHA (version 2002d) [12] in the framework of the CORSIKA Monte Carlo program version 6.600 [10]. For the electro-magnetic part the EGS4 [13] program library simultaneously with the NKG option has been used.

The US-standard atmospheric model [14] with planar approximation has been considered which works only for the zenith angle of the primary particles being less than 70°. The maximum primary zenith angle has been restricted to 45° here. The

EAS events initiated by primary protons as well as Iron nuclei and γ-ray have been simulated. The Monte Carlo simulation data library consists of 40,000 EAS events for each primary component p, He, Fe and γ-ray in the primary energy range from 10^{14} eV to $3x10^{16}$ eV followed a power law with a spectral index of -2.7 . A mixed sample has also been prepared from the generated showers taking 50% p, 25% He and 25% Fe events for better understanding of EAS observational results. We simulated EAS events based on the characteristics of several air shower arrays such as NBU, ARGO-YBJ, KASCADE and MT. CHACALTAYA. The magnetic fields are set accordingly. On ground level the kinetic energy thresholds are chosen as 50 MeV, 50 MeV, 3 MeV and 3 MeV for secondary hadrons, muons, photons and electrons.

3. SHOWER AGE PARAMETERS

According to the cascade theory, the developmental stage of a pure electromagnetic cascade can be expressed by a single parameter s_L, known as longitudinal shower age. This parameter is determined as the saddle point in the inverse Melline transformation of cascade transport equation. In approximation B, it is possible and natural to consider the value of s_L as

$$s_L = \frac{3t}{t+2ln\frac{E_O}{\epsilon_o}} \qquad (1)$$

where t is the (slant) atmospheric depth of observational level, E_o is the energy of the primary photon/electron, ϵ_o is the critical energy (in air $\epsilon_o \approx 81$ MeV).

Recent Monte Carlo simulation studies demonstrated universality for large EAS with primaries in the EeV energy range in terms of longitudinal age defined through the relation

$$s_L = \frac{3t}{t+2t_{max}} \qquad (2)$$

where t_{max} is the depth of the shower maximum. The longitudinal data sub-block of CoRSiKa output provides t and t_{max} for estimating s_L.

In the same theoretical framework Nishimura and Kamata solved numerically the 3-dimensional shower equations in approximation **B** to obtain the lateral distribution of electrons progressing in a constant medium. The density profile of cascade electrons was fitted by Greisen with the approximate form called NKG structure function, given by

$$\rho(r, s_{\square}) = N_e c(s_{\square})(\frac{r}{r_m})^{s_{\square}-2}(1+\frac{r}{r_m})^{s_{\square}-4.5} \quad (3)$$

where r_m is the Moliere radius which takes different values for different sites and $c(s_{\square})$ is a normalization factor.

$$c(s_{\square}) = \frac{\Gamma(4.5-s_{\square})}{2\pi r_m^2 \Gamma(s_{\square})\Gamma(4.5-2s_{\square})} \quad (4)$$

To obtain $s_{\square}$ the standard procedure in which simulated electron densities at different radial distances are fitted by the method of Chi-square-minimization through an iterative procedure based on the method of steepest decent to the NKG lateral distribution function [15] of electrons mentioned in equation (3).

For better estimation of shower age from experimental density distribution of electrons, Capdevielle introduced the notion of local age parameter (s_{Local}) [15]. From two neighbouring points, i and j, one can give a lateral age parameter for any distribution f(x) (where $x = r/r_m$) that characterizes the best fit by a NKG-type function in $[x_i, x_j]$:

$$s_{ij} = \frac{\ln(F_{ij}X_{ij}^2 Y_{ij}^{4.5})}{\ln(X_{ij}Y_{ij})} \quad (5)$$

Where $F_{ij} = f(r_i)/f(r_j)$, $X_{ij} = r_i/r_j$ and $Y_{ij} = (x_i+1)/(y_j+1)$. More generally, r_i approaches to r_j, this suggests the definition of the LAP s(x) (s(r)) at each point:

$$s(r) = \frac{1}{(2x+1)}\left((x+1)\frac{\partial lnf}{\partial lnx} + (2+\beta_o)x + 2\right) \quad (6)$$

If β_o =4.5, $f_{NKG}(r)$ with s=s(r) can be used to fit f in the neighbourhood of r. The identification $s(r)= s_{ij}$ for $r = (r_i+r_j)/2$ remains valid for the experimental distributions as long as they are approximated by monotonic decreasing functions versus distance: A typical behaviour of s(r) was inferred with a characterized minimum value of the parameter near 30-50 m from the axis followed by a general increase up to 300 m and again showing a decrement beyond it. A single average age parameter was estimated taking average of all local ages measured in different radial bands between first minima (45 m) and subsequent maxima (200 m) to incorporate important properties of shower initiating particles into it.

4. RESULTS ON GAMMA-HADRON SEPARATION

Based on Monte Carlo simulation studies, some important distinguishing characteristics of hadron and γ-ray initiated air showers have been investigated. The various observable parameters like shower size (N_e), muon size (N_μ), hadron number (N_{Had}), longitudinal age (s_L), lateral age ($s_\square$), local age (s_{Local}) and average age (s_{av}) are being used for this study.

A. ELECTRON-MUON AND ELECTRON-HADRON CO-RELATIONS

The average number of muons and secondary hadrons against the number of electrons are depicted in figures 1a and 1b. It could clearly be recognized that curves for hadron primaries are well above from that for the gamma-ray in both figures. For extensive air shower arrays examining higher energy regions for the selection of primary γ-ray (typically greater than 100 TeV or so), rejection of hadronic background based on the measured muon content remains a promising technique [17]. However, this technique becomes inefficient in regimes where the

expected muon number for protons/nuclei initiated showers is low due to lower primary energy and/or with wider geometrical spread in the shower profile. In such a situation protons/nuclei initiated showers are eliminated from γ-ray showers through the estimation of EAS events which are `secondary hadron-rich' with respect to the number of hadrons expected from γ-ray initiated showers [18].

B. VARIATION OF s_L WITH N_e

The penetration of the atmospheric matter by EASs is determined generally by the elasticity of the interaction defined as the fraction of energy carried by the leading secondary particle. The EASs initiated by γ-rays have large elasticity values compared to hadron initiated showers and by this reason the γ-ray induced showers penetrate more in the atmosphere, as can be distinguished from the comparison of their longitudinal ages [19]. In figures 2a and 2b, we have presented the results obtained on this feature corresponding to the photonic and the nucleonic origin of primary particles at three different depths.

C. N_e & N_μ DEPENDENCIES OF MEAN $s_\perp$

The correlation between mean lateral shower age and shower size in the shower size range (10^3 - 1.5 x 10^6) with the zenith angle interval (0° - 45°) for p, Fe, γ, mixed composition using QGSJet model and NBU results are put on view in figure 3b. It is important to perceive that the lateral shower age takes higher values for heavy nuclei compare to that of light and γ-ray primaries clearly indicating relatively flatter lateral distribution of electrons as one starts from gamma to Fe via p.

The variation of mean lateral shower age parameter with muon size in the primary energy range (10^{14}-3x10^{16} eV) in the zenith angle interval 0° - 45°) for p, Fe, γ-ray primaries is presented in figure 3a with Kascade data. The variation exhibits the same nature as obtained in the KASCADE experiment using NKG fitting for muons with slightly higher muon threshold energy [20]. The figure also exposes the fact

that γ-ray initiated showers are easily distinguishable from hadron showers in terms of s and N_μ but the discrimination between lighter and heavier hadrons at higher energies becomes gradually inappropriate. From our earlier simulation study it has been concluded that EASs from light primary components are younger in average.

D. RADIAL DEPENDENCE OF LOCAL AGE & DISTRIBUTION OF S_{av}

Using equation (5) we have studied the radial dependence of the local age (s_{Local}) for six different Moliere radii between 10-200 m for p, Fe and γ-ray primaries at Kascade site with different primary energies (figures 4a, 4b, 4c). The nature of variations of s_{Local} are almost identical irrespective of primary energy and mass. This behavior of the local age parameter leads to exhibit some kind of scaling feature of radial electron distributions. The radial variation of s_{Local} for p, Fe and γ, at three different altitudes (Kascade, Argo and Mt. Chacaltaya) are shown in figures 5a, 5b, 5c and they exhibit a very good indication of gamma-hadron separation. A very little shift of minima points is observed in s_{Local} vs r plot (figure 6) keeping overall shape unaltered for different altitudes. In figure 7 we have shown the frequency distributions of the estimated average age (s_{av}) and the early development of γ-ray initiated shower compare to hadron showers is revealed from it.

5. CONCLUSIONS

A simulation study has been made to separate the background cosmic rays constituted by hadrons from γ-ray primaries at energies above 100 TeV at four geographical sites. Our conclusions are as follows:

1. The well established fact that muons have higher discriminating power between γ-ray and hadron rather than secondary hadrons is verified once again.

2. It has been recognized from our present simulation study that γ-ray initiated showers are little younger than hadron showers of the same primary energy, zenith angle and observational level.

3. The longitudinal age parameter s_L could be useful for gamma-hadron separation for EAS experiments those equipped with optical detectors (CT & FD).

4. The experimental profiles of EAS cannot be expressed in terms of NKG function with a single age parameter. Consequently, though the lateral age parameter contains information of both hadronic cascading and primary composition, its determination can be biased while fitting the experimental distributions. The characteristic dependence of local age parameter with radial distance allows a more accurate determination of $s_{\square}$.

5. The lateral distribution of electrons in EAS exhibits some sort of scaling (energy, mass independent) behaviour in terms of the local age parameter at least in the energy range 100 TeV to 1 EeV and in few sites in the altitude range 110 m to 5300 m (however a little shift of minima in s_{Local} with altitude is noticed).

6. The local age parameter qualifies reasonably well as an estimator for gamma/hadron discrimination and may separate γ-ray showers from the hadronic background where muon measurements are not made (but array should be densely packed for precise density measurement i.e. ARGO-YBJ). On the other hand, s_{Local} may also be used simultaneously with N_μ in experiments such as GRAPES-3 with concurrent muon measurement facility.

7. The frequency distributions of s_{av} for p, Fe and γ-ray initiated showers exhibit a distinguishing character between γ-ray and hadron primaries.

ACKNOWLEDGEMENT

The authors are thankful to Professor J. N. Capdevielle from the University de Paris for several fruitful discussions. A. Bhadra would like to thank the Department of Science and Technology (Govt. of India) for support under the grant no. SR/S2/HEP-14/2007

REFERENCES

1. F Acero et al., HESS collaboration, http://arxiv.org/abs/0909.4651; V A Acciari et al., VERITAS collaboration, http://arxiv.org/abs/0911.0873 and A Abdo et al., Fermi collaboration, Astron., in press.
2. D J Bird et al. (Fly's Eye collaboration), Phys. Rev. Lett. 71, 3401 (1993).
3. R U Abbasi et al., (HIRES collaboration), Astrophys. J, 622, 910 (2005).
4. M Aglietta et al., Astropart. Phys. 20, 641 (2004).
5. T Antoniet al., Astro-ph/0505413, To appear in Astropart. Phys. (2005).
6. T Gaisser, Cosmic Rays and Particle Phys., Cambridge University Press. Oxford 1990.
7. S Nestnhoff et al., Astropart. Phys.4 (1995) 119-132.
8. H M Badran, T C Neekes, Astropart. Phys. 7 (1997) 307-314.
9. Engel J et al., 1999 Proc. 26th Int. Cosmic Ray conf. vol1, p349.
10. D. Heck et al., FZKA-Report 6019, Forschungszentrum Karlshruhe, (1998).
11. J N capdevielle and P Gabinski, J Phys G. Nucl Part. 16, 769 (1990).
12. H Fesefeldt Report PITHA-85/02 (RWTH Aachen) (1985).
13. W R Nelson, H Hiramaya, D W O Rogers, Report SLAC 265, (1985).
14. National Aeronautics and Space Administration (NASA), U.S. Standard Atmosphere, Tech. Rep. NASA-TM-X-74335 (1976); J Knapp, and D Heck, Tech. Rep. 5196B, Kernforschungszentrum Karlsruhe (1993).
15. K Greisen, Ann. Rev. of Nucl. and Part. Science, 10, 63 (1960).
16. Capdevielle J N, Gawin J and Procureur J 1978 J. Phys. G:Nucl. Phys. 4, 303; 1977 15th ICRC, Plovdiv 8 341.
17. T Stanev, T K Gaisser and F Halzen, Phys. Rev. D, 32, 1244 (1985).
18. Danilova T V et al., 1985, Proc. 19th ICRC 2, 260.
19. H J Drescher and G R Farrar, Phys. Rev. D 67, 116001 (2003).
20. T Antonio, et al., Astropart. Phys. 14, 245 (2001).

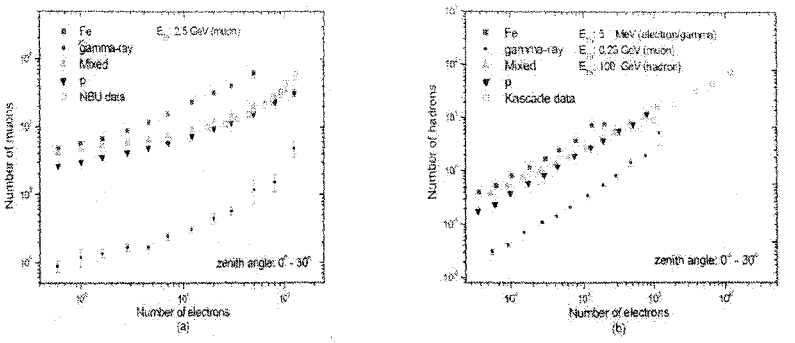

FIG.1: Number of muons[a] and hadrons[b] as a function of electron numbers for p, Fe, γ-ray, mixed composition and experimental data. Our simulated results with initial set of different threshold energies have been reduced to desired values through simulation as demanded for comparison with experiments.

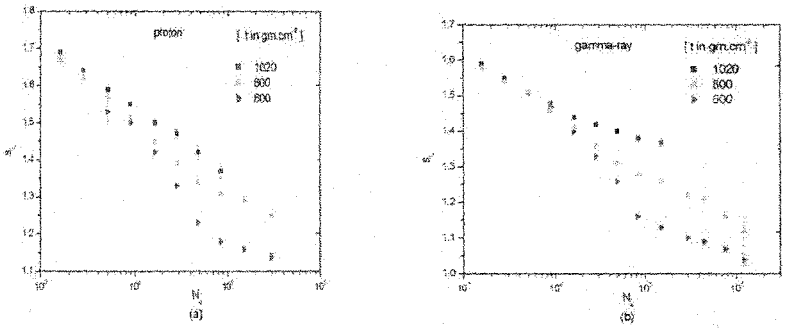

FIG.2: Variation of longitudinal shower age with shower size at three different atmospheric depths for CORSIKA generated simulated showers: [a] proton and [b] gamma-ray.

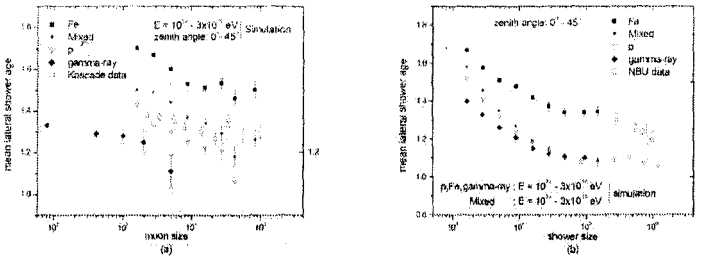

FIG.3: [a] Variation of mean lateral shower age with muon size. [b] Variation of mean lateral shower age with shower size along with NBU data. For comparison with Kascade data in Figure a, where the age parameter was estimated by NKG fits with r_μ as 420 m and also used truncated muon sizes N_μ^{tr}.

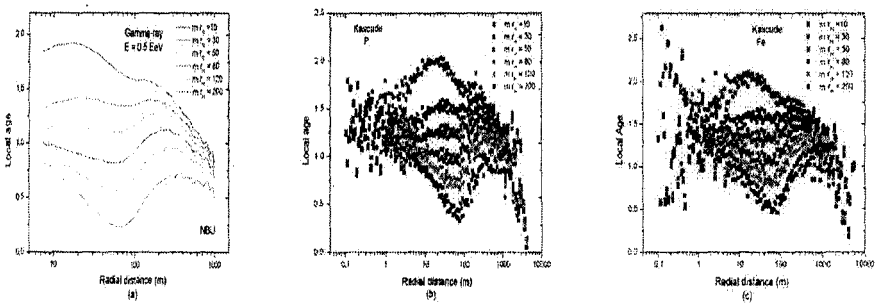

FIG.4: Local age parameter for different Moliere radii.

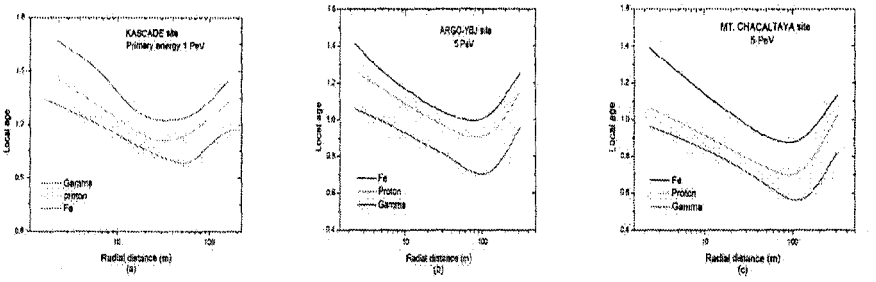

FIG.5: Local age parameter behaves as a good indicative parameter of gamma/hadron discrimination in different sites.

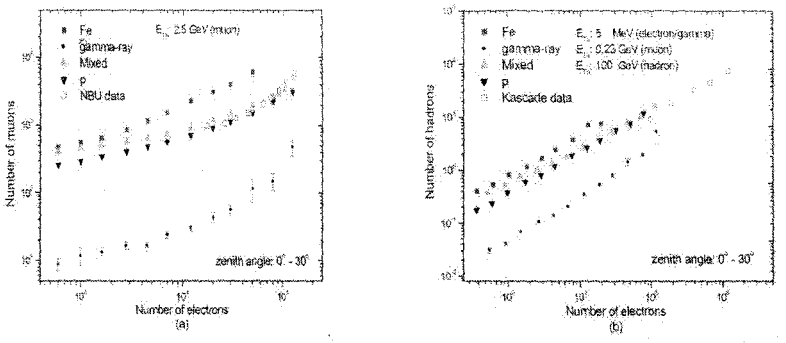

FIG.1: Number of muons[a] and hadrons[b] as a function of electron numbers for p, Fe, γ-ray, mixed composition and experimental data. Our simulated results with initial set of different threshold energies have been reduced to desired values through simulation as demanded for comparison with experiments.

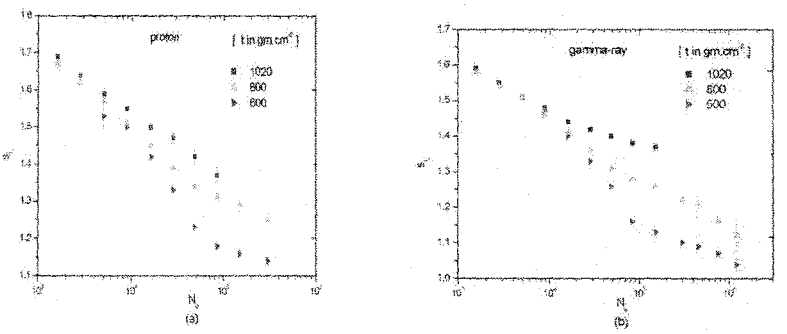

FIG.2: Variation of longitudinal shower age with shower size at three different atmospheric depths for CORSIKA generated simulated showers: [a] proton and [b] gamma-ray.

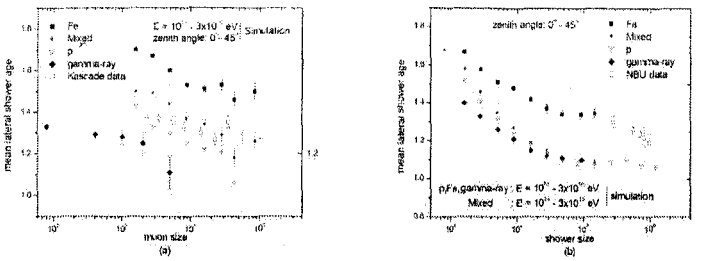

FIG.3: [a] Variation of mean lateral shower age with muon size. [b] Variation of mean lateral shower age with shower size along with NBU data. For comparison with Kascade data in Figure a, where the age parameter was estimated by NKG fits with r_μ as 420 m and also used truncated muon sizes N_μ^{tr}.

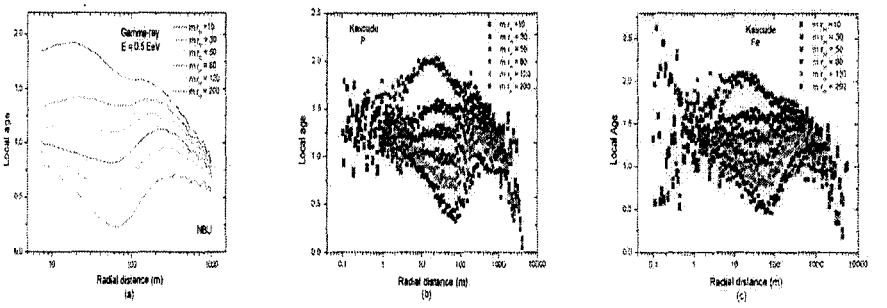

FIG.4: Local age parameter for different Moliere radii.

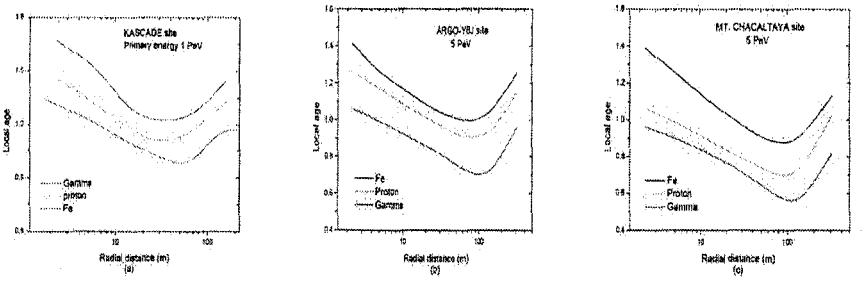

FIG.5: Local age parameter behaves as a good indicative parameter of gamma/hadron discrimination in different sites.

Behaviour of the EAS Age Parameter in the Knee Energy Region

R.K. Dey
Dept of Physics, Univ. North Bengal, Siliguri, WB 734013 India

A. Bhadra
High Energy & Cosmic Ray Research Ctr, Univ. North Bengal, Siliguri, WB 734013 India

J.N. Capdevielle
APC, Univ.Paris Diderot, 10 rue A.Domon, 75205 Paris, France

Analyzing simulated EAS events generated with the CORSIKA code, the characteristics of lateral distribution of electrons in EAS around the knee energy region of the primary energy spectrum have been studied and compared with experimental observations. The differences between the EGS4 and the NKG output of CORSIKA in respect to electron radial density distribution have been investigated. The relation between lateral and longitudinal age parameters has been studied after introducing the notion of the local age parameter that reflects the profile of the lateral distribution of electrons in EAS. The present analysis motivates the inclusion of the lateral shower age in a multiparameter study of EAS to extract information on hadronic interactions and primary composition.

I. THE DIFFERENT AGE PARAMETERS

The concept of shower age was introduced in cascade theory to describe the stage of development of an electromagnetic (e.m.) cascade. A synthesis summarizing the works of Greisen and Nishimura-Kamata under Approximation B of cascade development [1] in respect to shower age is the following: the longitudinal age s_L is defined here as

$$s_L = \frac{3t}{t + 2ln(E/\epsilon_0)} , \qquad (1)$$

where E_0 is the energy of the primary photon generating the cascade, t is the atmospheric (divided by the electron radiation lenth in air taken as 37.1 g-cm^{-2}), ϵ_0 being the critical energy of 82 MeV.

In this theoretical context the lateral density distribution of cascade particles given by Nishimura and Kamata can be approximated by the well known Nishimura-Kamata-Greisen (NKG) structure function,

$$f(r) = C(s_\perp)(r/r_m)^{s_\perp - 2}(1 + r/r_m)^{s_\perp - 4.5} , \qquad (2)$$

where r is the radial distance measured from the EAS core, r_m is the Moliere radius, $s_\perp$ is the lateral age : the normalization factor C($s_\perp$) is given by

$$C(s_\perp) = \frac{\Gamma(4.5 - s_\perp)}{2\pi\Gamma(s_\perp)\Gamma(4.5 - 2s_\perp)} . \qquad (3)$$

implying that for the density $\rho_{NKG}(r) = N_e f(r)$ thanks to the properties of the Eulerian function.

The relation $s_L = s_\perp$ was initially considered to hold for pure e.m. showers and it was admitted that the average steepness of the profile of the lateral distribution has a correlation with the longitudinal development.

Later the 3D diffusion equations were solved again by Uchaikin and Lagutin using adjoint equations and an improvement of NKG function was proposed by modulating r_m to s_L as follows:

$$\rho_{el}(r) = (mr_m)^{-2}\rho_{NKG}(r/m) \qquad (4)$$

with $m = 0.78 - 0.21s_L$.

The validity of this approach was demonstrated [3] by pointing out that the experimental distributions in EAS are steeper than the ρ_{NKG} but are in better agreement with Monte Carlo calculations of Hillas.

For better estimation of shower age from the experimental distributions, one of us (Capdevielle) introduced the notion of the local age parameter (LAP) s_{Loc} [3]: From two neighbouring points, i and j, one can give a lateral age parameter for any distribution $f(x)$ (where $x = \frac{r}{r_m}$) that characterises the best fit by a NKG-type function in $[x_i, x_j]$:

$$s_{ij} = \frac{\ln(F_{ij}X_{ij}^2Y_{ij}^{4.5})}{\ln(X_{ij}Y_{ij})} \qquad (5)$$

where $F_{ij} = f(r_i)/f(r_j)$, $X_{ij}=r_i/r_j$, and $Y_{ij}=(x_i+1)/(x_j+1)$. More generally, if $r_i \to r_j$, this suggests the definition of the LAP $s(x)$ (or $s(r)$) at each point :

$$s(r) = \frac{1}{2x+1}\left((x+1)\frac{\partial \ln f}{\partial \ln x} + (2+\beta_0)x + 2\right) \qquad (6)$$

If β_0=4.5, $f_{NKG}(r)$ with s=$s(r)$ can be used to fit f in the neighbourhood of r.

The identification $s(r) = s_{ij}$ for $r = \frac{r_i + r_j}{2}$ remains valid for the experimental distributions as long as they are approximated by monotonic decreasing functions versus distance: A typical behaviour of s(r) was infered with a characterised minimum value of the parameter near 30 – 50 m from the axis followed by a general increase at large distance and it suggests a relation $s_L \sim 1.25 - 1.3 s_\perp$.

After verification of the behaviour of the LAP through experimentally observed lateral distributions and particularly a detail study of the parameter with the Akeno data [4], this approach was validated by the rapporteurs of the ICRC from 1981 to 1985 [5]. This procedure was also used in extension to calculate the radio effect of very large EAS [6].

II. 3D SIMULATION OF EAS

In the present work, the high energy (above 80GeV/n) hadronic interaction model QGSJET 01 version 1c has been used in combination with the low energy (below 80GeV/n) hadronic interaction model GHEISHA (version 2002d) in the framework of the CORSIKA Monte Carlo program version 6.600 [7] to generate EAS events. The simulated shower library produced consists mainly of 10,000 EAS for each primary species Proton, Helium and Iron in the primary energy interval of 10^{14} eV to 3×10^{16} eV.

Taking the opportunity of calculating simultaneously the e.m. component via both the options, the EGS and the NKG option (implemented following [3] by exploiting the relation (4) in the subcascades treatment) as admitted in CORSIKA package, we have carried out parallel simulations. We ascertain that when the calculation of the electron component is carried out with relation (4), the situation with the NKG inspired procedure implemented in CORSIKA is more close to the experimental data and also to the calculation with the EGS, as shown in fig.1. The NKG option gives a slighly larger density with steeper radial distribution in compare to the EGS option. A small density excess appears for pure electromagnetic cascades near the axis for the Corsika NKG option. Such an excess appears also in proton induced air showers. However, over a large band of densities between the radial distance $10m$ up to $100m$ from the axis, a tolerable agreement is noticed.

For Fe primaries, both the options produce older profile near the axis with density excess (particularly in the case of NKG option) between $2 - 10m$ distance. The average energy of the positrons is quite small in the case of iron initiated showers and the cross section of positron annihilation becomes more important for the lower part of the cascade. This effect is probably enhanced by the longer path of the electrons in the geomagnetic field (and larger energy loss by ionisation). Therefore the NKG option is not a very good option

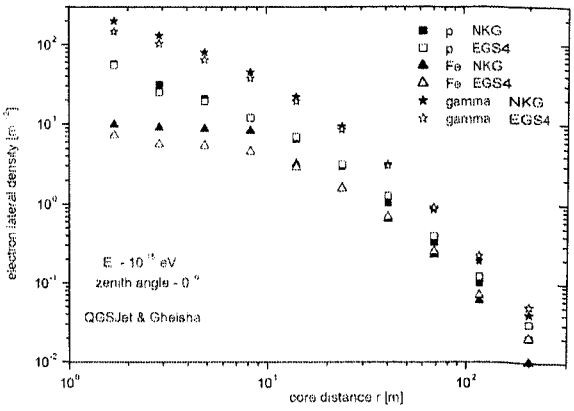

FIG. 1: Comparison of radial distribution of electrons for CORSIKA NKG and EGS options for proton and Fe primaries.

for the simulation of heavy nuclei initiated inclined showers after the maximum development of cascade. Near vertical showers in low altitudes are nevertheless acceptable. Conversely for very high energy primaries the average energy of the positrons remains important and for proton and photon showers NKG option is still useful to calculate a large number of cascades in a short time.

At larger distances a slight deficit in densities appears with the NKG option; it seems to come from the different treatment of the multiple coulomb scattering in the EGS and also may due to the enhanced path of the muons in the geomagnetic field which results in greater loss of energy by ionisation and subsequently their decay produces more electrons. The EGS takes into account the photoproduction inside the e.m. subcascades.

Through a smaller sample of events simulated in the energy band $10^{18} - 10^{20}$eV [9], we have also observed that the lateral distributions calculated at distances lower than 300m from the axis with the NKG option as well as the total longitudinal development do not differ much from those obtained with the EGS. Consequently, the NKG option in CORSIKA remains useful for faster calculations at ultra high energy initiated by a nucleon or nuclei. This circumstance allows the calculation of radio effect as in [6] as well as the fluorescent component via the NKG option. The Landau Pomeranchuk Migdal effect (LPM)(not included in the NKG option) limits however the employment of the option beyond 10^{18}eV for γ primaries.

The fluctuations in lateral shower age are much larger for proton initiated showers compared to those initiated by heavier primary.

This distribution (fig.2) can be fitted by an Extreme

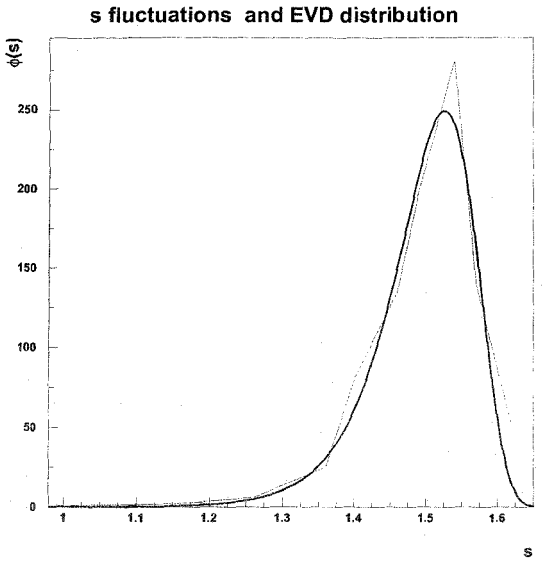

FIG. 2: fluctuation of shower age at fixed shower size $N_e = 10^4$ fitted by an E.V.D. function $\phi(s)$ (vertical showers, sea level, p primaries)

Value Distribution (E.V.D) defined through

$$\phi(s) = \frac{1}{\sigma} \exp(\pm\frac{\mu - s}{\sigma} - e^{\pm\frac{(\mu-s)}{\sigma}}) \qquad (7)$$

where the parameters μ and σ are related to the average size $\overline{s}$ and its variance V_s by $\overline{s} = \mu \pm 0.577\,\sigma$ and $V_s = 1.645\sigma^2$ (in the case of the histogram of fig.2, $\overline{s} = 1.495$ and $\sigma = 0.07$).

Comparing the results of the EGS and the NKG options with Kascade data [8] in the bin $Log(N_e)[3.9, 4.3]$, we observe that there are small discrepancies in densities even with the Lagutin NKG modified formula taking $s = 1.404, N_e = 11829$ as shown on fig.3

Those mentioned parameters (for Lagutin formula (4)) corresponds respectively to the average lateral age parameter and the average size in the size bin considered (calculated with the size spectrum in Karlsruhe).

III. LAP AND N_e DEPENDANCE

The dependance of the local age parameter $s(r)$ on lateral distance exhibits the typical dependance at the level of Akeno experiment with a minimum near 30-40 m distance and larger values near at small radial distances or at large distances from the axis. An example

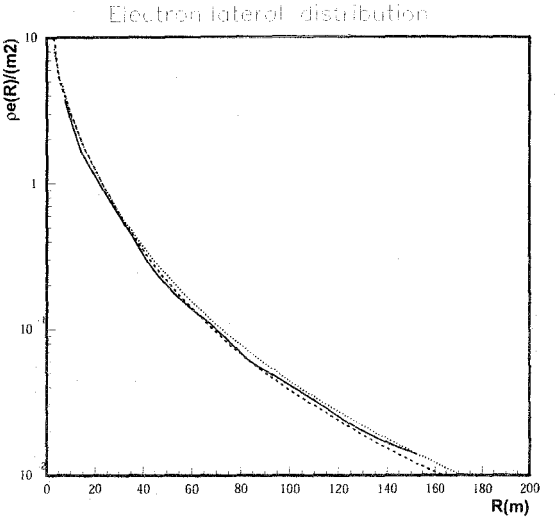

FIG. 3: Lateral electron distributions at Kascade level. Experimental(full line), NKG option(dashed), NKG-Lagutin modified function dotted

is given in the fig.4 for $N_e = 10^6$.

The comprehensive dependance of the lateral age parameter s on N_e is shown on fig.5

The lateral age parameter is obtained as the value of the l.a.p. s(r) averaged inside the shower disc up to the shower radius R_{lim} (distance where the average lateral distribution reaches a threshold density satisfying the trigger conditions and remains detectable by the scintillator detector used i.e. for instance $1el/m^2$ for a counter of $1m^2$ area). One of the most simple interpretations of the minimum near the knee on fig.5 could be a mixed component progressively enriched in nuclei after the knee as suggested half a century ago by the galactic leakage, according to the different Larmor radius of nucleons and heavier nuclei. However, for small energies the shower radius R_{lim} is lower than 40m whereas it exceeds 100m at large energies above the knee; the calculation of the average $s_\perp$ up to those different limits may be the reason for decreasing s below the knee and an increase in age beyond the knee.

IV. CONCLUSION

The experimental profiles cannot be expressed in terms of NKG function with a single age parameter. Consequently, though the lateral age parameter contains information of both hadronic cascading and primary composition, its determination can be biased while fitting the experimental distributions. The char-

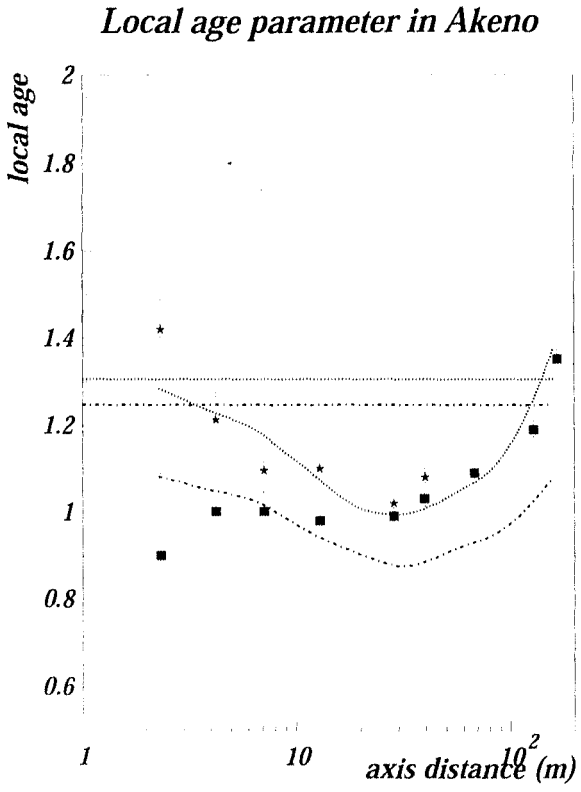

FIG. 4: Local age parameter versus distance at Akeno. Experimental points squares (thick scintillators), stars (thin scintillators), dotted line proton primaries, dashed line iron primary, horizontal lines longitudinal age parameter respectively for p and iron

acteristic dependance of local age parameter with radial distance allows a more accurate determination of $s_\perp$ as well as the conversion to s_L

A detailed study of dependence of $s_\perp$ on shower size, included in a multiparameter analysis (muon-electron abundance, absorption length) and comparison with the Akeno and the Kascade data (in progress) should help to understand the knee region in terms of primary composition.

Acknowledgments

AB would like to thank the DST (Govt. of India) for support under the grant no. SR/S2/HEP-14/2007

[1] G. Cocconi, Cosmic Rays, Handbuch der Physik, 46-1, 215, Berlin: Springer Verlag (1961) and references herein
[2] J. Nishimura, Cosmic rays, Handbuch der Physik, 46, 2,114, Berlin: Springer Verlag, (1967)
[3] J.N. Capdevielle and J. Gawin, J. of Physics G,8, 1317 (1982); M.F. Bourdeau, J.N. Capdevielle and J. Procureur, J. Phys.G, 6, 901, (1980); J.N. Capdevielle and F. Cohen, J.Phys. G : Nucl. Part. Phys., 31 (2005), 507-524 and references herein
[4] M. Nagano et al., Journal of the Physical Society of Japan, vol. 53, pp.1667-1681 (1984)
[5] S. Tonwar, Proc. 17^{th} ICRC, Paris, 13, 330 (1981); M. Rao, Proc. 18^{th} ICRC, Bangalore 11 (1983); R. Clay, Proc. 19^{th} ICRC, La Jolla 9, 323(1985)
[6] D. Suprun et al., Astrop. Phys., 20, 157-168(2003)
[7] D. Heck, J. Knapp, J.N. Capdevielle, G. Schatz and T. Thouw, FZK A report-6019 ed. FZK *The CORSIKA Air Shower Simulation Program*, Karlsruhe (1998); J. N. Capdevielle et al. KfK report-4998, ed. KfK *The Karlsruhe Extensive Air Shower Simulation Code CORSIKA*, Karlsruhe (1992)
[8] T. Antoni, et al., Astropart. Phys. 14, 245 (2001)
[9] J.N. Capdevielle et al, 36, J. Phys. G, 075203 (2009)

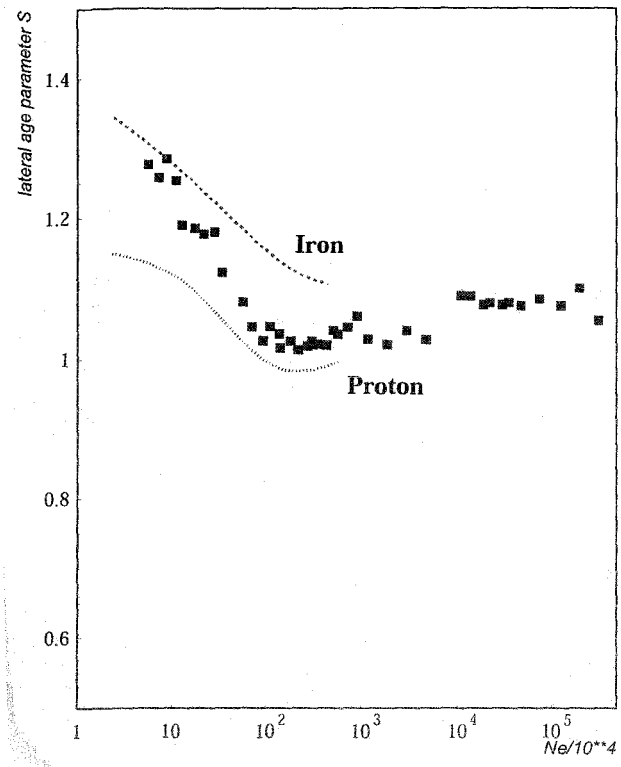

ateral age parameter versus size N_e at Akeno